# Deep Geothermal Drilling Using Millimeter Wave Technology

## Final Technical Research Report

**Project Number:** DE-EE0005504
**Project Period:** 30 September 2011 to 30 September 2014
**Date of Report Submission:** 30 December 2014

**Recipient Organization:** Impact Technologies LLC
**DUNS Number:** 141810494
**Recipient Address:** PO Box 35505, Tulsa OK 74153-0505

**Principal Investigator:** Kenneth D. Oglesby
President
kdo2@impact2u.com
918.629.6993

**Project Partners:** Dr. Paul Woskov at the Massachusetts Institute of Technology (MIT) Plasma Science and Fusion Center,

Dr. Herbert Einstein at the MIT Rock Mechanics Laboratory and the MIT Department of Civil and Environmental Engineering, and
Dr. Bill Livesay as a project consultant

**Federal Agency and Organization:** DOE EERE – Geothermal Technologies Program

**DOE Project Team:** DOE Contracting Officer – Michael Buck
DOE Project Officer – Michael Weathers
Project Monitor – Erik Swanton

# DISCLAIMER

## ABSTRACT

Conventional drilling methods are very mature, but still have difficulty drilling through very deep, very hard and hot rocks for geothermal, nuclear waste entombment and oil and gas applications. This project demonstrated the capabilities of utilizing only high energy beams to drill such rocks, commonly called 'Direct Energy Drilling', which has been the dream of industry since the invention of the laser in the 1960s. A new region of the electromagnetic spectrum, millimeter wave (MMW) wavelengths at 30-300 giga-hertz (GHz) frequency was used to accomplish this feat.

To demonstrate MMW beam drilling capabilities a lab bench waveguide delivery, monitoring and instrument system was designed, built and tested around an existing (but non-optimal) 28 GHz frequency, 10 kilowatt (kW) gyrotron. Low waveguide efficiency, plasma generation and reflected power challenges were overcome. Real-time monitoring of the drilling process was also demonstrated. Then the technical capability of using only high power intense millimeter waves to melt (with some vaporization) four different rock types (granite, basalt, sandstone, limestone) was demonstrated through 36 bench tests. Full bore drilling up to 2" diameter (size limited by the available MMW power) was demonstrated through granite and basalt samples.

The project also demonstrated that MMW beam transmission losses through high temperature (260$^{o}$C, 500$^{o}$F), high pressure (34.5 MPa, 5000 psi) nitrogen gas was below the error range of the meter long path length test equipment and instruments utilized. To refine those transmission losses closer, to allow extrapolation to very great distances, will require a new test cell design and higher sensitivity instruments. All rock samples subjected to high peak temperature by MMW beams developed fractures due to thermal stresses, although the peak temperature was thermodynamically limited by radiative losses. Therefore, this limited drill rate and rock strength data were not able to be determined experimentally. New methods to encapsulate larger rock specimens must be developed and higher power intensities are needed to overcome these limitations. It was demonstrated that rock properties are affected (weakening then strengthened) by exposure to high temperatures. Since only MMW beams can economically reach rock temperatures of over 1650oC, even exceeding 3000oC, that can cause low viscosity melts or vaporization of rocks. Future encapsulated rock specimens must provide sufficiently large sizes of thermally impacted material to provide for the necessary rock strength, permeability and other analyzes required.

Multiple MMW field systems, tools and methods for drilling and lining were identified. It was concluded that forcing a managed over-pressure drilling operation would overcome water influx and hot rock particulates handling problems, while simultaneously forming the conditions necessary to create a strong, sealing rock melt liner. Materials that contact hot rock surfaces were identified for further study. High power windows and gases for beam transmission under high pressures are critical paths for some of the MMW drilling systems. Straightness/ alignment can be a great benefit or a problem, especially if a MMW beam is transmitted through an existing, conventionally drilled bore.

## KEYWORDS

Drilling Direct Energy Drilling High Energy Beams Millimeter Waves Gyrotron
Geothermal Wells Nuclear Waste Storage Wells

# EXECUTIVE SUMMARY

Conventional drilling methods are very mature, but still have difficulty drilling through very deep, very hard and hot rocks for geothermal, nuclear waste entombment and oil and gas applications. In this project we laboratory bench demonstrated the capabilities of utilizing only high energy beams to drill such hard hot rocks, commonly called 'Direct Energy' (DE) Drilling. Full bore DE drilling has been a dream since the invention of the laser in the 1960s, but there are still no applications at this time. Military laser experiments (MIRCAL & COIL) in 1997-1999 showed the potential for 10-100 times faster than conventional drilling. Later research at Colorado School of Mines [4, 103] confirmed that potential. Foro Energy is developing a non-DE laser assisted mechanical drilling system using fiber optics to deliver a moderate power infrared beam to weaken the rock at a localize point immediately ahead of a bit cutting tooth . Infrared physics and laser technology are limitations to full bore DE IR based drilling applications, but millimeter waves (MMW) overcome these physics limitations and may reduce rock drilling to a fundamental interaction between energy and matter without the need for mechanical contact with the drilled surface.

Radio waves or electro-magnetic (non-ionizing) radiation in the extremely high frequency (EHF) range (between microwave/MHz and infrared/ THz classifications), between 30 to 300 GigaHertz (GHz) frequencies or 1-mm to 10-mm wavelengths ($\lambda$), are called millimeter waves (MMW). They are useful in near line-of-sight applications and can have efficient guided transmission. MMWs are generated using commercially available gyrotrons at efficiencies greater than 50% and at megawatt average power levels. Current applications of MMWs are- heating, communications (PAN), airport security, non-lethal weapons, radar, medicine, and astronomy.

The potential benefits of using MMW for drilling and lining wellbores include:

1) Commercially available efficient, megawatt gyrotron sources;
2) Simple, direct and efficient conversion of MMW energy into heat to melt and vaporize targeted rocks;
3) Simple system w/no rotation or mechanical components to wear out; Drill rate with depth is expected to be constant;
4) Drill cost with depth expected to increase linearly and not exponentially;
5) Rock hardness and temperature not limiting parameters;
6) Potential for vitrified liner with drilling, all in one process;
7) Flexible system with various MMW modes of delivery to the target;
8) Compatible with dirty environment and small particle plumes, due to Rayleigh scattering (note that 1 mm (MMW) has $10^{12}$X less scattering loss than 1 μm (IR) wavelengths);
9) Absorption of the beam by rock melt is more efficient in the MMW frequencies over IR;
10) Remote real-time diagnostic (radiometry, radar, spectroscopy) and monitoring technology available with MMW;
11) Efficient long distance, megawatt transmission technology;
12) Wavelengths and borehole sizes ideally suited for efficient beam delivery;
13) Inherent straight borehole to depth (may be difficult to re-enter conventionally drilled bores);
14) Inherent wellbore diameter control, but not necessarily resulting in a smooth bore; and
15) Potential monobore well construction to great depths.

The specific objective of this project was to further develop intense millimeter wave (MMW) radiation (non-ionized) technology (originally developed for fusion energy research) for ablation/ vaporization and melting of rocks for drilling deep geothermal formations and in other applications. The project work included: 1) theoretical considerations; 2) laboratory bench tests of rock ablation/vaporization with a gyrotron and furnace; 3) evaluation of the bench test melted rock specimens; 4) initial designs of an optimal drill system and key components; and 5) this Final Report. This Final Report covers: A) perform and evaluation all lab tests and designs; B) determine the development status; C) estimate costs; and D) identify further areas of research and design that are needed for using the MMW technology as a deep Enhanced/Engineered Geothermal Systems (EGS) drilling and borehole lining system. All were successfully performed.

In this project a lab bench MMW delivery waveguide and monitoring equipment / instruments were designed and built around an existing 28 GHz frequency, 10 kilo-watt (kW) gyrotron. Low wave guide transmission efficiency, plasma generation in/ on the rock sample and reflected power challenges were overcome. Real-time monitoring of the heating/ melting and vaporizing processes was demonstrated. A novel quasi-optical high power reflected power isolator was designed, built and is now in operation. A gap isolator with water loops was installed to capture scattered reflected beams. A focusing waveguide down taper was used to narrow the MMW beam diameter (now down to 2 cm) at launch with the goal of increasing the power density on the rock. The delivered peak power level to the rock face was raised to over 6 $kW/cm^2$ continuously at the 28 GHz frequency. Incident total power to the rock face was near 4.5 kW as limited by transmission losses. Radiative heat losses increased with temperature until equal to incident power, but are expected to be trapped in deep boreholes. However, even now, enough energy was being delivered to the rock specimens to reach up to 3000$^{o}$C, which is sufficient to melt granites and basalts, and partially vaporize limestone. Note that rock vaporization requires up to about 4 times the energy over just melting rocks, but that appears to be specific to the type/ mineralogy of each rock.

Over 25 rock specimens were tested on the gyrotron bench in 36 tests. A number of rock specimens were furnace melted for analysis of the native, thermally-affected and melt materials. The technical capability of using only high energy millimeter waves to melt (with some vaporization) four different types of rocks (granite, basalt, sandstone, limestone) was demonstrated using that MMW system. Most significantly, full bore drilling through solid granite and basalt using only the MMW beam was demonstrated in these bench tests, aided only by a predrilled drainhole and gravity.

MMW beam transmission losses through high temperature (260 $^{o}$C, 500$^{o}$F), high pressure (34.5 MPa, 5000 psi) nitrogen and helium gases over a 1 m path length was demonstrated to be below the error range of the test equipment and instruments utilized. To quantify those losses further to longer distances will require a higher sensitivity level of transmission tests. Impact borrowed MIT's MMW receiver and other instruments for these tests. Those tests were suspended when new gas absorption data literature was found and the current data obtained had too high an error range to be usefully extrapolated to long distances.

All rock samples that were subjected to high temperatures by the MMW beam developed fractures due to thermal stresses, even though the peak temperature achievable was limited by radiative heat

losses. Because of this fracturing drill rate, specific energies, economics and rock strengths were not able to be fully determined. New methods to encapsulate the rock specimens must be developed and higher power intensities are needed to overcome this limitation. The power intensity was limited by the gyrotron power and frequency, which was too low to focus smaller (diffraction limit). We demonstrated that rock properties are affected (weakening then strengthened) by exposure to high temperatures- via MMW beams or even just hot gases. Since only MMW beams can economically reach temperatures of over 1650$^{o}$C, or exceeding 3000$^{o}$C, that are capable to cause low viscosity rock melts and vaporization, all future encapsulated rock test specimens must provide sufficiently large enough sizes of thermally impacted material to provide for the necessary rock testing and analysis.

Systems, tools and methods to use MMW for drilling and lining in the field were identified. It was concluded that forcing a managed over-pressure drilling operation would overcome water influx and handling of hot rock particulates problems in the drilling process, while simultaneously forming the conditions necessary to create a strong, sealing rock melt liner. Materials for tools that can contact hot rock and melt surfaces were identified for further study. Straightness/ alignment can be a great benefit or a problem, especially if MMW is transmitted through an existing, conventionally drilled bore. Understanding borehole dynamics near the cutting edge was found important to understanding and optimizing the ultimate MMW drilling system design. Mineralogy was found to be a key factor in the thermal behavior of rocks under intense MMW exposure and may be critically important in the drilling and lining processes. Specifically, additives may be needed to line limestone intervals, since most of the drilling process appears to be by vaporization.

This project successfully demonstrated:

1) Full borehole guided energy propagation;
2) Reflected power (focused and scattered) isolation;
3) Collinear gas insertion and flow;
4) Collinear real time diagnostics (multiplexed signals);
5) Full bore melting and displacement (rock melt flow) in granite, basalt, sandstone and limestone samples;
6) Vaporization of limestone and possible partial vaporization of basalt, even at this low power level;
7) Full-bore Direct Energy ‘drilling’ using only MMW beams was demonstrated through basalt and granite rock slabs. Note that a small predrilled hole was used to simulate natural or created flow paths in the surrounding rocks in the expected drilling methods;
8) MMW transmission losses in high pressure nitrogen were found low, but the results were not definitive nor quantitative;
9) Initial thermal weakening of rocks started at 600$^{o}$C, but returned to near virgin rock strengths by 1650$^{o}$C, with no rock strength data above that temperature, yet;
10) New understandings of the rock melting and vaporization process under intense MMW beams were found for the drilling and lining processes; and.
11) Additives will be needed for drilling some zones- possibly limestones (due to high vaporization and low melt volumes) and water filled, highly fractured/ vugular zones (due to cooling). Those additives can then also form the wellbore lining across those zones.

# BACKGROUND

Current mechanical drilling technology is over a century old and is quite mature. Thus improvements in this drilling method will only be incremental. Abundant literature exists on the capabilities and problems of the overall mechanical drilling technology, as is given in the comprehensive review edited by Mitchell [29]. Basically, mechanical rate of penetration (ROP) is affected by formation strength and type, bit size and type, mud type (density, solid content, rheology), depth, temperature, pore pressure, bit weight, rotary speed and bit performance (tool wear, bit hydraulics) [30][70]. It is important to note that significant time (15 %) is lost to tripping, fishing, casing/cementing, repairs, logging and other non-drilling tasks [70]. A limited amount of deep, hot and hard rock EGS drilling experience for wellbores diameters of 12" or greater has been reported in the literature-

**Table 1**

| Location | Average ROP while Rotating- m/hr ( ft/ hr) | Overall ROP-m/ hr and (ft/ hr) |
|---|---|---|
| Fenton Hill, New Mexico [37] | 3.2 (10.5) | 0.49 - 0.39 (1.6 - 1.28) |
| Roesmanowes, England [37] | 4.0 - 6.3 (13.1-20.7) | 1.2-1.8 (3.9 - 5.9) |
| Animas Valley, New Mexico [38] | | 1.3 (4.2) |
| Cooper Basin, Australia [39] | | 1.2 (3.9) |

From the above discussion one can conclude that deep, hot and hard abrasive rock ROPs are drilled on the order of 0.4 to 1.3 m/ hr (1.3 to 3.9 ft/ hr). This is depressingly slow and expensive drilling. A new approach to drilling systems is necessary to overcome the limitations of mechanical drilling technologies at deep, hot hard rock geothermal conditions.

Mechanical drilling technologies encompass providing a downward force on a cutting tool (wear point) that is rotated (required delivered torque to tool) to gouge or scrape the rock surface face. The problems with this approach are the wear, shorted life and low efficiency when cutting very hard rocks (granites, basalts, etc…), as seen at great depths. Also transmitting that rotating torque to those great depths requires specialized pipe.

**Advanced and Direct Energy Drilling**

Therefore, new approaches are needed to make future major advances in increasing access to and reducing costs for underground energy resources. A number of novel techniques were proposed and reviewed by Maurer [1, 2] and Pierce [3, 40]. A liquid fueled, spinning, multi-flame jet system to spall and melt rock was patented by Potter and Tester [41]. Potter Drilling Technology with $4MM in Google funding and significant current DOE funding tested a supercritical water, chemical flame spallation method. Foro Energy, with significant private and DOE funding, is developing a laser assisted-mechanical drilling system using fiber optics to deliver a low power IR beam to weaken the rock and aid the drilling process. With DOE funding and private funding, Impact Technologies LLC developed a supercritical gas abrasive system, FLASH ASJ$^{TM}$, for fast drilling of hard rocks, but deep drilling proved elusive for that system.

Other research related to boring and tunneling are applicable to this investigation. Starting in the 1960s an electric extruder bit was tested at Los Alamos Scientific Laboratory (LASL), now Los Alamos NL (LANL) [71][95]. That study starting in 1972 was converted into the Subterrene Rock-Melting project under the US- Energy Research and Development Administration (ERDA, now DOE) with Atomic Energy Commission and National Science Foundation funding. That project investigated rock melting methods using an electrically heated carbide head for research directed toward horizontal tunneling, utility emplacement and drilling geothermal wells in hard rocks. They reported that 3 processes are needed: rock fracturing, debris removal, and wall stabilization. They reported that the element that makes innovative solutions possible is the liquid rock melt. The melt can be formed into a glass lining to seal and support the walls of the borehole. The rock melt also binds loose soil materials effectively into a stabilized liner [71][95].

Branscome [86] reported on several prior 'close contact' drilling systems in 2006, primarily related to military applications. Close contact in this case encompasses electric and nuclear decay heated drill heads. That thesis developed equations for drill rates as a function of contact temperature. It also had significant high temperature rock property information from many sources.

Direct Energy (DE) Drilling has been a dream since the invention of the laser in the 1960s, but over the 5 decades of research, there are still no applications at this time. The main advantages of using directed energy (DE) for drilling are: 1) no mechanical systems in the wellbore that could wear out or break, 2) no temperature limit, 3) equal ease penetrating any rock hardness, and 4) potential for replacing the need for casing/cementing by a durable vitrified liner. Laser DE drilling experiments started in the 1960s and continue to date [41][42][43] [44][45][46][47][6][7] [48][49] [50][51]. Military laser experiments (MIRCAL & COIL) in 1997-1999 showed the potential for 10-100 times faster than conventional drilling. Later research at Colorado School of Mines [4] confirmed that potential. A wealth of data has been collected with 1 to 10 μm wavelengths for lasers establishing the potential of directed energy drilling systems [4-7], but a transition to a practical system has so far proven to be elusive. The deepest rock penetration achieved to date with lasers has been only 30 cm (11.8 inches) [8]. There are fundamental physics and technological reasons for that lack of laser drilling progress. First, the rock extraction particle flow is incompatible with short wavelength energy which is scattered and absorbed before contacting the desired rock surface. Second, laser technology is deficient in energy, efficiency, and is too expensive.

Radio Waves or Electro-Magnetic (non-ionizing) radiation in the extremely high frequency (EHF) range (between microwave/MHz and infrared/ THz classifications), between 30 to 300 GigaHertz (GHz) frequencies or 1-mm to 10-mm wavelengths (λ), are called millimeter waves (MMW). They are useful in near line-of-sight applications and have efficient transmission and generation methods (greater than 50%) using gyrotrons. Current applications of MMW are- heating, communications (PAN), airport security, non-lethal weapons, radar, medicine, and astronomy.

By going to the MMW range of the electromagnetic spectrum for DE drilling, this impassable state of affairs can be changed. Longer wavelengths can propagate more efficiently (over 1000X laser wavelengths) through small particulate filled propagation paths. High power MMW sources are more energetic, efficient, and lower cost by a very large margin. For example, a million dollar class MMW source in Japan has produced more directed energy in eight minutes of operation at

megawatt power levels and 52% efficiency [9] than possible by any laser system in existence including the largest laser in the world, the billion dollar class National Ignition Facility (NIF).

In review, the potential benefits of using MMW for DE drilling include:

1) Commercially available efficient, megawatt gyrotron sources;
2) Simple, direct and efficient conversion of MMW energy into heating to melt and vaporize targeted rocks and metals;
3) Simple system w/no rotation, no weight on bit, no mechanical components to wear out;
4) High drill or penetration rates (via rock ablation / vaporization) with depth is expected to be constant;
5) Drill cost with depth is expected to increase linearly and not exponentially;
6) Rock hardness and temperature not limiting parameters, in fact hot temperatures will aid the rock degradation process;
7) Potential for vitrified (rock melt glass) liner while drilling, all in one process;
8) Flexible system with various MMW modes of delivery to the target;
9) Compatible with dirty environment and small particle plumes, due to Rayleigh scattering (note that 1 mm (MMW) has 1012X less scattering loss than 1 m (IR) wavelengths);
10) Absorption of the beam onto rock melt is more efficient in the MMW frequencies over IR;
11) Remote real-time diagnostic (radiometry, radar, spectroscopy) and monitoring technology available with MMW;
12) Efficient long distance, megawatt transmission technology;
13) Wavelengths and borehole sizes ideally suited for efficient beam delivery;
14) Inherent straight borehole to depth (may be difficult to re-enter existing conventionally drilled bores);
15) Inherent wellbore diameter control, but not necessarily resulting in a smooth bore;
16) fully scalable bore diameters from microholes (less than 4") to large bore drilling;
17) increased safety for personnel and environmental protection since the well is sealed as it is drilled; and
18) Potential monobore well construction to great depths.

That is the lure of using MMW for direct energy drilling, making the drilling process a simple and direct relationship between energy and matter.

**Project Objectives**

The overall objective of this project was to test a 10X breakthrough in rock penetration rates with 2X reductions in well costs by utilizing intense millimeter-wave (MMW) power. The original GETEM model indicated a 38% $/kwh cost reduction provided by this technology through faster drilling, no downhole tools to wear out, less tripping, monobore capabilities, insitu casing formation, and increased reservoir contact. A higher temperature rock penetration approach using newly available intense millimeter-wave (MMW) electromagnetic beams is proposed. It was fully differentiated from earlier direct energy drilling methods (primarily lasers) in that MMW beams are efficiently generated, can maintain coherence during transmission to depth, provide a very efficient contact with the ablating rock surface, and provide an efficient removal process of the melted or vaporized rock from the cutting surface and wellbore. Research on radiation interaction with rocks

and changes in rock properties were also to be studied for drilling optimization and liner vitrification. The specific objectives of this project were to verify theoretical calculations, understand and optimize the MMW drilling process, design and test key components leading to test the capabilities a full MMW system.

Theoretical considerations of millimeter wave (MMW) technology for rock melting and vaporization were earlier made using short, low power (5kW) bursts experiments on a few granitic rock specimens at a MIT laboratory bench (see Figure 5 below) for a current Technology Readiness Level (TRL) 2. At the end of this project the overall MMW technology is now at TRL4 for drilling, having made the key verifications of the theoretical calculations at higher power levels, but non-optimal frequencies, and for longer durations. Some components and processes are now up to a TRL7 level.

MMW has the potential to form a corrosion resistant, hardened, sealing wellbore liner while drilling for improved environmental safety, reducing the need for casing and cementing, as well as providing monobore capabilities for reducing (upper interval) bore, casing sizes and costs. Other stimulation benefits are also possible. Lowering these upfront costs by an estimated 38% will reduce EGS project risks and improve EGS economics. It may also improve EGS reservoir performance so that additional rock volumes are accessed and thus fewer wells are needed.

**Millimeter Wave Technology**

Intense millimeter-wave sources are more energetic, efficient, and at wavelengths (30 to 300 GHz) that are better suited to borehole penetration than lasers. This technology has recently been made available as part of an international research effort to develop fusion energy [52] [53] with much DOE support. These gyrotron sources are refered to as electron cyclotron masers [54]. Gyrotron tubes with continuous output power levels of 1 MW have been developed at 110 and 170 GHz with power conversion efficiencies of 52% [55]. Many gyrotrons are currently in use around the world in fusion research laboratories[56]: General Atomics with a 5 MW, 6-tube 110 GHz gyrotron system [57]; a 24 MW 170 GHz planned for International Thermonuclear Experiment Reactor (ITER) [58]; and the US Army has a mobile 100 kW, 95 GHz gyrotrons on a Humvee, therefore reliable for remote drilling.

The development stages envisioned are given in the Figure 1 below [102]. In that figure the range of available high energy beam generation systems are shown by power and frequency. The current project DE-EE005504 gyrotron is shown as a red dot. The next development level of testing will be in DOE contract DE-SC0012308 for nuclear waste storage shown as a blue dot in using the optimal 95 GHz frequency, but at a lower than optimal 100kW power level, where the anticipated required for commercial development is 95 GHz and 1-2 MW, shown as a yellow dot. The MMW frequency range, below infrared, is shown in green along the bottom axis.

The scientific basis, technical feasibility, and economic potential of directed energy millimeter wave (MMW) rock drilling at frequencies of 30 to 300 GHz (or 1000 times longer wavelengths than infrared lasers) are stong. It avoids Rayleigh scattering and can couple/transfer energy to a rock surface $10^{12}$X more efficiently than laser sources in the presence of a small particle extraction plume. Continuous megawatt power millimeter-waves can also be efficiently (>90%) guided to

great distances (>10 km) using a variety of modes and waveguide (pipes) systems, including the potential of using smooth bore coiled and jointed/ joined tubing.

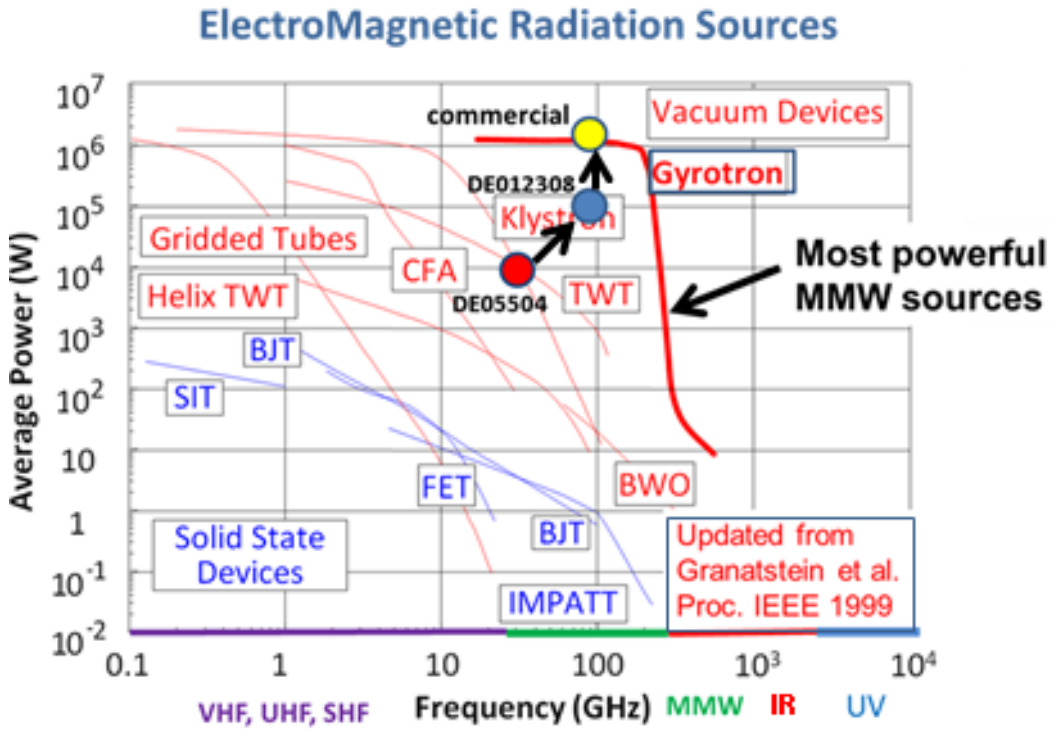


**Figure 1**. Planned Development Stages of MMW for Drilling and Lining [102]

**Theoretical Considerations**

Thermodynamic calculations suggest a penetration rate of 70 meters / hour (230 feet / hour) is possible in 5 cm (1.97 inches) bores with a 1 MW gyrotron that couples to the rock with 100% effeciency. Use of lower or higher powered sources (e.g. 100 kW to 2 MW) would allow changes in bore size and/or penetration rate. The total energy, H, required to melt then vaporize rocks was expressed by Maurer [1] in Equation 1. It is the sum of energies required to heat the rock to the melting point, then the required latent heat of fusion to melt the rock, then to heat the molten state to the vaporization point, and then the latent heat of vaporization into a vapor phase.

$$H = c_s\left(T_m - T_i\right) + H_f + c_m\left(T_v - T_m\right) + H_v \qquad \text{(Equation 1)}$$

where $c_s$ = mean heat capacity of solid rock, J/g/°C
$c_m$ = mean heat capacity of molten rock, J/g/°C
$T_i$ = initial temperature of rock, °C
$T_m$ = melting temperature of rock, °C
$T_v$ = vaporization temperature of rock, °C
$H_f$ = latent heat of fusion, J/g
$H_v$ = latent heat of vaporization, J/g

Tables 2 and 3 give the theoretical specific energies necessary to melt/fuse and vaporize rocks. As can be seen, its takes 4 to 5 times more energy to vaporize rocks than to melt them, but nano-sized particles result in easier hole cleaning [17][18][19]. Remarkably the specific energies derived by this analysis are in approximate agreement with the lower end measurements obtained with laser systems.

**Table 2.** Estimated Energy to Melt Rocks

| Rock | Specific Gravity | Mean Heat Capacity of solid[b] | Melting Temperature | Latent Heat of Fusion[c] | Total Heat of Fusion from 20 °C |
|---|---|---|---|---|---|
| | ($g/cm^3$) | (J/g/K) | ( °C) | (J/g) | ($kJ/cm^3$) |
| Granite | 2.7 | 1.05 | 1215 -1260[a] | 335 | 4.3 - 4.4 |
| Basalt | 2.8 | 1.05 | 984 -1260[a] | 419 | 4.0 - 4.8 |
| Sandstone | 2.2 | 1.04 | 1650[c] | 335 | 4.5 |
| Limestone* | 2.6 | 1.04 | 2600[c] | 498 | 11.0 |

* $CaCO_3$ decomposes to CaO at 895 °C, requiring 1.78 kJ/g.
[a] E. S. Larsen, "Temperatures of Magmas", *American Mineralogist*, Vol. 14, pp. 81-94, 1929,
[b]H. K. Hellwege, ed., Landolt-Börnstein Numerical Data …, Vol. 1, subvol. a, section 4.1, 1982,
[c]Maurer [2]

**Table 3.** Estimated Energy to Vaporize Rocks

| Rock | Molar Weight | Mean Heat Capacity of Melt[a] | Vaporization Temperature 1 - 3 Atm.[b] | Latent Heat of Vaporization[c] | Total Heat of Vaporization[d] |
|---|---|---|---|---|---|
| | (g) | (J/g/K) | ( °C) | (kJ/g) | ($kJ/cm^3$) |
| Granite | 69 | 1.57 | 2960 – 3230 | 4.8 – 5.3 | 25.7 – 28.4 |
| Basalt | 70 | 1.65 | 2960 – 3230 | 3.9 – 4.2 | 24.7 – 27.5 |
| Sandstone | 62 | 1.51 | 2800 – 3010 | 4.3 – 4.5 | 18.7 – 19.9 |
| Limestone | 51 | 1.61 | 3360 – 3620 | 6.0 – 6.5 | 30.9 – 33.4 |

[a] A. Navrotsky, "Thermodynamic Properties of Minerals", *Mineral Physics and Crystallography*, pp. 18-27, 1995, [b]V.A. Bornshten [24], [c]Trouton's Rule [25], [d]includes results of Table 7.

Having knowledge of the specific energy (S.E.) of vaporization from Table 3, it is a simple matter to determine the rate of complete rock vaporization for a given absorbed power density (P.D.):

$$ROP\left[cm/s\right] = \frac{P.D.\left[kW/cm^2\right]}{S.E.\left[kJ/cm^3\right]} \qquad \text{(Equation 2)}$$

Equation 2 is plotted in Figure 2 for three different rock specific energies 10, 20, and 40 kJ/cm. For a specific energy of 26 kJ/cm, representative of granite and basalt, and an absorbed power density range of 1 to 50 $kW/cm^2$, the MMW directed energy penetration rates would vary from about 1.4 to 70 m/hr with 100% absorption efficiency. Power densities greater than 50 $kW/cm^2$ are not recommended at atmospheric pressure to avoid plasma breakdown, where the energy will no longer be directed, but omni-directional reducing the forward penetration rate. Experiments at one atmosphere with short pulse gyrotron beams show air breakdown at minimum power densities over

1 MW/cm$^2$ [26]. Though this breakdown threshold would decease with continuous operation, it would also increase with fast gas flows and higher pressures that would be found in deep wells. Therefore plasma breakdown is not anticipated to be a problem in actual deep drilling applications.

The relation between power density and wellbore diameter (D) for a given total gyrotron power (P) is given by Equation 3 and plotted in Figure 3 above.

$$D = 2\sqrt{\frac{P}{\pi(P.D.)}} \qquad \text{(Equation 3)}$$

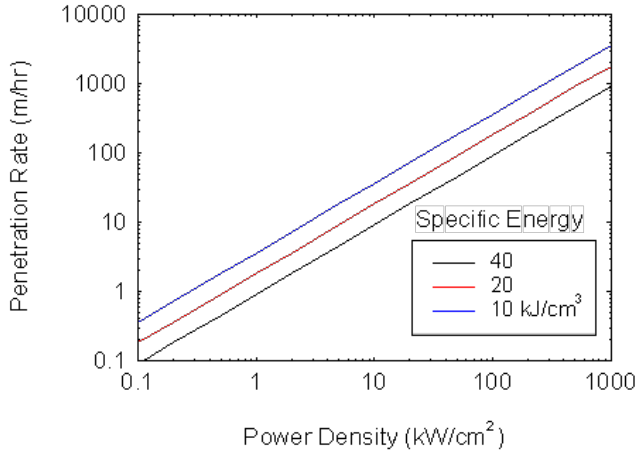


**Figure 2.** Relation between power density and rate of penetration for rock vaporization.

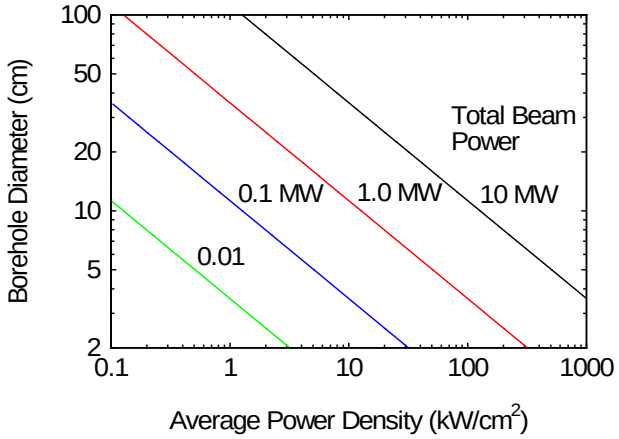


**Figure 3.** Wellbore diameter vs. power density

Figure 4 shows the relationship of Power, wellbore diameter and rate of penetration (ROP). From this relationship, a 5 cm (1.97 in) diameter wellbore could be penetrated via vaporization only at 50 m/hr (150 ft/ hr) with 1 MW of power. If we consider the Air Force's 2 MW gyrotron, we could penetrate (with full vaporization) a 15 cm (6") diameter wellbore at about 10 m/hr (30 ft/ hr) or a

30 cm (12”) bore at 7 m/hr (21 ft/ hr) independent of rock hardness. That same rate could be obtained via only melting using a reduced estimated 700 kW of power. Further, for EGS sizes, a 15” bore could be drilled (with full vaporization) at 80 m/hr (262 ft/hr) with a 10MW gyrotron, or only 2.5 MW if only melted. These ROP estimates would be reduced by the actual MMW absorption efficiency, which is currently estimated at 70%. As noted, they could be increased by not requiring 100% vaporization of all rocks encountered- resulting in utilizing only ¼ to 1/3 of the vaporization energy listed.

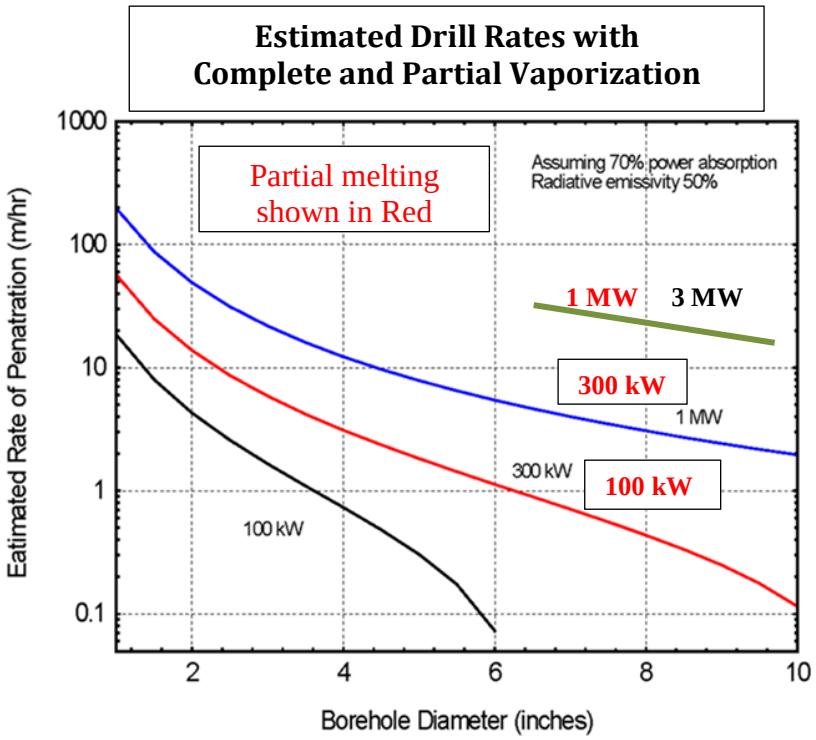


**Figure 4.** Drill Rate versus Borehole Diameter for Different MMW Power Levels

At the simplest level, a millimeter-wave (MMW) deep drilling system requires only one component in the well bore, the waveguide (i.e., drill pipe), which has only vertical motion of advancement into the hole as it is deepened. There are no other parts or mechanical movements in the borehole in this simplest method. The gyrotron energy output and compressed gas are injected at the surface. All the drilling, extraction, and vitrified liner formation will be done by the directional energy and concurrent purge gas flow. Figure 5 shows an elevation cross-section view of the bottom of a borehole with a cylindrical metallic waveguide as a conduit for the beam energy and purge gas flow. The metallic MMW waveguide is of smaller diameter than the borehole, which leaves an annular space for return exhaust. A larger concentric outer pipe may be desired, in some cases, for water/mud injection for additional cooling and wellbore pressure control. The reaming of the borehole to a diameter larger than the central waveguide is facilitated by the natural divergence of a MMW beam launched from a waveguide (drill pipe) [14]. The borehole itself (below the pipe waveguide) acts as a dielectric waveguide (like a long wavelength fiber optic) to

continue the propagation of the energy to the ablation surface, allowing for a large (>100 m) standoff distance, Z, between the central waveguide and vaporization front.

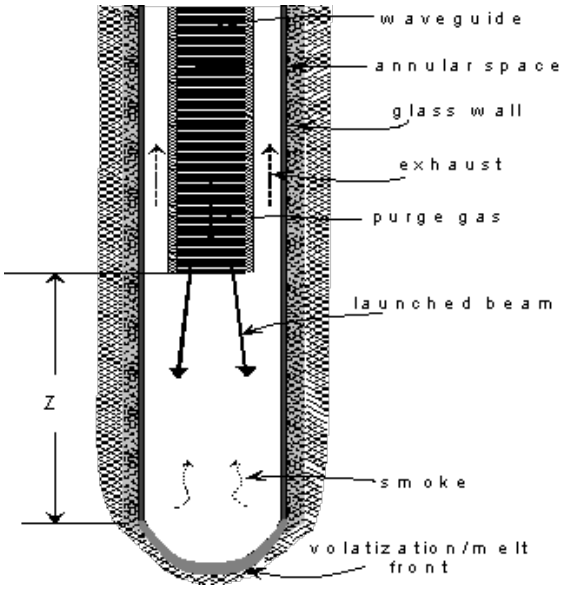


**Figure 5.** Simplest cross section of MMW Drilling System- Method #1

A fully surface-absorbed 1 MW beam with an average surface power density of 50 kW/cm$^2$ in a 5 cm (1.97 in) diameter borehole can raise the rock surface temperature to about 2900 °C (vaporization temperature of granite at 1 atmosphere) in about 1 ms [62]. Complete vaporization may not be necessary for extraction since the viscosity of the glass melt would be sufficiently low at 3000 °C (< 2 Poise) [21] to allow the wellbore pressure to drive part of the melt into the natural [22] or thermally induced micro-fractures in subsurface rocks. The formation of glass borehole liners by rock melting penetration has already been documented by research at Los Alamos [23]. Glass materials have the potential to be stronger materials and better sealing material than many rocks or high strength concrete [64, 65] and as a liner it would serve as a robust conduit for high temperature corrosive geothermal fluids.

Another potential benefit not previously mentioned is that the high pressures generated by vaporized *in-situ* water at temperatures ~ 3000 °C in a confined (or at least restricted) volume could reach 103 MPa (1000 atmospheres or 15,000 psi). This fracing potential demonstrates that there are other reservoir development activities possible with MMW.

**Levelized Cost of Electricity (LCOE) Estimate**

Penetration rates were discussed in earlier sections. Capital cost estimations for a deep 23,000+ft MMW drilling rig are based on the US Air Force 2 MW 95 GHz gyrotron system currently under development, total weight of 1900 lbs, that costs $2.1 million (MM$USD) [59][60]. Note- a 1MW gyrotron system cost is listed by one manufacturer at $1.1MM. Downhole piping/waveguides may cost $2.3MM (at $100/ft); specialized small rig structure, injector head, tools and controls may cost $8MM; and generator, compressor and pump systems may add $7.5MM. Total capital costs for

this first deep rig are thus estimated at $20MM, which amoritizes to $100K per well or $4.3/ft when amoritized over two hundred (200) wells that each reach 7 km (23,000 ft).

Operational expenses are estimated from- Electricial costs involved in drilling each well with an 8" bore, at 50% electrical efficiency, and 70% absorption would correspond to $4.5x10^6$ kW hrs or a total electricity cost of $450,000 (at a cost of $0.10 / kW-hr) or $64/m ($20/ft) drilled per the same amortization. Thus total drilling only costs (normally 1/3 of total well costs, but with lower interval casing/cementing now not needed and testing not included) would be estimated at about $72/m ($24/ ft) drilled. A 2X increase for profit, losses, repairs, downtime, etc.. would raise it to $144/m ($48/ft) drilled. For comparison, Impact estimated drilling (rig, drillpipe, bits, fluids) cost of a 21,000 ft EGS wellbore ending in a 7-7/8" bore in the GEECO study [70] at $286/ ft (for drilling only or 33% of $21M total well cost). In addition, such a MMW wellbore may already be suitably lined/ 'cased', forgoing the need of lower zone steel casing and cementing costs. Its monobore capabilites allows for a reduction in the upper casing sizes and bored holes.

It should be cautioned that we are assuming an idealized case with rock removed by vaporization only and that there are no power losses. The proposed research is needed to help determine how realistic these estimates are-

**Table 4.** Metrics Table

| Metric | Source | Conventional Costs | MMW Costs | Cost Factor for GETEM | Resultant GETEM Base = $9.255/kWh |
|---|---|---|---|---|---|
| Rate of Penetration, No Bit Wear, No Tripping, Topic Area 1 | GEECO report [70], MIT theoretical estimate on MMW 10X drill rate | $286/ft drill only rate representing 33% of the total well cost | $28.6/ft on 33% of total well costs | 0.73 on Expl, Confirm, Prod & Inj Well Costs | 8.446 (-8.7%) |
| Lining Well while Drilling Topic Area 2 | GEECO report [70] on 21kft well costs. Standard steel casing- higher for stainless (24X) or titanium (100X). | 20% of total well costs (below 10K to TD) | No cost since done while MMW drilling | 0.8 on Expl, Confirm, Prod & Inj Well Costs for standard steel | 8.656 (-6.5%) |
| Monobore Well Designs Topic Area 1 | Estimate only from GEECO report[70] ratio area 2 bore sizes from 20" > 10-5/8" | Intervals above 10Kft representing 50% of total well costs | Ratio for 72% off of 50% of well cost | 0.64 on Expl, Confirm, Prod & Inj Well Costs | 8.177 (-11.7%) |
| Increased Volume of Rock Contacted | 5X rock contacted by multiple small directed bores with connected fractures | 1.0 standard hydrofracing | Same cost, 5X times contacted rock volume | 0.20 factor on the thermal drawdown rate | 8.250 (-10.9%) |
| **Overall** | All | All | All | 0.373 on well costs plus 0.2 therm decline | 6.576 (-28.9%) |

# EXPERIMENT AND DESIGN ACTIVITIES

## Task 0 - Project Management and Reporting

The purpose of this task was to provide project management, DOE reporting and Peer Review technical papers. This task was successfully performed. The approach was to provide reports and other deliverables in accordance with the provided Federal Assistance Reporting Checklist. Additional deliverables included the 2012 and 2013 DOE Peer Review Meeting presentations. Developed test data will be entered into the National Geothermal Data System (NGDS). Multiple conference call and physical meetings between Impact and MIT were held before and during the project to discuss, outline and guide the project's research direction.

## Task 1.0 – MMW Bench Testing

The purpose of this task was to determine the key factors/ variables for MMW melting and ablation/ vaporization effectiveness on various rock samples for drilling and lining the borehole. This task was successfully performed as the methodology to drill was developed with this system and key data was obtained. The approach utilized was to upgrade an existing and available low 10 kilowatt (kW) power, non-optimal 28 Gigahertz (GHz) frequency CPI HeatWave Model VIA-301 gyrotron system at MIT. Then MMW bench testing of various rocks at intense MMW irradiation intensities for melting and ablation measurements were performed with that system. Measurements of all key factors would be made to optimize the system operation. It was determined early in the project that a higher frequency beam, closer to the 95 giga-Hertz level, was more optimal (for transmission and coupling to the rock) than the existing, but available, gyrotron unit. All this work was successfully done.

More time than expected was required to design and build the waveguide delivery system at this low frequency. Challenges overcome were low waveguide efficiency, reflective power off the samples back into the gyrotron (tripping the safety feature), plasma generation on the samples due to low pressure, launch aperature size (beam power density) and alignment issues. This project therefore required a constant feedback system of design-build-install-test-redesign commponent-build-test. Specifically, a new reflective (narrow frequency band) beam power isolator (Note- A technical paper on this feature was presented by Dr. Woskov at the IEEE June 2013 conference); a gap isolator was designed, built and installed to capture scattered reflected wavelengths; and a down-taper focusing tube was added to narrow the final beam diameter aperture to 2 cm (0.787 inches) at launch toward target. A schematic of the final designed system is given in Figure 5.

From this effort a successful design was made and emperical data on four (4) various rock types (granite, basalt, sandstone, limestone were obtained (See Appendix D). Data on high tempertaure thermodynamic properties, ablation products, tool standoffs, MMW operating modes, gases, fluids (fresh and salt waters, hydrocarbons), reflectivity, frequency and power parameters were obtained. Various MMW power levels, exposure times, stand-off distances, aperture diameters and other variables have been tested. Theoretical estimations were refined based on these tests. Melting and some vaporization occurred even at this low 28 GHz frequency and 10 kW (generated, less than 50% delivered to rock face) power level. Drilled full bores through basalt and granite rock slabs using MMW power and gravity only. Rock sample fracturing was a problem in all MMW exposed

samples due to differential thermal expansion. The samples were clamped/ braced to minimize fracturing, but to no avail.

Carrying out the intense millimeter-wave (MMW) directed energy rock exposure experiments required development of a specialized MMW transmission line system to protect the gyrotron from reflected power and to introduce gas flow and monitoring diagnostics beams collinear with the heating beam [73]. These transmission line features will also be needed in a practical gyrotron drilling system in the field. As part of the work on this project such technology was successfully developed and demonstrated on a small laboratory scale. The transmission line system went through a number of iterations as experience was gained with the experiments. It was found that backward protection for both spectrally and scattered reflected power was necessary, which was not present in the original transmission line configuration [74]. Figure 1 shows the final configuration in use at the end of the project period. The main technological challenges were due to working with the relatively low frequency of 28 GHz and small relative waveguide dimensions, only three wavelengths across, which effected transmission efficiency and the implementation of quasi-optical components.

The overall length of the transmission line from the gyrotron input side at the first parabolic up taper to the waveguide launcher inside the rock test chamber was about 13 feet (~4 m). It was constructed of copper and aluminum components. The output waveguide diameter from the gyrotron was 1.279 inches (32.5 mm), which was too small to make efficient waveguide bends or quasi-optical polarizers for reflected power isolation. Also, the waveguide mode at the gyrotron output was a circular $TE_{01}$ mode, which is an azimuthally polarized hollow beam that was unsuitable for isolation and for the experimental tests where a beam peaked on axis was desired. Circular waveguide up- tapers from 1.279 inches (32.5 mm) to 3.0 inches (76 mm) were designed and fabricated to make more efficient bends and to implement the polarizers in the larger diameter waveguide. However, because the conversion of the azimuthally polarized circular $TE_{01}$ mode to the linearly polarized circular $TE_{11}$ mode is more conveniently done in smaller diameter waveguide and the need to keep the beam as concentrated as possible for rock exposure tests, down tapers were also designed and used from 3.0 inches (76 mm) to 1.279 inches (32.5 mm). The many up- and down-tapers (four) and mode converters between $TE_{11}$ and $HE_{11}$ modes (up to three) used herein and the inherent inefficiencies of having a small ratio of waveguide diameter to wavelength caused extra inefficiencies. This will not be as much of a problem with higher frequency, higher power gyrotrons in the future.

The main components of the transmission line system going from the gyrotron to the rock sample can be described as follows, referring to Figure 5. First, the upwardly directed beam from the gyrotron cabinet enters a smooth walled parabolic taper [75] into a 3 inch (76 mm) diameter miter bend to make the turn into a horizontal direction followed by a down-taper back into 1.279 inch (32.5 mm) diameter waveguide. This is followed by a wiggle converter [76], which transforms the azimuthally polarized $TE_{01}$ beam into the linearly polarized $TE_{11}$ mode. Next the beam enters a $TE_{11}$ to $HE_{11}$ corrugated converter [77] followed by a corrugated up-taper to 3 inch (76 mm) diameter. The polarizers for rejecting backward spectral reflected power are configured in this 76.1 mm diameter corrugated waveguide to minimize gap losses [78]. The linear wire polarizer

is installed at a $45^0$ angle in a 4-port waveguide cross, followed by a miter bend with a grooved mirror, which circularly polarizes [79] the beam for transmission into the test chamber and linearly

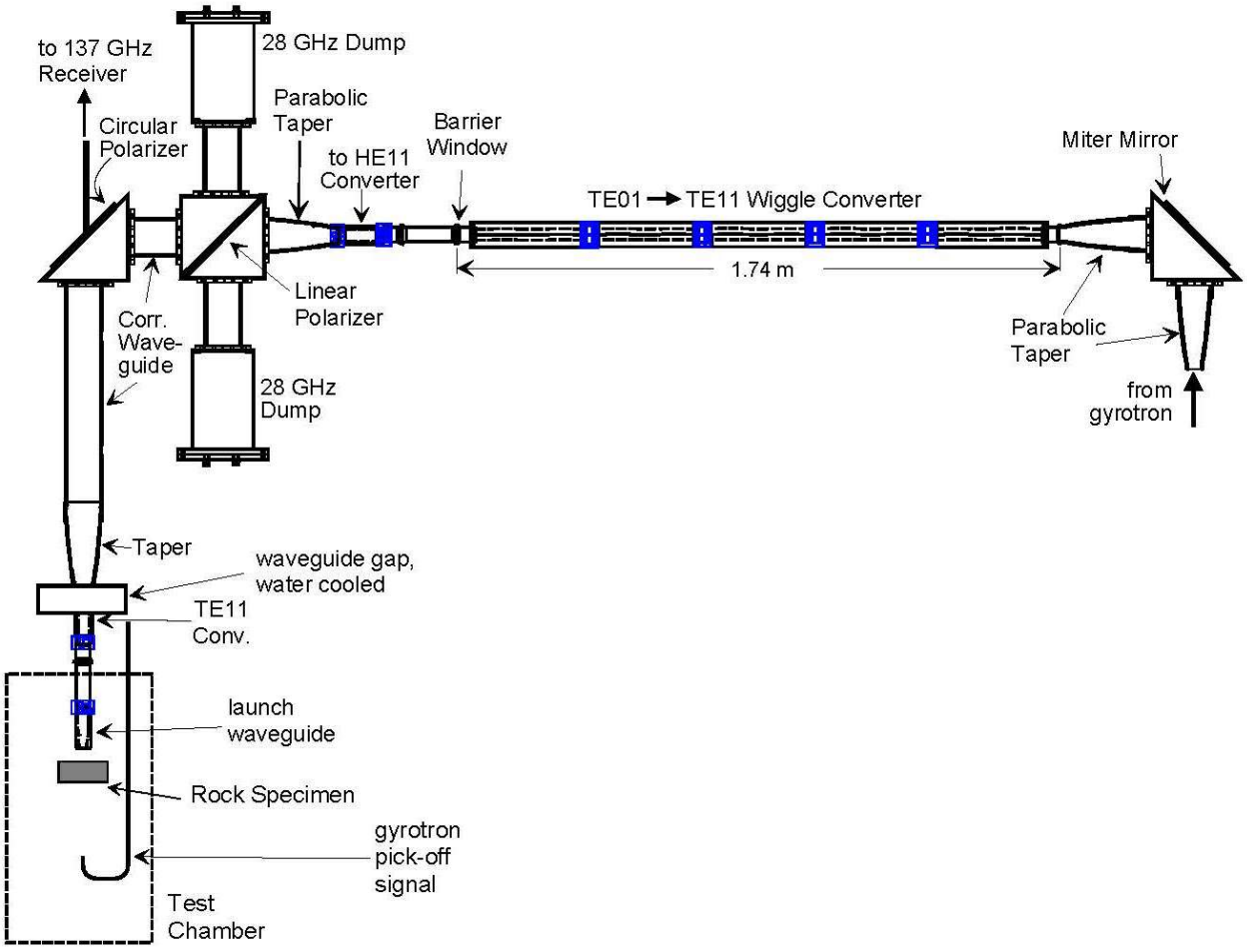


**Figure 5.** The 28 GHz transmission line system as finally implemented for the intense MMW rock exposure experimental research.

polarizes the specular back reflection into an orthogonal orientation relative to the forward power. Water loads connected to the cross ports of the 4-port linear polarizer absorb the rejected power. The waveguide below the second miter bend continues downward 24 inches (61 cm) in corrugated 3 inch diameter (76 mm) waveguide to a parabolic down-taper to 1.279 inch (32.5 mm) diameter. At this point a one waveguide diameter long gap is implemented to filter backward scatter radiation. This is flowed by a $HE_{11}$ to $TE_{11}$ converter and 1.279 inch (32.5 mm) diameter smooth walled waveguide into the test chamber. In the test chamber various waveguide launchers can be attached as needed, including a $TE_{11}$ to $HE_{11}$ mode converter or a smooth walled down-taper to $TE_{11}$ 0.787 inch (20 mm) diameter to concentrate the beam (i.e., launching a higher power density beam). Gas flow is introduced through one of the 28 GHz dumps and a 137 GHz radiometer view is implemented through a hole in the center of the miter mirror opposite the test chamber for real time monitoring of the surface sample temperature. This raw temperature is affected by waveguide

temperature as well.

### A. $TE_{01}$ to $TE_{11}$ Wiggle Converter

The $TE_{01}$ to $TE_{11}$ converter design was taken from ref. [76] having ten wiggle periods of 6.42 inch (16.3 cm) and a 4.7% peak axis deviation in 1.279 inch (32.5 mm) diameter waveguide. It was directly machined in aluminum sections with each one forming halve of two periods with the seam when assembled perpendicular to the $TE_{11}$ electric field to minimize leakage. Figure 6 shows a photo of two of the two period sections, one still split open and another assembled. The use of aluminum rather than copper, which eased machining, is estimated not to increase the losses by more than 1% from the demonstrated 96% efficiency [76].

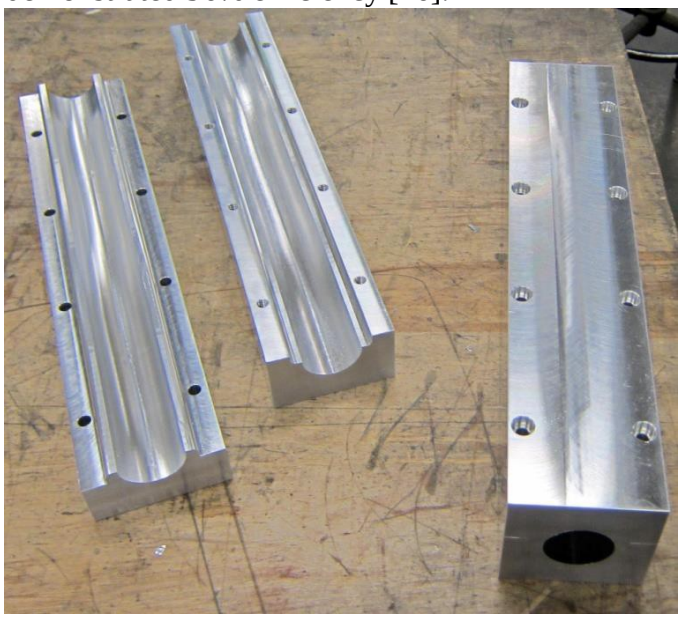

**Figure 6.** Two of the five machined two period sections of the wiggle converter.

### B. Parabolic Tapers and $TE_{11}$ to $HE_{11}$ Converters

Two 11.44 inch (29.1 cm) long smooth walled parabolic circular $TE_{01}$ tapers from 1.279 inch (32.5 mm) to 3.0 inch (76 mm) were used at the first miter bend above the gyrotron. After conversion to the linearly polarized beam, two 3.23 inch (8.2 cm) long $TE_{11}$ to $HE_{11}$ corrugated converters with a parabolic groove depth taper from ½ λ to ¼ λ [77] were used at the input and output of corrugated $HE_{11}$ parabolic tapers to convert from and back to the smooth wall $TE_{11}$ mode.

**Figure 7.** Internally corrugated $TE_{11}$ to $HE_{11}$ converter on left connected to $HE_{11}$ parabolic up taper

The parabolic tapers with ¼ λ deep grooves have an optimized minimum length [75] of 7.83 inches (19.9 cm). These components were machined in aluminum and are expected to have mode conversion losses < 1%. Figure 7 shows a photo of a corrugated converter and a parabolic taper.

### C. Copper Grill Linear Polarizer Cross

The linear polarizer was Electrical Discharge Machined (EDM) in a 1/32" (0.79 mm ) thick, 4.62 x .325 inch (117.5 x 82.6 mm) OFHC copper plate at an angle of 45**°** to the surface normal to produce a linear grill with 1/32" (0.81 mm) wide wires and a period of 0.128 " (3.25 mm) as viewed at normal incidence. With these parameters it was estimated that reflected power with the wrong polarization at 28 GHz would be attenuated by 25 dB [80]. Figure 8 shows a view of the grill and a cross-section of the resulting diamond shaped wires. This grill was orientated with the wires vertical in the diagonal of the 4-port cross. The $HE_{11}$ mode with E-field horizontal is transmitted through with no significant loss and E-field vertical component in the forward and backward reflected beams are rejected into the side ports with water load dumps. The main insertion loss is estimated as 2.8% (-0.13 dB) due to gap loss as determined by formula in reference [78] with the waveguide corrugations running up to the grill.

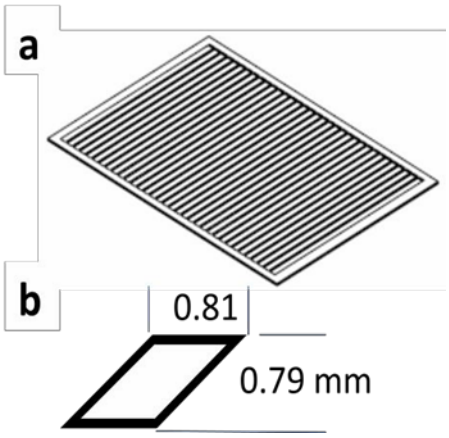


**Figure 8.** Copper grill linear polarizer made by EDM at a 45° angle relative to the surface normal; a) view of complete grill, b) cross-section of one of the wires.

Computer modeling with a heat transfer analysis code was carried out on this copper grill polarizer to determine if it could take the heat loading of the gyrotron beam due to copper resistive losses. The $HE_{11}$ mode Bessel profile was approximated with a Gaussian function having a $1/e^2$ diameter of 1 inch (25.4 mm). It was first assumed that the power loading on the grill would be due to absorption losses as given by the analytical formulas [78] using 1/3 ideal copper conductivity. This resulted in only about 0.6 W heating and a peak temperature rise of about 1 $^oC$ with a 10 kW beam. A more conservative assumption on absorption losses is to assume that the slits between the wires could be modeled as infinitely wide rectangular waveguides and use the $HE_{11}$ component $TE_{01}$ and $TM_{10}$ absorption coefficient of $2R_s/bZ_o$ where $R_s$ is the surface resistivity, $b$ the slit width, and $Z_o = 377\ \Omega$, the impedance of free space [81]. This results in about 8 Watts heating and a peak temperature rise of about 16 °C. The presence of higher order modes could increase absorption losses more, but peak temperatures would be reduced by larger beam diameters. Consequently, there was not any thermal problem with the copper grill linear polarizer and a 10 kW, 28 GHz beam, and it could be scaled to higher power levels. The copper grill was examined after extensive use in the present work and there was no sign of any thermal damage or discoloration.

### D. 137 GHz Radiometer View

A small 0.072" (1.83 mm) diameter, 1.54" (39 mm) long circular copper waveguide was inserted through the miter mirror circular polarizer above the test chamber along the central axis of the 28 GHz waveguide in the direction of the sample. This small waveguide was only inserted as far as the inside surface of the miter mirror so as not to obstruct the 28 GHz beam while giving a view to the sample. The 137 ± 2 GHz insertion loss from the miter bend to the output of the waveguide just above the sample surface was measured using a liquid nitrogen cooled black body. It was typically found to be about -12 dB. This is a large loss, but as long as it is known and remained at room temperature quantitative thermal measurements were possible. The analytic basis for using this 137 GHz radiometer for high temperature materials measurements was described previously [82].

The upper horizontal run of the transmission line is shown in Figure 8 with the radiometer attached to the left. The radiometer electronics box makes the connection to the small waveguide going through the copper miter mirror with a $90^o$ bend in small WR-06 waveguide and a transition from the rectangular to circular waveguide. Also, seen here are the large 3" (76 mm) inner diameter miter bend circular polarizer, the aluminum 4-port rectangular box containing the copper grill (shown in the insert) with the 28 GHz water dumps attached, and going off to the right the $TE_{01}$ to $TE_{11}$ wiggle converter. The many hoses seen here carry cooling water except for the small black line attached to the back of the 28 GHz dump, which brings in the forward gas purge.

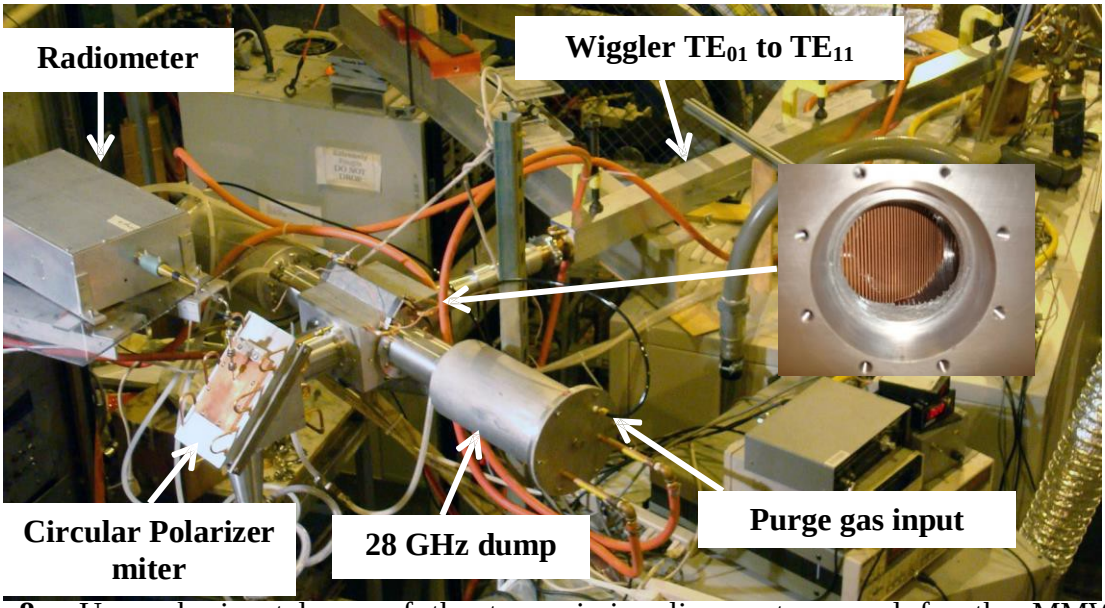


**Figure 8.** Upper horizontal run of the transmission line system used for the MMW DE experiments at 28 GHz. Insert shows the copper polarizer grill inside the 4-port rectangular block.

### E. Waveguide Gap

It was found early in the experiments with rock samples that the polarizer based reflected power isolator by its self was not sufficient in rejecting backward power. This is because this isolator works best if the reflected power is specular as from a mirror which does not distort the beam. In reality the melting surface deforms and scatters the backward power into higher order modes that are not rejected by the polarizer. To filter these higher order modes a waveguide gap was implemented. A gap introduces losses to all propagating modes, but these losses are much larger to higher order modes. In waveguide with a diameter of 1.279" (32.5 mm) at 28 GHz, the $HE_{11}$ mode suffers a transmission loss of 18% crossing a gap length equal to the waveguide diameter [78]. The slightly higher order circular $TE_{01}$ mode suffers a loss of 53% and the losses increase as the square of the Bessel function zero root for higher modes.

The waveguide gap was located below the circular polarizer miter bend after the waveguide diameter down taper to 1.279" (32.5 mm) just above the test chamber. Figure 9 shows a photo of the vertical arm of the transmission line and the location of the waveguide gap. It is enclosed by a 6" (15 cm) diameter aluminum pill box chamber with a Teflon tube water cooling loop inside the cylindrical wall to absorb the leaked 28 GHz power. Just below the waveguide gap there is a mode converter from $HE_{11}$ corrugated wall waveguide to $TE_{11}$ smooth walled waveguide with its own water cooling manifold. This converter is made necessary by the permanently brazed smooth walled copper waveguide for transmitting power into the test chamber.

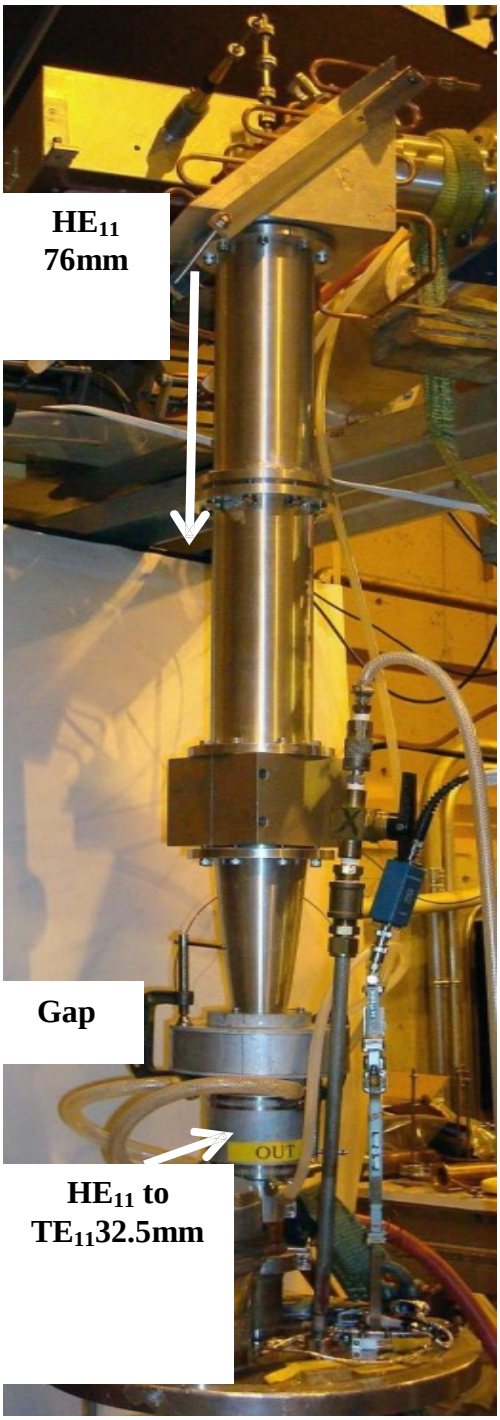


Figure 9. Vertical arm of the transmission line to the test chamber.

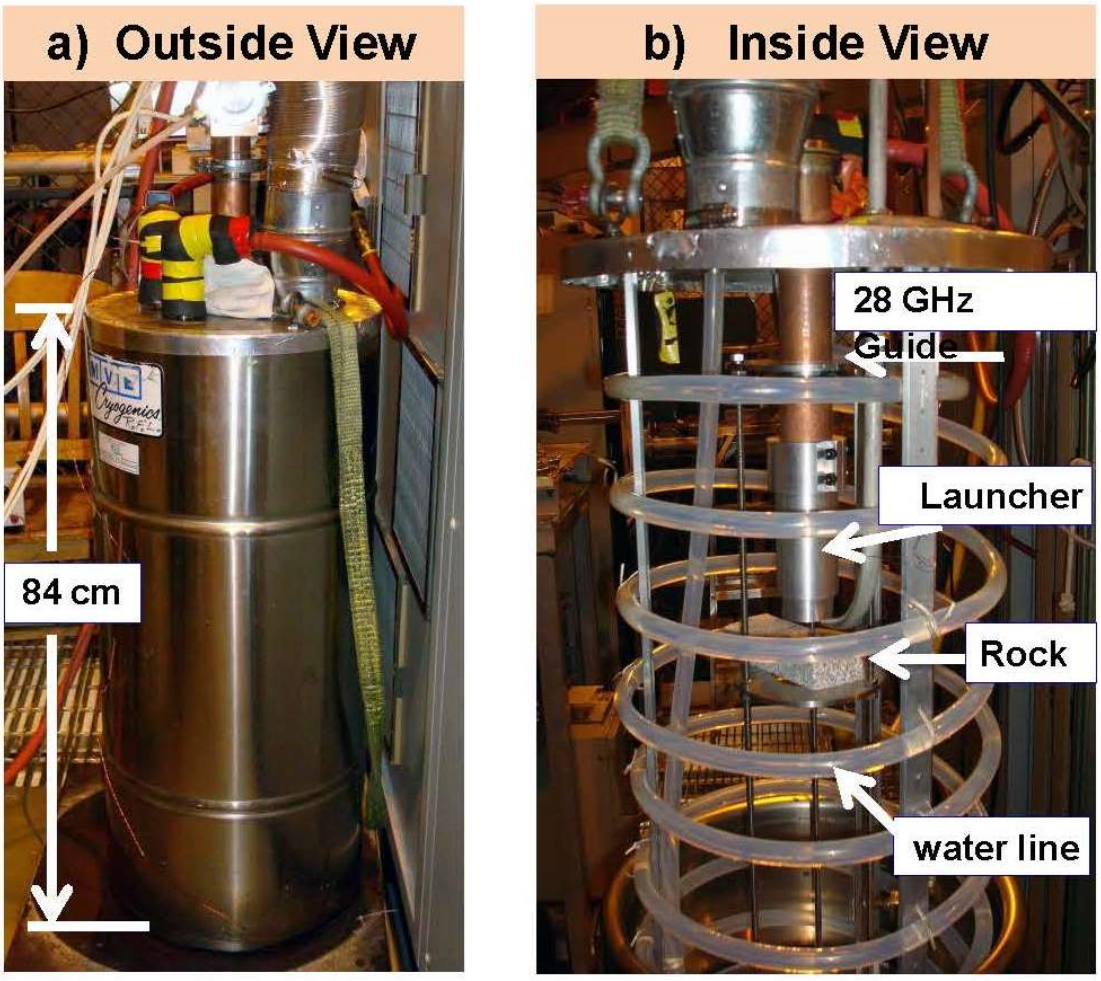


**Figure 10.** Outer and inner views of the rock Test Chamber used for the MMW exposure experiments.

### F. Test Chamber

The Test Chamber is a stainless steel Dewar with internal dimensions of 13" (33 cm) diameter and 30" (76 cm) deep. It is enclosed by a steel top to trap all 28 GHz power entering it for absorption by an internal coiled Teflon water line. The water flow and temperature rise were monitored to determine the power trapped inside the chamber. Without a test rock sample it was used to calibrate the gyrotron power. Figure 7 shows inner and outer views of the Test Chamber. Gas purge into the test chamber was exhausted through a 3" (76 mm) diameter metal mesh in the top through which 28 GHz could not pass. A flexible 4" (100 mm) diameter aluminum exhaust duct seen in Figure 10a directed the gas exhaust to a high efficiency particle filter and then through a water trap to clean any vaporization products that might be present in the exhaust.

The details of the inside construction in Figure 10b show the 28 GHz copper transmission line with an outside diameter of 1.66" (42 mm) entering through the center of the top. The gyrotron beam can be used directly as a $TE_{11}$ mode launched beam from this copper waveguide or a launcher waveguide section can be attached to convert the launched mode to something else for a given experiment. Shown in Figure 10b is an aluminum $TE_{11}$ to $HE_{11}$ converter to launch a near Gaussian profiled beam. We have also used a $TE_{11}$ down taper to 0.787" (20 mm) diameter to focus the beam. Other mode converters could be used to put more power loading on the walls for wall vitrification experiments. A converter from $HE_{11}$ to $EH_{12}$ was fabricated to increase wall loading by a factor of 10, but only used once in the present experiments due to lack of time. In a practical drilling application the launcher/ mode convert could be chosen as necessary along with beam power, frequency, and rate of penetration to control the borehole diameter and wall vitrification.

In the present experiments the rock sample was typically located ½ to 2 waveguide diameters away from the waveguide launch aperture. The actual distance was a compromised between having the sample as close as possible to maximized the power intensity on the rock before significant diffraction of the beam, but not too close to cause more back refection into the waveguide than could be handled by the reflected power isolators.

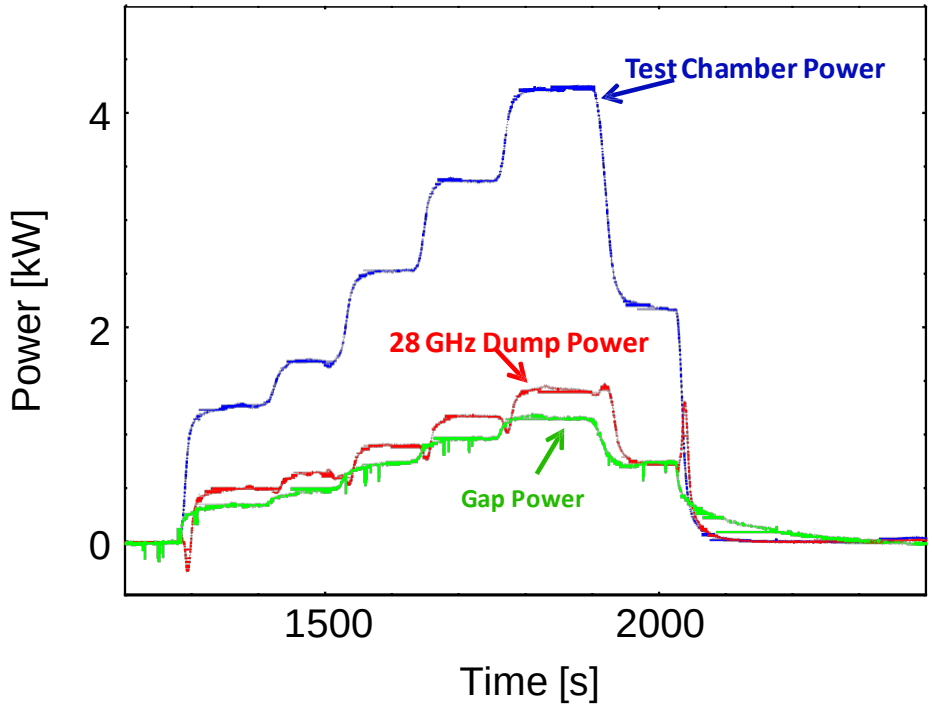


Figure 11. Measured water load powers for the final transmission line configuration without a rock sample in the Test Chamber.

## G. 28 GHz Transmission Line Calibration

In addition to the Test Chamber, the water flow and temperature rise of the cooling water to the 28 GHz water loads opposite the copper grill polarizer and to the gap were monitored. Figure 11 shows these power measurements for the final configuration of the transmission line that was taken without a rock sample in the Test Chamber as the gyrotron output power was stepped in 20% increments from 20% to 100% power. The top blue trace shows the power transmitted to the test chamber, which reaches 4.3 kW at 100% gyrotron output of 10 kW. At the same time the power lost in the 28 GHz reflected power dumps was 1.43 kW and in the waveguide gap 1.16 kW.

Other losses in the mode converters and miter bends also occurred, but they were not monitored. The power loss in the gap was expected, but the loss in the 28 GHz dumps without a reflective target indicates inefficiency in the $TE_{01}$ to $TE_{11}$ converter to produce a linearly polarized beam from the gyrotron launched circularly polarized $TE_{01}$ beam. The inefficiency of the transmission line system was one of the main limits on power for the present MMW rock exposure experiments. Such inefficiencies will not be as large with higher frequency, higher power gyrotrons, which put out a linearly polarized beam to start with and with larger waveguide to wavelength ratios that are not as prone to diffractive losses. Our laboratory gyrotron, in practice, could be operated above 100% and power levels up to 4.5 kW were used in the final experiments.

The effect on efficiency due to the complexity of the present transmission line system, with four waveguide diameter transitions between 1.279" (32.5 mm) and 3" (76 mm), up to three transitions between smooth walled and corrugated waveguide ($TE_{11}$ to $HE_{11}$ converters), and many gaps caused not only by the intentional one, but by the miter mirrors and the polarizer 4- port box is documented in the data shown in Figure 12. This figure shows the calibration of the forward power sensor signal at the gyrotron output to the power actually measured in the Test Chamber for various transmission line configurations. The top dashed plot is the power indicated on the front panel. The next plot below with circle points is the power transmitted by the circular $TE_{01}$ gyrotron output mode without mode conversion in smooth walled 1.279" (32.5 mm) diameter copper waveguide and two commercial CPI corrugated elbow waveguide bends following about the same path as the final transmission line. The 10 KW output is down only to about 8 kW in this case. The next curve down with square points is the present transmission line system without the waveguide gap above the Test Chamber. The 10 kW gyrotron output is down to 5.4 kW. The addition of the $TE_{01}$ to $TE_{11}$ mode converter, diameter changes, and polarizer grill more than doubles the losses of the simple mono-diameter transmission line. Adding the gap for scattered power isolation reduces the calibration curve to the lowest plots marked by open triangles. The increase loss due to the waveguide gap is 20% in close agreement with the theoretical loss of 18% [78]. Data was taken at two different times four months apart for these lowest plots after many experiments, disconnections and reconnections of some of the waveguide components with no change in performance.

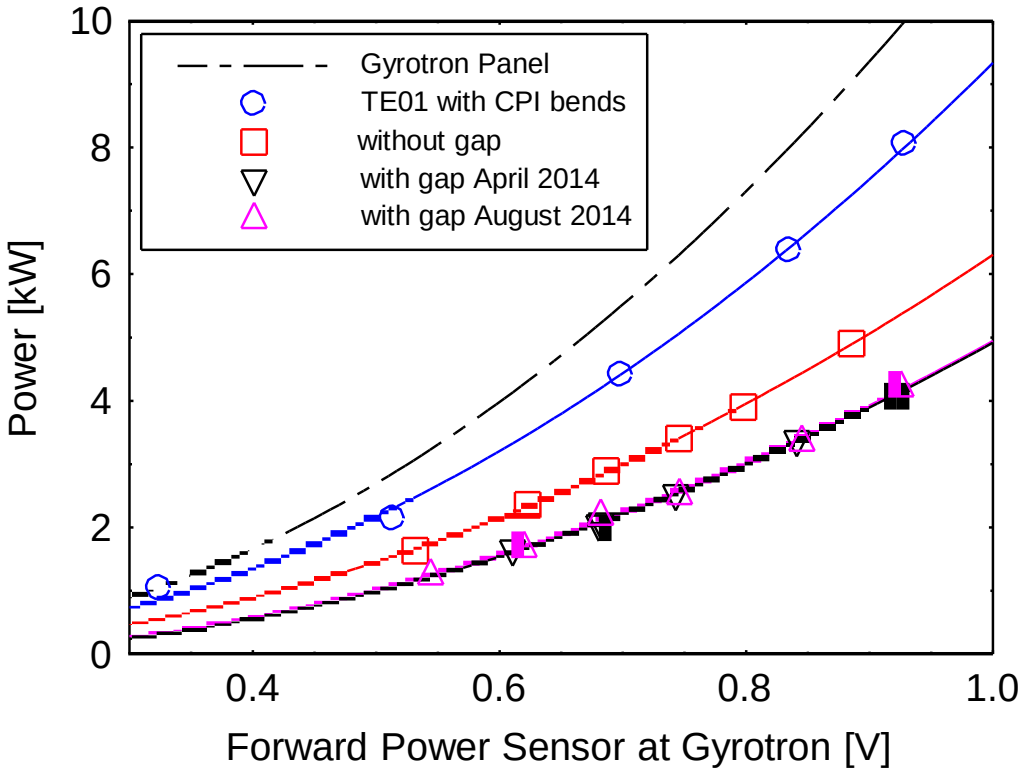


Figure 12. Calibration of the forward power detector signal at the gyrotron output to the power transmitted to the Test Chamber for various transmission line configurations.

### H. Discussion

The transmission line system developed here demonstrates most of the features needed to interface a high power gyrotron to a rock formation for full bore directed energy opening of a wellbore. These features include: reflected power isolation, forward gas purge, and beam collinear diagnostics that have not previously been a requirement in applications of gyrotrons to fusion energy research. In addition, we have used beam profile control through a specialized waveguide launcher. These features have been demonstrated together in a single gyrotron transmission system for the first time. It has made possible studies of rock melting and vaporization in this work showing that hard crystalline rocks can be penetrated full bore by millimeter-waves. Though the development accomplished here is on a small laboratory scale, the approach is compatible with being applied to much higher beam power. Most of the difficulty with inefficiency in the present experiments was due to not having a linearly polarized beam from the gyrotron source and to a frequency that is too low, causing significant diffractive losses in the quasi- optical components. Higher frequency, high power gyrotron sources with linearly polarized outputs will be more efficiently interfaced to directed energy drilling applications in the future.

## Task 2.0– Evaluation of Rock Specimens

The purpose of this task was to further the understanding of MMW generated rock melt and the rock melt glass liner and 'thermally affected' rock processes. This includes chemical reactions, if any, and methods to improve liner formation. The approach used was to test the rock specimens exposed to high power millimeter waves using MIT's uniaxial compression tests with simultaneous observation of the crack initiation, propagation and coalescence process leading to failure. A high temperature oven was used to supplement the MMW vitrified rock samples, but to a lower temperature (1650 versus 3000$^{o}$C). A high-speed video-camera allows seeing the detailed cracking process from initiation over propagation to coalescence. Size of the sample was also a problem, as many of the desired impacted areas were too small to test.

The unconfined density of selected Bedford MA granite samples that were exposed to furnace melting temperatures were measured and are shown in Table 5 below. Density drops before rising again to about non-thermally affected values with increasing temperatures. It is thought that confined rock samples would not see much of a density change.

**Table 5. Granite Temperature and Density**

| Maximum Exposed Temperature | **Density** |
|---|---|
| ~20 °C | 2.62 |
| 600 °C | 2.61 |
| 1200 °C | 1.90 |
| 1620 °C (melt) | 2.33 |

Selected furnace samples were send to a petrographic laboratory (see Appendix C for the full report #5EU) on November 12, 2013 for X-ray diffraction analysis and thin section photographs. These showed that selected minerals within the rock melted at increasing temperatures.

During bench testing, rock samples were fracturing during any significant MMW exposure due to thermal stress cracking. This greatly limited availability of rock samples for physical property testing. Furnace melts cannot get to the temperature that MMW exposure reaches (3000$^{o}$C versus 1650$^{o}$C). It is important to note that no fully melted rock glass specimens were tested, due to the thermal stress fracture problem of the samples. Also we cannot confirm that furnace and MMW beam melted rocks have the same properties. Neither can we confirm that melt form glasses have the same properties as vapor form glasses.

Bruno Gonçalves da Silva and Herbert H. Einstein, reported on bench testing of granite specimens that were obtained by P. Woskov from the Wilson Mill site in Bedford, Massachusetts, but that were partial furnace melted. Specifically, two specimens that were partially melted at temperatures of 1500 $^{o}$C and 1620 $^{o}$C in a furnace and solidified afterwards were tested. In addition, a natural (intact/ virgin/ unheated) specimen was tested for comparison purposes. The results of these tests as well as photographs of the specimens before and after testing are presented below. The results are somewhat unexpected in that the 1500 $^{o}$C specimen showed lower strength than the 1620 $^{o}$C specimen, and the latter roughly the same strength as the natural specimen. All specimens failed in

a brittle manner as the photos also show. However, the stress- strain curves are not as characteristic for brittle behavior as one would expect.

The most important message to take from all this is that a very systematic approach to such testing needs to be implemented in future MMW related testing. That approach will require more samples to test, a variety of rock types, improved confinement and larger sizes of the rock specimens that are subjected to MMW beam heating.

**Specimens IDs:** Melted (1500$^{o}$C and 1620$^{o}$C) and Intact/ Virgin/ Unheated Granite
**Tests Date:** 08/04/2014 for Melted specimens and 11/13/2014 for Intact/ Virgin/ Unheated specimens

**Table 6.** Summary Table

| | Maximum Temperature to which the samples were exposed | | Intact/Virgin Unheated Granite |
|---|---|---|---|
| | 1620$^{o}$C | 1500$^{o}$C | |
| Compressive Strength $f_c$ (MPa) | 106.9 | 74.0 | 100.4 |
| Vertical Strain at fc (%) | 1.75 | 1.41 | 1.71 |
| Young's Modulus $E_{50}$ (GPa) | 72.1 | 62.3 | 86.9 |

**Figure 13.** Melted Granite at 1620°C – Vertical Stress Vs Vertical Strain

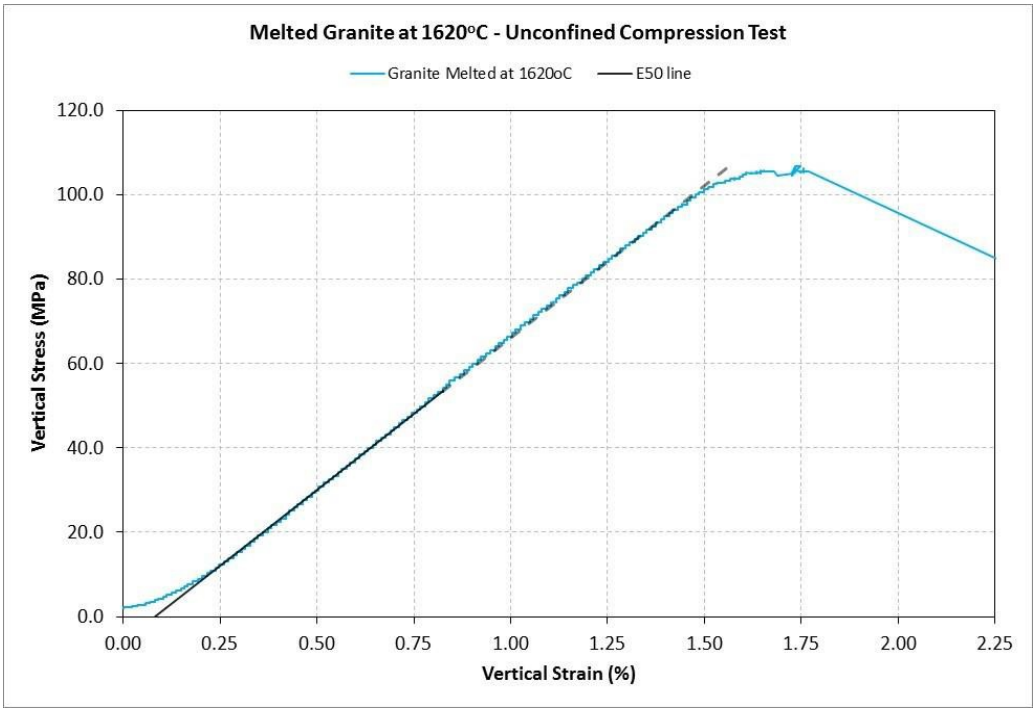


**Figure 14.** Melted Granite at 1500°C – Vertical Stress Vs Vertical Strain

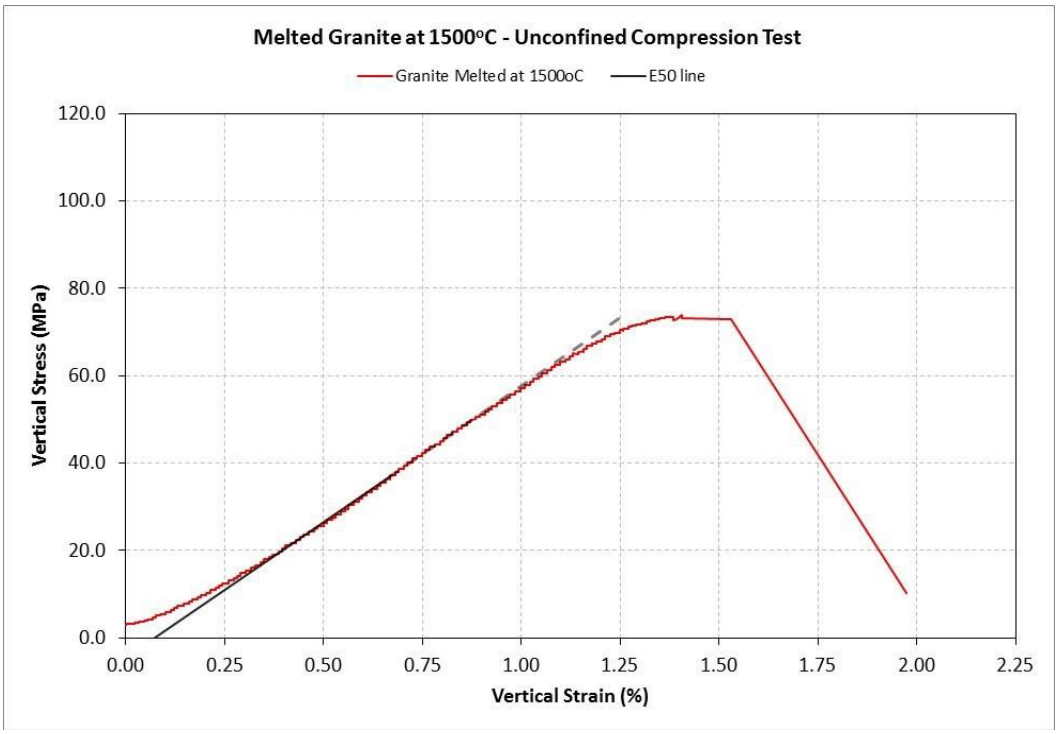

**Figure 15.** Intact Granite – Vertical Stress Vs Vertical Strain

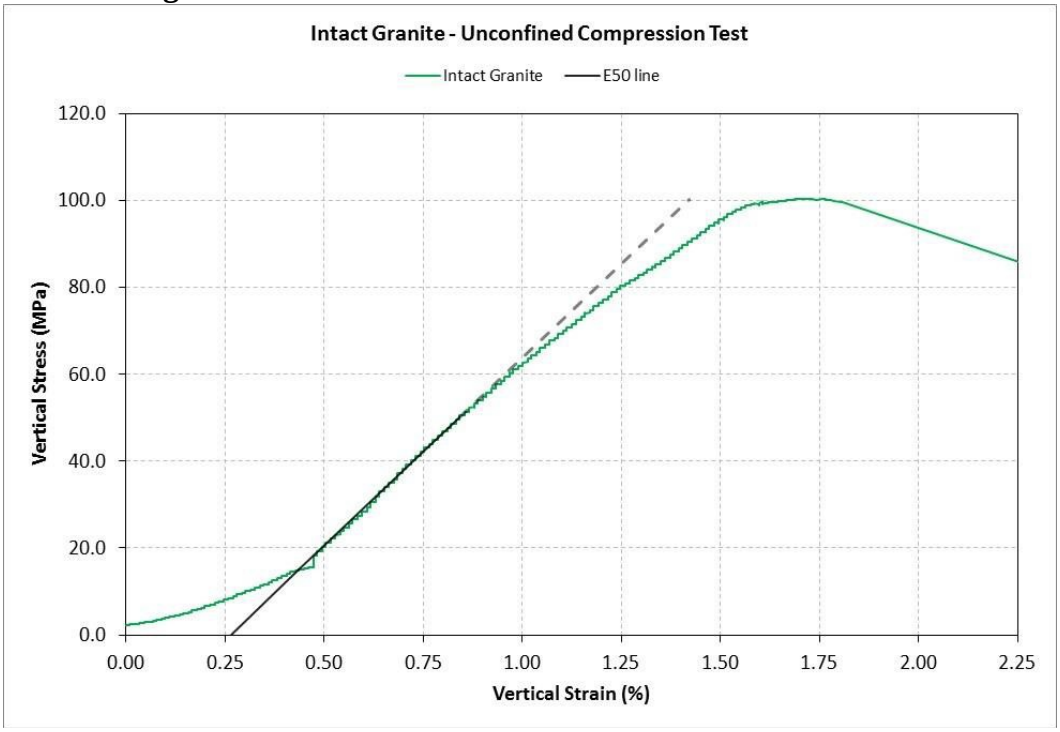


**Figure 16.** Intact/Unexposed and Melted Granite at 1620ºC and 1500ºC – Vertical Stress Vs Vertical Strain

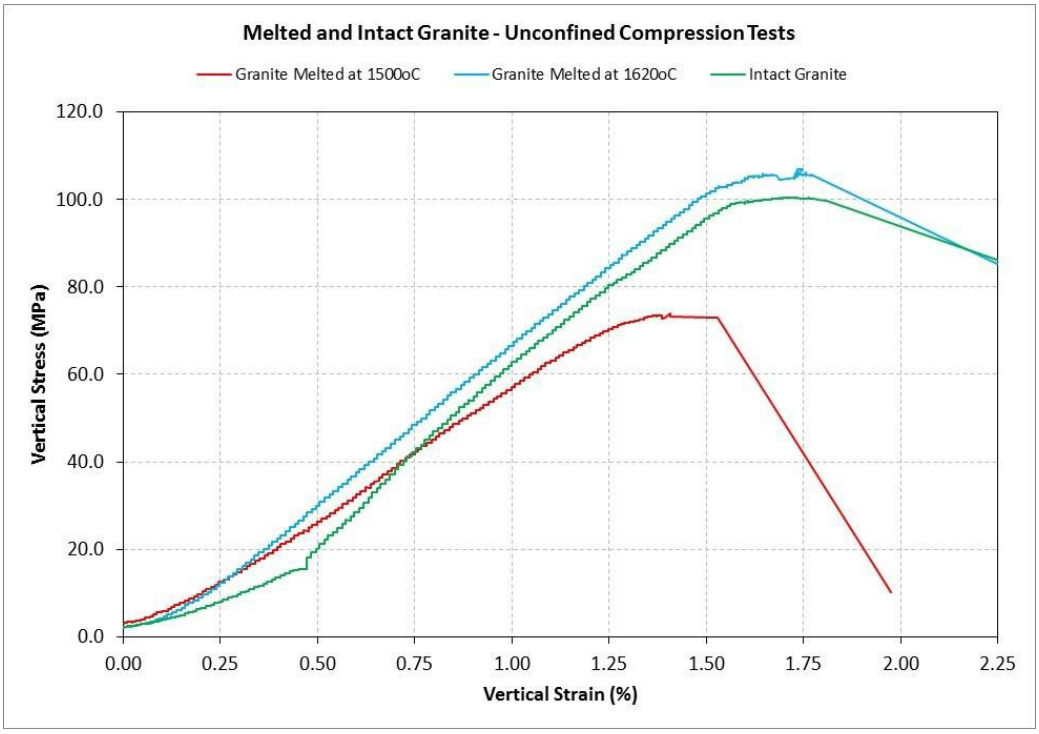

**Figure 17 a,b,c,d,e.** Initial Pictures - Before testing

a) Granite melted at 1620ºC

b) Granite melted at 1500ºC

c) Granite melted at 1620ºC on the left and granite melted at 1500ºC showing several voids on the right

d) Intact Granite specimen

e) Front view of the Intact Granite specimen where a closed fracture can be observed

**Figure 18 f,g,h,i.** Final Pictures - After testing Granite melted at 1620ºC

**Note:** The failure was extremely brittle, a large part of the specimen fragmented in very small pieces and a small pyramid with a base measuring roughly 30 mm × 30 mm with 35 mm of height.

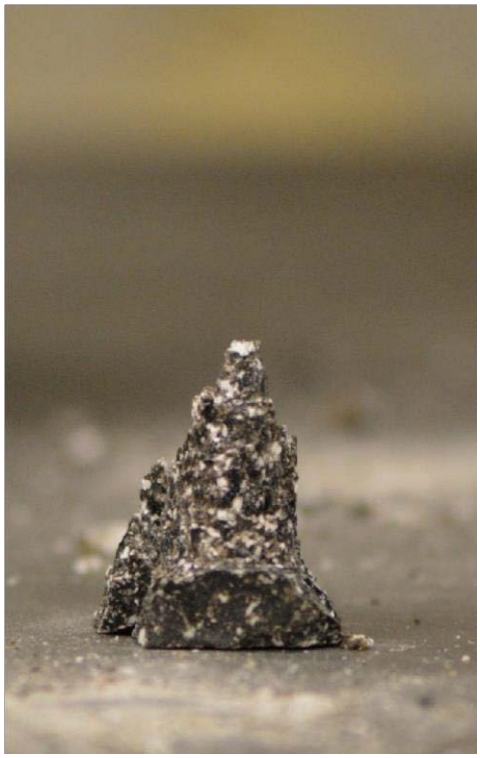

f) Front view of the granite specimen 1620ºC after testing

g) 3-D view of the granite specimen melted at melted at 1620ºC after testing

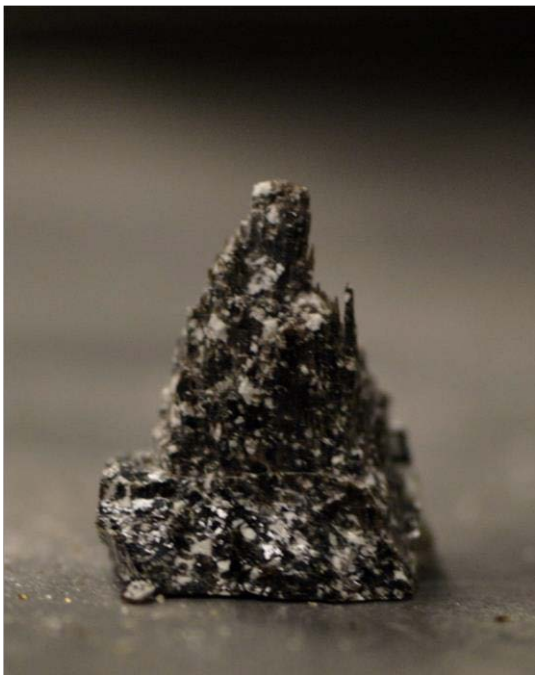

h) Side view of the granite specimen melted at 1620oC after testing

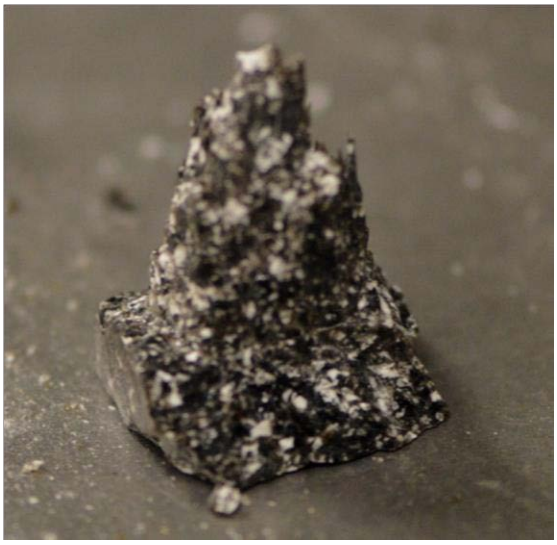

i) 3-D view of the granite specimen melted at 1620°C after testing

**Figure 19 j,k,l,m,n,o,p,q.** Final Pictures - After testing Granite melted at 1500°C

**Note:** The failure was very brittle, but not as explosive as the granite melted at 1620°C. The specimen fragmented into three large pieces and many smaller fragments.

j) Front view of the granite specimen 1500°C after testing

k) 3-D view of the granite specimen melted at melted at 1500°C after testing

l) Side view of the granite specimen melted at 1500°C after testing

m) 3-D view of the granite specimen melted at 1500°C after testing

n) Detail of the fractures created when the granite specimen melted at 1500°C failed

o) Detail of the fractures created when the granite specimen melted at 1500°C failed

p) View of the three large fragments produced when the granite specimen melted at 1500ºC failed

q) View of the three large fragments produced when the granite specimen melted at 1500ºC failed

**Figure 20 r and s.** Final Pictures – After testing Intact/ Un-Heated/ Virgin Granite

**Note:** The failure was extremely brittle, a large part of the specimen fragmented into smaller fragments, two of them larger than all the others

r) View of the various fragments produced when the intact/ unheated granite specimen failed

s) View of the two largest fragments produced when the Intact/ Unheated granite specimen failed

## Task 3.0 – Evaluate Experimental Results

The purpose of this task was to gather and analyze the theoretical and experimental results as to their meaning to the MMW process of drilling and liner formation. This was be used to set the requirements of the field test prototype components and system in later tasks. The approach was to obtain specific energies for rock penetration as compared to theoretical thermodynamic calculations and past (poor) results with laser systems. We wanted to then refine there estimates for potential millimeter-wave directed energy rock penetration rates, attainable depths, and trade-offs between borehole sizes, power, and rates. We expected to have a better understanding of the effect of water in the rock on MMW penetration, power and frequency requirements, sizing of the wave guide, standoff, rock materials, configurations and more factors. This task was to then demonstrate if significant improvements in technical performance and lower costs compared to the present technology can be achieved. The economic costs of millimeter-wave directed energy rock penetration and potential savings over current mechanical systems was to be based on the technical results of these tests. Significant advancements and understandings were made, but not all objectives of this task (costs and economics) were fully obtained.

Dr. Paul Woskov reported ("MW Directed Energy Rock Exposure Experiments and Analysis") the bench testing of 36 different rock samples that were exposed to intense MMW directed energy at a frequency of 28 GHz during the period of this project as described in Task 1. Some of these samples were exposed multiple times for a total of 65 tests. **Appendix D**, Table 1 chronologically summarizes all the MMW exposures that were carried out with the identification of the rock types, MMW power, and duration. In tests where there was transmission through a granite borehole to the sample, that borehole was not listed as a separate sample (except for the very first one). The sources of the rock samples are given at the bottom of that Appendix table. The majority of tests

were done with granites and basalt, the basement rock types that are of primary interest to heat mining for Enhanced Geothermal Systems (EGS), but a few tests with limestone and sandstone were also performed for additional insights. Typical samples are shown in Figure 21 below, which were sized to fit within the laboratory test chamber. In addition to those shown, some irregularly shaped granite samples picked up from the ground in Bedford, Massachusetts were also studied and one test was carried out on melting small (< 0.4" (1 cm)) granite fragments in a crucible.

During the course of these experiments the laboratory gyrotron- waveguide test setup evolved as experience was gained to control backward reflected power to the gyrotron source, which was prone to tripping off if the refection was too high. Details of the technology development are described in another section. It was not until April 2014 that the final experimental setup was reached with the addition of water cooling to the waveguide gap. After this point the maximum power intensities and time durations were achieved with the present gyrotron source for MMW exposure of the samples. These were an incident power of about 4.5 kW in a beam as small at 20 cm in diameter and a time exposure of over 1 hour 45 minutes in one test (Rock #35), though most of the thermal effect on the rock samples was achieved in the first 10 - 15 minutes due to attainment of a high temperature thermal equilibrium. These effects included fracturing, melting, and some vaporization of the rocks.

**Appendix D**, Table 2 summarizes the sample weight change and the maximum radiometer temperature signal observed in the tests where this data was recorded. In cases where the temperature signal significantly exceeds 3,000 $^{o}$C it is due to non-thermal plasma emission. In Appendix D, Table 3 the observed results are briefly commented on for each test.

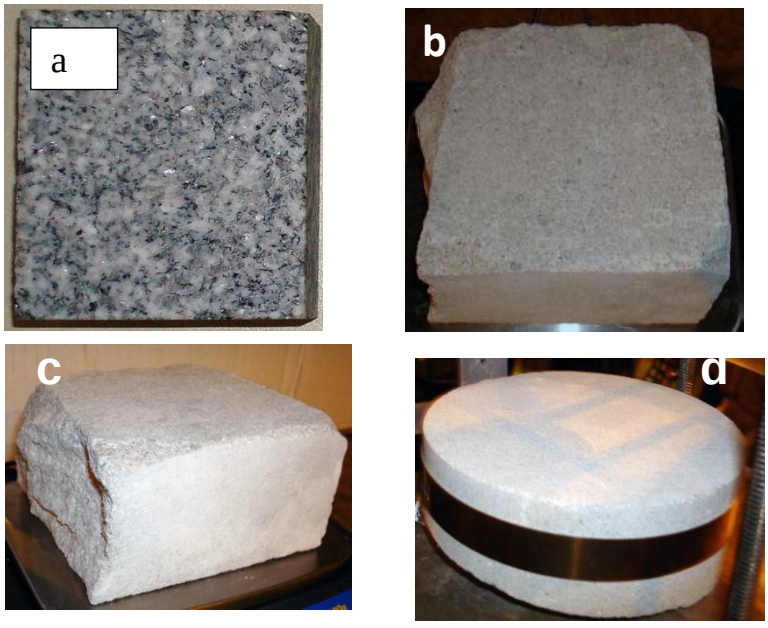


**Figure 21.** Typical rock samples tested where 4" (10 m) square or diameter and 1 to 2" (2.5 to 5 cm) thick, a) granite, b) basalt, c) limestone, and d) sandstone. A steel clamp is shown around the sandstone sample, which was required with all samples to reduce thermal stress induced fracture breakup during MMW beam exposure.

The experiments have reinforced the feasibility of MMW directed energy for full bore well formation. This is in addition to the previously identified physics and technology advantages of using the MMW range of the electromagnetic spectrum for this application [83]. The physics advantages include: 1) the capability of MMWs to propagate through infrared obscure, small particle plumes without scattering, 2) the higher efficiency of MMW absorption by melted rock relative to infrared laser beams, and 3) MMWs and typical borehole sizes are ideally suited for beam guiding and borehole diameter control. The technological advantages are: 1) commercially available, efficient (> 50%) megawatt gyrotron sources, 2) efficient long distance guided megawatt MMW transmission technology, and 3) the availability of real-time MMW – Terahertz remote diagnostic monitoring technology such as radiometry, radar, and spectroscopy. To these advantages the present experimental work adds the actual demonstration, for the first time, on a small laboratory scale the key features of a practical MMW gyrotron system for wellbore formation. These features include backward reflected/scattered power isolation, the introduction of a purge gas flow with the beam (listed in Appendix D, Table 2), beam collinear real-time monitoring diagnostics (temperature in Appendix D, Table 2), and MMW beam propagation and vitrification in a small granite borehole (Rock #13). Full bore DE MMW drilling was simulated in this project to demonstrate the feasibility of the proposed MMW drilling methods. These developments suggest that MMW directed energy should finally make full bore directed energy wellbore formation practical.

### A. Directed Energy versus Plasma Energy

The susceptibility for plasma breakdown and the advantages of directed energy over omni-directional heating were observed early in the experimental work. At atmospheric pressure and room temperature the air breakdown threshold for MMWs is over 1 $MWcm^{-2}$ [84]. However, with the presence of a hot rock surface we observed breakdown with as little as 1 kWcm-2. Figure 22 shows a TV image taken during the Rock #5 tests after the rock surface was heated to over 1000 °C with 2.2 kW power incident for about 100 s. There is a ball of plasma in the beam, near the surface, and blown sideways by a jet of nitrogen. In this test the nitrogen gas flow down the waveguide was 200 scfh. It was found that by increasing the gas flow the plasma could be extinguished and flows of over 400 scfh were eventually used in the experiments. The nitrogen gas flow was also replaced with air, which seemed to have slightly more resistance to breakdown. Increasing pressure would also increase the breakdown threshold [84] as would be the case in a deep drilling environment, but the present experimental test chamber was not designed for pressurization.

The superiority of directed energy over a plasma flame for heating rock is shown in Figure 23. With the same beam power of 4 kW much more surface rock melting is achieved with less heating time than without the plasma because all the energy is directed toward the surface and not radiated away into other directions. In a similar way, wellbore formation would be more efficient by directed energy versus undirected thermal sources such as flames or plasmas which operate with sufficient waveguide gas purge flow to prevent breakdown to maximize the rock sample heating with the available power. Plasma events are not expected to be a problem in downhole operations.

## B. Results on Flat Rock Surfaces

After optimization with transmission line development, standoff distance of the rock surface from the waveguide, and concentration of the power as much as possible with a waveguide down-taper to a 20 mm launch aperture, the maximum heating with the present experimental system was achieved. One class of experiments with flat rock samples had the surface orientated horizontally facing the vertical downward directed beam with no path for melt flow except displacement by the waveguide purge gas. Figure 24 shows representative melt craters formed with the 28 GHz MMW beam in the four rock types: granite, basalt, limestone, and sandstone introduced in Figure 21. Except for the limestone the appearance is similar, black glass with a raised perimeter and varying degrees of uniformity. The melts were most uniform with basalt (uniform black and smooth), least uniform with granite (white speckles and rough surface having out gassing voids), and the sandstone melt was in between. There was little mass change before and after exposure for these three rock types. In the case of limestone, however, there appears to have been significant vaporization before a white translucent glassy spot formed in the middle of the crater. In the following subsections a brief description is given of representative observations for each rock type.

### B. 1. Granite Tests

The rock sample shown in Figure 24a is Rock #28, a 10 cm diameter, 2.5 cm granite thick specimen with a starting weight of 578.0 g, which was initially located 20 mm from the 20 mm diameter waveguide launch aperture for the first two exposures (28a and 28b) and then moved to 25 mm for the 3rd exposure (28c) and 30 mm for the 4th exposure (28d). The $TE_{11}$ mode was used in all these tests and there was a forward flow of air at about 450 scfh. Also, the granite sample was banded with a steel clamp around the outer circumference to minimize thermal fracture breakup. The top plot in Figure 25 shows the power incident on the granite surface for test 28c. Steady power of 2.7 kW on the sample could be maintained, but when 3.0 kW was tried the gyrotron tripped shortly after due to high reflected power. The second plotted curve shows the part of the incident power not absorbed by the rock specimen, but by the water load in the test chamber. This water load power and the observed increase in reflected power in the isolator, when subtracted from the incident power indicates that the granite melt absorbs about 70% of the incident 28 GHz power, or in other words the emissivity of granite melt at 28 GHz is about 0.7.

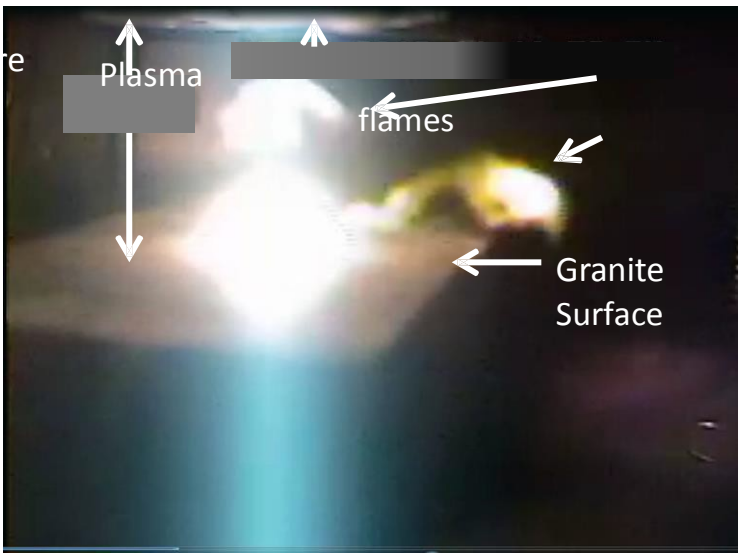


Figure 22. Plasma breakdown in the MMW beam between waveguide launch and the rock surface during Rock #5 tests after the granite surface becomes hot (> 1000 °C). In this image the beam power was 2.2 kW launched in $HE_{11}$ mode which results in about 1.3 $kWcm^{-2}$ peak intensity.

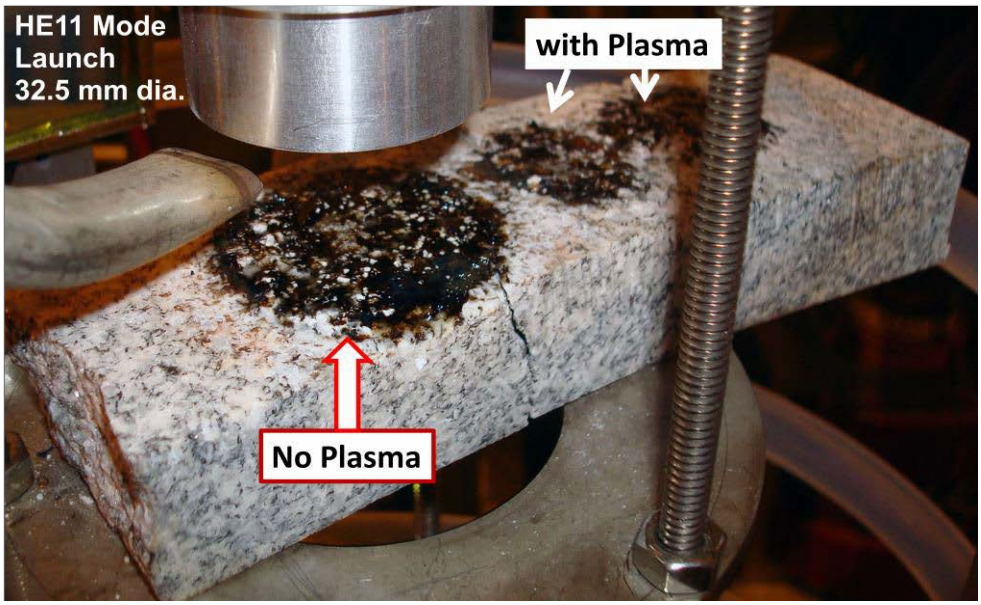


Figure 23. Granite melt spots on Rock #5 with the same incident beam power of 4 kW showing that when there is no plasma breakdown the rock is heated much more efficiently. The larger melting was achieved in only 4 minutes without plasma versus 16 minutes exposure for the smaller melt spots.

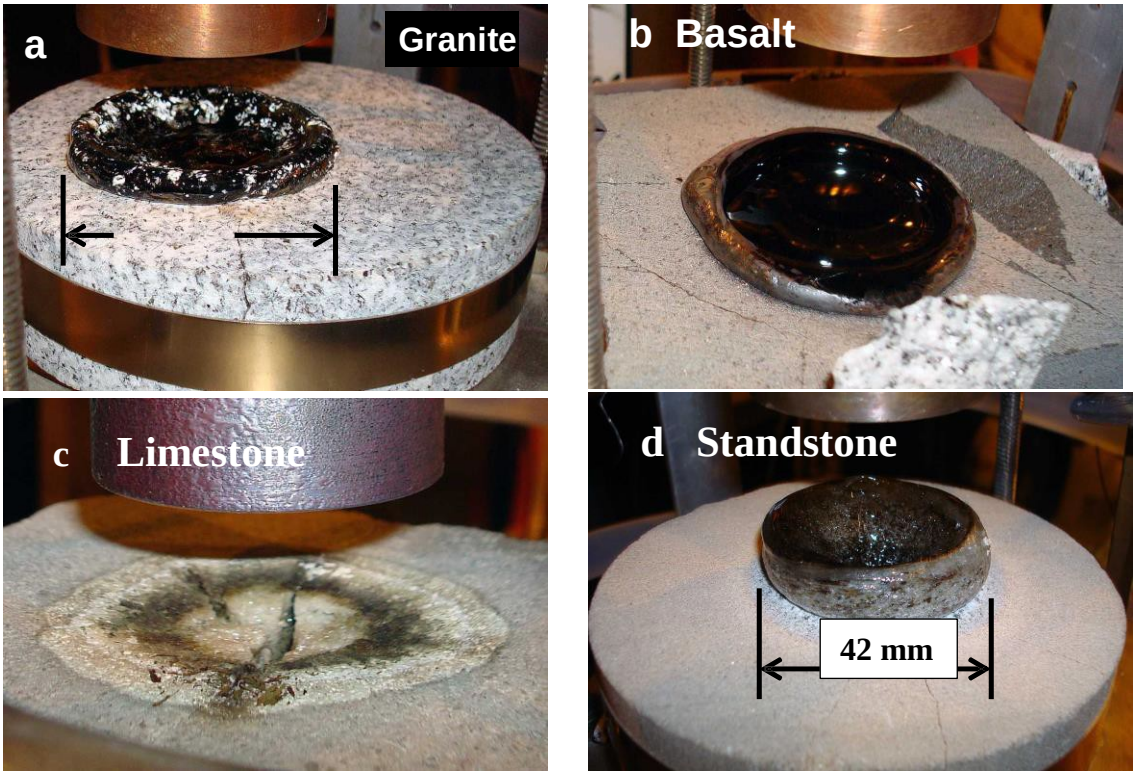


**Figure 24.** Results of 28 GHz MMW beam exposure of up to 4.2 kW for over 30 minutes with a $TE_{11}$ mode launched from a 20 mm diameter waveguide aperture; a) granite Rock #28c, b) basalt Rock #27c, c) limestone Rock #25, d) Berea sandstone Rock #29.

The surface thermal emission, which is a product of emissivity and temperature ($\varepsilon T$) was measured with a 137 GHz radiometer and is shown in the bottom plot of Figure 25. This signal as plotted is uncorrected for the emissivity of the melt surface and is also an average across the whole aperture of view. If we assume the emissivity at 137 GHz is the same as observed for 28 GHz, then the actual temperature would be 42% (1/0.7) higher than shown. There are rapid temperature signal fluctuations at high temperature, which could be melt surface turbulence or a surface plasma breakdown effect. When the incident power is changed, the major surface thermal signal follows, but the change is much smaller in magnitude. The thermal signal changes would have to be raised to a power of about three to be equal to the incident power changes. This suggests that radiative heat transfer, which goes as the fourth power is a major mechanism for heat loss and not conduction or convection which depend linearly on temperature.

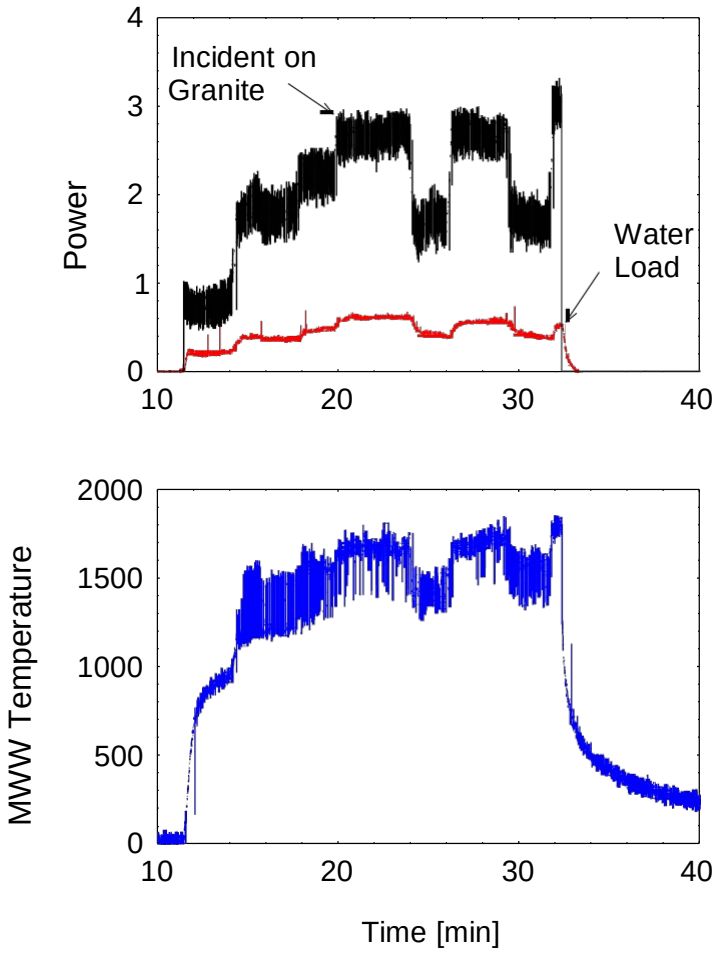


**Figure 25.** Data for third exposure of the 10 cm (4") dia., 2.5 cm (1") thick granite sample, #28c.

After all four MMW beam exposures of this sample the weight of the granite was down only 1.3 g, so there was no significant vaporization. This is consistent with the observation that maximum surface temperatures did not exceed 2500$^{o}$C (corrected for the assumed emissivity of 0.7), which is not thought to be high enough to reach the vaporization point of granite. Figure 26 shows the bottom view of this granite specimen after the 3rd MMW beam exposure (28c). The stalactite from the bottom surface is not a melt through from the top, but is due to a Fabry-Perot resonance at 28 GHz between the top and bottom surfaces. This 2.5 cm thick granite sample absorbs only 30% of the 28 GHz power on a single pass while a solid. After a melt spot forms on the top surface then transmission is cut off (see Figure 34) and the stalactite was frozen in size for all the subsequent tests on that rock.

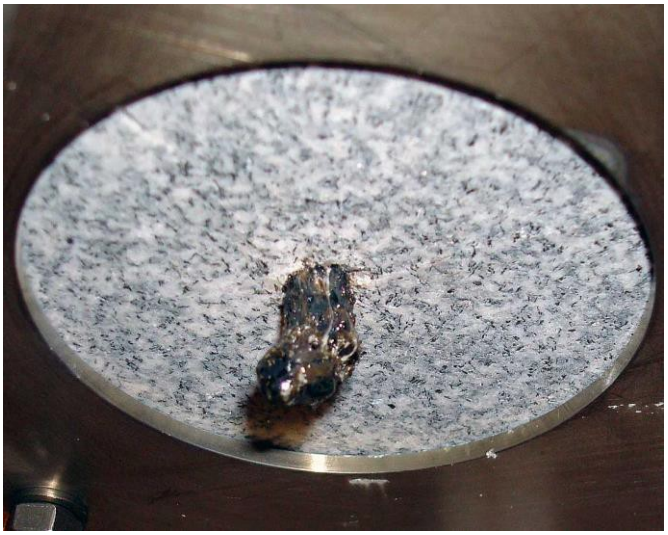

**Figure 26.** Bottom view of granite sample shown in Figure 24a.

B. 2. Basalt Tests

Basalt was very prone to violent thermal fracture. The first sample tested (Rock #22) completely broke apart within a few minutes of beam exposure as shown in Figure 27. In subsequent tests the square basalt samples were banded around the outside perimeter with a steel clamp and chips of granite wedged between the clamp and basalt sides to hold in the thermally fracturing rock during exposure. Some of the clamping granite chips can be seen in Figure 24b for Rock #27. Even with clamping around the side, rock fragments would spall from the top surface, which is also evident in Figure 24b.

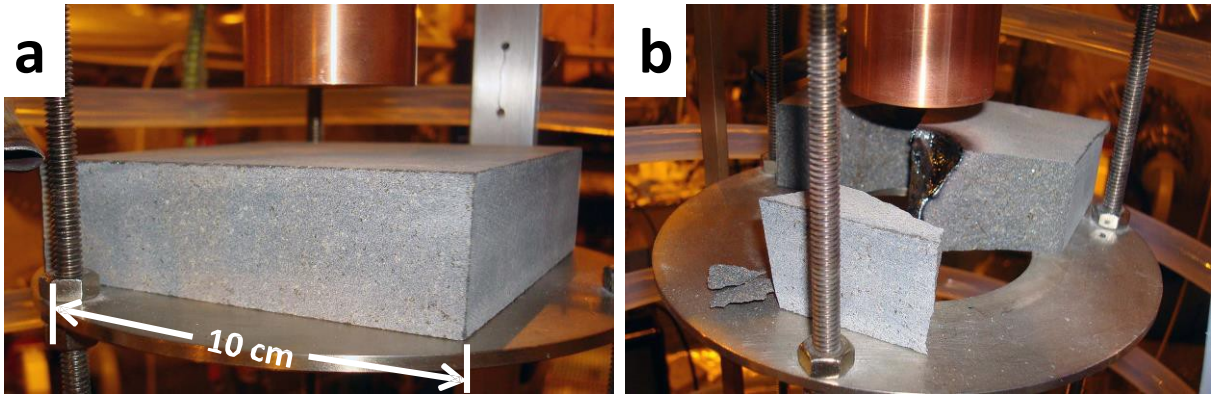


**Figure 27.** a) Basalt sample (#22) before exposure (100 mm (4”) square by 32 mm (1.25”) thick) setup under copper MMW waveguide, b) basalt sample as it appeared after being exposed to a 28 GHz beam of 2.7 kW, 32 mm diameter for 4 minutes. The heavy fragments were moved apart solely by the force of the MMW thermal fracture and broken basalt debris littered the bottom of the test chamber (not shown).

The basalt specimen #27 was exposed six different times with the distance from the waveguide launch aperture increased from 20 mm (0.787") to 40 mm (1.57") between tests. At 40 mm (1.57") distance it was possible to operate the gyrotron at full power without reflected power trip of the gyrotron. Figure 28 shows the power and temperature data for the 3rd exposure (#27c) when the sample was 40 mm distant from the waveguide launch aperture. The top plot shows that the maximum incident power could be maintained was 4.5 kW, at the limit of the gyrotron. The second plot shows the water load power. Combining this with the reflected power and subtracting from the incident power indicates that the basalt melt only absorbs about 50% of the 28 GHz power, not as good as granite.

The 137 GHz radiometer surface temperature signal in the bottom plot shows a behavior similar to that with granite. When the incident power is reduced by almost a factor of 2, the observed change in the surface temperature must be raised to a power of about 4 to follow, supporting the interpretation that radiative heat transfer dominates heat loss. If an emissivity of 0.5 (as observed at 28 GHz) is assumed for the radiometer signal, then the surface temperature reached 2930 °C on either side of the temperature dip when the power was reduced. The stair case like increase above this value toward the end of the temperature record is likely due to a change in surface figure of the melt crater which forms a focusing mirror like surface and is seen in other data.

The basalt fractures violently before melting with intense MMW beam exposure and fragments are expelled from surfaces that are not clamped. Fig. 24b shows the #27 basalt specimen with a surface defect to the right of the melt crater that was caused by an expulsion of a basalt fragment on first heating. Taking weight measurements are prone to the uncertainty of collecting all the small fragments that are scattered about the test chamber, but about 3.9 g was unaccounted for after all the tests on #27 and may have been to vaporization.

### B. 3. Limestone Test

The limestone sample #25 was 10 cm (4") square and 5.4 cm (2.1") thick with an initial weight of 1260.4 g. It was not clamped around the perimeter in this test and was located 20 mm (0.787") from the waveguide launch aperture. The power and temperature data for this test is shown in Fig. 29. It was possible to maintain 4.2 kW power incidents on the rock surface without tripping the gyrotron. The measured water load power and the reflected power in the isolator indicated that 28 GHz absorption efficiency of hot limestone is about 75%, better that granite or basalt. As with the other rock types tested, when the incident gyrotron power is varied by a factor of two as shown in the top plot the observed change in limestone surface temperature must be raised to approximately the third power to follow, again suggesting that radiative heat loss is the main limiting heat transfer mechanism. The maximum temperature observed, corrected for the observed 28 GHz emissivity (0.75), was 3770 °C. Limestone was found to vaporize before the remaining residue melts, which can have a significant impacts on the drilling and lining processes. The weight of the limestone sample was reduced by 51 g after the test and the inside of the test chamber was covered with a dark coating as seen on the copper waveguide in Figure 24c. Detailed views of this sample after exposure are shown in Figure 30. The sample had many fractures and broke cleanly into two halves after removal from the test chamber as seen in Figure 30a. The elevation view in Figure 30b shows a similar pattern of

discoloration as the top surface view in Figure 30a. There is an outer white region, a middle dark region and an inner white region with a glassy translucent white melt. After more handling the sample completely broke apart into many fragments with all the discolored heated regions crumbling into a fine mostly white powder.

### B. 4. Sandstone Test

The Berea sandstone test sample #29 was 10 cm (4") in diameter and about 3.81 cm (1.50") thick as shown in Figure 24d. The power temperature record is shown in Figure 31. The diameter of the black glass melt crater was smallest of the three rock types which produced a black melt crater and the height of the crater ridge was highest, making this the deepest, narrowest crater. An incident power of 4.2 kW could be maintained indefinitely without gyrotron tripping. The observed water load and reflected power indicates that the 28 GHz absorption efficiency of the high temperature melt to be about 65%, less than granite, but more than the basalt melts. The radiometer temperature signal becomes very noisy as the small deep crater develops suggesting plasma breakdown occurring within the depth where purge gas may not reach. The highest uncorrected temperature excursions go over 3200 °C. If we assume the bottom of the temperature excursions at about 2300 °C are representative of the surface temperature without breakdown and use the 28 GHz observed emissivity of about 0.65, then the surface temperature may be as high as 3500 °C. As with the other rock types the variation in incident power has a much smaller relative effect on the surface temperature also suggesting a radiative heat transfer limit. Another observation with the sandstone sample was a measured loss of mass of about 5 grams after exposure, more than with granite or basalt of similar weight, suggesting that there was more vaporization with this sedimentary rock versus the hard crystalline samples. This low vaporization may be related to the higher required temperature to melt, specific mineralogy within the sandstone sample, and/ or the more viscous sandstone melts that were seen.

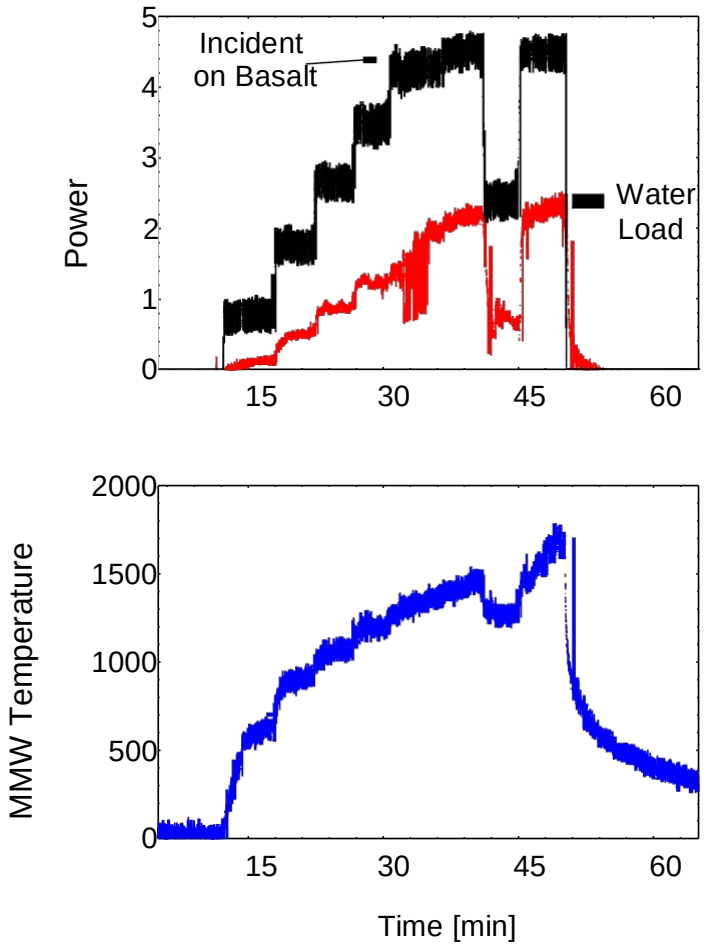


**Figure 28.** Data for test #27c, the third exposure of a 10 cm square, 3.1 cm thick basalt sample.

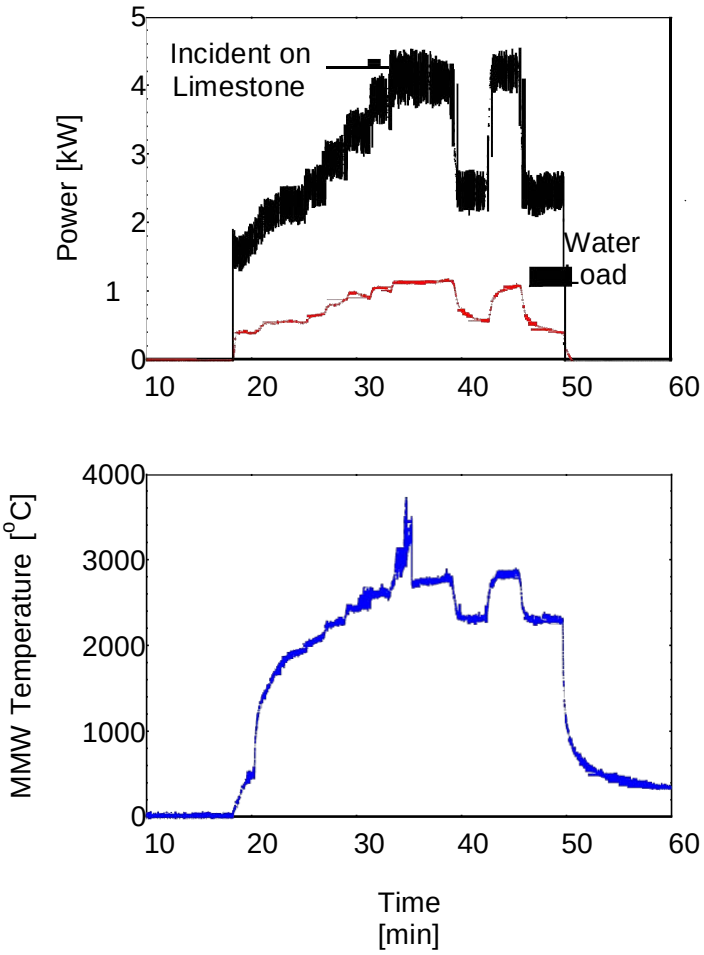


**Figure 29.** Data for exposure of 10 cm square, 52 mm thick limestone sample

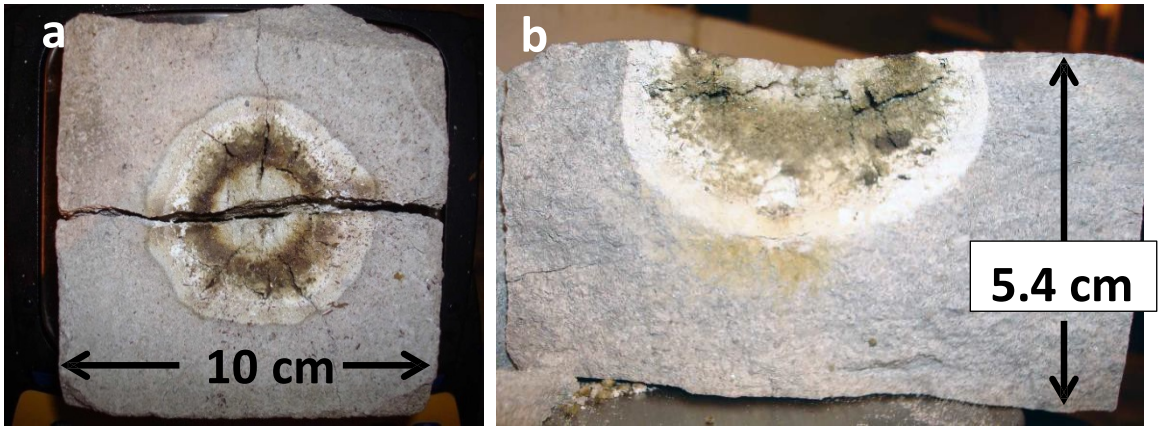


Figure 30. Views of limestone Rock #25 after MMW beam exposure.

B. 5. Summary of Rock Melt MMW Emissivity

**Table 7.** Approximate Observed High Temperature Rock Melt Emissivity at 28 GHz

| Rock Type | Emissivity |
|---|---|
| Granite | 0.70 |
| Basalt | 0.50 |
| Limestone | 0.75 |
| Berea Sandstone | 0.65 |

**C. Modeling and Analysis of Flat Rock Experimental Results**

Heat transfer modeling was carried out using a commercial finite element computer code (COMSOL) to provide insights into the observations. A number of assumptions and approximations are necessary to make the calculations possible because of the large temperature range from room temperature to over 3000 °C that is observed in the experiments. The thermal properties of the rock types studied are not really known to such temperature extremes and it was necessary to extrapolate trends of thermal properties from much lower temperatures. Also phase transition from solid to liquid could not be easily dealt with so an assumption was made that this transition and melt flow could be ignored.

The temperature behavior of the heat capacity of rocks is very similar for all rock types except for a magnitude difference [85]. We assumed for granite that the heat capacity at lower temperatures is given by as in [85]:

$$c_{p1} = -0.000273T^2 + 0.894T + 788 \qquad [\mathrm{J/\,kg/oC}]$$

for T < 1200 °C (Equation 4)

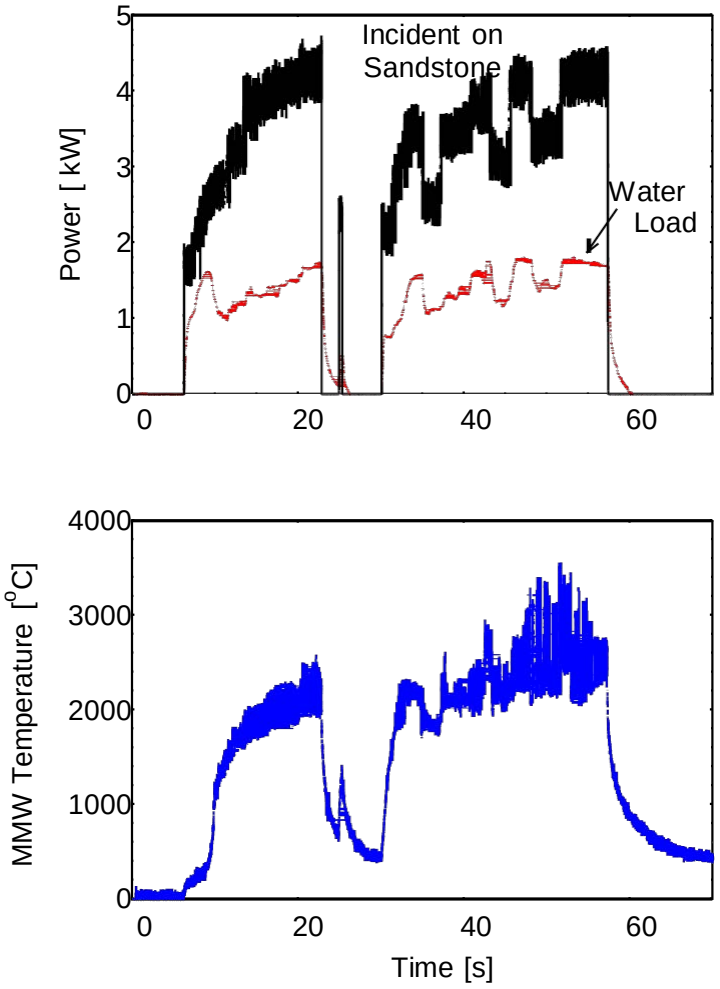


**Figure 31.** Data for exposure of 10 cm round, approximately 3.8 cm (1.50") thick Berea sandstone sample #29.

and linearly extrapolated to higher temperatures by:

$$c_{p2} = 0.184T + 1249.37 \quad [\text{J/ kg/oC}] \qquad \text{for T} \geq 1200\ ^{\circ}\text{C} \qquad \text{(Equation 5)}$$

These equations are plotted concurrently in Figure 32 by the curve that goes from 20 to 3000 $^{o}$C. For comparison, the data used by Branscome [86] and Waples [85] for granite are also plotted to their temperature maximums.

The temperature dependence of the thermal conductivity is also required for the modeling calculations. It has been shown that for most crustal rocks this parameter behaves in a similar way, initially decreasing with temperature [87]. At high temperature after melting the thermal conductivity of silica glass melts is about constant [88]. We assumed that the temperature

dependence of the thermal conductivity for granite at lower temperatures is given by formula [89]:

$$kh1 = (0.3514 + 0.00038T)^{-1} \ [W*m^{-1}*{}^{o}C^{-1}] \quad \text{for T< 800}^{o}\text{C} \qquad \text{(Equation 6)}$$

and extrapolated to higher temperatures by:

$$kh2 = 1.52 \ [W*m^{-1}*{}^{o}C^{-1}] \quad \text{for T > 800 }^{o}\text{C} \qquad \text{(Equation 7)}$$

These relations are plotted in Figure 33 and for comparison the data used by Branscome [86] for granite at lower temperature are also shown. The uncertainties in the thermal behavior of the heat capacity and thermal conductivity within scatter of the plots shown do not change the basic dynamic features in the calculated temperature behaviors that result, but do affect the absolute numbers.

The other input required for the modeling computations is the absorption of the MMW beam in the sample. In the case of our Barre granite samples we have measured the absorption coefficient at room temperature to be 0.14 nepers/cm [90], corresponding to about 30% absorption in a 1" (2.54 cm) thick sample. We also have measurements of the transmission through the sample from the 28 GHz pick off detector in the test chamber during the MMW beam heating. Figure 34 shows this measurement for grant sample #19. The initial transmission through the sample is rapidity cut off when the 137 GHz thermal emission jumps to a high value, which we interpret as the melt transition. The absorption coefficient is therefore modeled as a two-step function, before the rock melts it is assumed to be near the measured room temperature value and after melting it is increased about two orders of magnitude to restrict absorption mainly to the surface. The surface reflection of the 28 GHz heating beam is also assumed to be two stepped, 0.14 before melting calculated by The Fresnel Equations from the measured index of refraction of 2.24 at room temperature and 0.3 after melting as observed in the experiments.

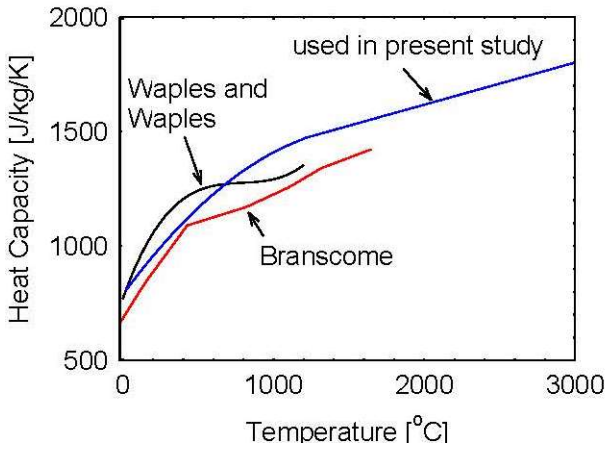


**Figure 32.** The Heat Capacity trend with Temperature used to model the experiments.

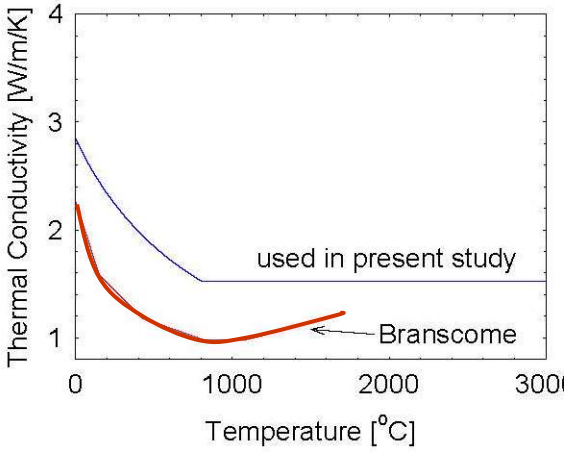


**Figure 33.** Thermal conductivity vs. Temperature assumption used to model the experiments.

The results of heat transfer modeling on a 4" (10 cm) square, 1" (2.5 cm) thick granite sample are shown in Figures 35 and 36. The 3D surface heat distribution is shown in Figure 35 for the end of a 550 second exposure with beam power 1.7 kW for the first 380 seconds and then increased to 2.7 kW. The beam is assumed to have a Gaussian profile with a 1/e power diameter of 0.80" (20 mm), approximately what is launched by our waveguide.

A plot of the peak surface temperature in the center of the heating beam is shown in Figure 36. The general dynamics of the temperature changes are similar to what are observed experimentally. When the sample initially melts there is an abrupt transition to a higher surface temperature as the volumetric absorption changes to a surface absorption. This is in agreement with the observation in Figure 34. Actually the experimental observed melt transition temperature change is larger because the melt initially starts 2 - 4 mm (0.08 – 0.16") below the surface and breaks through to the surface from below. The modeling shows that the temperatures peak below the surface, but does not model this solid-liquid phase transition. This is an interesting characteristic of MMW heating in that it penetrates below the surface and is less perturbed by high gas flow against the surface unlike heating with infrared lasers.

After a high temperature melt is established the change in surface temperature with incident power is much less than linear. For an incident power increase of 60% from 1.7 kW to 2.7 kW, the surface temperature increase is only 17%, which agrees with the experimental observation for granite illustrated by the insert in Figure 36 and Figure 25 for Rock Test #28c. Rock Test #28c is a previously melted sample and does not have the beginning dynamics of virgin granite that is modeled and shown for Rock Test #19 in Figure 34. The temperature scale difference between the calculated and experimental data can be due to the calculation being a real temperature at the peak of the heated profile and the experimental observation is uncorrected for emissivity and an average over the radiometer view, which includes lower temperature areas. Also small changes in the model assumptions affect the calculated temperature magnitude, but generally the change with power remains about the same percentage.

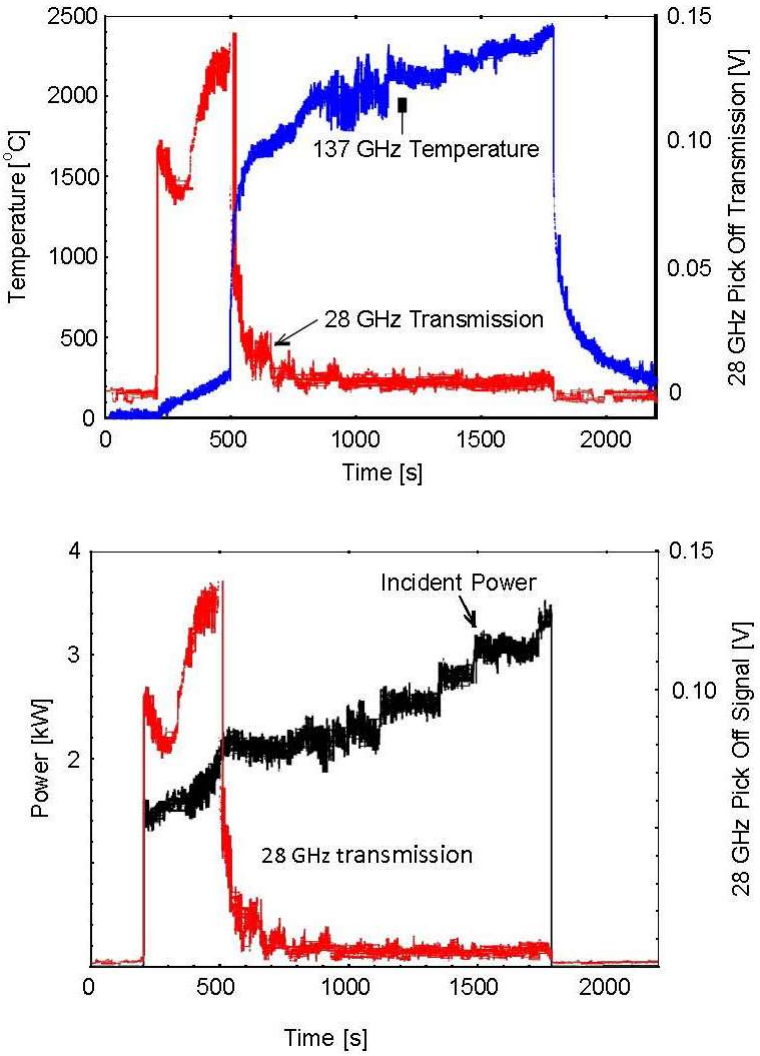


**Figure 34.** For granite sample #19 the recorded 28 GHz test chamber pick off signal, which is mostly due to transmission through the sample and the 137 GHz thermal emission signal uncorrected for emissivity in the top graph. Power incident on the granite is shown in the lower graph. There is a sharp cut off in transmission when the sample surface temperature jumps upward, which is interpreted as the onset of melting.

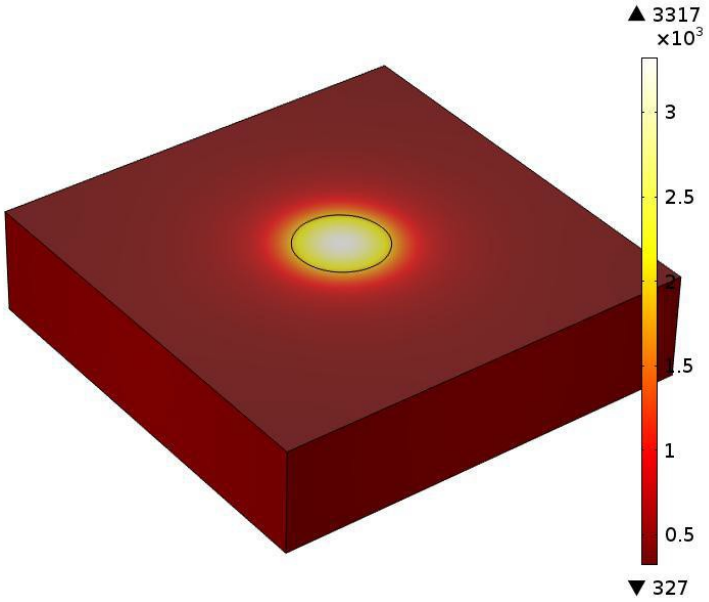


**Figure 35.** 3D image of calculated surface temperature (K) distribution of granite exposed to a 0.80”(20 mm ) 1/e diameter Gaussian 28 GHz gyrotron beam of 1.7 to 2.7 kW power for 550 seconds with assumptions in text.

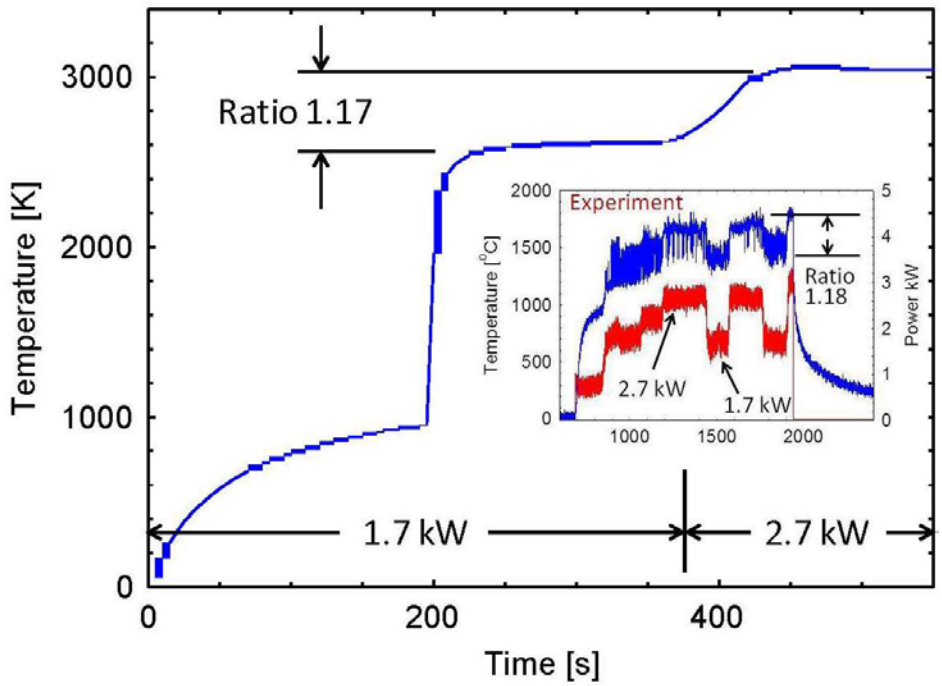


**Figure 36.** Calculated surface temperature as a function of time at the center of the MMW heating beam. Insert shows experimental data for test #28c, a previously melted sample. The calculated high temperature change of 17% with incident beam power change of 60% is the same as observed experimentally.

C. 1. Power Balance

The computer modeling heat transfer calculations confirm that the dominate heat loss mechanism when heating rock samples to high temperatures > 2,000 °C is primarily due to radiative heat transfer. Using this knowledge a power balance can be done on our data for the granite Rock Test #28c, which explains why our current laboratory experiments with flat samples are limited to crater melts and also reveals a significant advantage of using MMWs over infrared radiation for melting rock.

Analyzing the data for Rock Test #28C:

| | |
|---|---|
| Observed peak thermal emission- | 1700 °C |
| Corrected for emissivity (1700/0.7)- | 2430 °C (actual temperature) |
| Measured peak incident power- | 2.7 kW |
| Corrected for emissivity (2.7 x 0.7)-: | 1.89 kW (actually absorbed) |

The radiative heat transfer power loss is given by the Stefan-Boltzmann law:

$$q = \varepsilon_{IR} \sigma \, (T^4_{hot} - T^4_{cold}) \, A \qquad \text{(Equation 8)}$$

where $\varepsilon_{IR}$ is the infrared emissivity (at temperatures > 2,000 °C the black body emission peaks in the infrared), $\sigma = 5.67 \times 10^{-8}$ W/m$^2$/K$^4$ is the Stefan-Boltzmann constant, $T_{hot}$ is the temperature of the hot surface in Kelvin, $T_{cold}$ is the temperature of the surrounding environment in Kelvin, and A is the area of the hot surface. If we conservatively use 80% of the 49 mm diameter melt spot as shown in Figure 24a for the area, then for an infrared emissivity of $\varepsilon_{IR} = 1.0$ the calculated radiated power is 3.6 kW for a temperature of 2430 °C. This is obviously not possible because the absorbed power is only 1.9 kW. The only adjustable parameter in Equation 8 to achieve a power balance is the infrared emissivity. It needs to be reduced to about 0.5, and likely lower if we allow for convective and conductive heat losses and are less conservative with the hot area. Previously low infrared emissivity of basalt melts of about 0.5 and lower has been observed by Abtahi etal [91] and Vakulenko et al [92].

This analysis explains the limits of the present flat surface experiments and demonstrates the superiority of MMWs over infrared sources for full bore well formation. No more temperature increase or equivalently no more energy can be put into the rock samples because the heat losses are equal to input power. In these tests, the heat losses cannot be reduced by making the melt spot smaller because at 28 GHz the 20 mm diameter (0.787") waveguide launch aperture is already near the diffraction limit and the gyrotron output power is at its maximum. A higher power gyrotron and/or higher frequency will be needed to progress to complete vaporization to abate the rock in a horizontal flat configuration. Also the emissivity measurements and power balance analysis show that MMW absorption efficiency is higher than infrared absorption efficiency ($\varepsilon_{MMW} > \varepsilon_{IR}$). Therefore, less power will be needed to melt and vaporize rock with a MMW gyrotron versus an infrared laser.

**Figure 37.** Bedford granite for Rock Test 7b.

### D. Results with Non-Flat Rocks

With the ability to vaporized flat surfaces of rocks thermally limited in the present experiments, it becomes necessary to displace the melt to produce more rock penetration. In the early tests before the transmission line system was optimized and the thermal limits were fully understood, experiments were carried out with samples not having a level surface, which could allow melt flow. However, if the surface slope is not large, the melt forms a crater that flows into a horizontal orientation normal to the beam similar to the flat cut samples as shown in Figure 37 after Rock Test #7b. A sample with a very steep sloping surface is necessary and this was done in tests with granite Rock Tests #12 and #13, which achieved large melts flows.

The set up for Rock #13 inside the test chamber is shown in Figure 38. The corrugated aluminum HE11 launch waveguide is followed by a 1.25" (32 mm) thick granite slab 4" (100 mm) diameter in contact with the aluminum waveguide and having a 1.31" (33 mm) diameter hole that acts as a dielectric waveguide extension to corrugated aluminum waveguide. Located below the granite waveguide and in near contact (closest point 2-3 mm (0.08 -0.12") away) is granite Rock #13. The 28 GHz MMW beam transmission losses through the granite dielectric waveguide are calculated to be 17% [93]. The before and after views after Test #13 are shown in Figure 39. The incident beam power was in the range 0.8 – 2.3 kW for a total exposure time of 57 minutes for the sum of both tests. Waveguide purge air flow was 500 scfh. There was large melt flow extending 2.75" (7 cm) below the borehole, completely down the side of the granite sample and beyond in a stalactite. Both the rock sample and the inner wall of the borehole were melted and flowed.

A better view of the borehole wall melt from the bottom direction is shown in Figure 40. The melted wall only extends part way up from the beam output side of the borehole. The heat load on the wall due to the forward pass losses of the MMW beam decrease toward the output side of borehole as the beam is attenuated and would be insufficient to melt this wall at a maximum of about 390 Watts. The melting required the trapping inside the borehole of the upward radiated heat loss of about 2 kW maximum from the primary sample Rock #13. Controlling the diameter

of full bore directed energy well formation will require taking into account this radiated heat trapping, which would contribute to improving the efficiency of the directed energy penetration process.

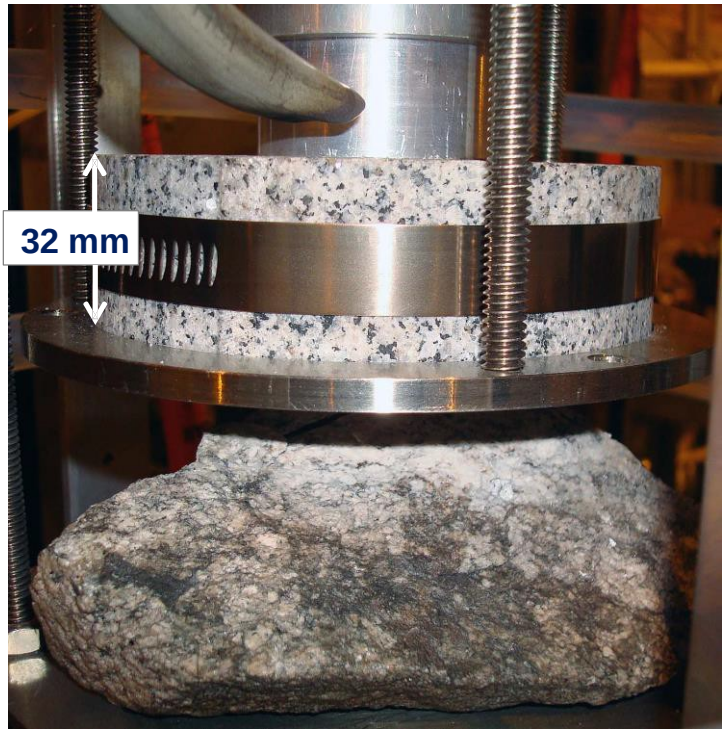


**Figure 38.** Set up for Rock Test #13 from top to bottom: aluminum corrugated waveguide, 4" (10 cm) diameter granite with 1.31" (3.3 cm) diameter borehole, and #12 granite sample.

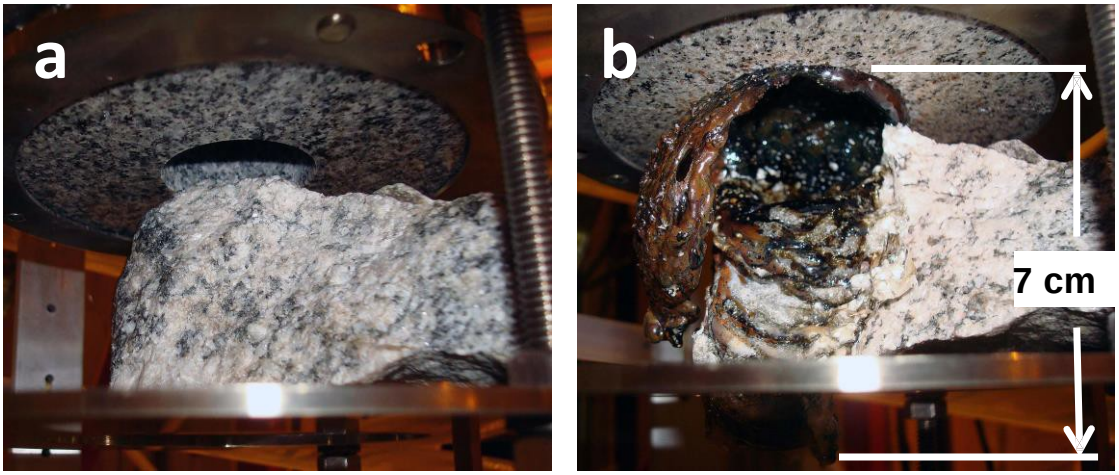


**Figure 39.** View from bottom of granite set up a) before and b) after Rock Test #3 (b). Melt flows from borehole and side of rock sample up to 2.75" (7 cm) from bottom of granite borehole.

**Figure 40.** Improved view into the borehole after Rock Test #13. Showing that the inside borehole melt does not extend into the MMW beam input end of the hole where the MMW beam power is maximum.

### E. Results with Pre-Drilled Leak Holes

Predrilling a small leak hole in the rock samples proved to be the most effective way to allow the melt to flow out of the way of the beam in the present experiments. While this experiment version utilizes only gravity to cause flow of the generated rock melt away from the 'drilling surface', it best represents the envisioned over-pressure methods that appear to be the most favorable for MMW drilling success. Full beam penetration of the Rock #33 sample with the 28 GHz gyrotron was achieve in basalt and granite rock specimens up to 3.1 cm (1.22") thick using a ½ "diameter leak hole located approximately in the center of the rock specimens. Figure 41 shows Rock #33, a 10 cm (4") square by 3.1 cm (1.22") thick basalt sample with a ½" (12.7 mm) hole before MMW beam exposure. A steel clamp with granite rock chips around the sides were used to hold in the basalt together when it thermally fractured.

Rock #33 was exposed to the 28 GHz gyrotron beam launched from the 20 mm (0.787") output aperture of the waveguide down taper waveguide propagating the $TE_{11}$ mode. The sample surface was located 35 mm (1.38") from the launch aperture. The power was on for a total of 41 minutes starting at 1.6 kW and increased to 4.5 kW for the last 17 minutes. Figure 42 shows this sample below the waveguide after exposure. Because the wavelength of the beam, 10.7 mm (0.42"), is large compare to the waveguide diameter, diffraction rapidly increases the size of beam to burn approximated a 50 mm (2") diameter hole in the sample. The top view of this exposed sample is shown in Figure 22a and the bottom is shown in Figure 42b.

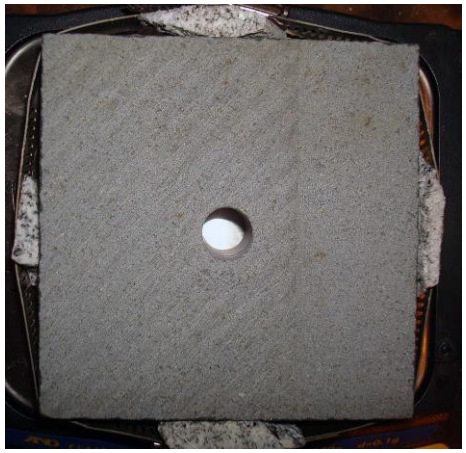

**Figure 41.** Basalt specimen Rock #33, a 10 cm square with ½" (12.7 mm) diameter leak hole for rock melt flow.

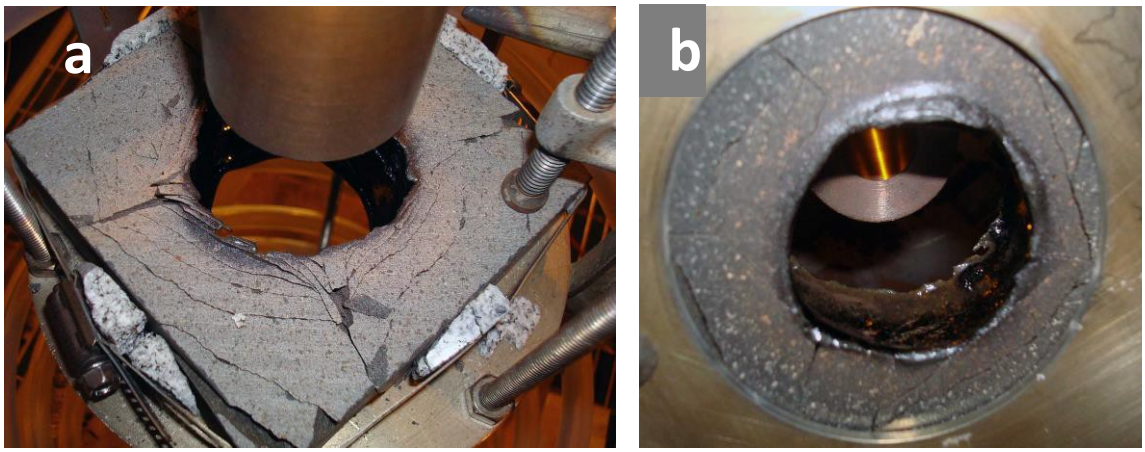


**Figure 42.** Basalt sample #33 after exposure to 28 GHz gyrotron beam launched from the 20 mm (0.787") diameter copper waveguide down taper. Beam power was 1.6 kW increasing to 4.5 kW over a 41 minute period; a) top view of the 52 x 49 mm (2.05 x 1.93") aperture burned into sample, b) bottom output of the hole was slightly smaller 45 x 43 mm (1.77 x 1.69").

**Figure 43.** The melt that collected in the bottom of the test chamber from the Test #33 basalt sample penetrated by the gyrotron beam. It appears as if it dribbled out in many drops. Total weight was 198 g.

The basalt sample weight with the leak hole before gyrotron exposure was 895.5 g and after exposure it was reduced to 686.7 g. Most of this missing mass was found as the melt flow from the sample collected in the bottom of the test chamber shown in Figure 43. The weight of the rock melt collected was 198 g. Only about 10 g is unaccounted for and could be due to fracture fragments and small melt glass needles that were not found or it was lighter components that were vaporized.

Another perspective of this basalt sample after exposure and removal from the test chamber is shown in Figure 44. A close inspection of the penetration made by the gyrotron beam shows that it was scalloped into a larger diameter inside as the diverging beam was increasing in size. The maximum internal diameter is about 60 mm (2.36”). However as the beam power dissipated it began to converge again on the output side. Another result is that the basalt sample is thoroughly fractured and will fall apart into dozens fragments if the outer clamp is removed. This happened with the first basalt sample #30 with the same ½” diameter starting leak hole. The burn-through results with Rock #30 were very similar to the result with Rock #33.

For basalt Rock Test #32 the launch waveguide was changed to the aluminum corrugated waveguide to launch the less diverging beam with the $HE_{11}$ mode to see if a more uniform diameter borehole penetration would be achieved. Unfortunately, the reflected power increased significantly and limited forward power to less than 75% of maximum. The resulting melting that occurred is shown in Figure 45. The starting melt penetration on top was much more collimated as expected, but the bottom of the melt facing the waveguide formed a focusing mirror that with the straight walled penetration redirected the back reflection much more efficiently, limiting maximum power. The reduced power limited the melt flow that could be achieved through the leak hole.

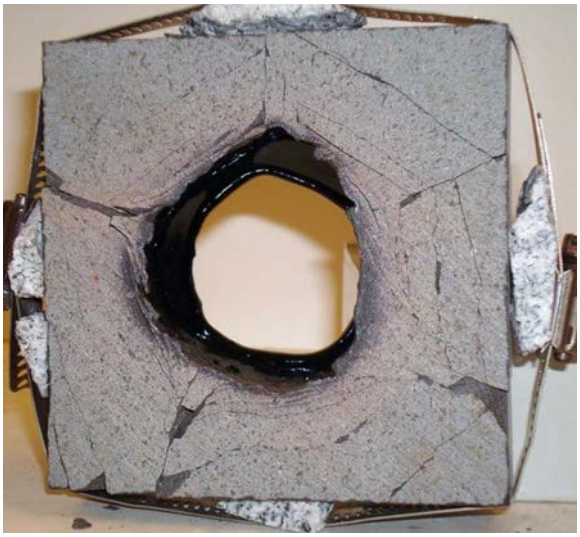

**Figure 44.** Front view of gyrotron beam exposed basalt sample from the MMW beam input side that started out with a 12.7 mm (½") pre-drilled leak hole for the melt flow.

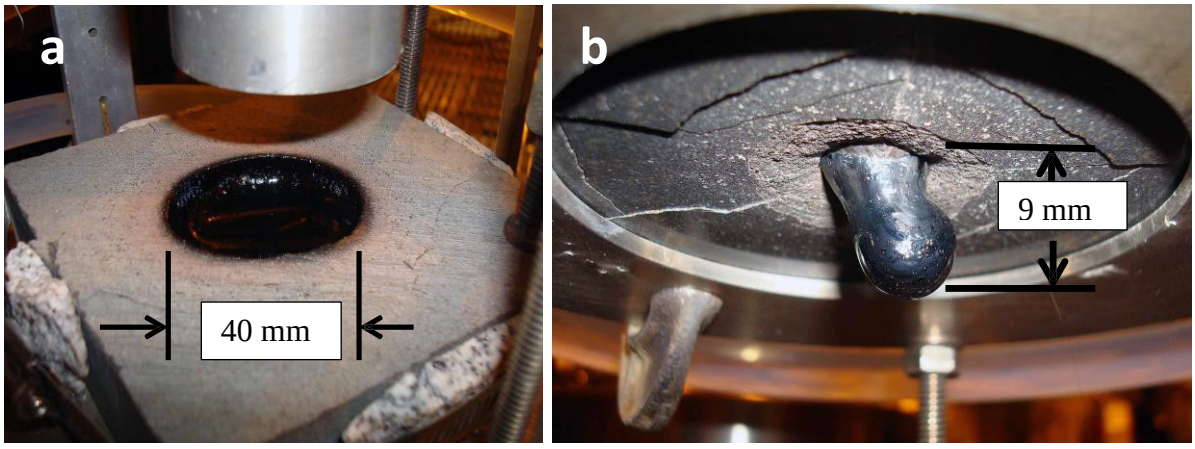


**Figure 45.** Basalt Rock #32 after MMW beam exposure up to 3.3 kW, an $HE_{11}$ mode launch beam a) top view of melt crater about 40 mm (1.57") diameter and 10 mm (0.39") deep, and b) bottom view a stalactite about 12 mm ( 0.50" ) diameter and 9 mm ( 0.35" ) long.

Predrilled granite samples were also studied. Rock #31 was a 10 cm square by 2.5 cm thick granite sample with a ½" (12.7 mm) leak hole. The bottom view of this sample with predrilled hole before exposure to the MMW beam is shown in Figure 46. After exposure the top and bottom of the sample are shown in Figure 47. Granite Rock #31 was exposed for a total of 61 minutes with varying power levels between 1.5 and 4.5 kW at a distance of 37 mm (1.47") from the waveguide launch aperture. The waveguide was the same $TE_{11}$ down taper that was used for basalt samples #30 and #33. It was possible to observe in the raw data that the melt through was not proceeding as efficiently in this granite sample as for the basalt samples. The viscosity of the granite melt is much higher than basalt melt at the same temperature (confirmed by a literature search [94]) and did not flow as freely. The diameter of the gyrotron

beam formed hole was about 3.9 cm (1.54") at the input side of the sample and tapered down to a smaller size on the output. At the end of the glass tube that formed it was less than 2.5 cm (1") inside diameter. The weight of the glass melt collected in the bottom of the test chamber was only about 25 g.

Figure 46. Granite specimen #31 with a ½" (12.7 mm) pre-drilled leak hole for melt flow, as viewed from the bottom inside the test chamber before gyrotron beam exposure.


**Figure 47.** The granite specimen #31 after it was exposed to the 28 GHz gyrotron beam of 1.5 to 4.5 kW for 61 minutes; a) top view, b) bottom view showing that the gyrotron beam formed a glass tube extending about 5 cm below the sample.

The granite borehole formed by the MMW beam is much rougher than that formed in basalt. A view through the hole formed in granite Test #31 is shown in Figure 48. Compare this with the view of the basalt hole in Figure 42b. It has been a consistent observation through all the tests, that when granite melts it does so non-uniformly with swells, bubbles, and a distribution of

white speckles through the black matrix. Basalt on the other hand melts into a uniform black glass that forms mirror like surfaces. Granite likely melts with a much higher viscosity and non-uniformity because of its more heterogeneous distribution of minerals, which can vary from sample to sample. The melt flow in our tests with granite was so marginal that in two other samples with ½" (12.7 mm) diameter leak holes (#34 and #35) we were unable to get a complete penetration with such a weak powered beam. Figure 49 shows the results for granite test #35 that almost penetrated completely through.

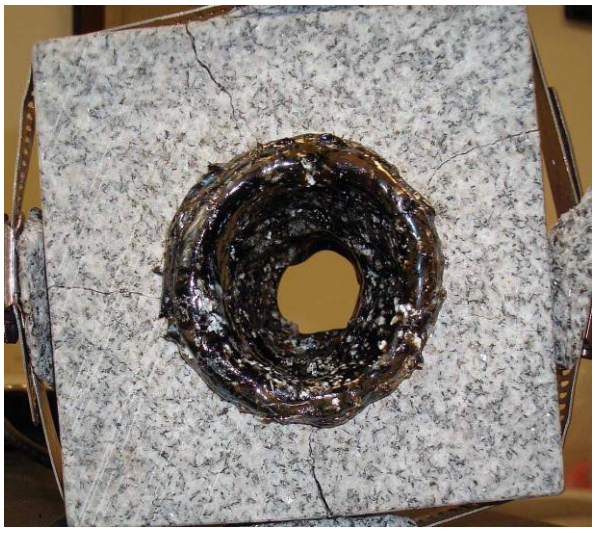

**Figure 48.** View through the hole and glass tube that together extend about 3" (7.5 cm) made by the MMW beam in granite Rock #31, (12.7 mm) diameter leak holes (#34 and #35) we were unable to get a complete penetration. Figure 49 shows the results for granite test #35 that almost penetrated completely through.

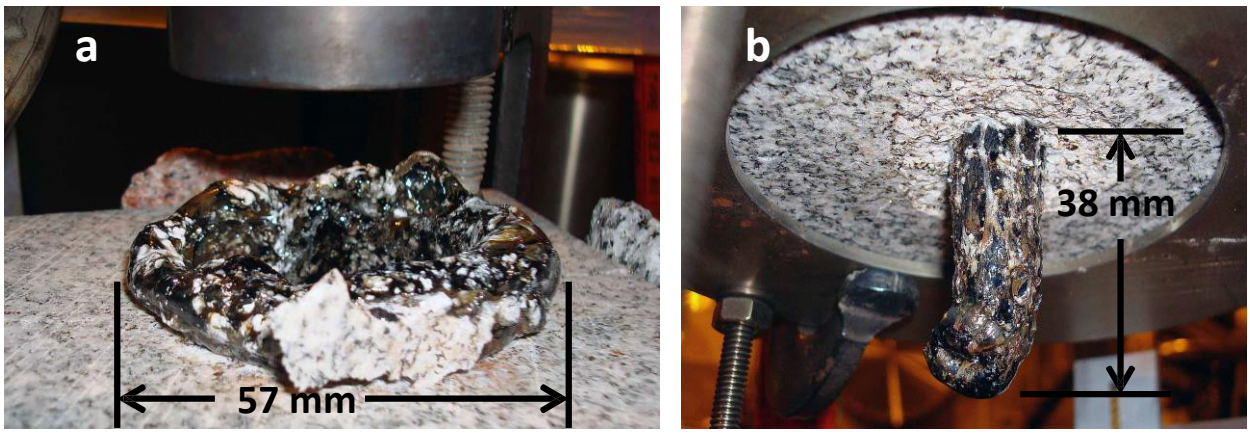


**Figure 49.** Result for granite Rock #35 with ½" (12.7 mm) leak hole after MMW beam exposure of 1.4 to 4.4 kW power and 20 mm (0.787") diameter $TE_{11}$ launch for 106 min- a) top b) bottom

### E. Crucible Test with Broken Granite Fragments

Tests (#9a- #9c) were carried out granite fragments, about 1 cm or less across, in a crucible with a top diameter of 2 ¾" (70 mm). The total starting weight of the granite was 280 g. Figure 50 shows a view looking down on the top of the crucible and its fill of granite fragments before exposure. The melt diameter is about 1.625" (41 mm). Figure 31a shows the crucible and fill after all three tests #9a- #9c. Pulling out the fused congregate of melt and granite it was found that the melt flow extend to about a depth of 1.25" (32mm) below the surface as shown, Figure 51b. The flow occurred with the high viscosity granite melt mostly under the influence of only gravity. If sufficient fracture voids are present or created this suggests that with some force behind the melt and higher temperatures to lower the viscosity, then rock melt could be displaced as a possible alternative to extraction. Alternatively, a directed energy wellbore formation process could include both displacement and extraction depending on the local rock formation environment.

**Figure 50.** Alumina crucible, 2 ¾" (70 mm) diameter, filled with granite fragments before MMW Beam exposure in MMW Beam exposure Tests #9.

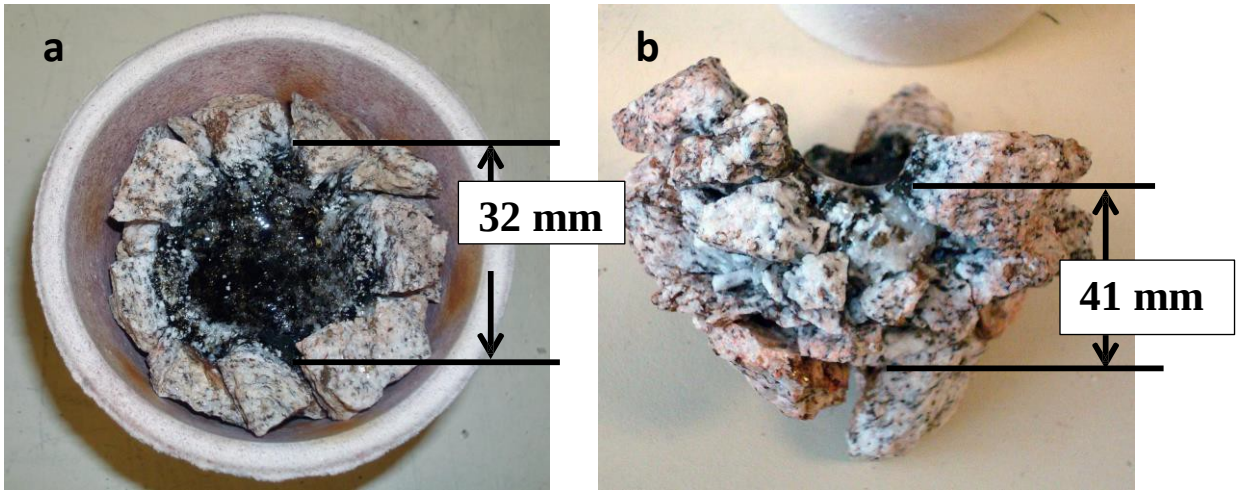


**Figure 51.** a) Top crucible view after MMW beam exposure Tests #9a - #9c up to 3.8 kW power. b) The congregate of melt and rock removed from the crucible.

### F. Discussion

Hard crystalline basement rocks, granite and basalt, can be readily melted with intense MMW energy. We were able to achieve heating, melting, and some vaporization to thethermodynamic limits imposed by the available incident power of 4.5 kW at 28 GHz in 20 - 32 mm (0.79 – 1.28") diameter beams. Temperatures in the 2,000 to 3,000 °C range were routinely achieved, and the analytical and experimental understanding gained indicates that higher temperatures and more material removal could be possible with higher power and/or higher frequencies. The physics and technology advantages of MMWs for full bore well formation as listed in the introduction are reinforced by the studies done here. The absorption efficiency of MMWs over infrared energy was directly observed. In addition we demonstrated for the first time, on a small laboratory scale, the key features of a practical MMW gyrotron system for wellbore formation. These features include backward reflected/scattered power isolation, the introduction of a purge gas flow with the beam, beam collinear real-time monitoring diagnostics, and MMW beam propagation and vitrification in a small granite borehole. These developments suggest that MMW directed energy should finally make full bore directed energy well formation practical where decades of research with other direct energy technologies have not.

## Task 4.0 – Design Key Drilling Components

The purpose of this task was to lay the preliminary designs and base drawings of certain key components and the full system for using MMW technology to drill the prototype test bores and for deep bores in the earth. The outcomes expected were basic concept, drawings and designs of some key components and the overall/ full rig configuration(s) will be the outcome of this effort. Operation and safety concerns will also be outlined for the system. This was accomplished in this task.

The approach utilzed the basic configuration and limitations of the MMW drilling technology was to come from Tasks 1-3. However, delays in completing those earlier tasks while still needing evaluation of the key components required an early **Initial Study for MMW Drilling and Lining** that looked at implementing MMW for drilling and lining in the field. That full report is given in Appendix A. A literature search was also performed to identify prior work in this area.

**Literature Search-**
In the Subterrene Project at DOE Los Alamos National Laboratory (LANL) [71] [95], a series of high temperature rock melt tests were performed using an electric powered tungsten carbide heating probe to melt various rocks. This study was reported earlier. It was found that a liner could be formed only with quartz rock. This restrictionwas not found in the current MMW tests, probable due to the difference in the lower temperatures (just above 2000$^{o}$C) that were attained in their tests versus almost 3000oC in our MMW tests. LANL hypothesized that quartz could be added to get a good melt liner. For our MMW needs, that quartz addition can be done, but if even quartz forms too brittle a material for sealing, then other additives/ materials can be added to form a stronger, more robust liner. This is a mineralogy and high temperature chemistry problem that must be studied further. The strength, brittleness and permeability/ sealing capability of different MMW generated rock melts to form a liner should be later tested.

Branscome [86], also discussed earlier, performed a detailed literature search and theoretical review of high temperature rock properties and tools for penetrating hard rocks.

**Initial Study for MMW Drilling and Lining-**
That Initial Study in Appendix A identified several important requirements for MMW drilling and lining, with a discussion of the key items listed:
1) high efficiency transmission fluid required to deliver the MMW beam from the surface to the bottom of the hole to cause rock removal and minimize wellbore heating;
2) avoid handling of high temperature solids/ vapors in the wellbore and at the surface;
3) absolute requirement to control and minimize water influx;
4) managed over- versus under-pressure drilling was optimal for attaining items 2,3and 4 above;
5) maintain tool alignment and straightness of the waveguide, and therefore wellbore;
6) waveguide construction for efficient transmission; and
7) cooling of the waveguide will be required.

**Waveguide Straightness and Cooling-**
Heating due to inefficient MMW beam transmission is important. Such undesired heating can be caused by inefficient gas transmission efficiency (heating the gas which then heats the waveguide), incorrect beam mode for the waveguide design, or by non-straight waveguides. Gas transmission efficiency will be discussed later. Equations for calculating MMW mode conversion losses due to waveguide imperfections can be found in reference [111]. For straightness concerns, if a bend or crimp in the waveguide occurs that causes a distortion of the beam (i.e., a partial mode change) with a 10% loss of a 2 Mega-Watt beam over a 100 foot bent section, that would cause 200 kilo-watts of power delivered onto that section of pipe, shown in Table 8. Without cooling by circulating water, standard 5” drill pipe, if the power was evenly delivered across that full section, would increase by 204$^{o}$C / 400$^{o}$F in just 8 minutes to the

temperature where degradation of the steel properties begin occurring (316°C / 600°F). Therefore, straightness of the hole that contains the waveguide is critical, otherwise hotspots in the waveguide could develop and destroy the drill string. This also means that any conventionally drilled hole where MMW will be used deeper must be straight enough to provide efficient beam transmission.

**Table 8-** Power Loss Conversion into Waveguide/ Pipe Heating

| Section Length | | Total Power | Power loss | Time 200> 600oF without cooling | | |
|---|---|---|---|---|---|---|
| feet | meters | MWatt | % | Hours | minutes | seconds |
| 1 | 0 | 2 | 10% | 0.00 | 0.1 | 5 |
| 10 | 3 | 2 | 10% | 0.01 | 0.8 | 48 |
| 100 | 34 | 2 | 10% | 0.13 | 8 | 476 |
| 1,000 | 341 | 2 | 10% | 1.322 | 79 | 4,759 |
| 10,000 | 3,408 | 2 | 10% | 13.22 | 793 | 47,593 |
| 20,000 | 6,816 | 2 | 10% | 26.44 | 1,586 | 95,185 |
| | | | | | | |
| **Required rate of cooling Water (80>200oF)** | | | | **11.38** | **gpm** | |

The required water circulation rate to remove this 10% loss (200,000 watts) power loss onto the steel pipe is only 11.4 gpm for a 120°F temperature rise. This can be reasonably accomplished with concentric tubulars. Cooling may also be possible with convection circulation in the annular space. However, this heat build calculation does not include heat conduction up the pipe from the tool head nor heat conduction/ radiation from the annular heated rock wall (primarily lower section).

**Waveguide Material and Design-**

Material, diameter and internal machined pattern of the waveguide are important for efficient MMW beam transmission. The most efficient waveguide beam propagating mode known is the lowest order, linearly polarized, hybrid transverse magnetic and electric field mode, $HE_{11}$ , in corrugated (specifically machined internal surface) metallic waveguide with a diameter at least 3 times larger than the wavelength. The second most efficient waveguide mode with 69% of the efficiency of the $HE_{11}$ mode in equivalent diameter waveguide is the azimuthally polarized transverse electric $TE_{01}$ mode in a smooth walled metallic waveguide. The lowest order linearly polarized mode in smooth walled metallic waveguide is the $TE_{11}$ mode, but it only has a transmission efficiency that is 37% of the best $HE_{11}$ mode.

For all these waveguide modes the higher the conductivity of the metal walls the better the transmission efficiency, with copper being a very high candidate. Some steels can also be candidates for efficient transmission. Note that this material must withstand the pressure and temperatures expected in the wellbore.

For the most efficient transmission, internal machining is required at very specific dimensions and patterns. In the most likely mode cases, a simple screw threaded type machine pattern at a specific thread depth, shape and frequency is required. This is possible today in short length (about 10 feet) sections.

Transmission efficiency also increases as one over the waveguide diameter cubed. Thus the larger the waveguide pipe the more efficient the MMW beam transmission. For a 2mm wavelength MMW beam, the minimum pipe/ waveguide diameter would be (3X) 6 mm (0.24 inches), well below the size needed in wellbore applications. An increase in diameter of only 25% will double the distance to which a beam can be transmitted assuming the same efficiency.

Since present commercial megawatt gyrotrons are designed to launch an $HE_{11}$ mode, corrugated metallic hollow waveguide will be the waveguide of choice.

**Gas Transmission -**
The transmission efficiency of the MMW beam through a gas at the required pressure and temperature was identified in the Initial Study as a key requirement for successful MMW systems. However, data for only nitrogen at a few psi was initially found in the literature. Later Dr. Woskov found additional literature [104][105][106][107] that could be evaluated, but not at the combined frequencies, pressures and temperatures required.

To test transmission fluids, a key component of the system, Task 5 was revised to design and build a Test Cell that was used to test the transmission efficiency of nitrogen and helium at up to 34.5 mega-Pascals (MPa / 5000 psig) and 260$^{o}$C (500$^{o}$F). MIT's Millimeter-wave heterodyne receiver, Boston Electronics 300C Analog Chopper, and Stanford Research SR830 Lock-In Amplifier instruments were on loan to Impact for those tests. That report is discussed further in Task 5. It should be noted that the results of those tests were inconclusive as to quantitative results, but still indicated relatively low losses. This is because the error range of the test was larger than the measured losses obtained.

Based on one literature finding, Dagg, Ressor, Urbaniak [107] that was published in 1973, a new Test Cell design can be utilized for future gas transmission tests. That more accurate Test Cell approach would use a resonant cavity to simulate a long distance waveguide, which reduces the overall % error of the test.

From this work 3 basic drilling methods and tools using MMW beams were outlined-

**MMW Direct Energy Drilling Method #1:**
An early study was performed in support of the earliest and simplest drilling method- to circulate gas down the wave guide (cooling from MMW transmission) and return all injected (cooling of rock and water vapors) and influx gases, rock dust and influx waters up the annulus and to the surface. The base drawing for this simplified Method #1 was given in Figure 5 previously. This method requires full vaporization of liquids and rocks, but the method can be performed in any pressure regime, underbalanced or overbalanced. This method requires no downhole sealing packer and minimal downhole tools. However, it is felt that the inherent problems of this

method outweigh the benefits in either mode except in the case where an existing well has a cased wellbore and MMW is used to deepen or complete the well in a deep basement rock.

The benefits of this Method#1, underbalanced MMW drilling version, are:
1) simple downhole tools;
2) inherently straight wellbore;
3) lower gas compression costs if maintained at low waveguide pressure;
4) lower gas losses to open formations;
5) potentially lower MMW beam transmission losses;
6) use of a lower pressure, but still high power, MMW window for the gyrotron;
7) cooling of the waveguide and the drilling debris is by the injected transmission gas; and
8) analysis of all produced liquids, rock and vapors at the surface would facilitate better understanding of the downhole process.

The problems of Method #1 in an underbalance mode are:
1) maintaining straightness of wellbore with centering and alignment of all tools;
2) the full wellbore is exposed, but influx of formation fluids would occur only where the wellbore was not fully sealed;
3) return pressure could be increased to lower liquid influx, but that may result in significant gas losses into the formation rocks, possible increased MMW power losses to the transmission gas and require a higher pressure rated MMW window or stop drilling;
4) differential pressure for flow is in the wrong direction (into the wellbore) resulting in it being less likely that a fully sealing liner will be formed during the drilling process;
5) water as liquid then as vapor coming up a long open wellbore below the waveguide end (ie., the standoff distance) would absorb a lot of the transmitted MMW beam power before it gets to the cutting surface at the bottom of the wellbore;
6) wellbore stability above and below the wave guide would also be a very serious concern due to hole collapse or, at least, hole diameter enlargement;
7) any hot rock particles over 312$^{o}$C (600$^{o}$F) can cause temperature degradation of the steel pipe on contact, leading to potential pipe holes or failure;
8) if any small % of the generated hot rock is not fully cooled and solidified before it reaches the waveguide, then it will deposit and build up in the long narrow cooler annular space to eventually stick the pipe; and
9) high velocities of the return gases with entrained particulate can create a severe erosion concern;

Method #1 in an over-pressure mode has the following advantages:
1) simple downhole tools;
2) inherently straight wellbore;
3) analysis of all produced liquids, rock and vapors at the surface would facilitate better understanding of the downhole process;
4) differential pressure for liner formation in the right direction (i.e., into the formation) resulting in it being more likely that a fully sealing liner will be formed simultaneous to the drilling process;
5) less erosion concerns due to lower return velocities in the upper annulus;

6) less water (liquid or vapor) in the open wellbore below the waveguide end (ie., in the standoff distance) for more efficient MMW beam power delivery to the bottom of the wellbore;
7) cooling of waveguide and all drilling debris is by the injected transmission gas; and
8) improved wellbore stability above and below the wave guide due to pressure differential and liner formation;

Method #1 in an over-pressure mode has the following disadvantages:
1) Higher gas compression costs;
2) higher losses to any open formations in the full wellbore that are not fully sealed;
3) potentially higher MMW beam transmission losses to the transmission gas;
4) high pressure and high power MMW window required to protect the gyrotron;
5) any hot rock particles over 312$^{o}$C (600$^{o}$F) can cause temperature degradation of the steel pipe on contact, leading to potential pipe holes or failure;
6) any small % of the generated hot rock that is not fully cooled and solidified before it reaches the waveguide, will deposit and build up in the long narrow cooler annular space to eventually stick the pipe.

***Hydraulic Flow and Pressure Modelling-***
Hydraulic analysis of this first / simplest direct energy MMW drilling method and approach required an assumed drill rate (10 meters/ hour or 32.8 feet/ hour) and hole diameter (20.3 cm or 8 inches) that gives a set volume of hot rock per hour. Note that this drill rate requires 4 MMW power levels. Also that all rock is assumed to have a heat capacity of granite and all rock is fully vaporized before getting to the bottom of the waveguide. Then the minimal rate of cooling gas (nitrogen) required to 'immediately' cool the rock vapors to below 312$^{o}$C (600$^{o}$F) to prevent melting and degrading of normal metals was calculated to be 3000 to 4000 scf/ minute. 'Immediate' in this case would be the first 500 feet above the end of the waveguide that can be made of expensive, high temperature materials. This would not prevent deposition of the particulate in the narrow annular space between the cooler rock wall and pipe. Lastly, we performed hydraulic flow modeling with the commercially available Schumberger owned SPT WellFlo modeling program to see if such flow rates were possible and the surface pressures required. The full report of that work is given in Appendix B. Figures 52 to 55 below show one the results for a vertical well with 30000 ft measured depth, 600 °F formation temperature at depth, 0 bpm water influx, 185.3 psig surface return pressure, 3.5 million (MM) scf/D nitrogen injection rate (minimum rate to cool the drilling rock debris).

These sets of hydraulic modelling runs show that lower pressure gas flow on the waveguide is possible under the most favorable circumstances.

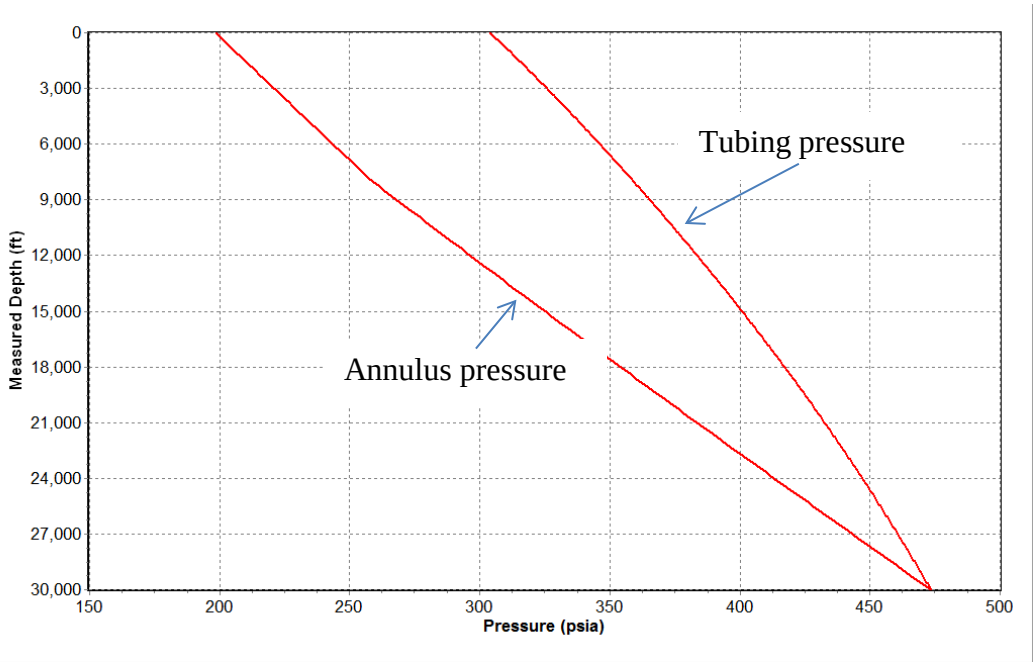


**Figure 52.** Pressure profile (185.3 psig surface return pressure, 3.5 MMscf/d injection rate, 30,000 MD ft well depth, 0 bpm brine influx, 600°F formation temperature at depth)

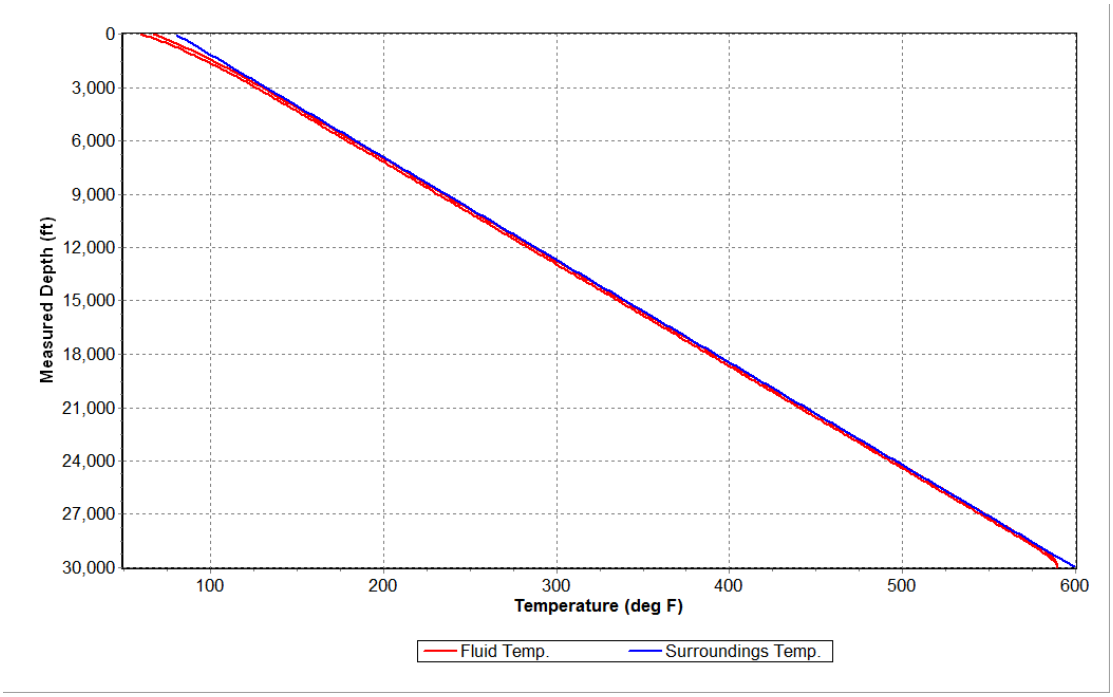


**Figure53.** Temperature profile (185.3 psig surface return pressure, 3.5 MMscf/d injection rate, 30,000 MD ft well depth, 0 bpm brine influx, 600°F formation temperature at depth)

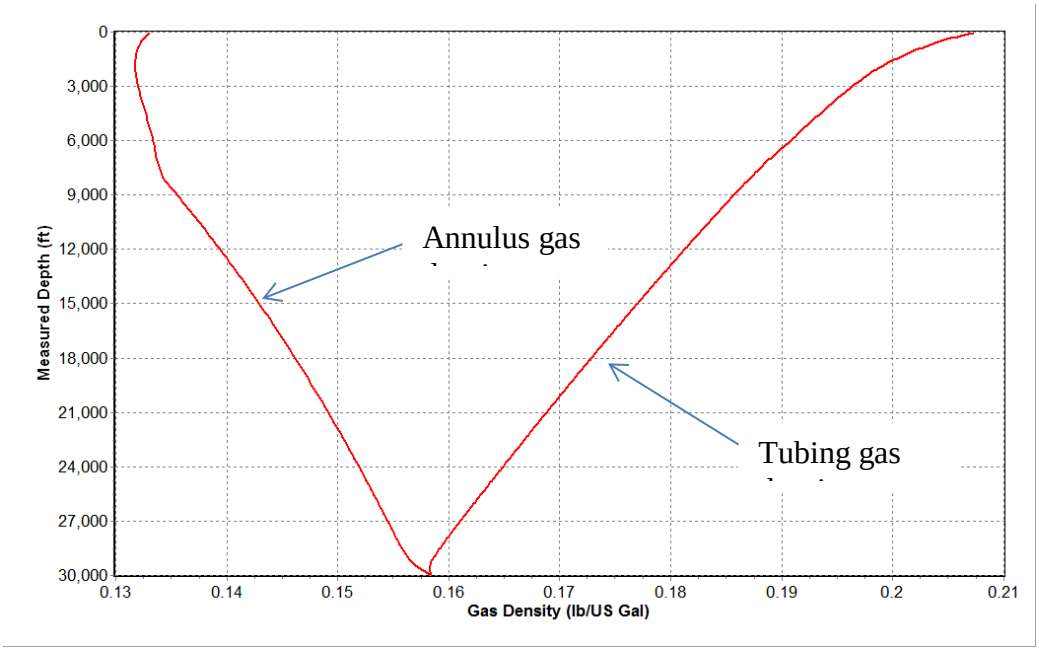


**Figure 54.** Gas density profile (185.3 psig surface return pressure, 3.5 MMscf/d injection rate, 30,000 MD ft well depth, 0 bpm brine influx, 600°F formation temperature at depth)

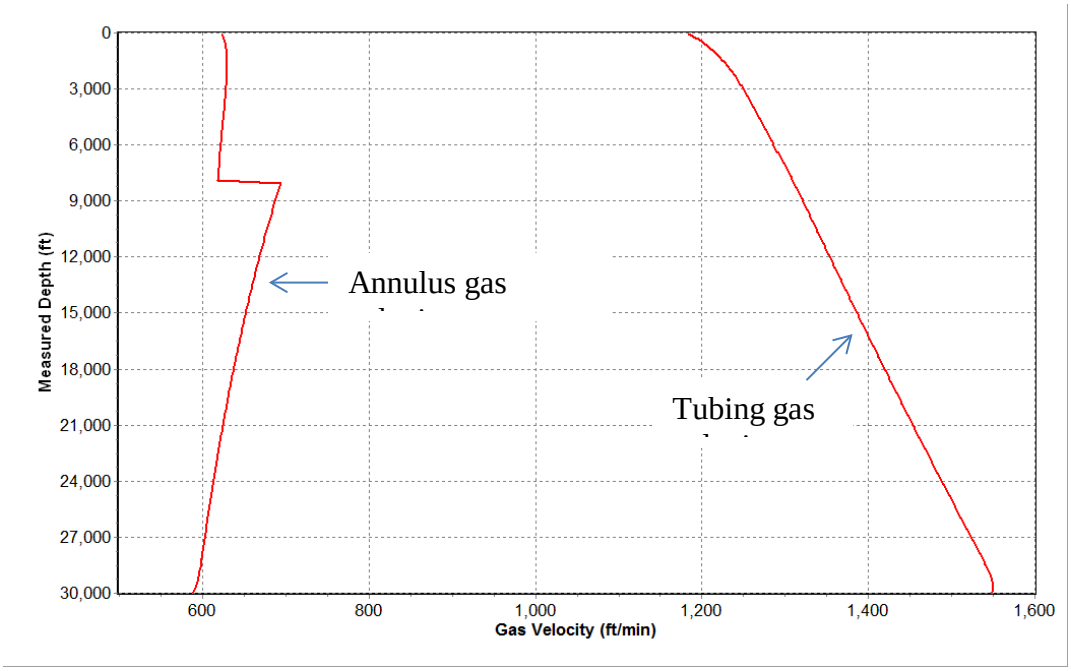


**Figure 55.** Gas velocity profile (185.3 psig surface return pressure, 3.5 MMscf/d injection rate, 30,000 MD ft well depth, 0 bpm brine influx, 600°F formation temperature at depth)

**MMW Direct Energy Drilling Method #2:**
To avoid the water influx and plume of rock particles (fully or partially vaporized) affecting MMW delivered power to the bottom cutting face, other direct MMW energy drilling options of modified managed (over-) pressure drilling were studied. Methods to implement those pressure conditions during MMW drilling and lining were conceived. Figure 56 below shows a modified Subterenne [71][95] version of a heating tool bit/ head that uses MMW power projected from the surface and delivered via a connected waveguide to heat it up to 2000°C to 3000°C to melt and (fully or partially) vaporize the contacted rock and pore fluids. Vaporization creates the pressure required for debris mobilization and removal out into the formation. Heavy-weight drill collars provide downward force on the tool head to counteract generated pressures below the tool head. The tool head is lowered by the pipe in tension as the encountered rock is melted and pushed out of the way. A smooth rock face with constant diameter wellbore and a sealing liner should be developed by this method.

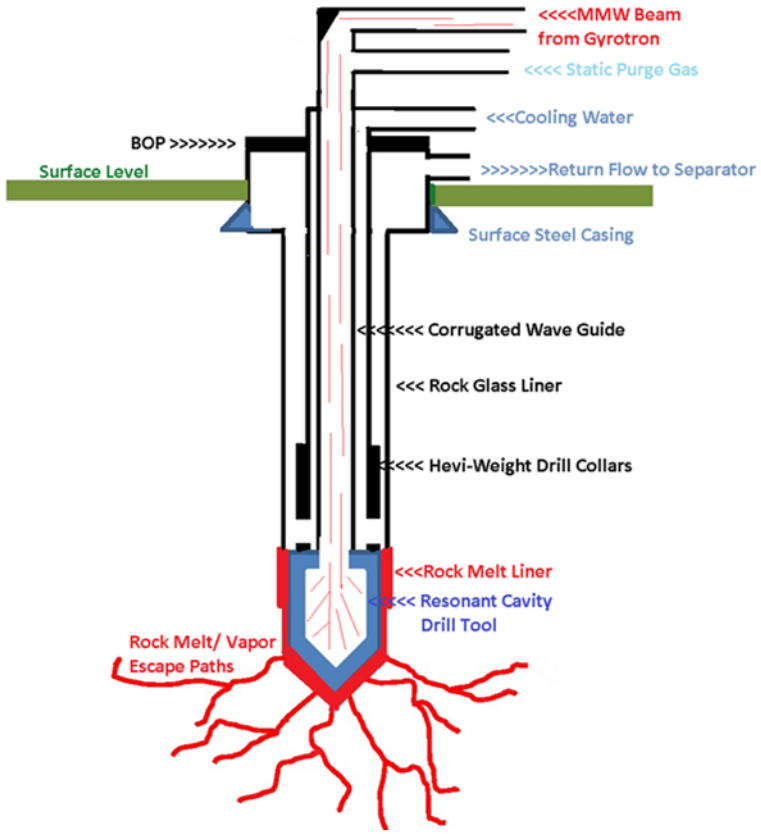


**Figure 56.** MMW Drilling Method #2, Resonant Cavity Drill Tool
Managed Over-Pressure Drilling below Tool

Rock contact, with both heat and abrasion, is mostly at the tool/ head bottom side, but also on the sides to maintain melt conditions. The side length must be long enough to provide a (non-absolute) seal between the tool and the (partially melted) rock wellbore wall to contain the

pressure below the tool. Some heating of the sides of the tool is desired to maintain a viscous rock melt sliding seal, but most of the heat should be directed to the bottom of the tool for drilling. This can be accommodated by the design of the cavity and the MMW beam mode utilized. The internal waveguide can be at low pressures allowing for a low pressure/ high power MMW window. Continued heating of the tool head will volatize and expand fluids and rocks in contact with the tool causing increased pressure below the head which will become much higher than formation pore pressure and rock stresses. This then first forces low(er) viscosity and highly mobile fluids below / ahead of the tool head out into the existing or induced formation pores, then forces slower heated and, lastly, the more viscous rock melt out into those same pores. Only as needed will rock be vaporized to move out of the way. Immediate cooling of the melted and/ or vaporized rock in those pores would form solid glass rock, effectively sealing those pores off from further flow and forming a strong glass rock liner where deposited.

Advantages of Method #2 are therefore:
1) allows lowest pressure waveguide window;
2) low transmission gas compression costs;
3) low gas transmission losses;
3) potentially higher transmission efficiency through low pressure gases; and
4) all high temperature drilling debris kept below the drill tool.

Disadvantages of Method #2 are therefore:
1) temperature degradation and abrasive wear due to the intimate and constant contact of rock melt on the metal/ ceramic drilling tool. Very limited high temperature (3000$^{o}$C and higher) and abrasive resistant materials exist While the highest temperature (3000$^{o}$C or higher) materials would be at and near the bottom of the tool, some high temperatures (2200-3000$^{o}$C) would be needed on the sides as well;;
2) drill rate is set by the maximum temperature possible on the material that makes up the drill tool head. Temperatures near and above 3000$^{o}$C were seen to be required to drill some basement materials.
3) long length of drill tool/ head, where length adds resistance to maintain drill rate; and
4) new method required to monitor and control rock melt viscosity along seal;
5) No surface monitoring of drilling debris for evaluating the drilling process; and
6) higher risk of tool/ head sticking in wellbore.

***Considerations of Requiring Extremely Straight Wellbores-***
Any deviation from a perfectly straight waveguide will degrade MMW beam power delivery to the bottom of the wellbore for drilling ahead. This requires any pipe waveguide to be in tension the full time of operation. This orientation can be vertical or directional, from the surface or a miter bend. Even conventionally drilled wells may have too much deviation (corkscrew pattern is normal) to re-enter successfully with MMW. A small diameter waveguide in tension inside of a large pre-drilled wellbore would minimize the bends and losses in the waveguide. The mode type and corrugation inside the waveguide can also be matched to minimize losses as well, if deviations are anticipated. Note that equations for calculating MMW mode conversion losses due to waveguide imperfections can be found in reference [111].

As discussed earlier, a severe bend can cause the full loss of beam mode and the delivery of the full transmitted power at that premature point. This would immediately melt the waveguide, circulating concentric pipe and fill the wellbore with rock and metal melt.

If either Method #1 were to encounter a high angle fault with vastly different rocks on either side, then differential drill rates would occur on either side with contact. A side force may occur due to this fact, but if the tool is sufficiently strong and long enough, then any deflection would be minor. Once direct physical contact is lost, then other lower efficient heating conditions are expected to occur to balance out the straight drilling process. Other direct MMW – rock interaction methods discussed may be more affected by this problem and would require drilling slower or taking more time to melt a full straight wellbore in this problem section, once identified.

***Considerations of Rock Removal during Over-Pressure Drilling-***
It is known and it was confirmed in this study that rocks becomes thermally stressed and will fracture when differentially heated very rapidly. Heat first degrades the strength of the rock before any significant melting occurs. Differential rock heating can occur by direct MMW beam contact, contact with the heated tool/ head, or contact with rock melts or vapors. Reduced rock strength, high over pressure and thermal fracturing should allow easier hydraulic fracturing of the rock by melts and vapors at this unconfined near wellbore position. In addition, the surrounding rock that becomes in contact with the flowing rock melt or vapors will be 'thermally affected' and pressure allowing extended fracturing. Once the melt or vapors get in contact with the cooler surrounding rocks, they would form a solid sealing rock glass plug in place.

Rock degrading process-A quick calculation of rock volume for drilling shows that for each 31 centimeters (1 foot) of drilled granite rock with 5% porosity to create a 20.3 cm (8 in) diameter hole, a total volume of 10,025 $cm^3$ (612 $in^3$) of rock would be removed (assuming no increase in volume due to heating).

Rock debris removal process- If no natural porosity or permeability exists, an induced dual-winged (mostly) vertically oriented (emanating mostly both up and down the exit pressure point) fracture with an azimuth perpendicular to the minimum stress within the formation would be formed for the melt/vapor flow to escape. If this fracture was 0.5 cm (0.2 in) wide and the same 31 cm (1 foot) tall, each wing would need to be 323 cm (127 inches) out of the wellbore to contain all the displaced melted/ vaporized rock. This assumes all rock melt goes into this one dual-winged fracture.

Creating of that fracture(s) and depositing the displaced rock would be very complex and dependent on the rate of rock melt creating, pressure differential, rock melt viscosity, temperature difference of the rock melt above its melting point, gas content and other impurities, temperature of the surrounding rock and many more factors. As the liquid rock melt or vapors initiates the fracture at the wellbore wall, it would penetrate into this newly opened fracture and quickly (dependent on temperature difference above melt temperature) solidify along the cooler walls, filling the void with rock glass if very thin or partially filling it if the fracture is wider. New liquid rock melt would continue to extend the fracture around this plug in the same

direction as before with entry then cooling along the newly created cool rock walls. If the resistance along this direction becomes too great, a new fracture direction out of the wellbore would be created, but one that would quickly reorient itself to become parallel to the original fracture path, due to insitu rock stresses. By this redirecting process, it is favorable that a $360^{o}$ rock melt glass pattern around the immediate wellbore could be formed.

Alternatively, if the rock has a natural porosity (assume 15%) and high permeability, the hot rock liquid melt may enter and become evenly distributed in the surrounding rock porosity/ flow paths due that immediate cooling and solidifying. The resulting rock glass wall would exist 16 cm (6.33 in) around the wellbore in the rock pores. Such a rock melt glass wall in a 25% porosity rock would be 10 cm (4 in) thick. The flow of rock melt and its interactions and effects on the native rock are very complex, but the near immediate solidification of the melt front upon contact with the cooler native rock would seem to favor a uniform distribution around the wellbore.

***Considerations of High Temperature/ Abrasive Resistant Materials-***
Sealing and containing the high pressure created by the heated rock and fluids below the tool head occurs on the tool's side length. This requires some minor but constant heating of the tool head sides to maintain a viscous liquid rock melt forming a seal to the tool head. Note that some pressure in the annular space is acceptable and even desired, but melt above the tool may cause some problems.

More research is needed on the materials in contact with this melt as they are the limit to the drill rate and the life of the MMW tool. Materials that can withstand both such high temperatures and abrasion are the concern and are very limited. Much more research will be required to find suitable materials. Tungsten properties are- melting temperature $3422^{o}C$ ($6191^{o}F$) melt temperature; 183.84 atomic mass; specific density of 19.3; thermal conductivity 173 W/m/K; ductile when pure but brittle in most alloys). Carbon / graphite also has a very high melt temperature, but it sublimes instead of melts. Mixtures of Tungsten and Carbon form Tungsten Carbide (a ceramic and not a metal), which is an important alloy for high temperature applications. Ultra High Temperature Ceramics (UHTC) are the general classification of such materials. This classification includes hafnium-dibromide ($3300^{o}C$ melting temperature) and zirconium di-boride ceramics. Silicon carbide and silicon nitride are also possible materials for the tool head for this drilling method. [Wikipedia] It is suggested that DOD, Oak Ridge and NASA laboratory be engaged to help find suitable materials in future ongoing research.

The shape of the cavity and bottom of the tool will also need to be studied for optimal heating.

***Considerations of Traversing Large Fractures/ Caverns-***
Another problem that would be encountered in drilling in the earth is large fractures or caverns filled with (salt) water and some gases. This Method #1 sealing method requires rock contact somewhere along the tool head side length. If the length is long enough this will occur successfully. If not, then the pressure cannot be contained. In addition, the surrounding water would drain away MMW beam delivered energy that is required to melt the forward rock and thus drilling would effectively stop. Methods to retrieve the head would be attempted but the cooling water contact may prevent that effort. If the tool head can be retrieved then plugging

agents can be put in place across and above the problem zone. A new head would be run and the plugging agents would be melted to enter the fracture/ cavern near the wellbore, immediately cool and solidify until a seal is formed. This process may require repeating until successful and allowing continued drilling ahead.

The shape and structure of the plugging agents placed in the wellbore at bottom is important and will be discussed later in this section. Long hollow tubes or large beads (large enough not to fall out of the wellbore) are needed. Placement of such structures would be by wireline or by pumping down. Material composition would be silicates/ quartz, metals and natural rock minerals/ materials of low melt temperature, but high melt viscosity.

***Circulation for Cooling –***
The wellbore annulus in all methods is sealed for well control purposes. In Method #2 it is by the rock melt liner, the surface valves and the tool head seal- and is therefore static. Heat conduction from the rock melt out into the formation would be the only natural cooling method, but this is fairly slow. Heat conduction up the pipe(s) from the tool head is a concern in using the more common steels and metals. Therefore, circulation will be needed to cool down the rock wall that forms and the normal metal pipe/ waveguide. This requires concentric pipe and some very expensive high temperature pipe on the bottom. This liquid circulation also cools down the waveguide from MMW power transmission losses, previously discussed. Any water leaks into the waveguide will adversely affect MMW power delivery.

***Considerations of Stuck Tool Head and Pipe-***
Recovering the tool head if it fails due to wear (reduced diameter or hole in the tool body) will be required. If fluids enter the waveguide or interior of the tool head, then it cannot be heated further and the rock melt around the tool head will solidify and stick the tool. If the sides of the tool head are not kept hot enough, then the tool head will stick in the wellbore. In these cases, the drill collars and/ or concentric pipe must be cut as deep as possible to allow their removal. Cutting of concentric pipe is problematic. Then a whipstock tool made of the highest temperature material and with a sloped face would be set above the remaining stuck equipment to force an offset around it. That offset would cause a bend in the waveguide with a permanent loss of waveguide efficiency. This requires a long bend radius to get around the 10 inches offset, depending on the MMW beam mode and waveguide corrugation used. A new tool head would then be run and drilling ahead could continue.

**MMW Direct Energy Drilling Method #3:**
Figure 57 shows a drilling head/ packer for a MMW drilling system that also utilizes high over-pressure to cause the correct pressure gradient direction into the formation to form a good solid glass rock liner/ seal. In this case the high pressure is below the packer seal and also transmitted up the waveguide to the surface. Therefore, a high pressure, high power window is now needed at the surface gyrotron. The wellbore diameter is controlled by the MMW mode and power level. In this case the well bore has a sealing glass rock melt liner created by the overpressure while drilling, but it is not at a constant diameter with smooth even wall. Weight on the drill tool head is provided to offset the high pressure below the packer. That force is furnished by the heavy walled drill collars (still with flow channels) above the tool. The upper drill pipe is kept in

tension to keep it straight. Circulating cooling flow is not needed as critically as in Method #2, but still needed for MMW transmission losses and rock wall cooling. The annular seal is formed by the bottom of the packer head onto a rock melt ledge. That rock melt ledge is formed from the last bottom location before the drill head is lowered the next round. When the drill head is ready to be lowered to the new bottom, special melt material can be added to the bottom of the hole, a MMW mode convertor (to a wall hugging mode) is inserted to slowly heat up the drill head bottom face and melt the existing upper rock ledge. The bottom of the wave guide may also be sealed during this operation. Once break-through of the upper ledge occurs, the drill head is lowered to the new bottom and sealed onto the new rock bottom and additives by heating and slowly lowering the tool once again. The mode convertor and sealing plug are retrieved and drilling ahead then resumes, at first slowly with reduced power levels due to the low open-hole volume and short standoff distance.

Required surface gas transmission pressures in the waveguide in Method #3 are expected follow the fracture gradient, the pressure required to hydraulically fracture the subsurface rocks. In many cases the fracture gradient is about 0.8 psi/ foot of depth (much higher than the normal pore pressure gradient) until high rock temperatures are encountered, but this is highly variable. Reducing that downhole pressure by the fluid column of the transmission gas at pressure and temperature yields the static surface pressure required for that downhole pressure. Transmission gas type and density are not known, but nitrogen at such high pressures would be close to that of water or 1 kPa/m (0.433 psi/ft). In all fluids, higher temperatures (due to normal gradient or MMW losses) would reduce its gravity and that fluid column gradient, increasing the required surface pressures. Therefore, the estimated required surface pressure of the gas transmission fluid in the waveguide on this difference basis would be – 3 km (10,000 feet) is 25.3 MPa (3,670 psi); 6 km (20,000 feet) is 50.6 MPa (7,340 psi) and at 9 km (30,000 feet) is 75.9 MPA (11,010 psi). As discussed, the thermally weakened rocks due to normal thermal gradient and MMW heating may significantly reduce this required surface hydraulic pressure to fracture the subsurface rock. This will only become known upon field testing.

The advantages of this Method #3 are:
1) full open path to bottom of hole allowing tool/ survey runs or insertion of plugging or transmission enhancement material additives;
2) shorter open wellbore sections which may be possible inefficient waveguides;
3) simple well diameter control method utilizing inversed MMW power density with increasing radius squared relationship;
4) only one controllable ‘high’ temperature metal seal section, that is non-moving and minimal abrasion during operation, is required;
5) cooling of the rock near and above the packer tool is not as critical;
6) Pressure developed by voliotales pushes all moveable material out of the drill path and into surrounding rocks; and
7) direct efficient MMW beam to rock contact and transfer/ converion of energy to heat.

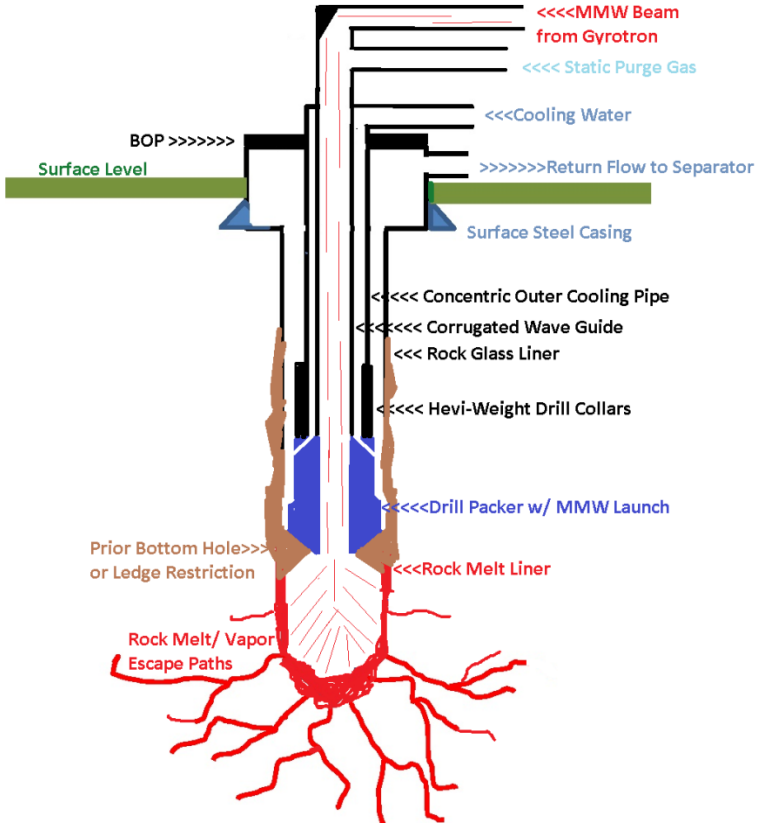


**Figure 57.** MMW Drilling Method #3a
Managed Over-Pressure Drilling with Bottom Seal Packer Tool

Some of the disadvantagess expected with Method #3a are the same as with Method #2. The disadvantages of this Method #3a are:
1) non- smooth diameter pipe walls with restricted diameter ledges where the packer was set;
2) direct rock melt contact to metal seal required, even if controlled;
3) additives may be needed to coat the open wellbore to improve transmission efficiency;
4) high cost gas compression for the high pressure (7000-11,000 psi) gas transmission;
5) finding a high efficiency transmission gas for the anticipated pressures;
6) obtaining high pressure concentric tubulars may a problem, especially if at high temperatures;
7) higher pressure gyrotron window is required that does not currently exist; and
8) less control over drill rate due to variable standoff distance from the waveguide end, such that drill rate affected now by beam power level, rock type heat capacity, and dielectric properties of the open hole rock wall.

The immediate concern is the requirement of a high pressure, high power window where none exists today. Wellbore wall smoothness may not be as fully rough as expected, since MMW beams do not like interference in its path and will focus on removing it. Some special high temperature pipe will be needed just above the drill head due to heat conduction during moves.

Another version of this fixed position Drilling Sealing Packer Tool with a bottom rock melt-packer seal has a sliding seal element within the Tool's internal bore that allows the waveguide to be extended downward as the drilling progresses. The sliding seal may be connected to the Packer Head or be floating on the waveguide. This Method #3b version keeps the standoff distance more constant and the drilling process more controllable. The modification of that Tool for this application is given in Figure 58, below. Not shown, that Head/ Packer may have an internal flapper valve that would close if the waveguide is pulled out.

**Additives for MMW Drilling:**

Several problems are immediately clear in drilling with MMW using the above methods. First is the problem of encountering large volumes of water in fracture/ caverns or just high permeability sections. Such contact of water with the MMW beam will create steam or supercritical water that can enter the wellbore/ waveguide and stop the drilling progress. Otherwise that steam/ hot water will be pushed out into the formation and new cooler water will enter the beam path with the same outcome of stopping drilling. Rock formations that vaporize over melting, such as limestones, may not form a full rock melt wall seal. Additives, that are non-soluble at elevated temperatures, must therefore be added to the wellbore and melted to form a new wellbore wall. The key features of this process are: material, construction and placement. The pre-melt shape and structure of these additives/ plugging agents that are placed in the wellbore is important. Long hollow tubes or large beads/ balls are needed to form a large flow path downward to allow additive melts to flow down and eventually enter the problem zone, where it will cool and solidify. The stacked height of the additives (i.e., volume of additive material) in the wellbore should reflect the anticipated volume needed to seal the problem zone. Placement of such structures would be by wireline or by pumping down to be above or at the depth of the problem zone.

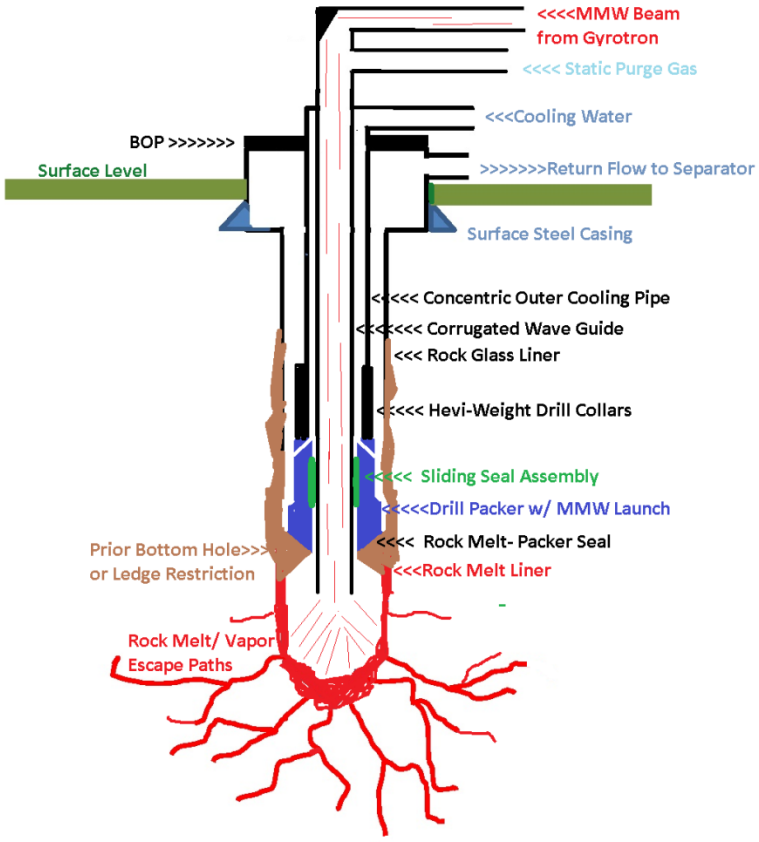


**Figure 58.** MMW Drilling Method #3b
Managed Over-Pressure Drilling with Fixed Bottom Sealing Packer Tool
and Slideable Waveguide Position

Favorable material composition would be silicates/ quartz, metals (e.g., copper) and natural rocks minerals (basalt)/ materials of low melt temperature. In some cases a high melt viscosity would be favorable. In general, the additive's melt temperature should be lower than that of the surrounding rock so that melting the additive is more likely than enlarging the wellbore diameter. Overpressure MMW drilling techniques would be required to melt the additives and force the melt into the problem zone near the wellbore. This process may require repeating until sufficient volume is placed into the problem zone and successful sealing is ensured that allows continued drilling ahead. Very thick problem zones would also require multiple treatments. The general steps are:

MMW drilling and lining (using Method #3b as an example) encounters a high water content problem zone or a zone that did not seal with virgin rock melt only, that then causes a stop in the drilling progress-

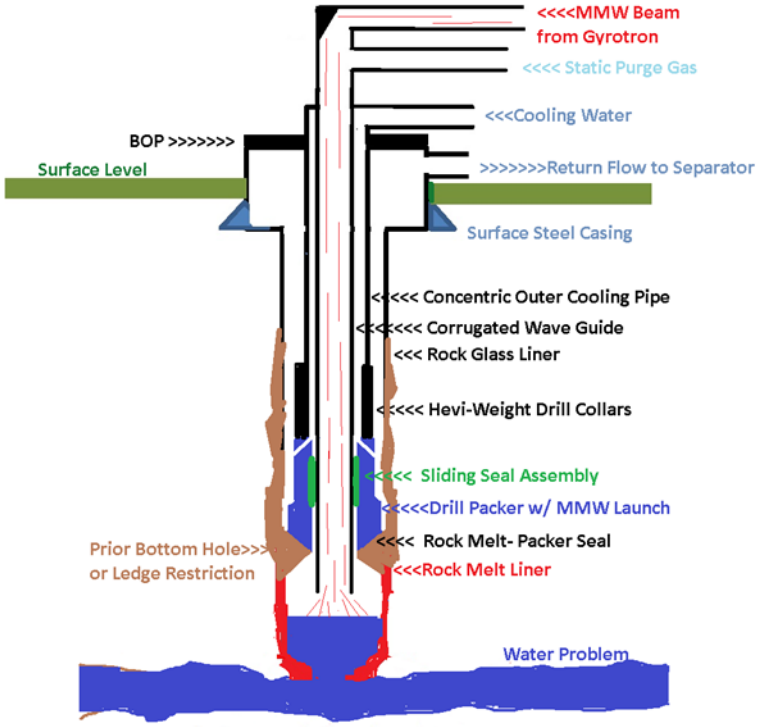


**Figure 59.** MMW drilling encountering a Problem Zone with High Water Content

Additive tubes are deposited at the bottom of the wellbore after drilling stopped-

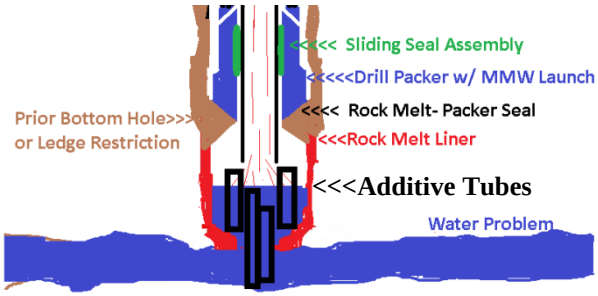


**Figure 60.** Inserting Additive Tubes at the bottom of the Wellbore

MMW power is slowly started which first vaporizes the water and forces it out of the wellbore, then melts the additives which flow downward with gravity and gas pressure. The melted additives occasionally re-solidifying until the MMW beam re-contacts it. Ultimately it reaches the problem zone where it is immediately cooled by the available water. The cooled re-solidified additive material builds up in the problem zone near the wellbore to start a wall. Multiple treatments may be needed to get enough volume of additive melt into the problem zone and form a competent seal. Drilling can then be resumed through the problem zone, Figure 61.

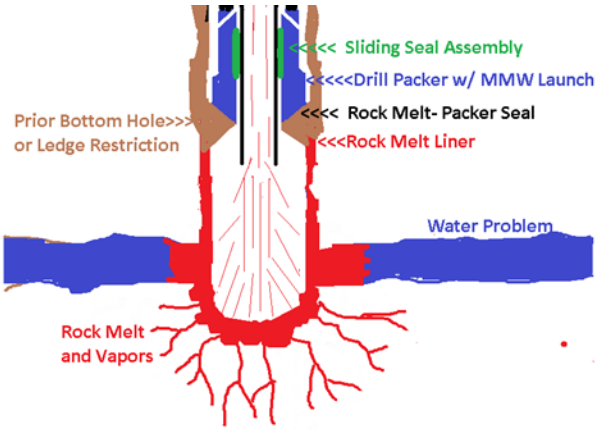


**Figure 61.** Problem Zone sealed off with Additive Melt and MMW Drilling resumes.

## Task 5.0 – Prototype and Test Drilling Components

The purpose of this task was to build and test selected key components of the drilling system. The original approach was to utilize Task 1-2 lab tests results, Task 3 rock evaluations and Task 4 concepts, designs and procedures to then preform Task 5- prototype and bench test selected key components. The amount of prototyping and testing depended on budget constraints and availability of the right gyrotron. However, the delay in getting the bench test system up and running and the lack of rock specimens to test prevented that work from being done. Therefore an Initial Evaluation Study of MMW Drilling and Lining Systems was performed to identify the key research needs and methods for MMW drilling and lining. That study is given in Appendix A and its key findings were discussed in Task 4. One of the key findings was that selecting a high efficiency transmission fluid was a critical path for MMW development. Since data for only nitrogen at a low pressures was initially found in the literature, it was determined that a Test Cell must be designed and built to test various gases for their transmission efficiency at the pressures and temperatures expected in the field. Therefore, to test transmission fluids, a key component of any MMW system, Task 5 was revised to design and build a Test Cell that was used to test the transmission efficiency of nitrogen and helium at up to 34.5 mega-Pascals (MPa / 5000 psig) and 260$^{o}$C (500$^{o}$F) in an electric furnace at Impact. This 1 meter (36 inch) Test Cell with an internal smooth wall steel waveguide was designed and built. Testing was accomplished using a millimeter-wave heterodyne receiver, Boston Electronics 300C Analog Chopper, and Stanford Research SR830 Lock-In Amplifier instruments that were on loan from MIT to Impact for those tests. Figures 62 through 64 show this test equipment at Impact's Tulsa shop.

In this testing process, a quartz window broke due to the combined high temperature and pressure on the upper end of the test envelope, see Figure 64. This endangered the expensive heterodyne receiver. Minimal additional testing was conducted with a dual quartz window on each end using both helium and nitrogen. It should be noted that the results of these tests were inconclusive as to quantitative results due to the test errors being greater than the instrument accuracy, but they still indicated relatively low losses.

**Figure 62.** Insulating the high temperature electric furnace at Impact.

**Figure 63.** Waveguide ending at nitrogen cooled black body during calibration.


**Figure 64.** Cracked quartz glass before converting to a double window design.

Based on one later literature finding, Dagg, Ressor, Urbaniak [107] published in 1973, a new Test Cell design should be utilized for future gas transmission tests. That more accurate test cell approach would use a resonant cavity to simulate a long distance waveguide, which reduces the overall % error of the test. Their design is given in Figure 65 below.

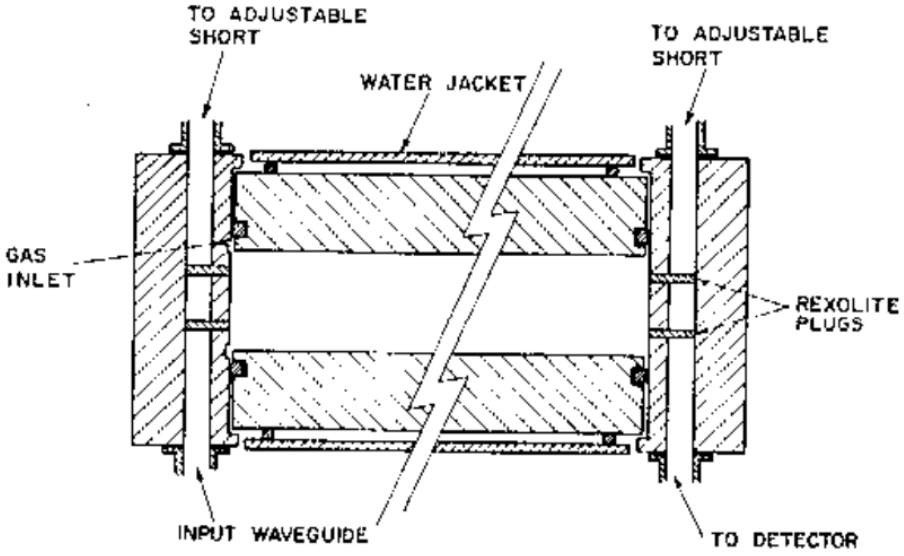


FIG. 1. The 70 GHz resonant cavity.

**Figure 65. D**esign of a Resonant Cavity Test Cell after Dagg, et. al. [107]

## Task 6 – Evaluation of Project MMW Drilling / Lining Testing

The purpose of this task was to evaluate all laboratory, shop and field test data in the project for understanding and optimization of the MMW drilling and completion process for feasibility of commercial utility. The approach was to: collect all theoretical calculations and understandings of the processes at work in MMW drilling; collect all bench test data and results performed in the project; collect all theoretical and resultant liner formation and evaluation (logs, thickness, strength, chemical composition, etc.) data; collect all theoretical implementation designs and shop prototyping and performance data; then evaluate all data for safe operations, effective environmental protection, optimal and possible operational envelopes. Determine specific areas of research and design needed to move this technology to commercialization. This work was successfully accomplished and was discussed in earlier Tasks.

However, in addition to the above effort, this task was to evaluate operational efficiency, costs of operation and cost/foot metrics; evaluate all data for liner formation, thickness, strength, and sealing effectiveness; make cost and efficiency metric comparisons to current drilling and liner practices; develop a full realized operational envelope with costing and comparison to current drilling and liner installation practices sufficient to identify that continued research required or commercialization efforts should be started. These actions could not be done due to delays in MMW bench testing and lack of non-fractured rock samples for testing. However other investigations were accomplished in their place.

***MMW Drilling and Lining Processes-***

The MMW drilling processes as now envisioned will use a chromatography separation process to reduce and remove the rock in progressive increasing temperature states. This temperature will be set by residence time of a given rock mineral particle in the wellbore, by the MMW power level, and by the particle position in the wellbore (on wall or at the bottom) relative to the MMW mode type. Fluids in the pores will vaporize immediately and be forced out into the surrounding rocks pores or induced fractures. The lightest rock mineral components will melt or vaporize first and move out of the wellbore path into the surrounding formation rock by pressure. The heaviest components (as compared by melt temperature, viscosity at temperature above melt, and vaporization temperature) will remain in the wellbore path until sufficiently heated and melted to move out of the way, but they will be last and will push the prior lighter components even deeper (reheating and melting them upon contact, if needed). A thick build up of unmobilized heavy ends will block MMW waves from contacting new rock, until they are heated sufficiently to mobilize. These heaviest component will set the drill rate and form the majority of the final rock melt/ glass liner around / in the wellbore wall. They are therefore the most important mineral component to understand (% distribution in rock and their melt temperature) in the rocks to be drilled. This will take more involved rock mineralogy and volcanic (rock melt) research in the future.

**Benchmarking with Specific Energy-**

First used by Maurer [1,2] for all drilling, and most recently for conventional drilling by Mensa-

Wilmot [109], mechanical specific energy (MSE) as a drilling efficiency (DE) quantification methodology, is defined as the energy input per unit rock volume drilled. MSE is an evaluation tool that focuses only on the mechanical aspects of DE, with the minimum being desired. Researchers at the DOE- NETL's Extreme Drilling Lab recognized that the traditional MSE equation consists of a set of interrelated parameters (eg., weight on bit, bit type, rock type, revolutions per minute, hydraulics, etc..). Hamrick [108] expanded upon that effort, re-writing the MSE equation in terms of each parameter and adding bench testing data.

From an overall efficiency drilling (DE) standpoint, MSE is not the sole consideration since other factors may supersede MSE reduction strategies- improvements in downhole tool life, borehole quality, directional drilling, hole cleaning, vibrations control and transitional drilling. In all of these instances, the effect of ROP on MSE and the subsequent association to DE are overshadowed by the need for improved operational efficiency. Most of these issues are deemed more critical than MSE minimization, but can be effectively addressed during project planning of conventional well drilling. Hydraulics also plays a key role in any drilling process.

MMW drilling via melting or vaporization has few of those other issues (except for tool material strengths), thus comparison to conventional drilling methods must be on the efficiency of the overall process of: 1) rock dislocation and 2) removal of failed rock. That combined process depend on formation hardness and are heavily influenced by both mechanical, hydraulic and thermal factors. Removal of failed rock is heavily dependent on hydraulic (flow rate, velocity, viscosity) factors in conventional drilling systems. In the MMW drilling systems discussed herein, 'rock dislocation' is rock melting and, if needed, vaporization. There is a large range of energy requirements required for that process, but it deals with finding the lowest energy required to reduce the particle size and melt viscosity to allow removal from the cutting face. MMW's version of 'removal of failed rock' is a function of that particle size / viscosity, the self-generated (by vaporization) pressure differential into the formation and rock fracture pressure. On this basis, conventional bit bench tests can be compared to the current study's pre-drilled drain-hole MMW beam bench tests based on net power delivered to the rock.

Only granite and basalt samples were fully drilled through enough to overcome the initial heating effort as being dominate. In addition, heating was continued past end breakthrough. Therefore, these MMW rock tests had significant 'end effects' which will lower the overall efficiency. MMW granite Rock #33 test had 1915 watt-hours= 6.894 Mega-Joules of generated energy to melt and move (by gravity only) the rock to 'drill' a hole through the full sample. Much of this energy was used to start heating up the rock at the beginning of the test and was therefore not at a steady-state condition. Also, only about 50% of that gyrotron power was actually delivered energy to the rock (ie., deducting energy lost in the waveguide or reflected). Much of the reflected energy in an actual deep wellbore would remain in the wellbore to perform additional heating.

On a weight basis Rock #33 started with 895.5 grams, with the pre-drilled hole installed, and 686.7grams at the end of the test for 208.8 grams of granite rock removed. This is a generated specific energy of 33 kilo-joules/ gram for granite in Rock #33 tests and a net power specific energy closer to 16.5 kilo-joules/ gram.

On a Volume basis: Rock #33 removed a net rock volume of 81.97cm$^3$ (32.27in$^3$). The specific energy based on power generated at the gyrotron would then be 84.1 kilo-Joules/ cm$^3$ (216.4 kilo-joules/in$^3$), or about 42 kilo-joules/cm$^3$ (108 kilo-joules/in$^3$) based on net power delivered.

In comparing MSE values in the literature from Hamrick [108] and the DOE DeepTrek study, the average mechanical specific energies (MSEs) were 94.6 to 324 ksi (ksi is assumed to be 1000 lbm-force per square inch, for 4.57 to 15.5 kilo-joules/cm$^3$ and higher) that included Basalt (240 MPa/ 34.8 ksi unconfined compressive strength, UCS) and sandstone (131 MPa/ 19 ksi UCS). The most efficient MSE from Deep Trek Test #28 was 7.173 kilo-joules/cm$^3$ (150,000 ft-lbs/ft$^3$). Therefore our MMW bench test on Rock #33 was 3 times higher in these reported MSE conventional drilling values, but still within reach using the anticipated higher power and more optimal frequency in upcoming tests.

**Cost Estimating-**

Capital cost estimations for a deep 23,000+ft MMW drilling rig are based on the US Air Force 2 MW 95 GHz gyrotron system currently under development, total weight of 1900 lbs, that costs $2.1 MM [59][60]. Note- a 1MW gyrotron system cost is listed by one manufacturer at $1.1M. Downhole piping/waveguides may cost $2.3M (at $100/ft); specialized small rig structure, injector head, tools and controls may cost $8M; and generator, compressor and pump systems may add $7.5M. Total capital costs for this first deep rig are thus estimated at $20M, which amoritizes to $100K per well or $4.3/ft when amoritized over two hundred (200) wells that each reach 7 km (23,000 ft).

Operational expenses are estimated from- Electricial costs involved in drilling each well with an 8” bore, at 50% electrical efficiency, and 70% absorption would correspond to 4.5x106 kW hrs or a total electricity cost of $450,000 (at a cost of $0.10 / kW-hr) or $64/m ($20/ft) drilled per the same amortization.

Thus total drilling only costs (normally 1/3 of total well costs, but with lower interval casing/cementing now not needed and testing not included) would be estimated at about $72/m ($24/ ft) drilled. A 2X increase for profit, losses, repairs, downtime, etc.. would raise it to $144/m ($48/ft) drilled. For comparison, Impact estimated drilling (rig, drillpipe, bits, fluids) cost of a 21,000 ft EGS wellbore ending in a 7-7/8” bore in the GEECO study [70] at $286/ ft (for drilling only or 33% of $21M total well cost). In addition, such a MMW wellbore may already be suitably lined/ ‘cased’, forgoing the need of lower zone steel casing and cementing costs. Its monobore capabilites allows for a reduction in the upper casing sizes and bored holes.

**Future Research Needs and Directions-**

Based on this work and theoretical considerations, testing at higher frequencies is required to get to field prototyping and commercial operations. Higher frequencies and the larger gyrotrons will allow direct utilization of optimal modes, provide a higher transmission efficiency and prove MMW beam-rock coupling efficiencies. Higher power- 100 kilo-Watt, 500kWatt, 1 MW, 2 MW continuous gyrotron units are commercially available in the 95 GHz frequencies. The DOD-Army has 100 kiloWatt 95 GHz gyrotrons in use for fixed and mobile applications, see Figure

56. DOD also has a 2MW, 95 GHz gyrotron full unit designed and partially assembled for mobile use. Impact and MIT are working with DOD- AFRL in a follow-up DOE project, DE-SC0012308 to utilize their 100kWatt, 95 GHz gyrotron. New waveguide components are required to be designed and built for this work.

**Figure 56.** DOD- Army's existing System 1
95 GHz, 100kW mobile gyrotron unit for "Active Denial'

It is critically important that a gas or fluid is found that can efficiently transmit MMW power at 95 GHz at high pressure, 13.8 to 82.7 MPa (2,000 to 12,000 psi), and high temperatures, 24 to 316 $^{o}$C (70- 600$^{o}$F) . Losses less than 10% of the generated power are desired to minimize waveguide heating. Nitrogen, Argon, Helium and possibly Hydrogen are potential gases for this function. Other liquids are also potential. The Dagg [107] resonant cavity test cell design should be utilized for this testing, to be done at MIT. The gas transmission capabilities will set the method of MMW drilling and lining.

It is critically important that a high power (2 MW) 95 GHz window be developed at increasing higher pressures to meet those commercial levels. This window capability will also set or limit the method of MMW drilling and lining. Various designs have been studied and considered. Any pressure capable window will allow surface testing under some pressure to better simulate the desired MMW drilling and lining system.

Larger samples of MMW melted rocks are needed for physical strength testing in the upcoming higher GHz testing. A large number of samples of each rock type are required for these tests. To obtain such samples, longer and wider rock specimens that are enclosed in steel pipe (to reduce fracturing) are required. Some shale samples, not tested in this project, should also be included.

High temperature materials should be identified and specified for contact points of downhole tools and rock melts. Abrasive resistant materials at these elevated temperatures may also be needed for some MMW drilling and lining methods identified. Sandi National Laboratory, Oak Ridge National Laboratory, and National Air and Space Administration should be contacted about such materials.

# CONCLUSIONS

Millimeter wave in the 30 to 300 GigaHertz (GHz) frequencies or 1-mm to 10-mm wavelengths ($\lambda$) are favorable for drilling and lining wellbores. The experiments have reinforced the feasibility of MMW directed energy for full bore well formation. This is in addition to the previously identified physics and technology advantages of using the MMW range of the electromagnetic spectrum for this application [83]. The physics advantages include: 1) the capability of MMWs to propagate through infrared obscure, small particle plumes without scattering, 2) the higher efficiency of MMW absorption by melted rock relative to infrared laser beams, and 3) MMWs and typical borehole sizes are ideally suited for beam guiding and borehole diameter control. The technological advantages are: 1) commercially available, efficient (> 50%) megawatt gyrotron sources, 2) efficient long distance guided megawatt MMW transmission technology, and 3) the availability of real-time MMW – Terahertz remote diagnostic monitoring technology such as radiometry, radar, and spectroscopy. All enumerated significant benefits remain possible for MMW drilling and lining. All testing performed helped refine theoretical estimates.

The MMW transmission line system developed in this project demonstrated most of the features needed to interface a high power gyrotron to a rock formation for full bore MMW directed energy drilling for the first time. These features included: reflected backward and scattered power isolation, forward gas purge, and beam collinear real-time monitoring diagnostics. In addition, a beam profile control was made through a specialized waveguide launcher. Limestone, basalt, granite and sandstone rock samples were tested using MMW beams. Full bore directed energy drilling through granite and basalt samples was simulated utilizing the expected methods of drilling and lining. These tests reached the limit of the 28 GHz gyrotron system with only 5 kW of delivered MMW power. MMW beams only demonstrated

Thermal weakening of rocks was identified below 1500 $^{o}$C exposure, but rock strength then rose to near virgin rock strengths by about 1650 $^{o}$C. Tests above 1650 up to 3000$^{o}$C are still needed. More testing is needed to confirm the overall strength of the rock melt formed glass liner.

Three basic MMW drilling and lining methods were identified. Various aspects of those system were discussed: preference for over-pressured drilling to prevent handling of hot rock particulates and vapors and simultaneous lining the wellbore; requirement for extremely straight wellbores and alignment of tools to hold the waveguides; requirement for cooling of the waveguide and downhole tools; methods to transverse water filled fractures and caverns utilizing additives; testing of MMW gas transmission losses; specific energies of MMW drilling compared to conventional values.

Based on this work and theoretical considerations, testing at higher frequencies is now required to get to field prototyping and commercial operations. Higher frequencies and the larger gyrotrons will allow direct utilization of optimal modes, provide a higher transmission efficiency and prove MMW beam-rock coupling efficiencies. Commercial MMW drilling will require gyrotron powers in the 1 to 4 MW range. The DOD-Army has 100 kiloWatt 95 GHz gyrotrons in use for fixed and mobile applications, see Figure 56. DOD also has a 2MW, 95 GHz gyrotron

full unit designed and partially assembled for mobile use. Impact and MIT are working with DOD- AFRL in a follow-up DOE project, DE-SC0012308 to utilize their 100kWatt, 95 GHz gyrotron. New waveguide components are required to be designed and built for this work.

It is critically important that a gas or fluid is found that can efficiently (<10% losses) transmit MMW power at 95 GHz at high pressure, 13.8 to 82.7 MPa (2,000 to 12,000 psi), and high temperatures, 24 to 316 $^{o}$C (70- 600$^{o}$F) . It is critically important that a high power (2 MW) 95 GHz window be developed at increasing higher pressures to meet those commercial levels. High temperature materials must be identified and specified for contact points of downhole tools and rock melts. Abrasive resistant materials at these elevated temperatures may also be needed for some MMW drilling and lining methods identified.

Much work remains to go to a field demonstration with a mobile 95 GHz MMW gyrotron unit, even if it is not at the preferred power range.

# PRODUCTS / DELIVERABLES

**Training and Professional Development:** Graduate students were utilized in this project at MIT.

**Publications, Conference Papers, and Presentations:**

- Presentations were made to DOE GTP Peer Review Meetings in May 2012 and April 2013 in Denver.
- Dr. Woskov presented a paper on the MMW reflective power isolator at the June 2013 IEEE meeting. Dr. Woskov made a presentation at the GE Whiting Symposium on Unconventional Fuels and Mining in October 2013.
- Dr. Woskov made a presentation at the APS-DPP in Denver, CO on 10-15 November 2013.
- A Canadian Institute of Mining, Metallurgy and Petroleum (CIM) magazine article was prepared in November-December 2013 and published in January 2014, entitled “Rock Melting Waves. How miners could stop drilling bit by bit”. Link at- http://magazine.cim.org/en/2013/December-January/upfront/Rock-melting-waves.aspx
- Dr. Woskov presented a paper at the September 2014 IRMMW-TeraHertz Conference in Tuscan AZ. The paper was entitled “Penetrating Rock with Intense Millimeter-Waves”. Dr. Woskov was a keynote speaker at the conference.

**Patents and IP:** Original prior-project MIT patent, US 8393410 B2 in 2013. Additional patents are anticipated and are now being discussed.

**Other Products / Deliverables:** www.impact2u.com website for the MMW project. MIT website- http://www.psfc.mit.edu/library1/catalog/reports/2010/14rr/14rr011/14rr011_full.pdf

# REFERENCES

1. W. C. Maurer, Novel Drilling Techniques, Pergamon Press, London, pp. 87-91, 1968.
2. W. C. Maurer, Advanced Drilling Techniques, Petroleum publishing Co., Chap. 17, 1980.
3. K.G. Pierce, B.J. Livesay, J.T. Finger, "Advanced Drilling Systems Study", Sandia National Laboratories, SAND95-033 1, 1996.
4. R. M. Graves, D. G. O'Brien, StarWars laser technology applied to drilling …, Proc.SPE Ann. Tech. Conf. & Exhibition, v Delta, Drilling & Completion, pp. 761-770, 1998.
5. J. S. Bacon, S. Russell and J. P. Carstens, "Determination of Rock Thermal Properties", UARL Report No. L-911397-4, NTIS AD755218, Jan. 1973.
6. R.M. Graves, A.A. Ionin et al, "Interaction of pulsed CO and CO2 laser … with rocks", High-Power Laser Ablation II, C, R. Phipps, Ed., SPIE Vol. 4065, pp. 602-613, 2000.
7. M. R. Hallada, R. F. Walter, S. L. Seiffert, "High power laser rock cutting and drilling in mining operations: initial feasibility tests", High-Power Laser Ablation II, C, R. Phipps, Ed., Proc. SPIE Vol. 4065, pp. 614-620, 2000.
8. B. G. Gahan, ""Processing Rock", Indust. Laser Solutions, pp. 16-18, Sept., 2005.
9. A. Kasugi, K. Sakamoto, K. Takahashi, K. Kajiwara and N. Kobayashi, "Steady-state operation of a 170 GHz - 1 MW gyrotron.", Nuclear Fusion, vol. 48, 054009, 2008.
10. K.L. Felch, B. G. Danly, H. R. Jory, "Characteristics and Applications of fast-wave gyrodevices" Proc. IEEE vol. 87, 752-781, 1999.
11. G.S. Nusinovich, Introduction to the Physics of Gyrotrons, John Hopkins Studies in Applied Physics, 2004.
12. J. Lory et al, "Practical experiences with the 6 gyrotron system on the DIII-D tokamak", 20th IEEE/NPSS Symp. on Fusion Eng. (IEEE Cat. No.03CH37469C), pp. 228-31, 2003.
13. J. Jacquinot, "Plasma heating and current drive systems for ITER ….", 17th IEEE/NPSS Symposium Fusion Engineering (Cat. No.97CH36131), vol.1, pp. 399-404, 1998.
14. L. Rebuffi and J. P. Crenn, "Radiation Patterns of the HE11 mode …", Intern. J. of Infrared and Millimeter-Waves, vol. 9, pp.291-310, 1988.
15. L. L. Frach, S. J. Mclean, and R. G. Olsen, "Electromagnetic Properties … Basalt Rock", 1–110 GHz", IEEE Trans. Geosci. & Remote Sensing, vol. 36, pp. 754-766, 1998.
16. P. P. Woskov, S. K. Sundaram, W. E. Daniel, Jr., D. Miller, "Molten Salt dynamics in glass melts …", J. of Non Crystalline Solids, vol. 341/1-3, 21-25, 2004.
17. R. D. Whitlock and G. M. Frick, "Particle size distributions of aerosols formed by laser ablation of solids at 760 Torr", *J. Mater. Res.*, vol. 9, 2868-2872, 1994.
18. D. M. Hunten, R. P. Turco, O. B. Toon, "Smoke and Dust Particles of Meteoric Origin in the Mesosphere and Stratosphere", *J. of Atmospheric Sci.*, vol. 38, 1342-1357, 1980.
19. A. T. Zimmer, "The influence of metallurgy on the formation of aerosols", *J. of Environ. Monit.*, vol. 4, 628-632, 2002.
20. J.L. Doane and C.P. Moeller, "HE11 mitre bends and gaps in a circular corrugated waveguide," Int. J. Electronics, vol. 77, pp. 489-509, 1994.
21. P. Richet, "Viscosity and configurational entropy of silicate melts", *Geochimica et Cosmochimica Acta*, vol. 48, 471-483, 1984.
22. V. Nikolaevskiy and I. Garagash, "Earth crust structure as a result of rock fracturing…", in Coupled Thermo-Hydro-Mechanical Chemical Processes in Geo-Systems, O. Stephansson, J. A. Hudson, and L. Jing, eds., pp. 727-732, Elsevier, Amsterdam, 2003.
23. R.J. Hanold, "Rapid Excavation by Rock Melting", Los Alamos Nat. Lab., LA-5979-SR, 1977.
24. V.A. Bornshten, Physics of Meteoric Phenomena, D. Reidel Publishing, Dordrecht, 1983.

27. Communications and Power Industries, Inc., private communication, 2009.
28. J.W. Tester et al, The Future of Geothermal Energy, MIT, Chapter 1.5 and Fig. 1.8, 2006, http://geothermal.inel.gov/.
29. Petroleum Energy Handbook, Vol. II, SPE, R. Mitchell, ed., 2007.
30. A. T. Bourgoyne and F. S. Young, "A Multiple Bayesian Approach to Optimal Drilling and Abnormal Pressure Detection", SPEJ, Transactions AIME, 1974.
31. F.E. Beck, J.W. Powell, M. Zamora, "The Effect of Rheology on Rate of Penetration", IADC/SPE Drilling Technology Conference, Amsterdam, 1995.
32. E. K. Morton and W. R. Clements, "The Role of Bit Type and Drilling Fluid Type in Drilling Performance", Int'l. Meeting on Petroleum Engineering, Beijing, China, 1986.
33. E. Aliko, T. Hunt, M. George, J. Nicol, H. Christensen, "New-Generation PDC Bits Allow Drilling at Record Rates of Penetration and Increased Durability in Challenging Algerian Applications", IADC/SPE Drilling Technology Conference, Orlando, Florida., 2008.
34. C. Elsberg, J. Carter, R. Cox, "High Penetration Rate Drilling with Coiled Tubing", SPE Int'l. Conference on Horizontal Well Technology, Calgary, Canada, 1996.
35. A. Hameed, A. Al-Rushaid, "Deep Wells Bit Optimization", IADC/SPE Drilling Technology Conference, Bahrain, 1997.
36. S. Alkhamees et al., "Drilling Demanding 16" Hole Section in Deep Gas Fields, Saudi Arabia Challenges and Advances", IADC/SPE Drilling Technology Conference, Abu Dhabi, UAE., 2003.
37. H.C.H. Armstead, J.W. Tester, Heat Mining, Chap. 11, E. & F. N. Spon, London, 1987.
38. R.A. Cunniff and R.L. Browers, "Finial Report Enhanced Geothermal Systems Technology, Phase II", U.S. DOE, DE-FC07-011D14203, 2003.
39. Copper Basin Project Updates, ASX Announcements, Dec2008 – Jan 2009. www.geodynamics.com.au
40. K.G. Pierce, B.J. Livesay, J.T. Finger, "Advanced Drilling Systems Study", Sandia National Laboratories, SAND95-033 1, 1996.
41. R.M. Potter and J.W. Tester, United States Patent No. 5771984, 1998.
42. R. B. Jurewicz, Rock Excavation with Laser Assistance, *Int. J. Rock Mech. Min. Sci. & Geomech.* Vol. 13. pp. 207-219, 1976.
43. R. M. Graves, D. G. O'Brien, StarWars laser technology applied to drilling …, *Proc.- SPE Ann. Tech. Conf. & Exhibition*, v *Delta, Drilling & Completion*, pp. 761-770, 1998.
44. M. R. Hallada, R. F. Walter, S. L. Seiffert, "High power laser … drilling…", High-Power Laser Ablation II, C, R. Phipps, Ed., Proc. SPIE Vol. 4065, pp. 614-620, 2000.
45. R. Parker, "Drilling Large Diameter Holes …", ICALEO, (504), 2003.
46. B.R. Jurewicz, "Rock Excavation with Laser Assistance", *Int. J. Rock Mech. Min. Sci. & Geomech. Abstr*, Vol. 13, pp. 207-219, 1976.
47. J. S. Bacon, S. Russell and J. P. Carstens, "Determination of Rcok Thermal Properties", UARL Report No. L-911397-4, NTIS AD755218, Jan. 1973.
48. B. G. Gahan, *GasTIPS*, Spring2002, pp.4 – 8, 2002.
49. Z. Xu, C. B. Reed, R.A. Parker, R. Graves, "Laser spallation of rocks …," *Proc. of 23rd Inter. Cong. on App. of Laser & Electro-Optics*, San Francisco, CA, Oct. 4-7, 2004.
50. Z. Xu *et al*, "Specific energy for pulsed laser rock drilling", *J. Laser Applications*, vol. 15, pp. 25-30, 2003.
51. K. H. Leong, Z. Xu, C. B. Reed, and R. A. Parker, "Laser and Beam Delivery for Rock drilling", *Report ANL/TD/TM03-01*, Argonne National Laboratory, 35 pages, 2003.
52. K.L. Felch, B. G. Danly, H. R. Jory, "Characteristics and Applications of fast-wave gyrodevices" *Proc. IEEE* vol. 87, 752-781, 1999.
53. R.J. Dowling *et al*, "Progress in fusion technology in the US magnetic fusion program", *Fusion Engineering and Design*, vol. 11, pp. 23-34, June-July 1989.

54. G.S. Nusinovich, Introduction to the Physics of Gyrotrons, John Hopkins Studies in Applied Physics, 2004.
55. A. Kasugi, K. Sakamoto, K. Takahashi, K. Kajiwara and N. Kobayashi, "Steady-sate operation of a 170 GHz - 1 MW gyrotron for ITER", *Nucl. Fusion*, vol. 48, 054009, 2008.
56. T. L. Grimm, K. E. Kreischer, and R. J. Temkin, *Phys. Fluids B*, vol. 5, 4135-4143, 1993.
57. J. Lory *et al*, "Practical experiences with the 6 gyrotron system on the DIII-D tokamak", *20th IEEE/NPSS Symp. on Fusion Eng.* (IEEE Cat. No.03CH37469C), pp. 228-31, 2003.
58. J. Jacquinot, "Plasma heating and current drive systems for ITER ….", *17th IEEE/NPSS Symposium Fusion Engineering* (Cat. No.97CH36131), vol.1, pp. 399-404, 1998.
59. M. Blank *et a*l, "Development … of a Multi-Megawatt 95 GHz Gyrotron …", *35th IEEE Conf. on Plasma Sci.*, Karlsruh, Germany, IEEE 978-1-4244-1930-2/08 2008.
60. Communications and Power Industries, Inc., private communication, 2009.
61. L. L. Frach, S. J. Mclean, and R. G. Olsen, "Electromagnetic Properties … Basalt Rock", 1–110 GHz", IEEE Trans. *Geosci. & Remote Sensing*, vol. 36, pp. 754-766, 1998.
62. K. D. Hagen, Heat Transfer with Applications, Prentice-Hall, Inc., see Eq. 5-10, p.171 and rock thermal properties Appendix D, 1999.
63. S.T. Han et al., "Low-Power Testing of Losses in Millimeter-Wave Transmission Line for High-Power Applications", *Intern. J. of Infrared and Millimeter-Waves*, vol. 29, 1011-1018, 2008.
64. The Engineering Tool Box, http://www.engineeringtoolbox.com/young-modulus-d_417.html
65. O. Katz, Z. Reches, J-C. Roegiers, "Evaluation of mechanical rock properties…", *Intern. J. of Rock Mechanics & Mining Sci.* vol. 37, pp. 723-728, 2000.
66. M.K. Thumm, "Passive High-Power Microwave Components', *IEEE Trans. on Plasma Sci.*, vol. 30, pp. 755-786, 2002.
67. P.P. Woskov and S. K. Sundaram, "Thermal return reflection method for resolving emissivity and temperature in radiometric methods", *J. Appl. Phys.*, vol. 92, 6302-6310, December 2002.
68. L.N.Y. Wong, H.H. Einstein, "Using High Speed Video Imaging in the Study of Cracking Processes in Rock", *Geotechnical Testing Journal*. Vol. 32, No. 2, 2009.
69. Internal MIT Report #PSFC/RR-09-11, September 2009
70. Paul Dunn, K.D. Oglesby, et. al., "Baseline System Costs for a 50MW Enhanced Geothermal System" DE-EE0002742-002, preliminary report to DOE, March 2011, GEECO and Impact Technologies.
71. John H. Altseimer, et., al., THE SUBTERRENE ROCK-MELTING CONCEPT APPLIED TO THE PRODUCTION OF DEEP GEOTHERMAL WELLS, Los Alamos National Lab, LA-UR-76-1302, Q-23, 1976
72. blank
73. P. P. Woskov, H. H. Einstein and K. D. Oglesby, "Penetrating Rock with Intense Millimeter-Waves", 39th International Conference on Infrared, Millimeter, and Terahertz Waves, Tucson, Arizona, MIT Report PSFC/JA-14-17, 2014.
74. P. P. Woskov, "A Reflected Power Isolator for a 10 kW, 28 GHz Gyrotron", Microwave Symposium Digest (IMS), 2013 IEEE MTT-S International, 3 pp, Seattle, WA, 2-7 June 2013.
75. J. L. Doane, "Parabolic Tapers for Overmoded Waveguides", Int. J. Infrared and Millimeter Waves, vol. 5, no. 5, pp. 737-751, 1984.
76. M. Thumm, "High Power millimeter-wave mode converters in overmoded circular waveguidesusing periodic wall perturbations", Int. J. Electronics, vol. 57, no. 6, pp. 1225-1246, 1984.
77. M. Thumm, A. Jacobs and M. S. Ayza, "Design of Short High Power TE11-HE11 Mode Converters in Highly Overmoded Corrugated Waveguides", IEEE Trans. Microwave Theory and Techniques, vol. 39, no. 2, pp. 301-309, February 1991.
78. J. L. Doane, C. P. Moeller, "HE11 mitre bends and gaps in a circular corrugated waveguide", Int.J. Electronics, vol. 4, no. 4, pp. 489-509, 1994.

79. J. L. Doane, “Grating Polarizers in Waveguide Miter Bends”, J. Infrared Milli Terahz Waves, vol.13, no. 11, pp. 1727-43, 1992.
80. R. Ulrich, T. J. Bridges, and M. A. Pollack, “Variable Mesh Coupler for Far Infrared Lasers”, Applied Optics. vol. 9, no. 11, pp. 2511-2516, 1970.
81. R. E. Collins, Foundations of Microwave Engineering, New York: McGraw-Hill Book Co., 1966.
82. P.P. Woskov and S. K. Sundaram, "Thermal return reflection method for resolving emissivity and temperature in radiometric methods", J. Appl. Phys., vol. 92, pp. 6302-6310, 2002.
83. P. P. Woskov and D. R. Cohn, “Annual Report 2009 Millimeter Wave Deep Drilling for Geothermal Energy, Natural Gas and Oil”, MIT Plasma Science and Fusion Center Report PSFC/ RR-09-11, 2009.
84. A. Cook, M. Shapiro, and R. Temkin, “Pressure dependence of plasma structure in microwave as breakdown at 110 GHz”, Applied Physics Letters, vol. 97, 011504, 2010.
85. D. W. Waples and J. S. Waples, “A Review and Evaluation of Specific Heat Capacities of Rocks, Minerals, and Subsurface Fluids. Part 1: Minerals and Nonporous Rocks”, Natural Resources Research, vol. 13, No. 2, June 2004.
86. E. C. Branscome, “A Multidisciplinary Approach to the Identification and Evaluation of Novel Concepts for Deeply Buried Hardened Target Defeat”, PhD Thesis, George Institute of Tech., 2006.
87. A. G. Whittington, a. M. Hoffmeister, P. I. Nabelek, “Temperature-dependent thermal diffusivity of the Earth’s crust and implications for magmatism”, Nature, vol. 458, 319-321, 2009.
88. H. Shibata1, A. Suzuki and H. Ohta, “Measurement of Thermal Transport Properties for Molten silicate Glasses at High Temperatures by Means of a Novel Laser Flash Technique”, Materials Transactions, vol. 46, No. 8, 1877-1881, 2005.
89. L. Eppelbaum, I. Kutasov, A. Piltchin, Applied Geothermics XVIII, Springer-Verlag, Berlin, 2014.
90. P. Woskov and P. Michael,” Millimeter-Wave Heating, Radiometry, and Calorimetry of Granite Rock to Vaporization”, J Infrared Milli Terahz Waves, vol. 33, 82-95, 2012.
91. A.A. Abtahi, A.B. Kahle, A.D. Abbott, A.R. Gillespi, D. Sabol, G. Yamada, D. Pieri, “Emissivity Changes in Basalt After Eruption From PU’UO’O, Kilauea, Hawaii”, American Geophysical Union, 2002AGUFM.V71A1263A, (2002).
92. V. O. Vakulenko, D. D. Dzhigiris, Yu. N. Dem’yanenko, B. M. Shutov, “Emmissivity of Basalt Melts”, Glass and Ceramics 35, 530–532 (1979).
93. E. A. J. Marcatili and R. A. Schmeltzer, “Hollow Metallic and Dielectric Waveguides for Long Distance Optical Transmission and Lasers” The Bell System Tech. J., v43, 1763, 1964.
94. M. Hobiger , I. Sonder, R. Büttner, B. Zimanowski, “Viscosity characteristics of selected volcanic rock melts”, Journal of Volcanology and Geothermal Research, vol. 200, 27–34, 2011.
95. P. E. Armstrong, et. al., “Subterrene Electrical Heater Design and Morphology”, part of the Subterrene Project at Los Alamos National Lab, LA-5211-MS, February 1974
96. Ken Pierce, John Finger and Bill Livesay, “Advanced Drilling Systems: Sandia National Lab, 95-0331, June 1996.
97. John Finger and Bill Livesay, personal note on their Sandia NL wellbore liner.
98. Sandia NL and MIT study DE-AC04-94AL8500,National Advanced Drilling and Excavation Technologies (NADET), 1996 via NTIS.
99. Erik Lassner, Wolf-Dieter Schubert (1999). Tungsten: properties, chemistry, technology of the element, alloys, and chemical compounds. Springer. p. 9. ISBN 0-306-45053-4.
100. M Gasch, D Ellerby, E Irby, S Beckman…Processing, properties and arc jet oxidation of hafnium diboride/silicon carbide ultra high temperature ceramics”, Journal of Materials, 2004 - Springer
101. J Cheng, R Roy, D Agrawal, “ Radically different effects on materials by separated microwave electric and magnetic fields”, Material Research Innovations, 2002 – Springer

102. G.S. Nusinovich, MKA Thumm, MI. Petelin, “The Gyrotron at 50: Historical Overview”, Journal of Milli-Terahz Waves, 2014.
103. RM Graves, DG O’Brien, “StarWars laser technology applied to drilling and completing gas wells”, SPE Annual Technical Conference proceedings, pp 761-770, 1998.
104. W. Ho, I. A. Kaufman, Po Thaddeus, “Pressure-Induced Microwave Absorption in $N^2$", 14 June 1968
105. A. Rastogi and RP Lowndes, “ Collision-induced far-infrared absorption in nitrogen gas at high densities?”, Journal Physics, B Volume 10, No. 3, 1977
106. G. Birnbaum and AA Maryot, “ Collision-Induced Microwave Absorption in Compressed Gases. I. Molecular Electric Quadrupole Moments”, Journal of Chemical Physics, Volume 36, Number 8, April 1962.
107. I.R. Dagg, G.E. Reesor and J.L. Urbaniak, “ Collision Induced Microwave Absorption in N2, CH4 and N2-Ar, N2-CH4 Mixtures at 1.1 and 2.3cm-1”.
108. T. R. Hamrick, “Optimization of Operating Parameters for Minimum Mechanical Specific Energy in Drilling”, Dissertation to the College of Engineering and Mineral Resources Department of Mechanical and Aerospace Engineering at West Virginia University, 2011
109. G. Mensa-Wilmot, S. Southland, P. Mays, P. Dumrongthai, and D. Hawkins, and P. Ilavia, “Performance drilling – definition, benchmarking, performance qualifiers, efficiency and value”, Drilling Contractor, July/August 2009, Innovating While Drilling,
110. F.E. Dupriest and L. Koederitz, “Maximizing Drill Rates With Real-Time Surveillance of Mechanical Specific Energy”, SPE/IADC 92194, February 2005.
111. M. K. Thumm and W. Kaspareck, "Passive High Power Microwave Components", Plasma Science, vol. 30, No. 3, pp. 755-786, 2002.

# BIBLIOGRAPHY

## from Hamrick [108] for drilling

Well Drilling School. "http://welldrilliHistoryofWellConstruction." *http://welldrilliHistoryofWellConstruction* n. pag. Web. 20 Apr 2010. <http://welldrillingschool.com/courses/pdf/HistoryofWellConstruction.pdf>.

American Society of Mechanical Engineers. "Hughes Two-Cone Drill Bit." *Historic Mechanical Engineering Landmark* 2009: Web. 27 Apr 2010. <http://files.asme.org/MEMagazine/Web/20779.pdf>.

Lambert S W, Rogers J D, Williamson J R, Boyer C M, and Frantz J H. "Benchmarking Deep Drilling Technologies." *2005 SPE Annual Technical Conference and Exhibition.* SPE Editorial Committee: Dallas, TX, Society of Petroleum Engineers. 2005.

Teale R. "The Concept of Specific Energy in Rock Drilling." *International Journal of Rock Mechanics* . 2. (1965): 57-73.

Gerbaud, Menand, and Sellami. "PDC Bits: All Comes From the Cutter/Rock Interaction." *IADC/SPE 98988 Drilling Conference*. Miami, FL, International Association of Drilling Contractors and Society of Petrolleum Engineers. 2006. Web. 11 Jun 2010.

Rashidi B, Hareland G, and Nygaard R. "Real-Time Drill Bit Wear Prediction by Combining Rock Energy and Drilling Strength Concepts." *SPE 117109-PP 2008 Abu Dhabi International Petroleum Exhibition and Conference*. Abu Dhabi, Society of Petroleum Engineers. 2008.
Zeuch D H, and Finger J T. "Rock Breakage Mechanisms With a PDC Cutter." 60*th Annual Technical Conference and Exhibitionof the Society of Petroleum Engineers.* Society of Petroleum Engineers: Las Vegas, SPE . 1985.

Wojtanowicz A K, and Kuro E. "Dynamic Drilling Strategy For PDC Bits." *SPE/IADC 16118 1987 SPE/IADC Drilling Conference*. New Orleans, LA, Society of Petroleum Engineers and International Association of Drilling Contractors. 1987.

Huang S L, and Wang Z W . “The Mechanics of Diamond Core Drilling of Rocks.” Int. J. Rock Mech. & Min. Sci. 34:3-4, paper No. 134.

Ersoy A, and Waller M. "Drilling Detritus and the Operating Parameters of Thermally Stable PDC Core Bits." *International Journal of Rock Mechanics*. 34.7 (1997): 1109-1123.

Ersoy A, and Atici U. “Performance characteristics of circular diamond saws in cutting different types of rocks.” *Diamond and Related Materials* 13 (2004) 22–37.

Caicedo H, and Calhoun W. "Unique ROP Predictor Using Bit-specific Coefficient of Sliding Friction and Mechanical Efficiency as a Function of Confined Compressive Strength Impacts

Drilling Performance." *AADE 2005 National Technical Conference and Exhibition*. Houston. TX, American Association of Drilling Engineers. 2005.

Armenta M. “Identifying Inefficient Drilling Conditions Using Drilling Specific Energy.” *SPE 116667. SPE Annual Technical Conference and Exhibition*. Denver, CO. Society of Petroleum Engineers. 2008.

Koederlitz W and Weis J. “A Real-Time Implementation of MSE.” *AADE-05-NTCE-66 AADE National Technical Conference and Exhibition*. Houston, TX, American Association of Drilling Engineers. 2005.

DuPriest F. “Comprehensive Drill Rate Management Process to Maximize Rate of Penetration.” *SPE Annual Technical Conference and Exhibition*. San Antonio, TX, Society of Petroleum Engineers. 2006.

Remmert S, Witt J, and DuPriest F. "Implementation of ROP Management Process in Qatar North Field." *SPE/IADC 105521 Drilling Conference*. Amsterdam, The Netherlands, Society of Petroleum Engineers, International Association of Drilling Contractors. 2007.

Burmaster K, Chando J, and Vaczi K. “Execution Success in Platform Drilling Campaign." *SPE/IADC 119262 Drilling Conference*. Amsterdam, The Netherlands, Society of Petroleum Engineers, International Association of Drilling Contractors. 2009.

Kilroy D, and DuPriest F. “Practices Implemented to Achieve Record Performance in Narrow Margin Drilling in Bass Straight Extended Reach.” SPE 125246. *SPE Annual Technical Conference and Exhibition*. New Orleans, LA, Society of Petroleum Engineers. 2009. Print.

Roehrlich M, and Belohlavek KU. “ROP Enhancement in Ultra-hard Rock.” *IADC/SPE 99045 IADC/SPE Drilling Conference*. Miami, FL, Society of Petroleum Engineers, International Association of Drilling Contractors. 2006. Print.

DuPriest F. “Maintaining Steerability While Extending Gauge Length to Manage Whirl.” *SPE/IADC 119625 Drilling Conference*. Amsterdam, The Netherlands, Society of Petroleum Engineers, International Association of Drilling Contractors. 2009. Print.

Reddish D J, and Yasar E. “A New Portable Rock Strength Index Test Based on Specific Energy of Drilling.” Int. J. Rock Mech. & Min. Sci. 33:5 pp 543-548. 1997.

Stavropoulou M. “Modeling of Small Diameter Rotary Drilling Tests on Marbles.” Int. J. Rock Mech. & Min. Sci. 43. Pp 1034-1051. 2006.

Abd Al-Jalil Y Q. "The Mechanics of Indentation of Rock –A Critical Review." The 41st U.S. Symposium on Rock Mechanics (USRMS)ARMA/USRMS 06-1082. American Rock Mechanics Association: Golden, CO, American Rock Mechanics Association. 2006.

Mosley S G, Bohn K P, and Goedickemeier M. “Core Drilling In Reinforced Concrete Using Polycrystalline Diamond (PCD) Cutters: Wear And Fracture Mechanisms.” *Int. Journal of Refractory Metals & Hard Materials* 27 (2009) 394–402

Hamade R F, Manthrib S P, Pusavec F, Zacny K A, and Taylor L A. "Compact Core Drilling In Basalt Rock Using PCD Tool Inserts: Wear Characteristics And Cutting Forces." *Journal of Materials Processing Technology*. 210. (2010): 1326–1339.
Black A D, and Judizs A. “Optimization of Deep Drilling Performance – Development and Benchmark Testing of Advanced Diamond Product Drill Bits & HP/HT Fluids to Significantly Improve Rates of Penetration.” Topical Report, March, 2006, Contract DE-FC26-02NT41657, prepared by TerraTek, Inc. for NETL. Morgantown, West Virginia: National Energy Technology Laboratory (NETL). 2006.

Langeveld C J. "PDC Bit Dynamics." 1992 IADC/SPE Drilling Conference. IADC /SPE 23867: New Orleans, LA, American Society of Petroleum Engineers. 1992. Print. 30 Langeveld C J. "PDC Bit Dynamics. (Supplement to IADC /SPE 23867" 1992 IADC/SPE Drilling Conference. IADC/SPE 23873: New Orleans, LA, American Society of Petroleum Engineers. 1992.

Mensa-Wilmot, Graham, Fear, and Martyn. "The Effects of Formation Hardness, Abrasiveness, Heterogeneity and Hole Size on PDC Bit Performance." 2001 IADC/SPE Drilling Conference IADC/SPE 67698: Amsterdam, The Netherlands, American Society of Petroleum Engineers. 2001.

Warren T M, and Sinor, L A. "PDC Bits: What’s Needed to Meet Tomorrow Challenge." University of Tulsa Centennial Petroleum Engineering Symposium, IADC/SPE 27978: Tulsa, OK, American Society of Petroleum Engineers. 1994.

# Appendix A

# Feasibility Study of MMW Technology for Drilling and Lining

# Feasibility Study
## for
# Drilling and Lining Deep Wells
## using
# Millimeter Wave (MMW) Technology

## DOE Project Contract Number DE-EE0005504

## Initial 24 May 2013
## and Revised 20 December 2014

## CONFIDENTIAL

### INTRODUCTION

This report covers an initial (because no additional bench tests are available) study of using Millimeter Wave (MMW) technology for drilling and lining deep wellbores. It started with a project meeting of Dr. Bill Livesay and Ken Oglesby (Impact Technologies LLC) on 4February2013 in Del Mar, California. The purpose of that meeting was to initiate the understanding the key processes, benefits and limitations of MMW technology and look at how they would be applied in a future MMW drilling and lining system. That meeting and this report includes consideration of prior discussions, emails and reference materials from Dr. Paul Woskov and Dr. Herbert Einstein both at MIT.

That initial study was reviewed and revised in December 2014 once all experimental data was obtained and analyzed. Little change to the study was warranted at that time.

This report was written by Ken Oglesby (Impact) with edits by Dr. Livesay and Dr. Woskov (MIT).

## EXECUTIVE SUMMARY

The key points discussed and considered, listed from the most to lesser importance, include:

1. The ongoing project study at MIT on rock melting/ vaporization/ reduction using MMW power on various common rock types including- granites, sandstones, shales, limestones/ dolomites, non-quartz and non-crystalline rocks, must show and quantify positive indications of rock reduction effectiveness (i.e., “Show Stopper”).

2. The ongoing project study at MIT on rock melt properties must show sufficient strength and dielectric properties for various common rock types (listed above). The current study on the strength and properties of the rock melt is important. Specifically, the dielectric properties of MMW rock melt of various rocks is a “show stopper” if NO or only a few rocks can provide a conductive wellbore for efficient MMW wave propagation. Sealing capabilities of rock melts within formation pores is important and must be studied later.

3. The ongoing project must study MMW transmission efficiency through a variety of fluids/ gases (supercritical or not) at elevated pressures and temperatures. At least one relatively low cost, efficient and safe (non-toxic) transmission supercritical fluid should be found and tested at the pressure and temperatures expected in the waveguide and wellbore (this is a “Show Stopper”). This test also requires the design and bench testing of an efficient, high pressure, low temperature window for 100 kilo-watts up to 2 megawatts of MMW power. Such transmission tests were conducted at Impact’s shop in 2013 and 2014, but not at high power levels.

4. Because of the influence of water and fluids on MMW power, the proposed system must not allow such (much) fluids - especially water as a liquid or vapor - into the waveguide (pipe or open rock wellbore). Fluids, in particular water, will strongly absorb MMW power and interfere with the power delivery to the cutting rock face and thus reduce drill rate.

5. The MMW drilling process must not bring the reduced/ created very hot rock particles and produced fluids to the surface, because - A) the interference of the rising vapors and particles plume on the MMW beam; and B) difficulty delivering and surface processing the required fluids (most likely water) for cooling the drilling debris on top of that needed for cooling the pipe/ waveguide and transmission fluid.

6. Because of above items 4 and 5, the MMW process must dispose of hot rock particles/ melts/ vapors and produced fluids within the drilled formation and preferably at the immediate cutting point. The penetration of such rock melt is only a few meters. If rock reduction can be kept down to the particle/ melt reduction energy level (and not requiring vaporization), the MMW process will be 4-5 times more efficient.

7. Because of above items 4, 5 and 6, the MMW drilling process at the cutting/ melting point must occur in an over-balanced (just above rock pore pressure), if not extreme over-balanced (above fracture initiation or rock tensile failure) pressure condition. The

combination of thermal weakening/ fracturing with hydraulic pressure should lower the threshold requirement of both.

8. Due to equipment and process limitations, there are three MMW drilling methods – A) fixed or constant stand-off distance from waveguide end to the rock face; B) variable stand-off; and C) a combination method (including constant rate advancement). A competent downhole seal of the waveguide-wellbore wall is required for all findings and methods. A low pressure transmission system (at least at the surface and in the waveguide) would require a high temperature downhole MMW window. It also complicates pipe collapse issues. A high pressure transmission system (advocated in the findings, if possible) would need a much easier low temperature, high pressure, high power MMW window at the surface. However, this option complicates pipe burst and surface well containment issues.

9. Required Later Testing- Theoretical review (started) and bench testing of the influence of materials (rocks, cladding, …) and imperfections (bends, ovality, ID restrictions, etc…) on the wave guide (smooth & corrugated pipe, in both the pipe and the open borehole rock melt liner). Predictive methods are needed for MMW performance, heat build-up and pipe failure.

10. Helpful Later Bench Testing- Bench testing to characterize the reflective energy measurement response (Giga to Tera-Hertz range of frequencies) to various rocks (identify types) and fluids (identify types and amount) is important to prove, understand, optimize, and provide robustness to MMW drilling systems. Also use as a method to predict errant MMW behavior downhole in the wave guide(s).

11. Required Later Modeling- Heat/ Energy balance modeling would help evaluate the temperature of the downhole system, including waveguide. This would include basic radial heat conduction and heated mass flux components.

12. Helpful Later Modeling- Understanding the dynamics of the open rock wellbore/ standoff region is important to optimize MMW drilling efficiency and the overall system design. This includes vectors and velocities of rock and fluid particles/ melts/ vapors (plume) by population/ number, size, density and position in the wellbore, all while under high power MMW bombardment in the open borehole. This should be studied as a function of distance from the rock cutting face and bore pressure (relative to rock pore pressure). This is a non-trivial problem that will not be accomplished in this project.

13. Required study on the influence of doglegs in the waveguide. Understanding the degree of dog-leg severity (degree/100ft) that can be tolerated by an MMW beam without melting the waveguide (even with cooling) is required. It may be determined that no conventionally drilled upper hole is straight enough to transmit a high powered MMW beam through it. It may be possible to mitigate any heating with sufficient cooling flow in a concentric pipe or to utilize a small diameter waveguide inside a much larger pre-drilled hole, with tension on the wave guide pipe to maximize straightness.

## KEY DRILLING EQUIPMENT AND SYSTEMS

The key physical sections or systems of a future Millimeter Wave (MMW) drilling and lining system (with much overlap and inter-relationships) and their key components were identified. It tries to honor our current understanding of the MMW processes. It is recognized that these system will change as the MMW processes mature over time. This section is organized/ listed in order of position on the earth- surface to bottom of the hole.

### Top Side

The desired hole size and drill rate sets the required MMW power level to be delivered to the deep rock cutting face {see plot by Paul Woskov}. The size of the largest unit indicates the mobility concerns and the overall system footprint.

A future commercial MMW system that drills an 8" diameter hole at a desired 4 meters (12 feet)/ hour drill rate sets the total gyrotron power to 2 MegaWatts (no known portable units of this size exist and they may be too big to become portable) OR, most likely, multiple smaller (assume 4 portable 500 kiloWatt, partially developed by GA) gyrotrons in parallel with a beam combiner that may require special frequency output controls. {a possibility from ITER, per P. Woskov}. To deliver that MMW energy generation (at 50% efficiency) it will take a 4 MegaWatt electric grid source and transmission lines (doubtful that any utility would do this for a temporary activity) OR, most likely, 4 separate and frequency synced 1 MegaWatt electric generators each coupled to a 1500 horsepower (total of 6000 horsepower onsite) diesel engines with appropriate diesel fuel storage. The surface waveguide piping and mirrors/ miter bends will need a separate cooling system.

The transmission fluid/ gas system will need a compressor or fluid pump (either rated for the required pressure and estimated loss rate) powered by electricity from the grid or a direct coupled diesel engine. Storage tanks will be needed for both the transmission fluid/gas and the diesel fuel. These will be very large tanks that are most likely pressurized and cryogenic.

The waveguide needs cooling (at 10% to 30% losses of total power, 110$^{o}$F temperature rise allowed) rated at 28-80 gpm of a water based fluid or about 10X that rate if the cooling fluid were a gas (heat capacity differences). With those conditions the transmission fluid could cool the pipe as it was pumped down, if sufficient downward flow rate occurred.

If a separate cooling circulating system is needed, it must be rated for 5000 psig. Pressure for that rate will depend on downhole pipe size and that is based on the hole size and other required downhole paths/ pipes in the allowed annular space- all going to total depth. The waveguide and the separate cooling fluid path would be best configured as a concentric pipe- cooling fluid in sheath surrounding the wave guide. That cooling system would need water tank storage, cooling towers, chemical pumps, triplex pumps, diesel engines with fuel storage space (or electric motors and grid lines/ electric generator).

If desired, a cooling / downhole jet pump operation circulation system for lifting and cooling drilling debris would require fluid manifolds, separation, storage space, high volume fan driven air coolers/ towers, triplex pumps (rated for 5000 psi pressure and an estimated 140-800 gpm rate [cooling alone is 70-420 gpm, jet pumps are 50% efficient at best and multiple lift points may be needed], allowing a 110$^{o}$F temperature rise) requiring a diesel engine/ electric motor and fuel storage. The fluids used for transmission cooling and the jet pump operation with drilling debris cooling can be combined for, possible simpler operation. The return flow for all fluids is up the annular space.

If the downward pumped transmission fluid can be used to circulate out the drilling debris up the annular space, this would require storage, separation, cooling towers, high pressure and high rate compressors/ pumps, diesel engines and fuel tanks. IF the return flow contains gases, special pressure control and variable choke restrictions precautions must be taken to prevent sand blasting effects of the pipes and surface equipment. If the transmission fluid is non-water or a gas, it will have much lower heat capacity and will require much higher flow rates to accomplish drilling debris cooling. Treating after separating from the other fluids, will be needed to reuse the transmission fluid. Separation may be a problem as all water (even vapor) must be removed from that fluid.

Corrugated surface piping from the gyrotrons to the downhole waveguide connection is the most efficient transmission line approach. Each gyrotron window (high pressure, low temperature) will be manifold to combine all 4 MMW beams into 1 beam. A vertical sliding sleeve with high pressure gas seals will incorporate an enlarging diameter wave guide to allow for a full 30-40 foot pipe movement for connections. MMW wave transmission modes are set by specialized mode conversion steps and miter bends are needed for efficient beam conditioning and focus into the vertically moveable waveguide/ drill pipe going downhole. Between the MMW wave introduction and the downhole waveguide connection will be a special port for transmission fluid/ gas introduction (via multiple slits that are less than 1/3 of the MMW wavelength) going into the vertically mobile waveguide assembly (surface and downhole) at the set pressure.

The number of flow paths from the surface down to the end of the downhole waveguide varies by what is desired to be performed downhole. The minimum paths needed is 1 downward and 1 upward path- A) MMW waveguide with flowing cool, pressurized transmission fluid going down, B) annular space for transmission flow upwards. If a separate cooling/ operating fluid circulating system is desired then there are minimum 3 paths-

A) MMW waveguide with pressurized transmission fluid going down (all one way paths),
B) waveguide cooling fluid going down,
C) annular space flowing upwards.

Extra separate downward flow paths be desired for the power fluid to operate a downhole jet pump(s) and for cooling drilling debris- these would be combined into 1 flow path with the return in the annulus.

For an 8” drilled hole, a minimum 4” ID / 4.5” OD wave guide is needed. The wave guide cooling fluid (if separate) will require a minimum 2.5” equivalent diameter flow path. Concentric pipe (one inside the other) can be used to provide 2 downward flow paths- especially good for an inner waveguide and outer cooling fluid path. Such concentric pipe is very favorable for use of coiled tubing. In concentric form around the waveguide- the 2 path concentric diameter extends to 5.0” ID/ 5.5” OD. The annular upward flow path required (space between wellbore 8” ID and the pipe(s) ODs) where all cooling fluids (and drilling debris) can be brought back up to the surface. With the waveguide and cooling sheath of 5.5” inside the wellbore already, this leaves 2.5” clearance or an ample equivalent flow diameter of a 5.9” pipe ID. However, the 1.25” clearance on each side of the inside pipe, if centered, is the minimum desired for drilling operations (tool/ packer movements, hole collapse, fishing.,,,). *There is not enough space in the wellbore for another separate circulation pipe for the above calculated rates required.*

If waveguide cooling and rock cooling/ jet pump operation circulating paths were combined into a minimum 4” equivalent flow diameter, the outer sheath would then be 6” ID / 6.5” OD. This leaves a 1.5” total clearance (0.75” on each side, if centered) for the total combined return flow rate (100-500 gpm) and for drilling operations. Also the debris cooling process would heat the waveguide cooling fluid in counter flow heat exchange. *This is insufficient for the flows expected and for normal drilling operations and thus it is doubtful that a cooling path for drilling debris can exist*, unless the monobore hole size is increased (reduced drill rate for the same power) or a smaller waveguide size is possible (higher energy losses). Nor is this configuration good for properly cooling the waveguide.

Pipe handling (lifting, raising/ lowering and laying down) of the downhole pipe type (smooth or corrugated, continuous or jointed or both), with pipe racks/storage is required. This is normally performed with a mast based system, but may be a hybrid system (mast with a coil reel setup) if coiled tubing use is desired. A special surface system (also discussed later) would be needed if CT is used for continuous pipe movement during MMW drilling.

For constant standoff type MMW drilling where the waveguide is lowered with bore advancement, internal system pressure would be lost at each connection unless check valves/ plugs are run into the waveguide and set at some depth after the MMW beam is stopped and pipe movement is desired. In this regard, continuous pipe (CT) would be better with longer lengths and fewer connections required. CT allows better well control with no upsets/ smooth outer pipe, no loss in pressure and continuous movement.

***Personnel Safety-***

Surface MMW stray power monitors are needed for immediate gyrotron(s) shutdown. MMW generation will then immediately stop. Fixed and mobile MMW absorbing barriers can also be placed in areas were personnel are expected. Heavy water mist was

considered to be used to absorb stray MMW power, but that creates steam which is not beneficial.

***Well Containment-***

There are normally multiple layers of safety to keep the well under control. In conventional systems, the first line of defense is the heavy drilling mud for an over-balanced condition (wellbore pressure > rock pore pressure at all depths of open wellbore) and, if needed, heaver mud is circulated down; second protection is providing a flow restriction which showing up as a pressure surface pressure reflected to depth; the third protection is a annular bag type seals; the fourth are pipe rams that seal around all existing pipe in its way; and the fifth barrier is a shear ram that cuts all pipe in the way and seals the well up. Industry and regulators will expect these levels of control/ isolation on an MMW well. All piping paths (into and out of the well) will need isolation and control with full opening and safety shut-in valves.

In addition, an annular Blow-Out-Preventer (BOP) and pipe rams (set for the number, size and position of all pipes) will be needed to close off and/or contain the well during operations and in well control events. Multiple pipes make annular sealing with a BOP difficult, but still possible. Sealing of concentric strings is also difficult as each string would have to be sealed, but possible. It is a concern on the method to makeup multiple joints while maintaining downhole pressure- a real concern if the downhole temperature is over 212$^{o}$F and the release of pressure would allow boiling off downhole fluids. The good news is that only the waveguide may be pressurized and have this concern- and that is fixable. All equipment must be rated at the maximum operating pressure and temperatures with appropriate safety factors. Burst and collapse conditions must be calculated for all strings – top to bottom- with temperature degradation to be considered.

***Returns Processing-***

All solids and fluids returned to the surface must go through a manifold then to a multiphase flow-back separation, such as a Gas-Liquid-Solids cyclonic separator. This process will handle hot pressurized fluids, (if brought to the surface) solidified rock vapors as very small particles and produced fluids/ water. Large volume/ rate, field separation technology can efficiently separate gases from liquids and large solid particles out of liquids. They currently clean solids out of liquids only down to 20-50 microns, while condensed vapors are much below this size level and thus are very difficult to process and recover. Field centrifuges can remove particles down to about 5 microns. For cost savings, often a portion of the full fluid volume is disposed and replaced to dilute the small particle. This cannot be done where water is expensive or unavailable. To remove these smaller particles, higher speed centrifuges would be needed in field settings- or collecting them should be avoided.

***Surface Measurement of Downhole-***

Measuring key downhole operations is important for safety and maintaining efficiency of the drilling operation. *One very favorable aspect of MMW power for drilling is the potential of surface monitoring reflected beams/ waves for measuring various downhole conditions.* This capability was demonstrated in the current MIT studies by Dr. Woskov.

Some of the key monitoring elements that would be helpful or required are: depth of plume/ depth of cutting face in real time for current postings, calculation of drill rate and therefore efficiency, identification of downhole problems preventing advancement; temperature at (various and at maximum) depth; un-intended MMW wave mode change especially for mode conversion within the waveguide(s) due to imperfections, bends; and geological (commonly called 'mud') logging- drilled rock composition (inferring rock type) and fluids (water/ brines, hydrocarbons) which need rock/ fluid response characterizations.

**Power Transmission**

It is estimated that 10-30% of the generated MMW power will be lost in the waveguide(s)- pipe and open wellbore- and converted to heat {per P Woskov}. Cooling of the waveguide/ pipe will be required. Waveguide pipe size (larger for less energy loss), material (high electrical conductance desired) and type (continuous or jointed, single or concentric, smooth or corrugated ID, imperfections/ bends) is extremely important as it ties to the drill method and performance. The most strong, fairly conductive, most available and lowest cost material for the piping is some steel alloy. Steel alloys are easily machined and welded. For the waveguide, steel alloys are not the most conductive material available (and therefore higher MMW energy losses in transmission), as compared to copper or aluminum or gold, but it has superior strength (for the depth required) and temperature resistance (natural EGS and induced MMW sources). To decrease transmission losses, internal plating, coating or cladding can be added to the pipe prior to use. Some alloy of copper would be the most conductive material to utilize, but testing must be done to determine the steel-cooper's bonding strength at the extreme temperatures changes expected.

Pipe can be delivered in long joints (30-40 ft and possibly 60 feet) or continuous (coiled tubing, CT), delivered in coiled form and can be laid out to straighten. No pipe is perfectly straight and smooth. Smooth and round pipe is the most available, but those properties change with time, pressure, handling, tools running through, and stretch due to loading in the hole and roughness of the ID of the pipe. Corrugated pipe with special and expensive internal groove or thread machining is more efficient MMW transmission in most modes, but those grooves will change with time. Their grooved dimensions will change with pressure, axial loads, wear from internal tool/ flows, corrosion and age- and might not be worth the price and handling problems. This trade-off between performance and cost will ultimately need to be tested.

Special tool-joints are needed for the wave guide to makeup with minimize gaps (1/3 of a wave length or less) that can cause MMW losses/ heating. Such small gap tool joint types are breechblock and also the patented Hughes type connections.

Each time the joint connection is made internal fluids and pressure can be lost – a special downhole check valve/ plug can be run into the waveguide and set at some depth. Joint makeup and disconnecting is slow and contributes to non-drilling time. It also will have an upset on the OD at each joint connection to keep the internal diameter

constant, but this will make surface preventer sealing more challenging. It also restricts the flow paths causing higher pump pressures.
If continuous pipe, such as coiled tubing, is used it will have a lateral or longitudinal weld line that may interfere with the MMW transmission. Such continuous pipe would be faster tripping (pulling out and/or running into the well) for less downtime. It is safer due to a smooth outer bore for sealing in the surface preventers. However, it has thinner walls than typical jointed pipe and therefore less strong in tensile and collapse. Coiled tubing is attractive but comes with its own problems from the way it is manufactured.

The various cooling needs (fluid, pump rate, drilling debris, circulation path) were discussed earlier and will extend from the surface connections to the wave guide or packer end depth.

Many of the MMW drilling methods outlined require a downhole packer/ seal / anchor to provide tension to the waveguide for straightness, provide a seal between the waveguide and the rock wall (trimmed/ smoothed/ conditioned). In one method, a continuous pipe (CT) can be slid through a seal in the bore to allow advancement of the waveguide end. This is a difficult sealing application due to the heated environment. The most likely method (needing a packer/ seal) will keep a packer and waveguide end at a fixed depth until the wellbore energy losses are too large. An all metal packer version was used at Soultz and will be investigated further.

At the end of the waveguide will be a mode convertor to change the beam mode from one of transport to outward vectors for lining or downward vectors for drilling the bottom of the hole. If a low pressure transmission is required a low pressure, high temperature MMW window will be needed.

Very high temperatures may surround the downhole pipes and tools, thus it is important that correct materials (titanium, ceramics, others…) are selected to survive those downhole conditions.

The open wellbore will also be a waveguide below the pipe waveguide end and the bottom cutting surface. It must be smooth and straight enough for MMW transmission. It also must have the right dielectric properties for efficient transmission, if long distances (therefore longer/ fewer packer moves) are desired. Additives may be added to downward transmission fluid flow to impart some transmissibility improvements to the rock melt liner. The types and size and chemistry of such additives and their method to inject must be studied later.

**Rock Reduction**

Recently concluded MMW rock melting tests at MIT by Dr. Paul Woskov using the low power 10 kilowatt, non-optimal 28 GHz CPI gyrotron with all associated systems, demonstrated the ability to melt and remove various rock types (including sandstone, limestones, granite and basalt). Higher powered MMW drilling tests are being

contemplated in a current DOE project. These tests will help identify and quantify the influence of key factors in bottom hole rock reduction rates.

This can be a simple downhole system. The only other equipment needed for rock reduction is a special wave mode converter at the end of the wave guide to condition the MMW beam to have a mode that has a mostly downward vector.

**Rock Removal and Disposal**

Reduced rock must be cleared out of the way so that new, virgin rock can be impacted by the MMW power and drilling can be advanced. MMW power is thought to penetrate (a few centimeters at most) below the surface of the rock to cause melting and vaporization – expansions that can cause rock failure before MMW melting and vaporization. Following the above discussion, the rocks and fluids encountered by the bore will expand in volume as they are converted from solid into liquid into vapors- thus initially clearing the cutting surface from this expansion. But in a very small closed space, pressure will rise due to the expansion and ultimately something will give-way and fail. We prefer it be the rock that fails. However, this pressure will be reflected back to the surface and must be within the capabilities of the pipes and containment equipment. Disposal of the debris is best kept downhole, thus no further equipment for this section is required.

The design of the downhole assembly at the end of the waveguide may be complicated, due to cooling and circulation. But not if the MMW transmission fluid is the total cooling fluid, then no other downhole equipment (mode convertor only) is needed. The full system, wellbore included, will be at that operating pressure condition. This can be for either surface return/ recovery or for downhole disposal techniques. If it is a gas, then the surface pressures will be higher than if a liquid.

However, for most systems identified, the downhole assembly must incorporate a packer element to seal the space between the waveguide pipe and the hot, rough rock melt lined wellbore. A German company provided an all metal packer for the Soultz project. This company was not found, but any moving components of such a downhole tool that would encounter rock melt or even fine rock particles would not release and could not be removed. Therefore a new seal mechanism is required- use a rock melt seal.

In this seal mechanism, the hot rock melt contact point in the wellbore needs to be partially cooled (to below 2500oC before contact is made and weight is placed on the drill tool this seal is engaged. The seal keeps the return flows and annular fluids (most likely water) from entering the lower open wellbore (stand-off region). It also keeps the working high pressure region below the drill tool. That operating / working fluid (having already cooled the transmission line) will then circulate back up the annulus to the surface.

**Lining the Bore**

The ongoing rock melt strength and property testing at MIT by Dr. Herbert Einstein was hoped to shed light on the capabilities of MMW created rock melt to form a permanent seal on/in the wellbore wall face. Future tests will be needed on the most common rock types to be encountered in the earth to investigate this as needed.

Casing and cementing EGS wellbores are about 50% of the total well cost. Thus, lining the open rock wellbore while drilling (a success in itself and discussed above) versus a separate post-drilling function are important benefits. Step-wise lining (drill and lining wellbores) using expandable casing is the closest to that capability currently. ***However, in this MMW application all the casing and cementing costs are potentially saved***! No rig non-drilling time is required for this lining process, as well, if the over-pressure, downhole disposal method is performed.

Rock melt liners may be temporary and used to stabilize the wellbore and fluid flow just until steel casing can be inserted upon finishing drilling the well or segment. This is important unto itself as it can save multiple sized strings and reduced wellbore diameters as it maintains mono-bore capability. It's even better if the rock melt liner can be permanently used for huge well cost and time savings. This can occur in time.

For separate liner installations or for liner repairs, special wave modes exiting the waveguide are needed to focus and distribute the MMW power to the rock walls. This is a simple procedure and has/ can be further demonstrated with the MIT experiments conducted by Dr. Paul Woskov in this study. Tools to ensure minimum bore diameter and for smoothness (to not catch tools later) will be required.

Additives may also be needed to repair especially difficult problems, such as large fractures, caverns, or just post- drilling lining operations. Methods of introducing balls or granules of selected additives into the waveguide or wellbore must be determined, preferably added at the surface. These additives maybe used for coating the waveguide for transmission improvements, or for initial wellbore sealing, or for repairing an existing wellbore seal. This is difficult because there would not be flow through a pack of additive materials, because MMW melt would immediately solidify in additive's pores and plug the flow. But all material will ultimately melt, then vaporize and be pushed out into the rocks.

If required for packer/seal moving and placement, it is important to understand the length of time needed for temperature cool-off by slow conduction cooling into the earth before cold water (rapid cooling) is circulated across the liner. This may be important to prevent thermal shock damage of the formed rock melt liner.

The high temperatures by the constant energy waves passing through the wellbore may cause the wellbore rock wall to be in a constant state of melt and flow. Both the wellbore pressure and gravity will influence the wellbore lining smoothness, minimum diameter and transmission efficiency. Tools may be needed to identify these cooled flows and smooth out these rock wall imperfections.

## Directional

MMW directional capabilities are not the focus of this project. MMW bores will naturally want to go in a straight direction. Also gravity works, and downhole tools tend toward vertical. However some directional control may be needed during drilling and for directional bores for completions. MMW beams in a waveguide can only turn gradually (kilometers) without significant heat buildup and waveguide failure. Otherwise, MMW beams of the correct modes can be immediately turned at most angles with cooled MMW mirrors or miter bends. The later immediate turns would allow for multiple directional bores from a primary bore to another wellbore or fracture nest. This requires that the created rock melt/ vapors and fluids are prevented from blowback onto the mirror. Such bores would be straight in the direction initiated.

The gradual turn method also allows for some directional capabilities, which also change the Top Side equipment and setup. One special case of the gradual turning bore is for use of continuous (or very long segment) tubing (delivered coiled, but laid out for straightening) drilling multiple wells extending outward from one central surface well site. Each bore would start with a very shallow angle then gradually directional turn the bores into vertical over kilometers. This will allow targeting spread-out reservoir locations at depth.

## Industry Acceptance

It is important to note that the estimated total vaporization drill rates from Paul Woskov's plot, when compared to conventional methods, are ***NOT*** by themselves persuasive enough to industry to justify MMW systems. If melt drilling can be achieved, then the economics are much more favorable, the simplified systems and other MMW benefits (e.g., lowering other costs, less non-drilling time, case-while-drilling, etc…) will gain industry interest. Prototype demonstrations and proof of performance will bring acceptance.

However, many regulatory hurdles must also be overcome. Regulators are conservative and reluctant to change a 'working' system or be out of their comfort range. MMW changes must be clearly described and demonstrated. Rock melt liners are not 'comfortable' steel with known cement behind it- although this is not always the best seal. Further, all conventional EGS, geothermal, hydrothermal, oil & gas casings / liners must be pressure tested to ensure integrity and thus must be done on MMW rock lined wells for the same reasons and to prove their capabilities. Instrument logging tools (often acoustic in nature) are used to verify cement bond and adherence (to rock and pipe) and something similar can be developed and used on MMW liners.

The application of MMW for drilling will start with shallow prototype drilled bores, going to increasing depths for specialty applications. Targeting solutions for especially difficult conventional drilling problems (eg., very hard, hot rocks) would be the next step necessary for industry acceptance. Getting to EGS depths will take many years of building success and reliability.

**Cost Estimating**

Real cost analysis will only be possible in estimated form until a system is built, tested and used in the field. Total system cost will be the capital cost to build and the operational cost. Furthermore, the system will change and thus costs will be refined over time. We will need to develop system cost based on the cost of the individual equipment and estimates from similarly complicated systems.

There are likely to be some rock types and environments that this technology may work best and other environments that it will work poorly. But overall cost and performance must be better than the best available process to drill, control the environment and line/case for subsequent use as an engineered geothermal (power) system. Better performance must be clearly based on testing and backed up by rigorous theoretical considerations, not hypothesized. A broad brush cost/ performance analysis will be provided in this project and then it get more detailed, piece by piece, as data becomes available.

## DISCUSSION OF MMW DRILLING PROCESSES

*Listed by Importance to the Process*

Overall, a better understanding of the MMW process and its actual performance and effects of various factors must occur before heading into commercial applications or even prototyping. However, certain essentials of the MMW process are known and those can be considered for implementation into a full MMW drilling system. The following discussions build on the prior Key Systems section and include identification of problems and propose various solutions to those problems.

### Rock Reduction

This discussion covers topics over and above the basic ongoing tests of MMW drill rate and efficiency for various rocks (especially limestones,…) completed at MIT by Dr. Paul Woskov and Dr. Herbert Einstein. The first bench tests by Paul Woskov were on rock surfaces. Later bench tests will be in predrilled bore in the rock samples with the waveguide at the upper tip of the rock hole and with / without gas flow. The millimeter wave would bombard the rock surface or propagate into the predrilled bore, for studies of ablation efficiencies and bore wall vitrification, measuring particle sizes that escape, changing mode/waveguide, measuring a range of reflected power with temperature for characterizing rock types, different rocks (sandstone, granite, limestone, dolomite,…), energy input, etc… It is also known that fluids, especially water, absorb significant MMW power and thus will reduce MMW drilling efficiency. Another challenge to doing the tests include overcoming reflective power shut-down of the gyrotron. Solving this problem can be applied toward larger systems and other applications.

**Problem #1**- Can MMW power efficiently reduce or drill rock? What are the minimum power levels and optimum frequencies for commercial applications? What are the various factors that impact MMW rock reduction? How to overcome reflective power?

**Solution to Problem #1**- Ongoing bench tests at MIT using low power and frequency and extrapolated to desired higher power and frequencies. These tests are critical to determine whether MMW power can be used for drilling (and lining). One method to harness reflective power has been designed and is being tested.

**Problem #2**- **WATER EXISTS EVERYWHERE IN THE EARTH** below about 3000 feet (i.e., the water table) in the surrounding rock pores and in natural fractures. Water fills pores (2-25% by volume) that exist in all rocks, water fills natural micro-fractures, large natural fractures and in large canyons (mostly shallow).

Water and other fluids vaporize easier than rocks, and thus water and fluids will absorb the delivered MMW power before it impacts the rock. Water (as liquid or steam) existing at the cutting surface or even in the wellbore will reduce MMW power to the rock cutting surface. The reason it is easier to vaporize an equal volume of water is that water (and most all liquids) requires much less energy to vaporize:

vaporization/ boiling point-100$^{o}$C, 212$^{o}$F
specific heat capacity- 1J/g/K, 0.24 BTU/lb/$^{o}$F, and
heat of vaporization- 2260 J/g , 972 BTU/lb

when compared to most rocks first going through the melting stage:
melting point - 1000 - 2600$^{o}$C, 1832- 4712$^{o}$F
vaporizing/boiling point- 2800-3600$^{o}$C, 5072- 6512$^{o}$F
specific solid heat capacity- 1 J/g/K, 0.24 BTU/lbm/$^{o}$F
latent heat of fusion (melting)- 335-500 J/g,
specific heat of rock melt heat capacity- 1.6 J/g/K, 0.38 BTU/lbm/°F
heat of vaporization 4000-6000 J/g, 1720-2581 BTU/ lbm

Vaporizing a cubic centimeter of rock with a specific density of 2.7 starting from room temperature requires about 25 kJ, 23.7 BTU, to vaporize while for the same volume of water only 2.3 kJ, 2.2 BTU are required.

Therefore stagnant water (and other fluids) that is only a small fraction of the rock volume will cause a only small perturbation on the drilling efficiency, but large liquid flows could present a problem. Flowing liquids will absorb much of the delivered MMW power before that power can significantly impact any exposed rock. Thus, it is very important in MMW drilling to prevent water (whether as a liquid or as steam?), and maybe any liquids, from entering the wellbore, so that the millimeter wave power can efficiently transmit from the waveguide to the cutting rock face.

**Solution to Problem #2**- Push all water and liquids away from the wellbore and cutting surface and out into the surrounding rock (pores, fractures either natural or induced) by momentum forces, over pressure, thermal shock/ cracking, thermal expansion (converted into pressure) or other means PRIOR TO OR CONCURRENT WITH THE MMW POWER HITTING THE CUTTING ROCK SURFACE. Since this directed energy drilling process will operate at high temperatures > 1000 °C, thermal expansion of water / fluids will cause local over pressure to counter any inflow, this is a realistic direction to pursue. See later discussion on creating voids in the rock.

**Problem #3**- MMW drilling of a bore encountering water filled ‘canyon’ or very large fracture (even with overpressure- discussed later) whose large fluid influx stops the MMW drilling process.

**Solution to #3**- Steps would include dropping/ pumping seal material in multi stages into the wellbore at the offending zone, melt the pellets with MMW power until the zone is filled and sealed (method discussed further in the wellbore lining section). It might take a large volume of pellets and significant non-drilling time to cure this problem. Also running expandable casing is possible once the segment is <u>somehow</u> drilled.

**Problem #4-** The rock and fluids at the cutting surface will literally explode with application of MMW power. This is because the MMW power can penetrate the rock several centimeters and vaporize pore fluids and rock material {P Woskov}. It is very

important to understand the conversion of solid rock into particles, then into melt, and then into vapor under severe MMW bombardment. It is important to note that as the particle size (not a cloud array or aggregate) decreases to less than 1/4 a wavelength (General atomics 170 to 110Ghertz, 95 GH for army active denial= 3 mmw wave length thus ¼ = .75 mm particle sizes), they will become invisible to and be less or not impacted by the MMW beam. All of this phase conversion causing volume expansion will occur within and mostly at the bottom of the wellbore (with fixed walls), resulting in an increase in upward velocity. Wellbore pressure in the wellbore will hold down this upwardly mobile plume to some extent. It is important that this plume does not enter the waveguide- existing at some safe standoff distance. Such a plume may impact the MMW power delivered to the rock cutting face as well.

**Solution to Problem #4**- This rock-to-melt-vapor-melt-solid conversion process must be modeled (vectors, velocities, size, distribution,…) and then bench tested at some later time. Temperature control/ cooling with fluid/gas flow from the surface may also be possible and can be estimated to moderate standoff pressure.

**Problem #5**- Significant heat (sufficient to melt or vaporize rock at about 3000$^{o}$C) will be generated during the MMW rock reduction process. For every 1 MW of beam power directed down hole, all (except for a small amount of reflected energy) will be converted into heat. A small amount will escape the wellbore by conduction into the surrounding rocks. An unknown amount will be lost by mass transfer/convection/ transport into the surrounding rocks or (known) lifted to the surface. On its own, that delivered power is sufficient to vaporize 10 feet of dry rock in an 8” diameter per hour at that 1 MW power level.

Heat will be generated in the waveguide by energy loss (set by pipe type and mode) over the entire length down to EGS depths. The losses will depend on the frequency, waveguide diameter and conductivity, and the uniformity of the inner dimensions. The design goal will be to keep these losses under 30%. Heat will also be generated when the energy wave mode is (even temporarily) converted to a lesser mode when it encounters bends, abrupt shape changes/misalignment, or other imperfections in the waveguide.

Due to the potential for large amount of heat created and stored in the rock surrounding the wellbore, care must be exercised when the waveguide will be eventually advanced into this heated wellbore/rock wall environment, unless cooled by time or injected fluids. Also problems (deposition of hot particles on wellbore wall and drill pipes) exist if the drilling debris is brought to the surface (discussed in more detail elsewhere).

**Solution to Problem #5**- Study the heat transfer characteristics of a propagating melt front in rock with *fluid flows from the surface* to minimize heat losses away from the working melt/vaporization front. The thermal conductivity of rock is very low; therefore if the penetration front advances quickly enough heating sideways into the walls could be kept small.

Also, investigate the possibility of not bringing drilling debris to the surface- dispose insitu. The required procedure when stand-off distance gets too great is to- stop drilling, wait for natural cooling, circulate water until returns are cool, advance the waveguide, set the packer/ seal, provide low-MMW power to remove water until the wellbore is dry, slowly increase MMW power to resume drilling. Also, must use high temperature components materials on lower portion of the drill string/ waveguide/ circulation pipe.

If the drilling debris is not removed from the wellbore to the surface, where can it go?

**Rock Removal and Disposal**

In all drilling processes, it is important that the drilled debris be removed from the virgin rock face so that new/ virgin rock can be exposed to the ongoing drilling process.

Providing sufficient downhole cooling of such hot drill debris materials, the waveguide and rock walls may not be possible. That cooling flow can be estimated from the MMW power sent downhole, but that estimate is additive to the required cooling of the waveguide. If drill debris is circulated up the annulus uncooled, it will deposit / scale onto the drill pipe / waveguide and rock wall which can stick the drill pipe and cause loss of the wellbore.

Reduction of the rock is merely the first step, disposal of drilling debris is a critical issue. DOE Los Alamos National Lab conducted the Subterriene Project (about 1985-1990) with engineering assistance from DOE Sandia NL. They used an electric tungsten carbide heating probe to melt various rocks. It was found that a liner could be formed only with quartz rock. It was hypothesized that quartz could be added to get a good melt liner. Conversely, if quartz forms too brittle a material for sealing, then additives/ materials may be needed to quartz rocks to form a stronger, less fragile liner, e.g., ceramics. This is a chemistry problem that can be studied further. Layered glass is more flexible than a solid thick layer, better for in-pore formed glass. The capability of different MMW generated rock melts to form a liner should be tested.

**Problem #6**- The condensing point of the rock (approx. 5432$^{o}$F, 3000$^{o}$C) is higher than the temperature at which steel properties start degrading (about 600$^{o}$F, 316$^{o}$C), so that any direct contact of the rock and steel pipe would damage and may destroy the waveguide/ pipe. It may be possible that very large standoffs and pressure drops between the waveguide and the bottom rock face may cool off the particles enough to not damage the lower steel pipe/ waveguide and mode conversion end.

Returning any hot rock particulates or fluids to the surface is not desired. Surface discharge of such a large amount of fluid is problematic due to environmental considerations and permitting. Discharge all drill debris at the depth found.

**Problem #7**- Rock debris must go somewhere. If a large temperature drop cannot be achieved in the wellbore, the system cannot bring the created hot rock materials (as

vapors, melts or particles) and hot produced brines to the surface, because the cooler temperature at the upper depths and the resulting depositional problem onto the rock wall and pipe that will occur. This will stick the pipe/ waveguide in the well and potentially junk the well.

**Solution to Problem #6&7** - The only method left is to deposit all the drilling debris (rock and water) back into the rock as the wellbore is drilled AND, if possible, not even allowing the debris to come into the wellbore. This requires that a void(s) be created in the rock at (best) or near the cutting/ drilling depth by a singularly or in combination of methods - thermal cracking (high temperature difference between the adjacent rocks, possibly causing enlarged wellbore and unstable well bore walls), shear dilation (relieving existing in-situ geologic stress), by simple tensile rock failure (ie., exceeding the rock's tensile strength or fracture/ parting pressure) by hydraulic means or melt compression.

Within the well bore, it is important that the reduced rock particles are reduced or melted sufficiently that they can enter/ be pumped into/ otherwise forced into the existing pores or created voids. The 1/3 rule on particle bridging would apply- the rock particles must be less than 1/3 of the opening aperture or they will likely bridge and plug the opening. Note that MMW power will vaporize the rock into nano-sized particles or will continue to reduce particle size until they are at least less than 1/10th of the millimeter wavelength {per PW email and prior discussions}, the size at which they will not be affected by the millimeter wave, unless they reach a high population density (e.g., bridging at aperture). For a 100 GHz the MMW wavelength would be 3 millimeters/ 0.12 inches {per PW email}, thus unpacked, stabilized particle size would be about 0.3 millimeter (0.012 inch, 300 micrometers). Steam, melts and these smaller particles would have no problem entering even small openings.

*This proposed insitu disposal process provides a very beneficial '**casing-while-drilling' capability**. It also provides the system a 10X lower energy requirement (particles/melting than vaporizing all rock) for drilling. It also provides a built in **drilling balancing or stabilization action** where the energy required for minimum rock reduction (particles reduced in size, melted then vaporized) is balanced by the earth's/wellbore's disposal capacity at that exact time and for that current wellbore to pore pressure difference. If, for example, a tight deep rock with no permeability is encountered and MMW generated particles are too big go anywhere, they will remain in the wellbore and be further reduced in size by higher cumulative MMW energy absorption. If it remains in the wellbore long enough it would transition it into smaller and smaller particles, then into melt then into vapor. An opposing trend on the disposal side exists by the increasing temperature causing higher thermal cracking in that area and the local over-pressure due to high temperature will cause wider and deeper fracture openings to take the largest size particle or melt or vapors that exist in the wellbore at that time. Conversely, in a highly porous/ fractured rock, larger particles would be flushed out of the wellbore in minimal time and minimal MMW power expended. Also high temperature rock melt is a non-Newtonian fluid that can be compressed to a smaller volume than the starting solid rock, thus creating additional*

*voids. Such high temperature flows will affect the solid rock that it contacts as well as vice-versa.*

**Pressure Regime**

The only method to prevent water/ fluids entry into the wellbore and / or to push existing water/ fluids and rock debris away from the wellbore, requires multiple actions- create and maintain an internal pressure condition, within a mostly sealed and limited volume, that is greater than the pore pressure in the surrounding rocks. The creation of such a high(er) pressure condition will likely be from the MMW process itself- high temperature and vaporization of material expands their volume and within a fixed space the pressure will increase until something fails and releases the built up pressure. Preferably it will be a rock pore/fracture, or if pressure is higher the rock will fail at its tensile fracture pressure. Such a created fracture at deeper depths will mostly be near vertical (perpendicular to local minimum stresses). Also, the desired internal pressure can be controlled and maintained by injecting fluids at the surface. The pressure range for an assumed 20,000 feet (6.1 kilometers) wellbore with an assumed compressed gas (0.7 specific gravity) transmission fluid is-

To ***just balance the rock pore pressure*** (normal pressure gradient range of 0.43 to 0.5 psi/ft, normally near 0.45 psi/ft) the required bottom hole pressure would be 9,000 psi. The required surface pressure to obtain this downhole pressure would be about 3,000 psi assuming the stated fluid gradient. This is manageable with current technology.

To ***fracture the rock*** (fracture gradient range of 0.6 to 1.0 psi/ft, often near 0.8 psi/ft) the downhole pressure would be 16,000 psi. The surface pressure required to obtain that downhole pressure would be 10,000 psi, a very high challenge and above current technology. A higher density transmission fluid, if one could be found, would lower that surface pressure requirement. This means that the MMW transmission fluid must operate efficiently at these higher pressure (and temperature) conditions- ***TO BE TESTED see transmission section***. It is assumed now, but to be tested further, that the MMW process' thermal stress cracking at the cutting surface would lower this required fracture pressure. Furthermore, deeper, hotter rocks often fail at lower pressures than the normal gradient due to shear dilation, temperature degraded strengths, chemical changes and other factors.

After the creating the required pressure condition, a sealed volume is required to maintain that pressure. This is because that pressure cannot be sustained if internal volumes leak off/ cool off faster than what can be created or injected. If injected at the surface, it cannot be afforded due to high cost of the transmission fluid and the expense of compression/ pumping. This then requires a fully sealed wellbore steel or rock melt casing /liner OR a sealing packer to isolate it away from the operating zone. It also needs the entire standoff interval mostly (not fully) sealed as well. Maintaining this pressure condition by fluid injection requires a low cost (due to potentially high losses) transmission fluid to constantly pump into the well at the surface.

Over pressure in the wellbore (ie., a pressure over the pore pressure) will aid all other methods to push all rock particles/ melts / vapors into the created rock opening or into existing pores and fractures, initially bridging at the face (due to particles of too large a size) until they are reduced in size further or melted by the MMW bombardment when they can flow out into the created void. Higher wellbore pressure (from the transmission or wellbore fluid) can also be applied to cause additional failure of the rock and widen the rock opening exit from other methods.

Over pressure minimizes the plume (consisting of the rock particle/melt/vapor and water/supercritical steam) that can block the MMW power from the cutting/ reduction face. Such absorbing would reduce or stop the drilling advance. This disposal method eliminates the need for high rate circulation to cool and remove the heated particles and produced brine to the surface. Such injected water may deleteriously find its way into the borehole with the MMW power. Such rock vapor cooling would also prevent cooling of the waveguide from MMW transmission losses. This disposal method eliminates the concern of vapor/particle/melt deposition on the upper/shallower pipe and rock walls which can stick the drill pipe in the well and/or permanently damage pipe due to high temperatures, at a minimum.

Per the above requirement of depositing the drilled debris (rock and water as particles, melts or vapors) into the rock as it is drilled, preventing of rock debris, especially water, from entering the wellbore from open wellbore rock pores or natural fractures, certain pressure regimes in the wellbore are required.

Maintaining this overpressure condition requires a low cost transmission or pressurizing fluid **(liquid or gas)** due to potentially high losses into the rock. Being a gas or supercritical gas with a lower density, most of the required downhole pressure will be reflected to the surface where the surface equipment must be able to safely handle and even generate and maintain that high pressure regime. This is also a non-trivial issue.

This must also cover even highly over-pressured (12-15 ppg mud equivalent) zones encountered in the earth.

**Problem #8**- The open hole above the cutting depth must be fully sealed to prevent cooling fluid losses. A method to test this seal while drilling and to repair such leaks in the rock wall must be developed.

**Solution to Problem #8-** Placing/ stacking/ dropping pellets or tubes of MMW meltable materials (copper, quartz, etc…) at or above the leak and melting them with MMW power at a suitable mode and with over-pressured transmission fluid would force/ pump that melt into the leaking rock to repair it. The sealing additive material can be selected for its melt temperature and flowing viscosity. Quartz and its mixes are a natural choice since our experimental tests showed such favorite characteristics.

Drilling over-balanced **will** require that we have a method to seal (at surface or surface / downhole) the wellbore as it is drilled. This is a non-trivial issue. In many options identified, a downhole seal is required between the waveguide and the hot rock melt

lined wall due to MMW drilling. That sealing section will need to be cooled then trimmed/smoothed before a packer/ seal is placed exactly on it.

**Transmission**

Transmission equipment and systems were discussed earlier. It is best to provide a high efficiency cladding to the pipes before utilization. However, improvements in the transmissibility performance may be obtained by adding highly conductive materials in additives/ pellets/ beads/ grains into the MMW power path for melting and distributing along the waveguide. It may also be possible to increase transmission efficiency by increasing the diameter and frequency of beams in operation, since ohmic losses decrease as one over diameter cubed and frequency squared.

HE11 or TE01 modes are anticipated to be the most efficient for transmission down long waveguides/ pipes. HE11 requires corrugated or internal machined waveguides. The machined grooves required are specific for the wavelength and can be 'screw' or continuous helical thread types for easier, but still costly machining. The specifications of such machined grooves would change with bends, axial loads (hanging in the well), erosion of pumped fluids and slurries, corrosion and just normal wear and tear. The TE01 mode can be used in smooth circular pipes with an efficiency that is 69% of the HE11 mode, but would require internal corrugations to achieve changes in drilling direction without mode conversion. In either mode, at imperfections or irregularities (ID restrictions, ovality, etc…) in the pipe or rock wall or with bends using any mode, a partial mode conversion may occur that may generate heat. Sufficient heat may be generated to anneal or melt even steel pipe possibly causing the loss of the well. Methods to identify when this is occurring are needed for a robust MMW system.

The "waveguide" system is critical to efficient delivery of the MMW energy downhole to the rock cutting face and includes the pipe and the rock wellbore. The efficiency of drilling across large borehole standoffs can determine the preferred method of drilling and the pipe types possible. Other than plume size, density and material, the wellbore smoothness and dielectric constant are important in determining the maximum standoff distance. The wellbore dielectric constant is a function of rock type and its melts on the bore walls as it related to borehole transmission efficiency. Transmission is not strongly affected / dependent (weak) by material di-electric constant. Not as important to the process. Methods may be needed to smooth out imperfections and add higher dielectric materials onto the walls to improve efficiency. Partially true (true for diameter restrictions) It is interesting to note that for a directed energy MMW drilling process transmission could be self-correcting to imperfections because losses to an imperfection would increase until it is corrected after which the losses decease and the beam continues to propagate forward. It is also possible that a mode change would cause heat and can occur after the imperfection- needs testing.

**Problem #9:** The transmissibility of various fluids at such high pressures and temperatures is unknown and must be bench tested. The cost of such fluids in high volumes and their safety/ properties must also be determined. Leak and losses add

cost. Can a high efficiency MMW transmission fluid/ gas be found for pressures up to 10,000 psi? No data is available for pressures much above ambient. No data is available for such fluids at elevated temperatures as well.

**Solution to #9:** Perform bench tests of various potential transmission fluids/ gases at pressures from 0 to 5000 psi and temperatures from 70$^{o}$F- up to 500$^{o}$F degrees using comparable MMW transmission to measure transmission efficiency. This work is beginning at Impact shop with measurement help from Dr. Woskov at MIT. Because of losses the fluids must be readily available.

Water in liquid form is detrimental to MMW power delivery to the rock, but is it in its vapor/ steam state or even in supercritical state?

**Problem #10**- The MMW gyrotron window must be strengthened to operate in this higher pressure regime. Such a design must be made, built and tested. It must also operate at the anticipated higher power levels of 1 to 2 MegaWatts. Such windows do not exist at this time.

**Solution to Problem #10**- Bench test various MMW window materials for up to 5000 psi in the diameters anticipated. This is being done in the current project at minimal power levels for testing transmission fluids at elevated pressures AND temperatures.

**Problem #11-** Need to understand the effect of such imperfections on millimeter waves, the heat generated and its profile along the pipe. Monitoring the impact of such imperfections/ changes in MMW modes is important.

**Solution to Problem #11-** Perform theoretical studies and bench testing of the influence of imperfections (bends, ovality, ID restrictions, etc…) in the waveguide (both pipe and borehole), including rock (and their melts) types.

With the use of a high temperature or all metal packer, tension can be pulled to straighten out the pipe/ waveguide fully for improved transmission efficiency.

**Problem #12-** A waveguide (herein, pipe) can be made out of any material (highly conductive material is better) or shape. It is just a question of size (diameter) and uniformity. A high power beam that is capable of melting material must form an efficient size (within waveguide diameter) before it will propagate forward. It is just a question of power and diameter. However, in downhole applications the diameter is somewhat fixed. Therefore a ‘show blocker’ to MMW drilling will be if the whole open wellbore section of the diameter allowable cannot be a good waveguide because of non-conductive rock melt material and non-smoothness, irregular shape and imperfections in the rock wall ID. This needs to be tested and understood.

**Solution #12**- Bench test wellbore conductivity, transmissibility of various rock melts. This work is partially being performed at MIT in this project. Investigate options of adding conductive materials to be vaporized and allowed to coat the wellbore lining.

**Top Side**

The most likely drilling methods possible and envisioned are-

1. Constant stand-off drilling using continuous waveguide/ pipe advancement - where the waveguide is moved with the advancing/ deepening hole to keep a specified stand-off distance to the cutting surface. MMW beams react directly on the rock face. Over pressured versions are preferred. The benefit of this method is that the influence/ inefficiency of using the open borehole as a waveguide are minimized. But it is important that the waveguide not get too close to the bottom rock face being drilled, due to temperature and particle velocity effects. In the option that a packer or seal between the waveguide and the rock wall or cased wall is not used, then the full open hole is at the operating pressure. The detraction of this method is that inner and outer pipe cooling by cooling liquid circulation is not normally possible without a packer/ seal assembly. A sliding seal (outer waveguide surface to packer) within a packer with a rock melt seal is required to isolate the annulus from the lower operating region and allow cooling fluid circulation via concentric pipe. Continuous pipe strategies may be possible with this version. Disposal of the gas transmission fluid also used as a coolant to the waveguide into the open hole is also possible.
2. Variable stand-off drilling with staged packer/ pipe movement - where the waveguide is attached to a packer/seal drill tool which is sealed to the rock wall or set casing at some depth. In this method the standoff distance (waveguide tip to the rock face) increases as the hole is drilled down. There is direct MMW beam to rock interactions. Circulation for pipe cooling is possible in this version by using concentric pipe (SEE DRAWING #1) and the annulus for return flow. Each pipe can be run separately. At some standoff distance the drilling efficiency in the open hole bore decreases and drilling stops. A caliper tool and certain instruments (for rock and fluid type determination) can be run through the waveguide (consider wear on corrugated machining) to survey the drilled distance below the packer assembly/ wave guide end to total depth. Another expanding milling tool can then be run through the waveguide to near the bottom and opens up to mill a smooth interval for the next packer assembly placement, similar to an under-reamer now used with expandable casing. The packer/seal & fixed waveguide are then released from the wall by MMW heating and moved down to and reset at the new deeper location. Drilling then resumes as before. Jointed or continuous pipe can be used. This method requires knowing that the bore will provide a decent waveguide that has good conductivity materials (rock type) and not too many imperfections. Otherwise, methods to add conductive material to the wellbore wall will be required. The rock melt wellbore created by this method will not be smooth, but will have a minimum diameter based on the packer / seal diameter. MMW beams do have a self-regulating feature to them since larger diameters spread the beam too wide to be useful in heating.

3. Drilling Head/ Tool with Indirect Heating- Transmitting MMW beams downhole to a resonant cavity residing within a drilling head/ tool at low pressure is also possible. Using the MMW beam to heat the drilling head to temperatures of 2200oC to 3000oC which would then heat and vaporize the pore fluids and melt/ vaporize the rock below it. This method is highly dependent on the materials available to withstand the temperatures and abrasiveness required. Weight on the Tool Head would counter act the generated pressure below the tool and force it deeper as the rock is displaced out into the surrounding. The required seal would be from the length of the Tool and would use hot rock melt. With either jointed or coiled tubing the pipe can be advanced continuously.

Concentric pipes (waveguide within a cooling fluid pipe conduit) can be used with the annulus as the return flow to cool the waveguide and rock wall. The pipes can be joined or run separately and sealed downhole.

Multiple wells on 1 surface wellsite location can use a continuous long pipe that is stretched out on a 2500 foot rail system. The gyrotron, electric generator, gas compressor/ liquid pump and tanks would be on the end of the pipe and move with the pipe as it is inserted/ well drilled. The surface angle would be a low <30 degrees from horizontal that slowly turns vertical over some great distance (kilometer) to minimize transmission losses and heat buildup. Such early/shallow high angles can normally be a problem in very deep wells due to increased drag or resistance to rotation, but these are not as much of a concern with MMW drilling systems. The continuous pipe would be moved to the well site in coiled racks of 2500 feet. It would be rolled out on racks parallel to the rail and that pipe would be processed (heated with MMW and pulled with tension) to straighten out it. The internal diameter of the pipe would then be milled/polished onsite to smooth for efficient MMW transmission.

The bottom hole assembly with the waveguide must be ceramic or other high temperature alloy (tungsten, titanium, ceramics,….?) because of the generated heat and retained in the rock(s). Need to look at the gas turbine technology for some material suggestions since high temperatures are utilized in almost all gas turbines.

Another Top Side pipe handling version, is to have a teardrop shape structure (low and thin away from the well rising up going to the well) that would hold continuous (or even jointed) pipe and gradually increase the height as it nears the well, but then allow a rapid decline near the well so that is becomes vertical at the wellhead/bore. Away from the far end of the tear drop, a rail system would be used for connecting the gyrotron, generator and gas source so that it would travel with the pipe end. That method for drilling with continuous pipe is only possible if an additional length (of stroke desired) of continuous pipe is used before connecting the gyrotron assembly to avoid lifting those heavy pieces of equipment.

**Wellbore Lining**

Extreme overpressure MMW drilling discussed earlier allows an immediate lining of the wellbore during well drilling. Regulatory bodies would not (immediately/ soon) allow use of only a melt liner for isolation across fresh waters, brines, oil and gas zones. Those are mostly shallower than EGS zones. Testing of melt liner can be by pressure testing and by instrument (mostly acoustic) wireline logging.

Rock type is important -very interested in testing limestone, shales and dolomites for how they perform in lining the bore and in MMW transmissibility performance. The wellbore diameter and MMW frequency need to be appropriately sized to conduct the MMW beam in the wellbore. Additives may be used at extra expense, if needed,

Lining repair method - to go back and fill gaps that are still leaking or don't hold pressure. This can possibly be done with additives, such as silicate or other materials in the form of tubes, balls or pellets, that are deposited/ placed in the bore and then melted with MMW energy and over pressure. That combination would cause the additives to melt and flow into the porous rocks zones. With contact of the cooler rock the melt immediately sets up and seals.

We also believe expandable casing with an external seal coating may be helpful, as those jobs are being done right now in casing drilling. Each length would be about 3000 feet. To do this, it is very important to know that MMW can create a fairly controlled ID in the open hole section to be able to use the existing and commercially available expandable casing reamers – run through the waveguide, then open and rotate using downhole motors to dress the bore. These casing means and tools come from the oil and gas casing- drilling side of the business.

**Measurement**

It is important to note the reflected MMW power isolator to prevent damaging reflective power from reaching the gyrotron may also serve to allow measurement of downhole operation- if response characteristics can be determined for each need. Dr Woskov already has a patent on one version of this capability. Measurements of interest are - depth to the rock face or the cloud/ plume of rock/water vapors, temperature, plume composition.

Composition would help determine the lithology that we would be drilling through, and maybe the pore fluids. It is important to determine whether we have water coming in the bore and that it is what is stopping MMW drilling advancement. It is thus very important to test the responses/ characterization of different rock and fluid types over the frequency ranges. If we can identify when we have a water plume in the wellbore, then we can take certain steps to remedy that problem by increased pressure to push the plume out of the bore. A caliper would be also important to determine the ID for casing and the deviation would be of interest if that could be determined. Identifying errant MMW behavior may show how practical MMW drilling can become.

**Directional Capabilities**

MMW directional must be very, very gradual or very abrupt -nothing in between. Also MMW power does not care what direction (inclination or azimuth) it is going. However, it does want to go perfectly straight without interference. If a very gradual turn is desired it may take a full kilometer or more to obtain a 90 ° bend. The limiting reason of the bend rate is the resultant heat rise that would occur within a waveguide bend. The greater the bend the greater the heat generated. In fact, too high a bend would result in a loss of transmission mode and waveguide burnout/ melting for a parting of the pipe and that pipe dropping down into the well making the bore junked.

One option for field development would be to directly target the desired bottom hole location from the surface and drill a straight hole to that location. Many well could be drilled from the same surface location with minimal rig moves. This would results in a downward conical, wheel spoke pattern.

Conversely, gradual directional build and control can be obtained in its simplest form by offsetting the bottom waveguide end in the borehole slightly off center. In a vertical hole, utilizing such an offset tool to displace the axis continuously in one azimuth direction would yield a slow bend in the borehole trajectory. The amount of displacement will result in the rate of angle build. Since an MMW pipe does not need rotation, then only a vertical movement is needed and maintaining the desired direction displacement is easier. Directional surveys at regular intervals would still need to be run through the waveguide end. The problem come in with a large standoff distance (waveguide to borehole end) since the existing bore will have one set orientation and the offset orientation will be slightly different. The offset tool will follow the existing bore to a large extent.

For the other end of the spectrum of directional drilling, a cooled mirror (as used at the surface) can be attached to the bottom of the wave guide for immediate directional turning (ie $90^{o}$ turn in 0 distance). It can be oriented by pipe rotation and verified by survey tools run down the waveguide initially. Its depth can be set by the waveguide depth and verified by the survey tools. It must be cooled to prevent melting. The length of the created directional bores by this MMW mirror method will depend on the frequency and well bore diameter. With a 100 GHz frequency and a 4 inch bore it can be a thousand feet long and multiple bores can be placed in dense patterns. Such bores would be melt lined if performed pressure overbalanced. Overpressure and disposal of drilling debris must be at the drilling tip for mirror directional drilling, since high velocity hot rock particles must not directly impact/ contact the mirrors or miter bends. Also, such mirrors must also be cooled continuously during operation which requires a circulation loop to the surface. This directional capability would be very important for EGS, nuclear waste storage/ entombment, especially for microbore array drilling.

# Appendix B

# SPT WellFlo
# Hydraulic Modeling Study

**Chapter 1 Results for the well with 10000 MD ft, 400 °F formation temperature at depth, 1 bpm brine influx, 50 psig surface return pressure, 10 MMscf/D injection rate**

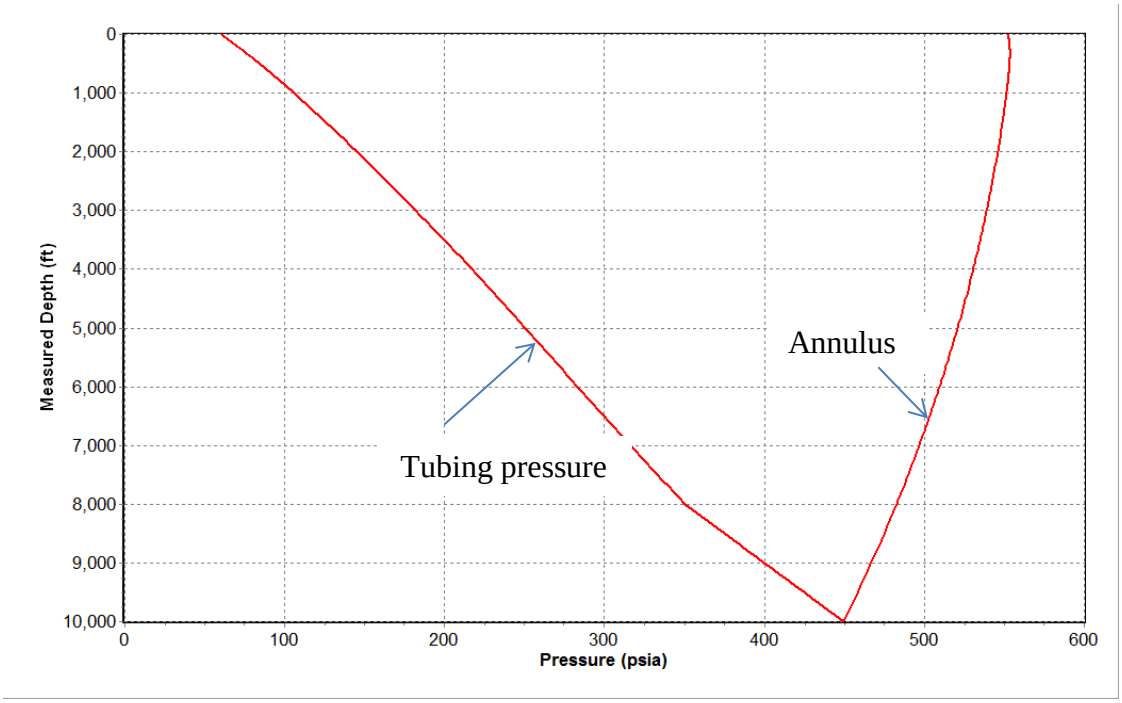


Figure 1-1 Pressure profile
(50 psig surface return pressure, 10 MMscf/d injection rate, 10,000 MD ft well depth, 1 bpm brine influx, 400°F formation temperature at depth)

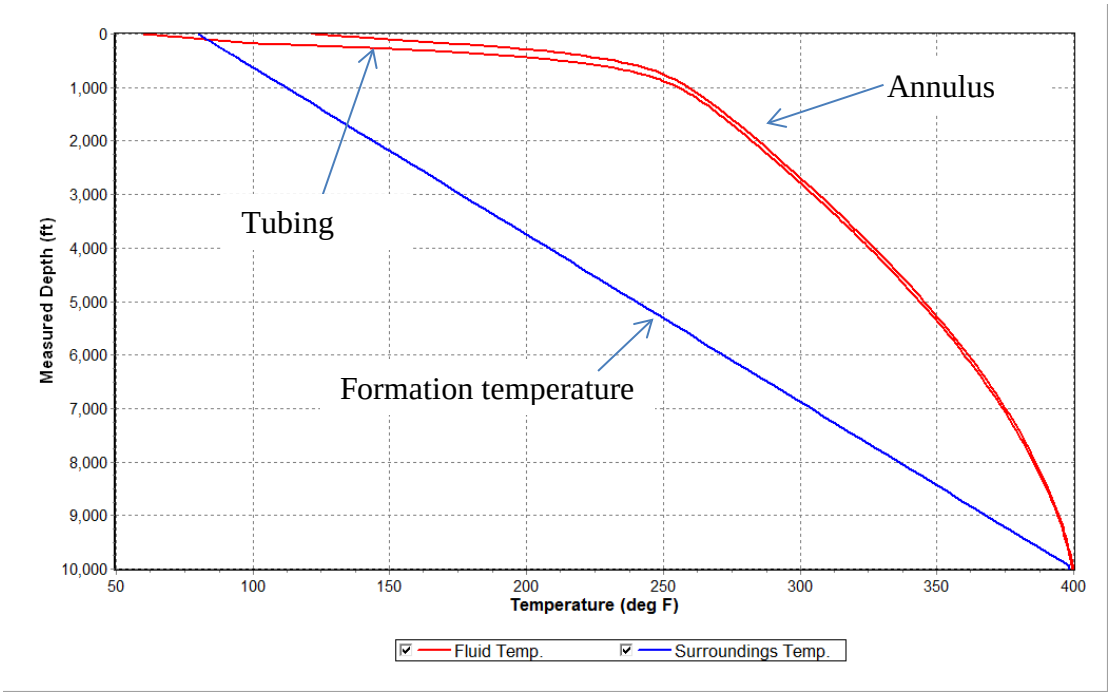


Figure 1-2 Temperature profile. (50 psig surface return pressure, 10 MMscf/d injection rate, 10,000 MD ft well depth, 1 bpm brine influx, 400°F formation temperature at depth)

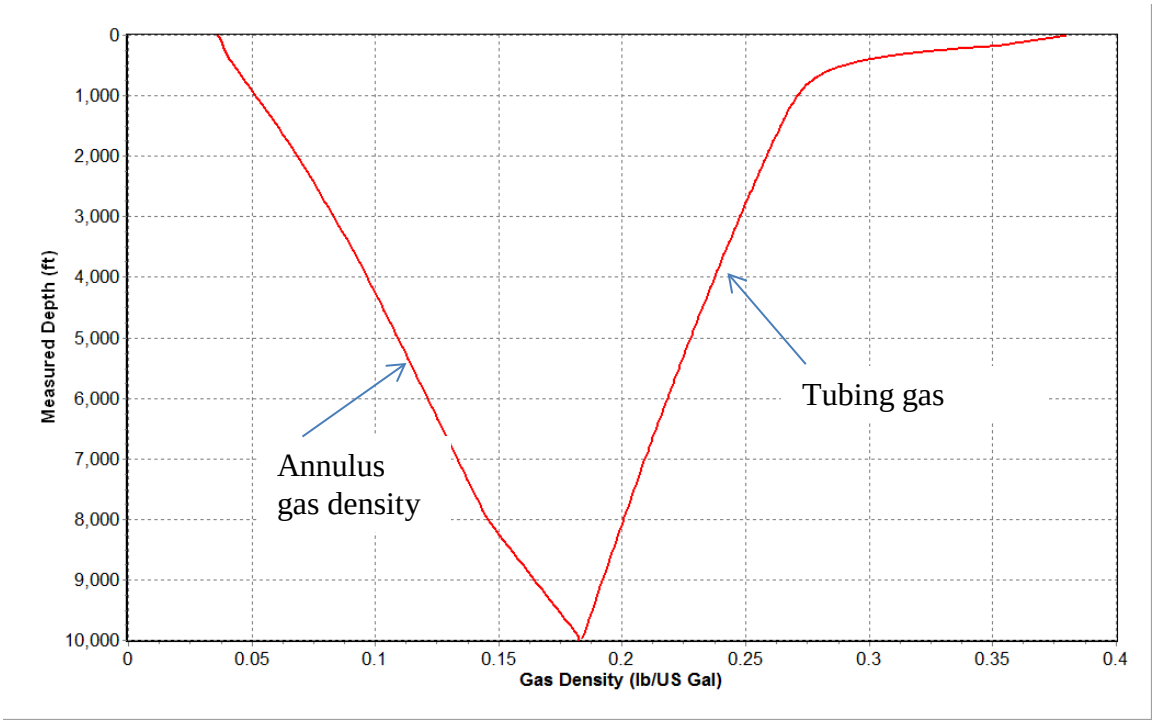


Figure 1-3 Gas density profile. (50 psig surface return pressure, 10 MMscf/d injection rate, 10,000 MD ft well depth, 1 bpm brine influx, 400°F formation temperature at depth)

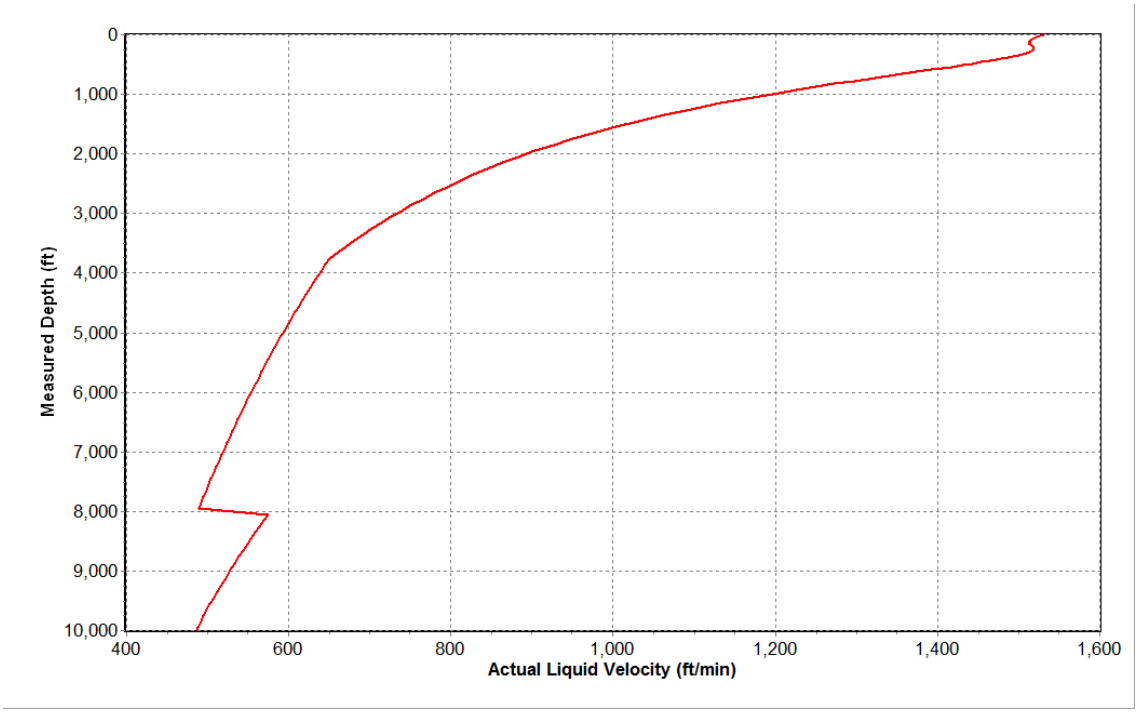


Figure -4 Liquid velocity profile

(50 psig surface return pressure, 10 MMscf/d injection rate, 10,000 MD ft well depth, 1 bpm brine influx, 400°F formation temperature at depth)

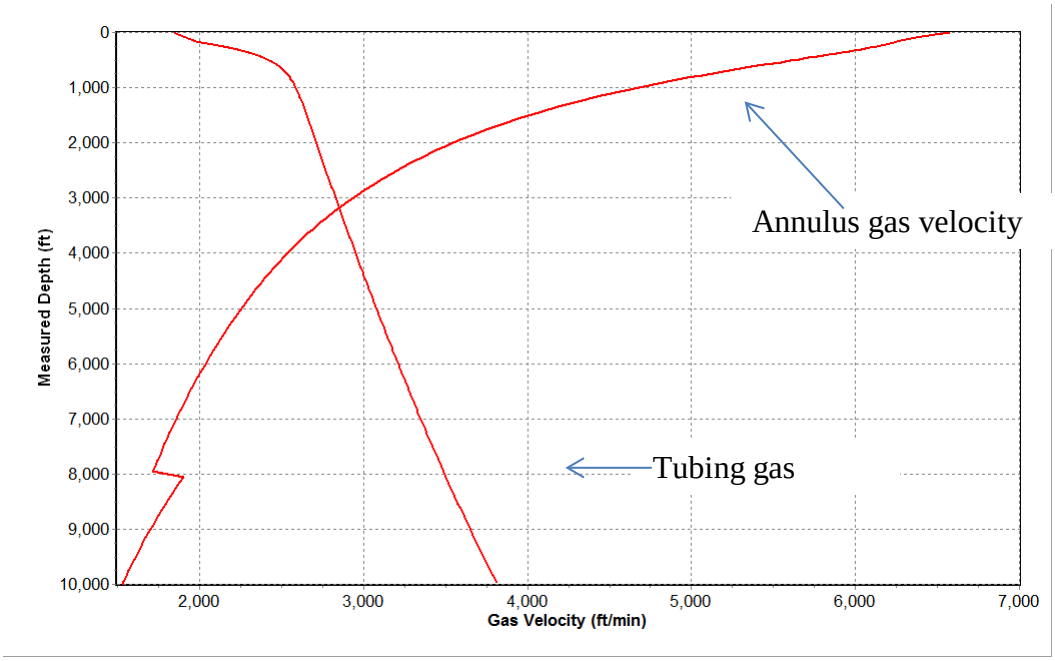


Figure 1-5 Gas velocity profile (50 psig surface return pressure, 10 MMscf/d injection rate, 10,000 MD ft well depth, 1 bpm brine influx, 400°F formation temperature at depth)

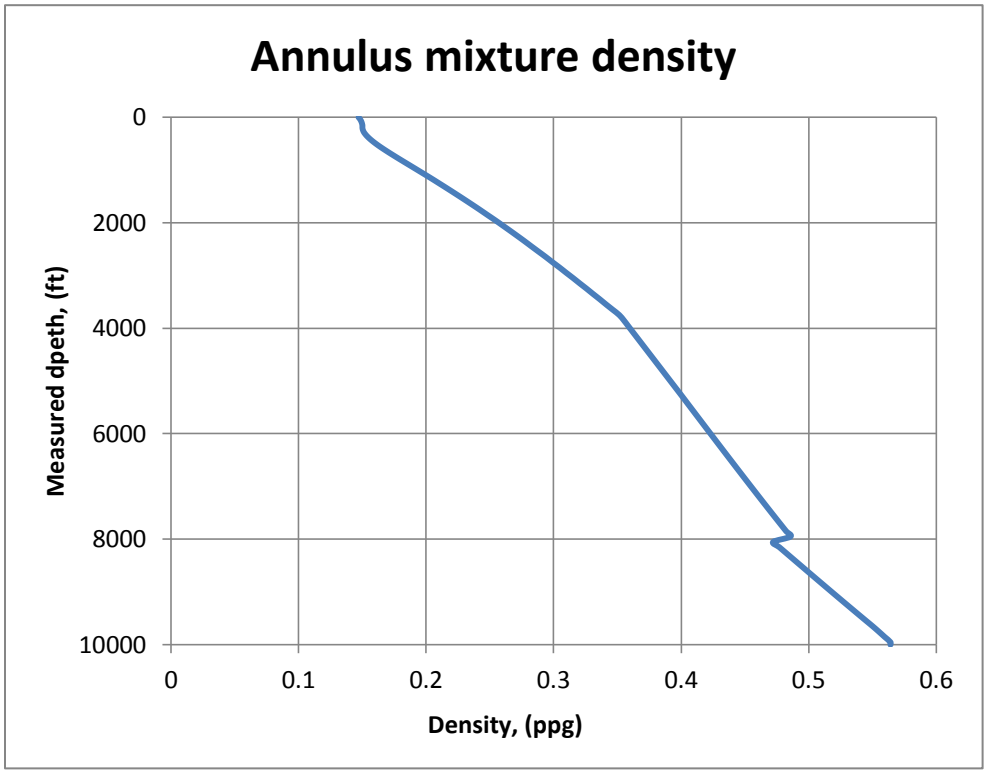


Figure 1-6 Annulus mixture density profile
(50 psig surface return pressure, 10 MMscf/d injection rate, 10,000 MD ft well depth, 1 bpm brine influx, 400°F formation temperature at depth)

## Chapter 2 Results for the well with 10000 MD ft, 400 °F formation temperature at depth, 1 bpm brine influx, 50 psig surface return pressure, 3.5 MMscf/D injection rate

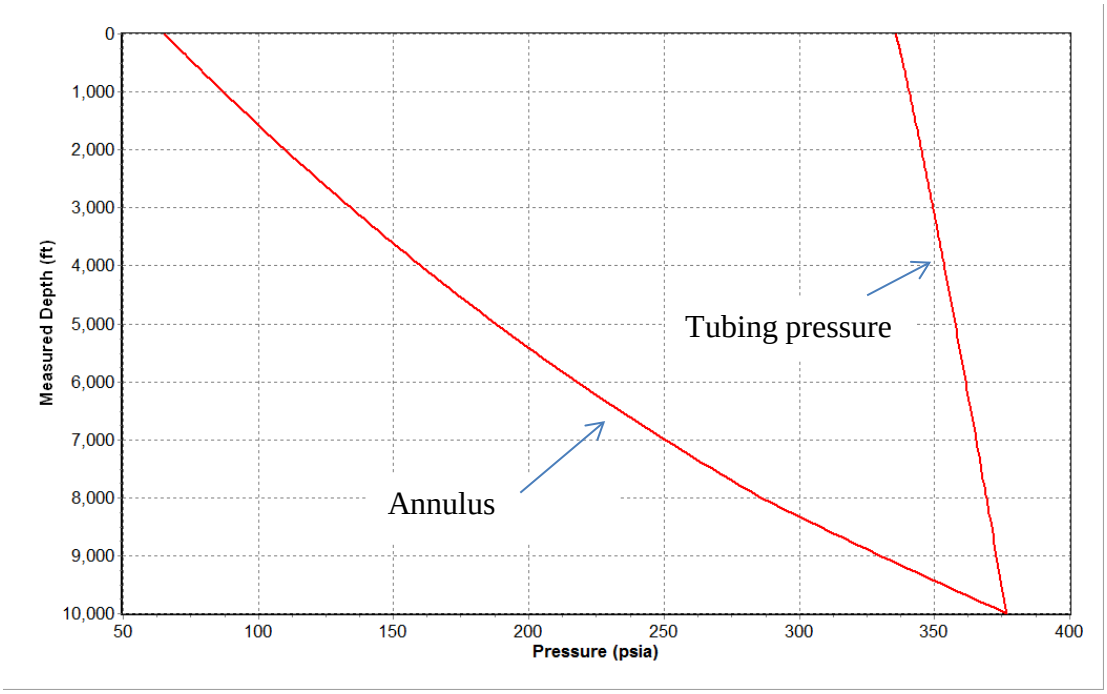


Figure 2-1 Pressure profile (50 psig surface return pressure, 3.5 MMscf/d injection rate, 10,000 MD ft well depth, 1 bpm brine influx, 400°F formation temperature at depth)

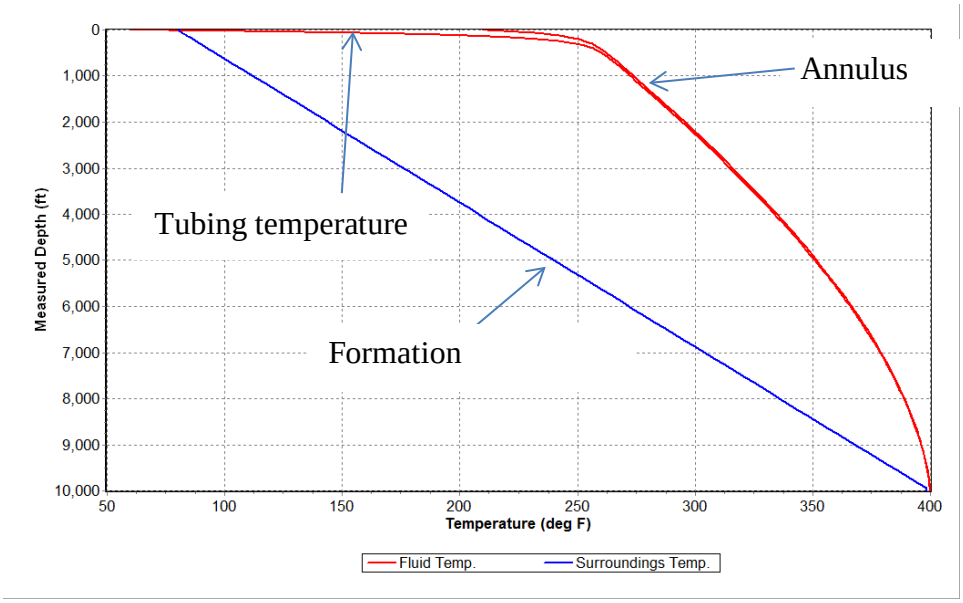


Figure 2-2 Temperature profile (50 psig surface return pressure, 3.5 MMscf/d injection rate, 10,000 MD ft well depth, 1 bpm brine influx, 400°F formation temperature at depth)

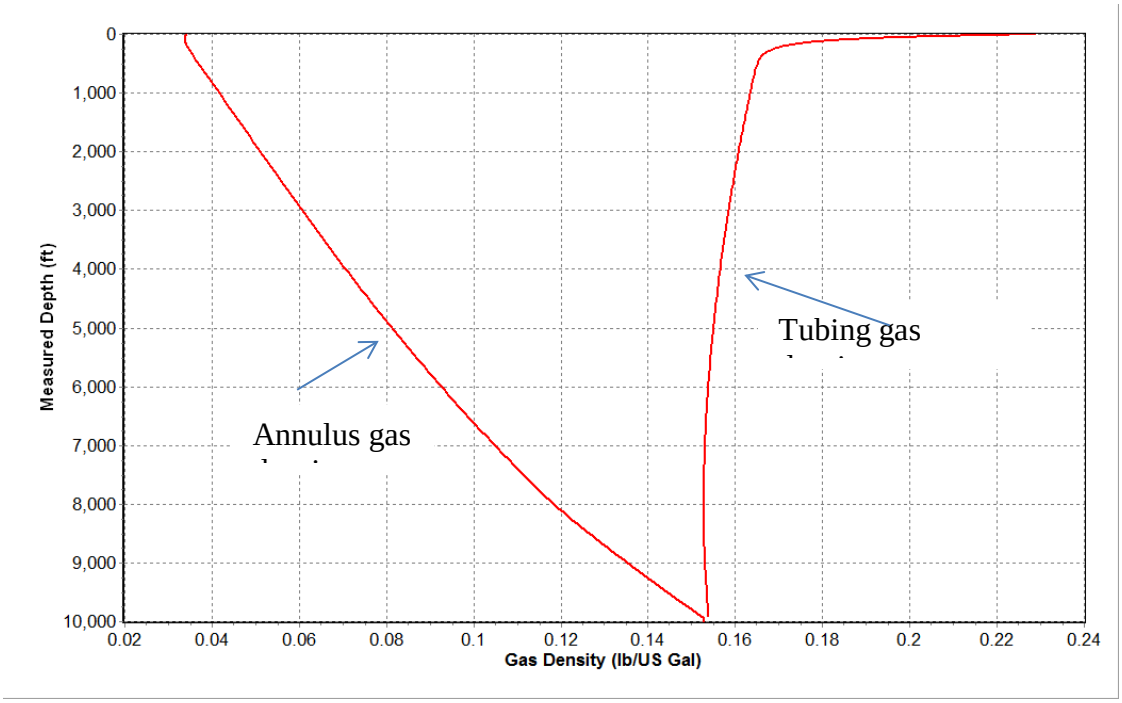


Figure 2-3 Gas density profile (50 psig surface return pressure, 3.5 MMscf/d injection rate, 10,000 MD ft well depth, 1 bpm brine influx, 400°F formation temperature at depth)

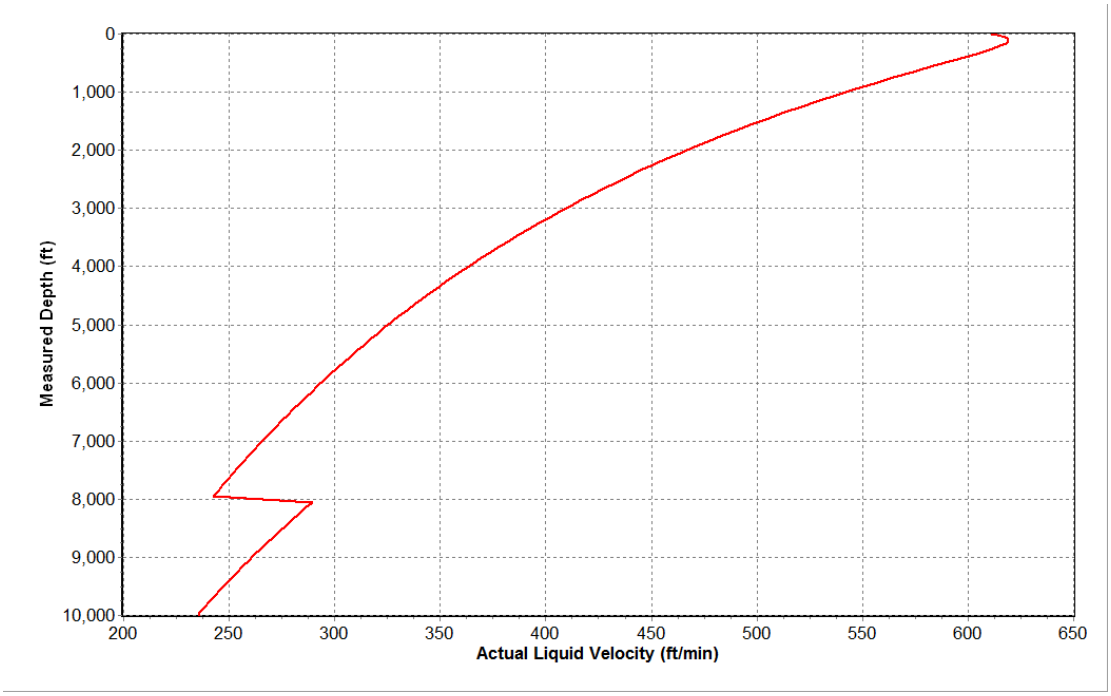


Figure 2-4 Liquid velocity profile
(50 psig surface return pressure, 3.5 MMscf/d injection rate, 10,000 MD ft well depth, 1 bpm brine influx, 400°F formation temperature at depth)

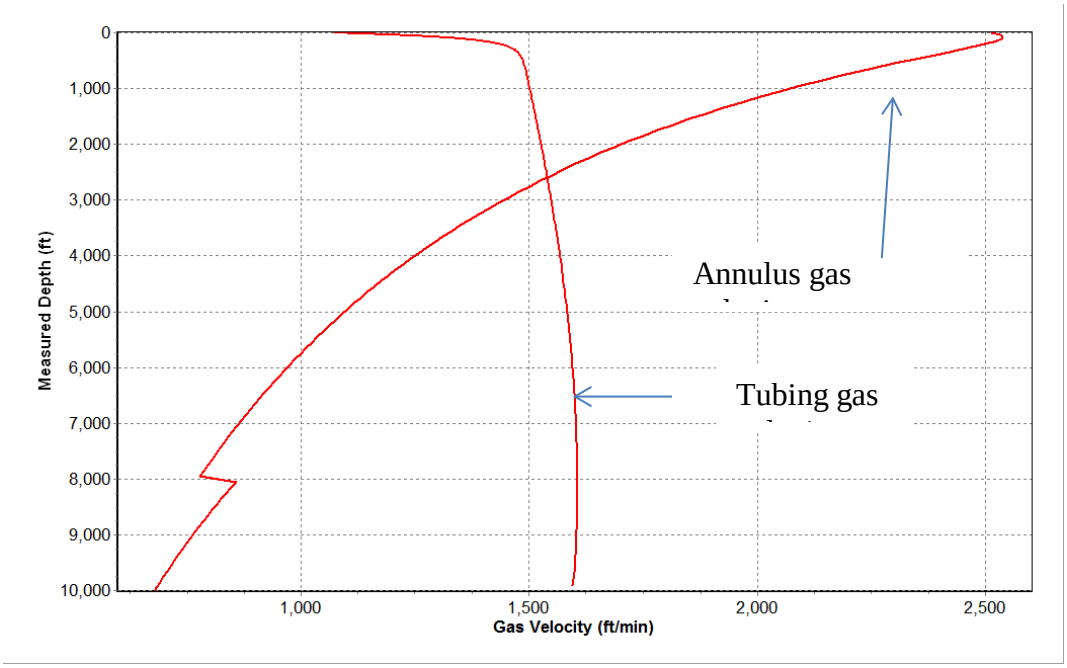


Figure 2-5 Gas velocity profile
(50 psig surface return pressure, 3.5 MMscf/d injection rate, 10,000 MD ft well depth, 1 bpm brine influx, 400°F formation temperature at depth)

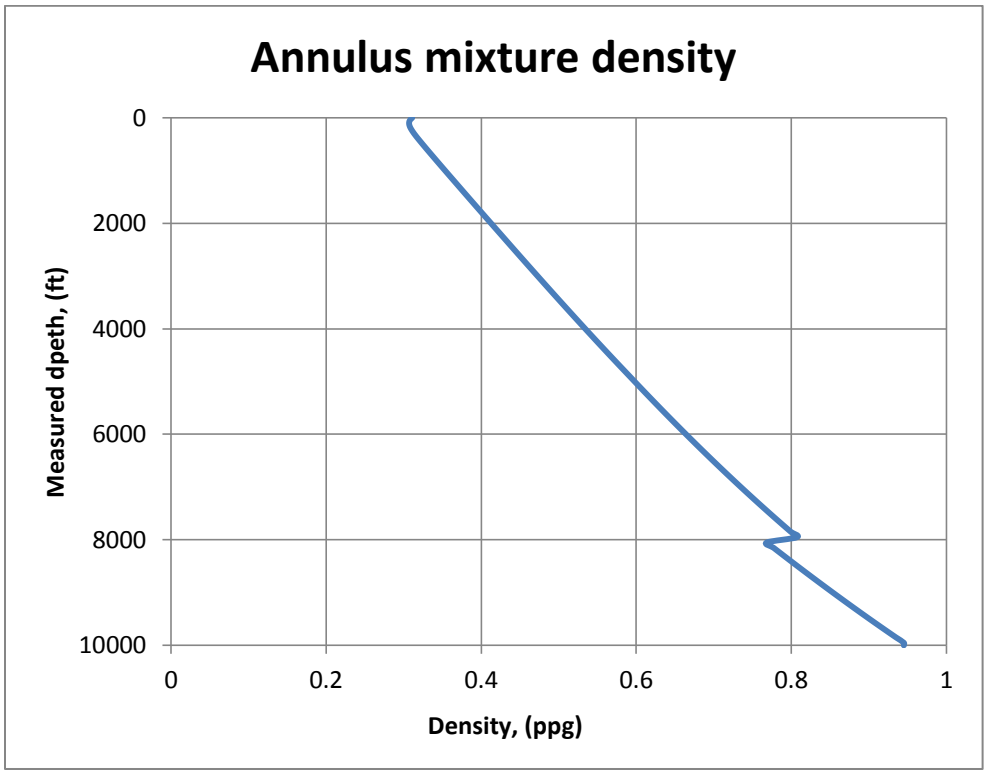


Figure 2-6 Annulus mixture density profile
(50 psig surface return pressure, 3.5 MMscf/d injection rate, 10,000 MD ft well depth, 1 bpm brine influx, 400°F formation temperature at depth)

## Chapter 3 Results for the well with 20000 MD ft, 600 °F formation temperature at depth, 0 bpm brine influx, 50 psig surface return pressure, 10 MMscf/D injection rate

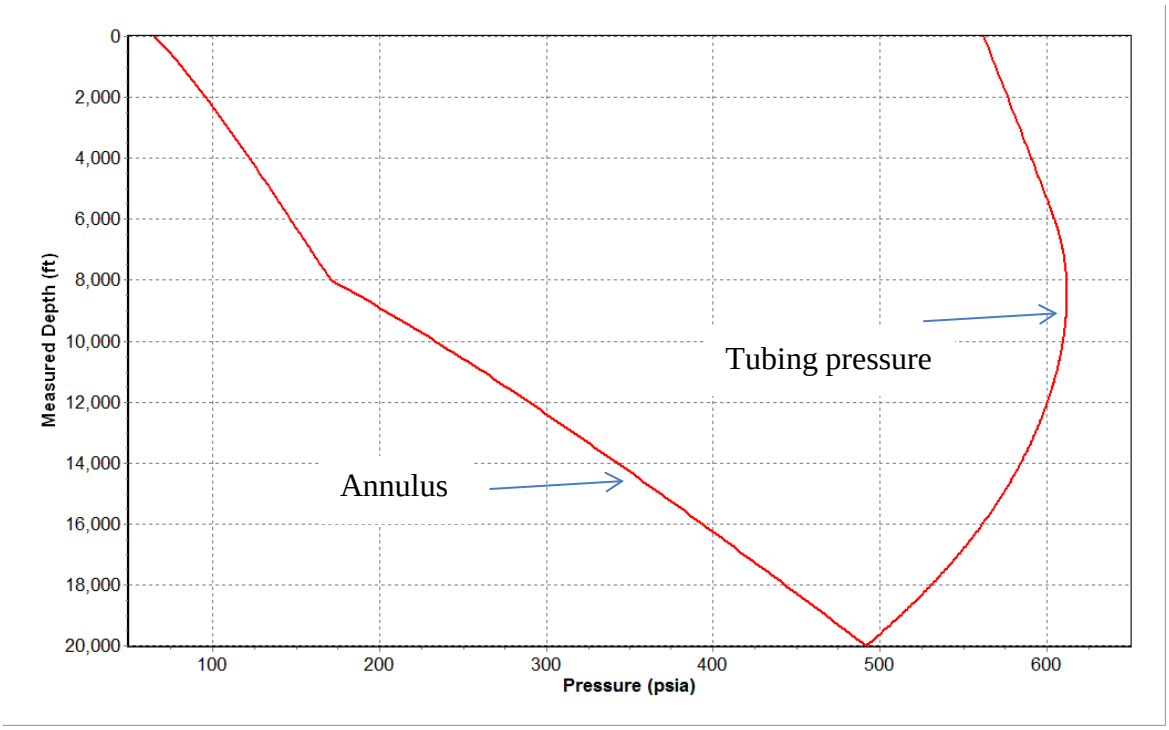


Figure 3-1 Pressure profile
(50 psig surface return pressure, 10 MMscf/d injection rate, 20,000 MD ft well depth, 0 bpm brine influx, 600°F formation temperature at depth)

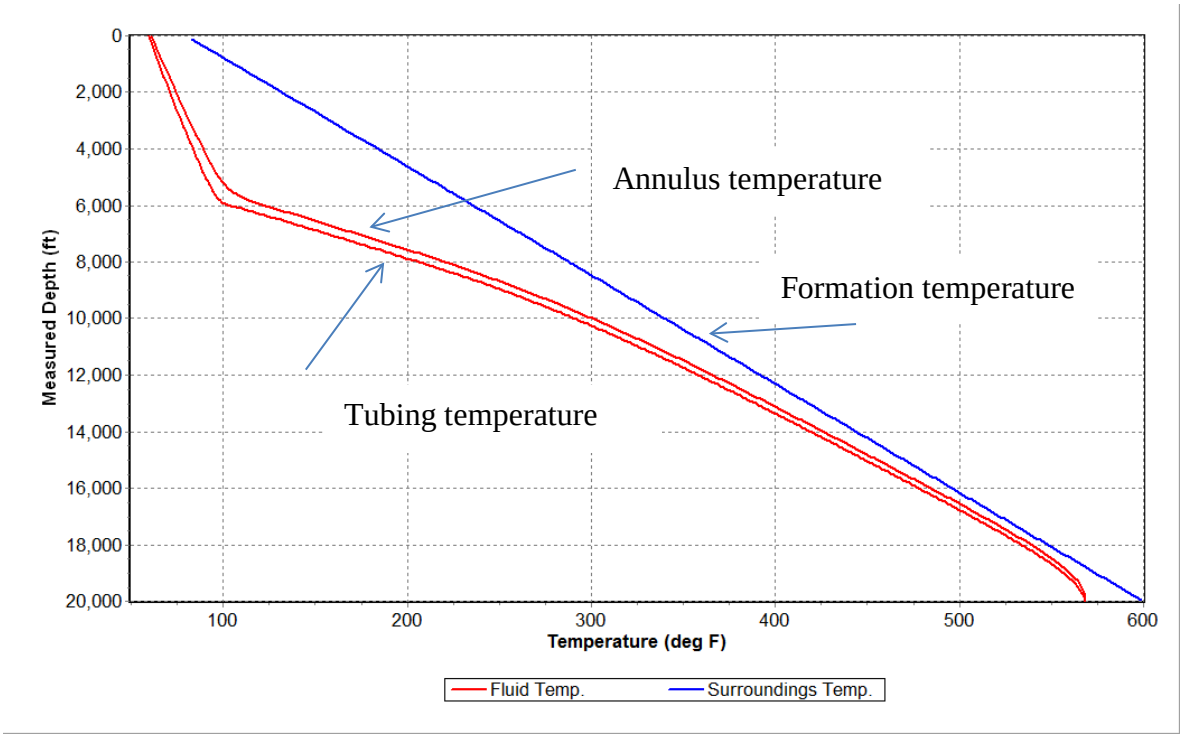


Figure 3-1 Temperature profile (50 psig surface return pressure, 10 MMscf/d injection rate, 20,000 MD ft well depth, 0 bpm brine influx, 600°F formation temperature at depth)

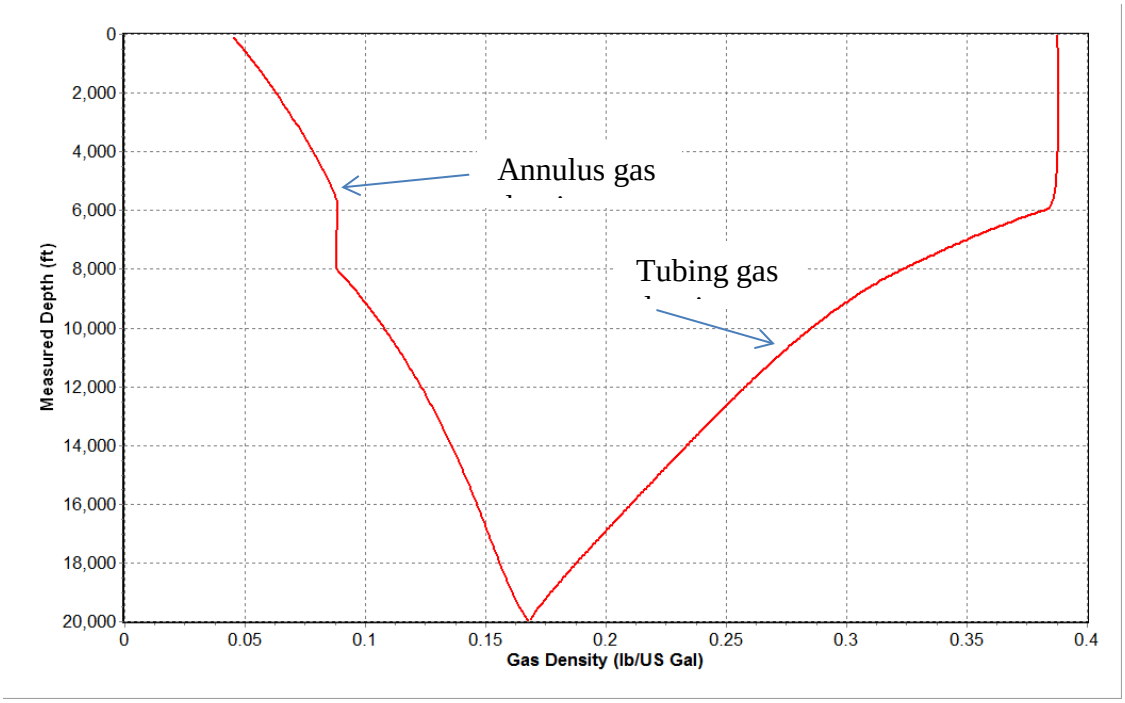


Figure 3-3 Gas density profile (50 psig surface return pressure, 10 MMscf/d injection rate, 20,000 MD ft well depth, 0 bpm brine influx, 600°F formation temperature at depth)

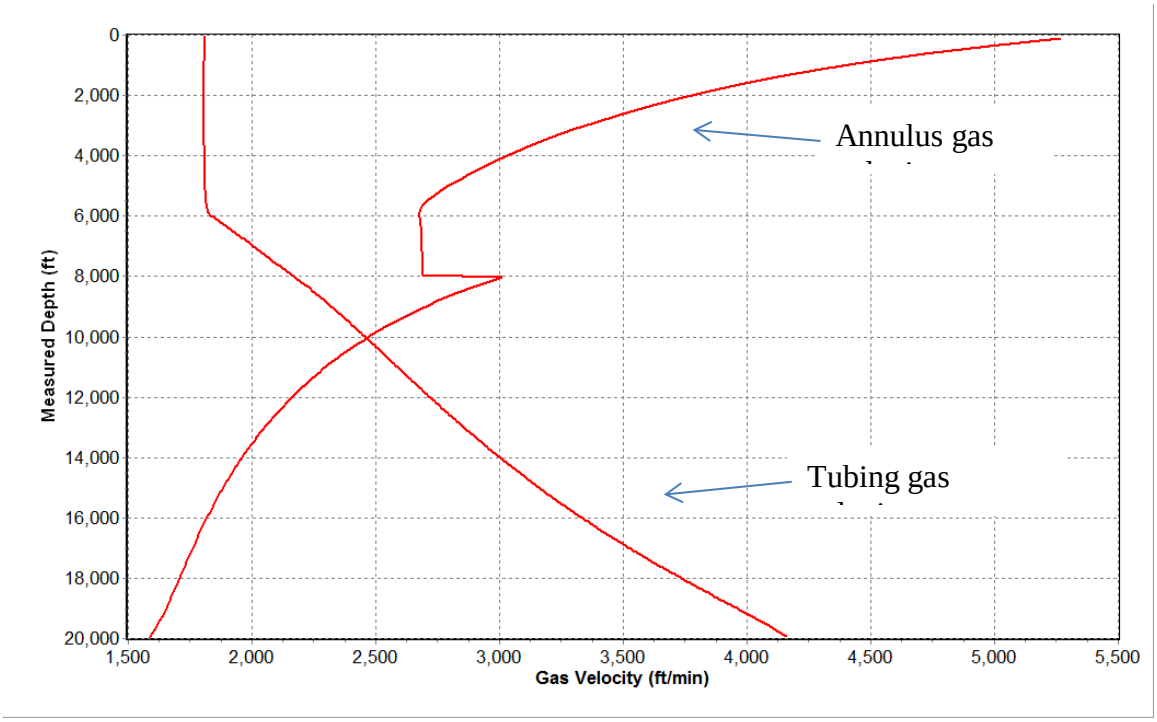


Figure 3-4 Gas velocity profile
(50 psig surface return pressure, 10 MMscf/d injection rate, 20,000 MD ft well depth, 0 bpm brine influx, 600°F formation temperature at depth)

**Chapter 4 Results for the well with 20000 MD ft, 600 °F formation temperature at depth, 0 bpm brine influx, 50 psig surface return pressure, 3.5 MMscf/D injection rate**

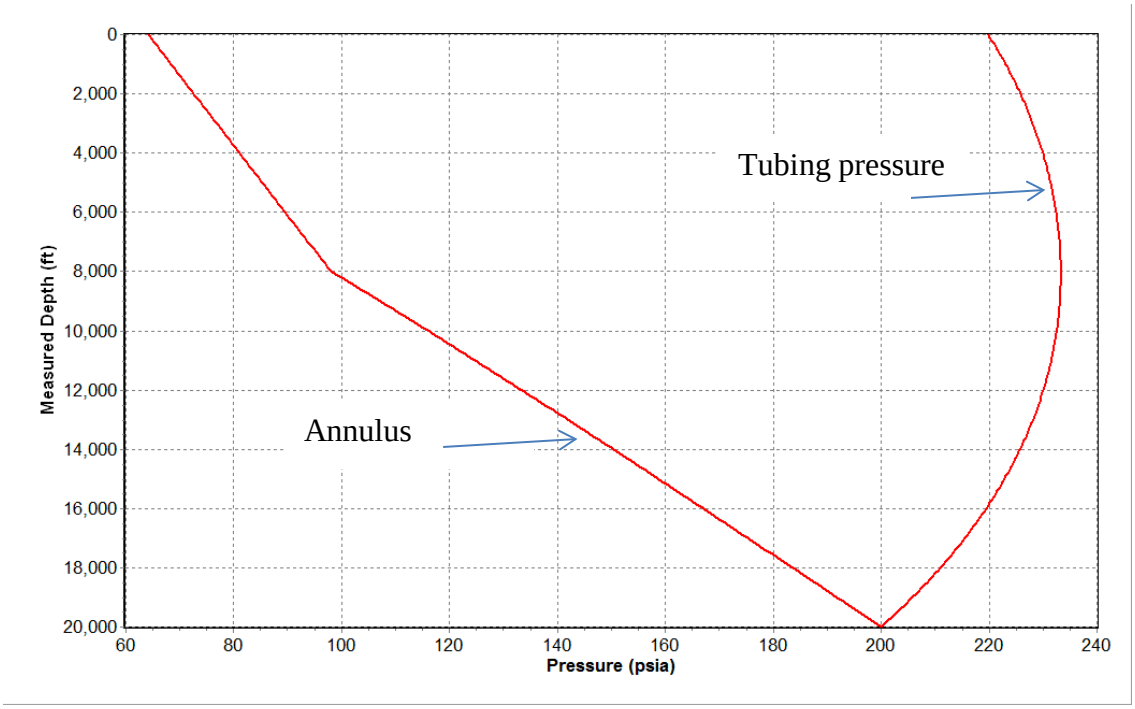


Figure 4-1 Pressure profile
(50 psig surface return pressure, 3.5 MMscf/d injection rate, 20,000 MD ft well depth, 0 bpm brine influx, 600°F formation temperature at depth)

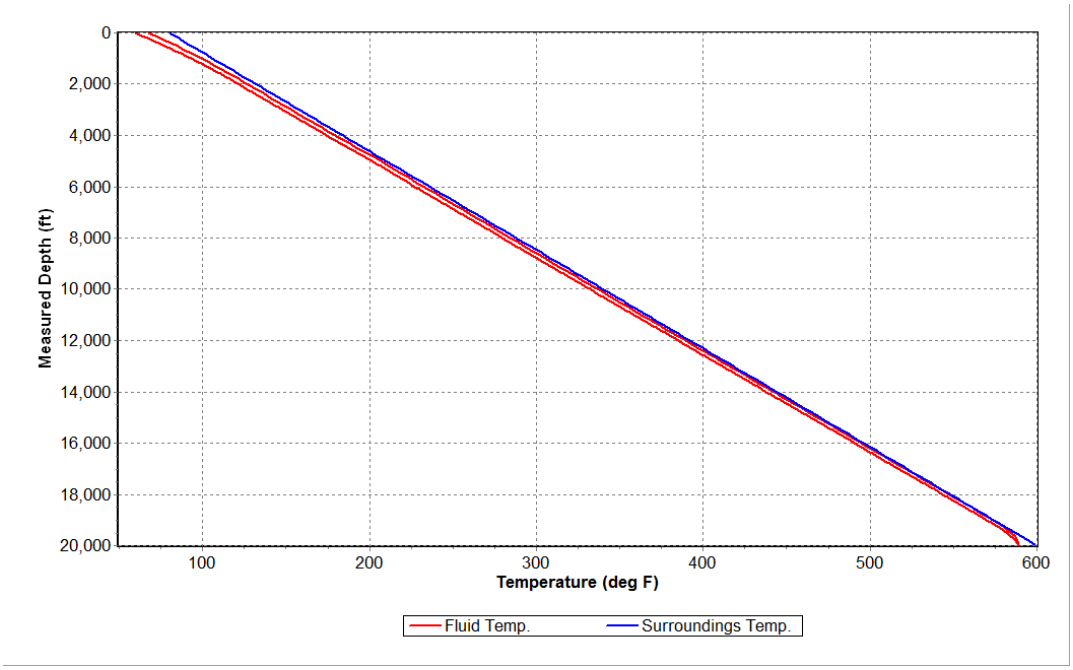


Figure 4-2 Temperature profile
(50 psig surface return pressure, 3.5 MMscf/d injection rate, 20,000 MD ft well depth, 0 bpm brine influx, 600°F formation temperature at depth)

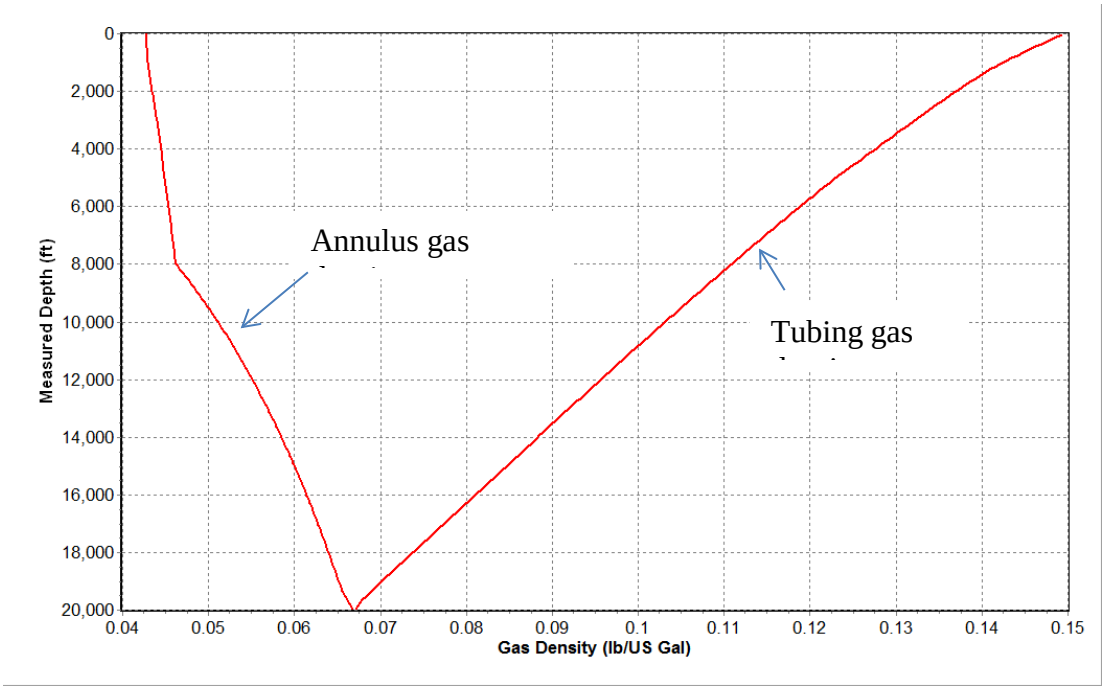


Figure 4-3 Gas density profile (50 psig surface return pressure, 3.5 MMscf/d injection rate, 20,000 MD ft well depth, 0 bpm brine influx, 600°F formation temperature at depth)

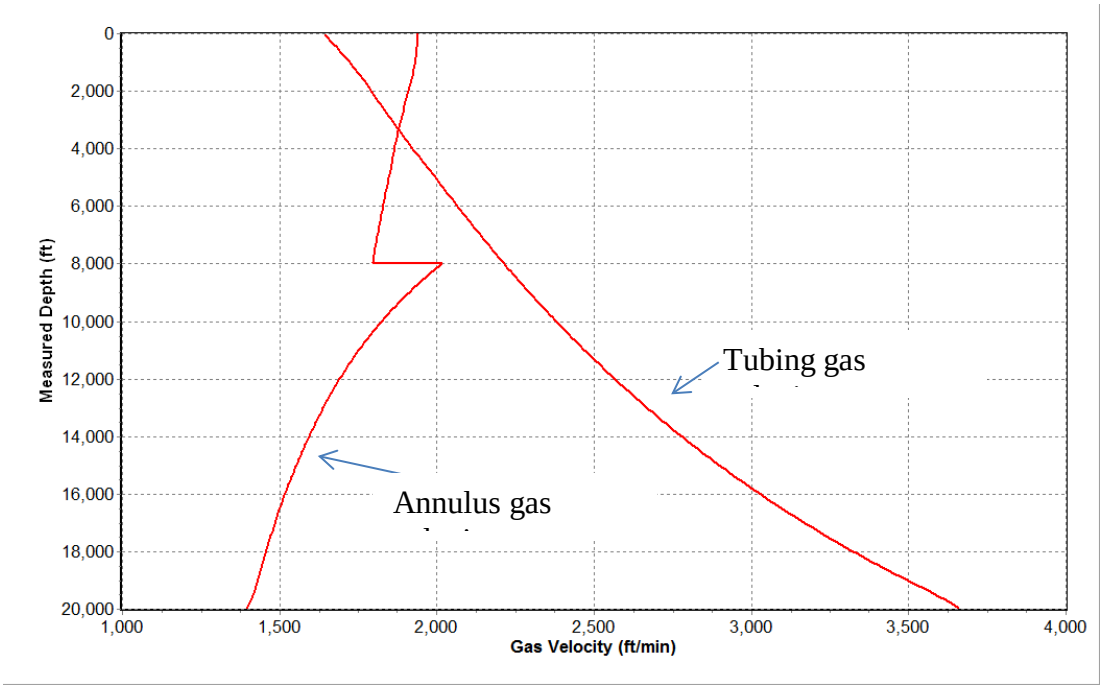


Figure 4-4 Gas velocity profile (50 psig surface return pressure, 3.5 MMscf/d injection rate, 20,000 MD ft well depth, 0 bpm brine influx, 600°F formation temperature at depth)

## Chapter 5 Results for the well with 20000 MD ft, 600 °F formation temperature at depth, 0 bpm brine influx, 185.3 psig surface return pressure, 10 MMscf/D injection rate

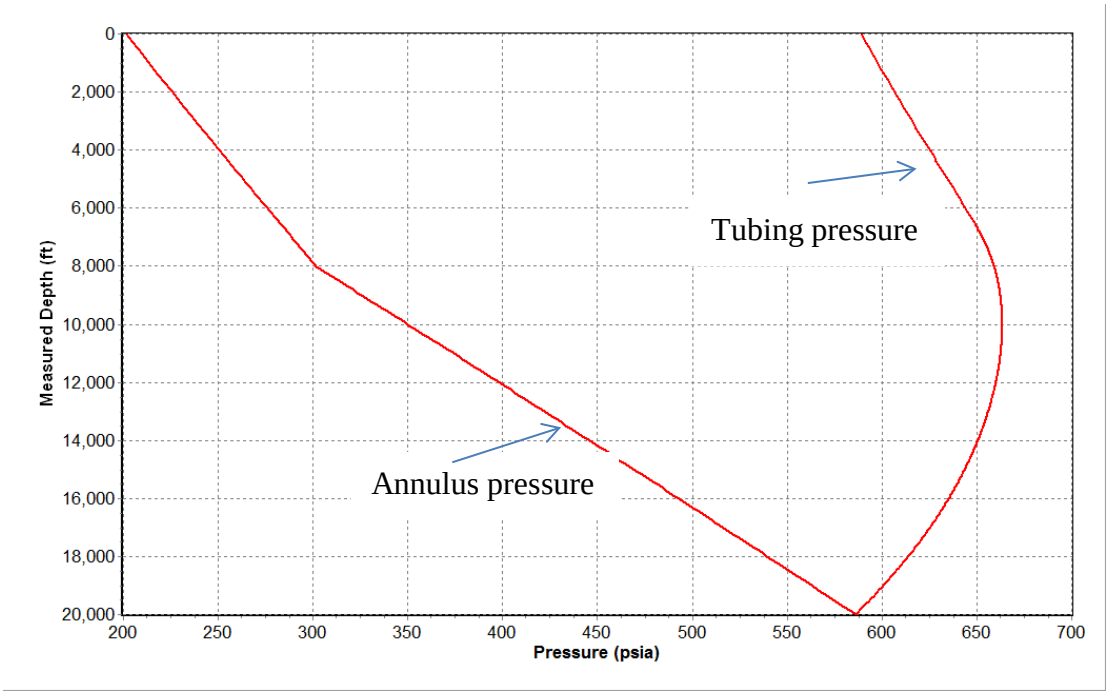


Figure 5-1 Pressure profile (185.3 psig surface return pressure, 10 MMscf/d injection rate, 20,000 MD ft well depth, 0 bpm brine influx, 600°F formation temperature at depth)

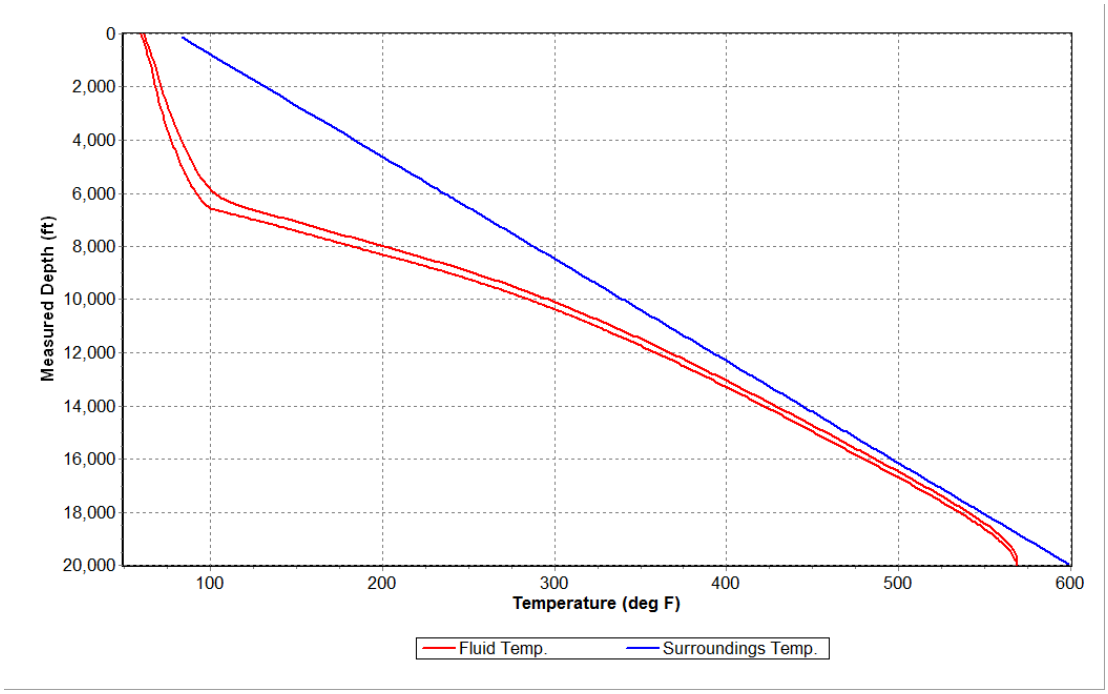


Figure 5-2 Temperature profile (185.3 psig surface return pressure, 10 MMscf/d injection rate, 20,000 MD ft well depth, 0 bpm brine influx, 600°F formation temperature at depth)

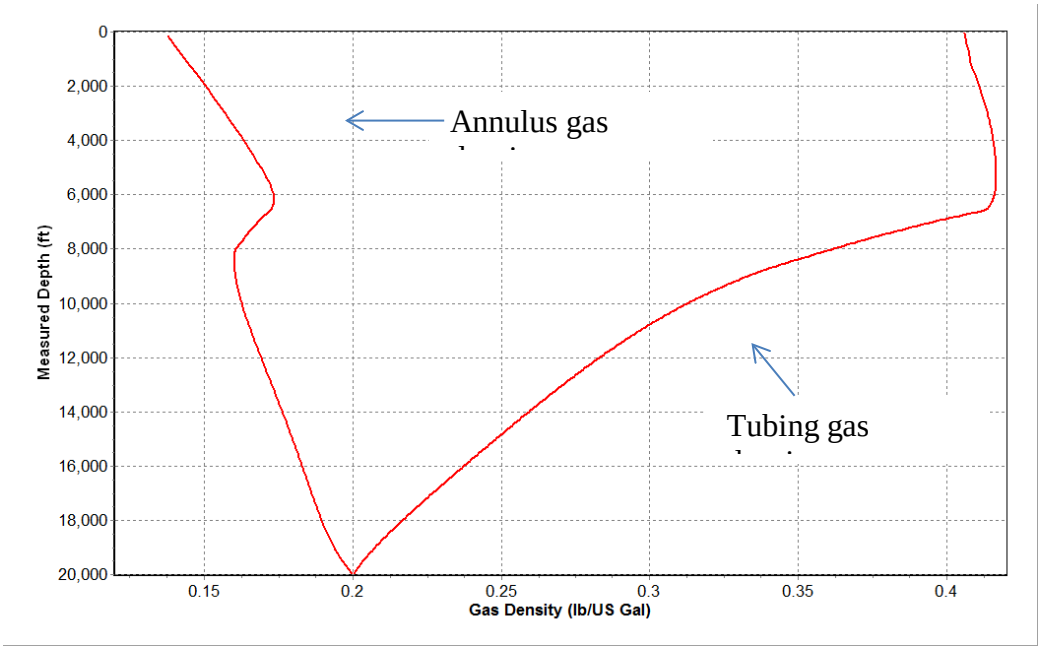


Figure 5-3 Gas density profile (185.3 psig surface return pressure, 10 MMscf/d injection rate, 20,000 MD ft well depth, 0 bpm brine influx, 600°F formation temperature at depth)

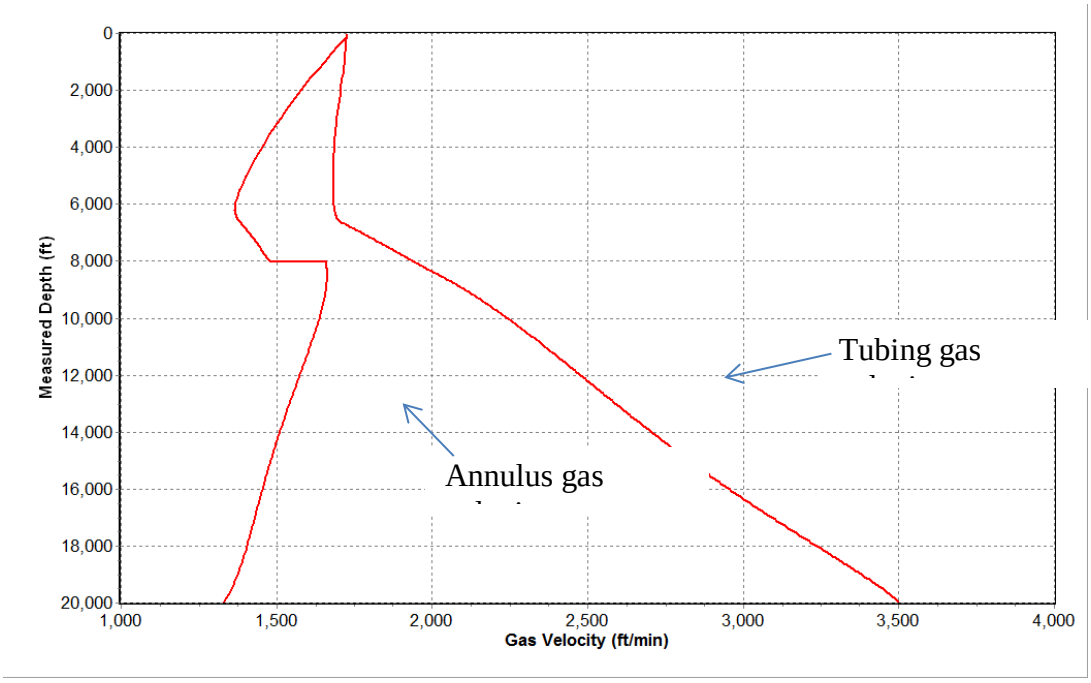


Figure 5-4 Gas velocity profile
(185.3 psig surface return pressure, 10 MMscf/d injection rate, 20,000 MD ft well depth, 0 bpm brine influx, 600°F formation temperature at depth)

## Chapter 6 Results for the well with 20000 MD ft, 600 °F formation temperature at depth, 0 bpm brine influx, 185.3 psig surface return pressure, 3.5 MMscf/D injection rate

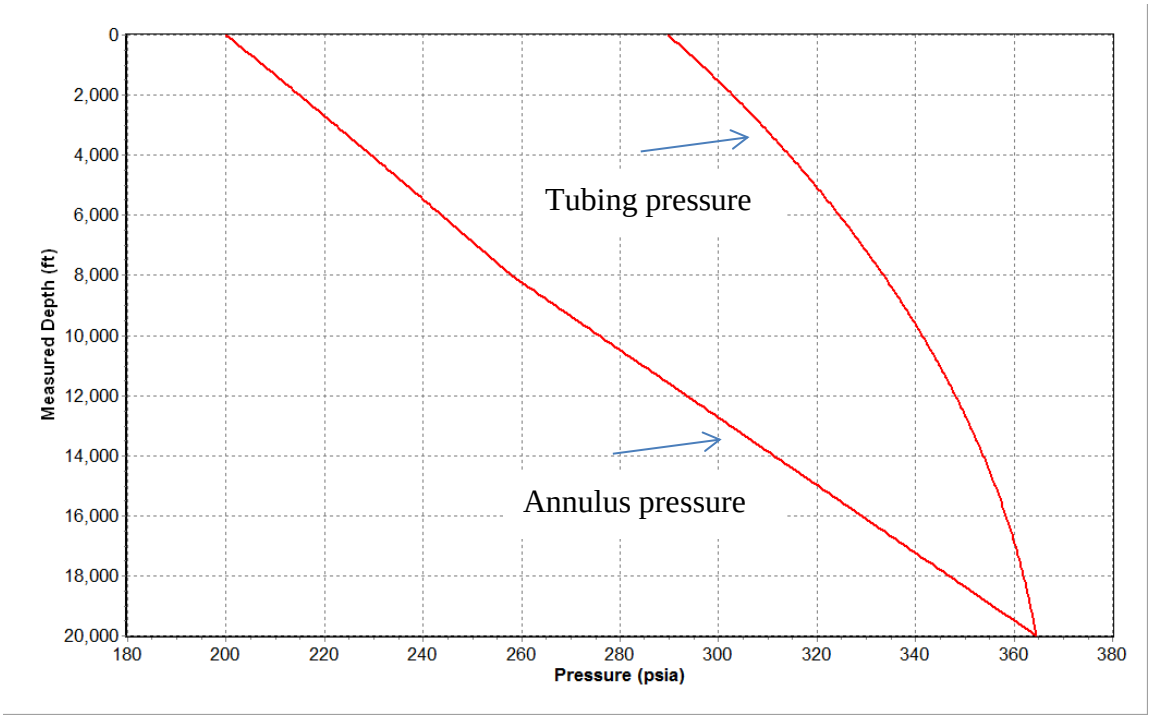


Figure 6-1 Pressure profile (185.3 psig surface return pressure, 3.5 MMscf/d injection rate, 20,000 MD ft well depth, 0 bpm brine influx, 600°F formation temperature at depth)

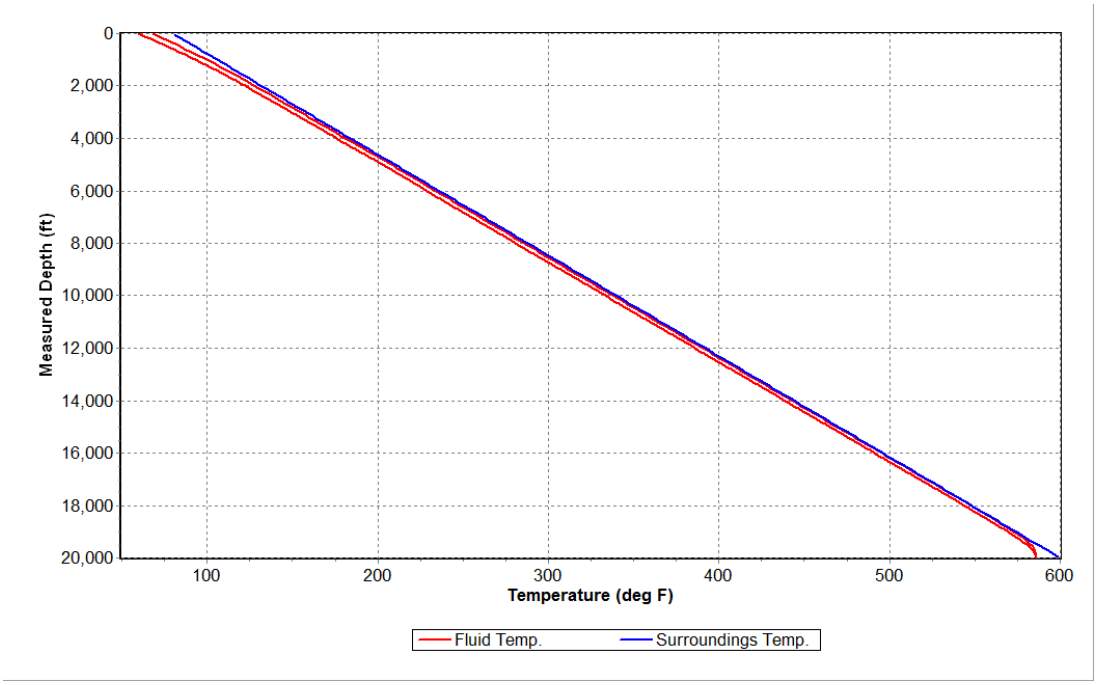


Figure 6-2 Temperature profile (185.3 psig surface return pressure, 3.5 MMscf/d injection rate, 20,000 MD ft well depth, 0 bpm brine influx, 600°F formation temperature at depth)

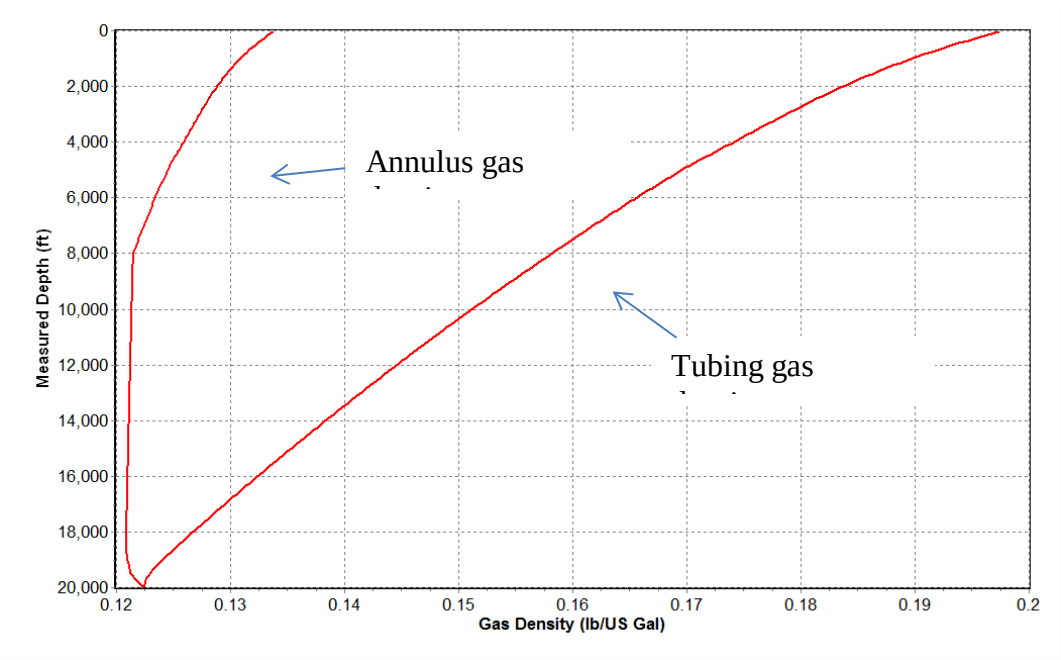


Figure 6-3 Gas density profile (185.3 psig surface return pressure, 3.5 MMscf/d injection rate, 20,000 MD ft well depth, 0 bpm brine influx, 600°F formation temperature at depth)

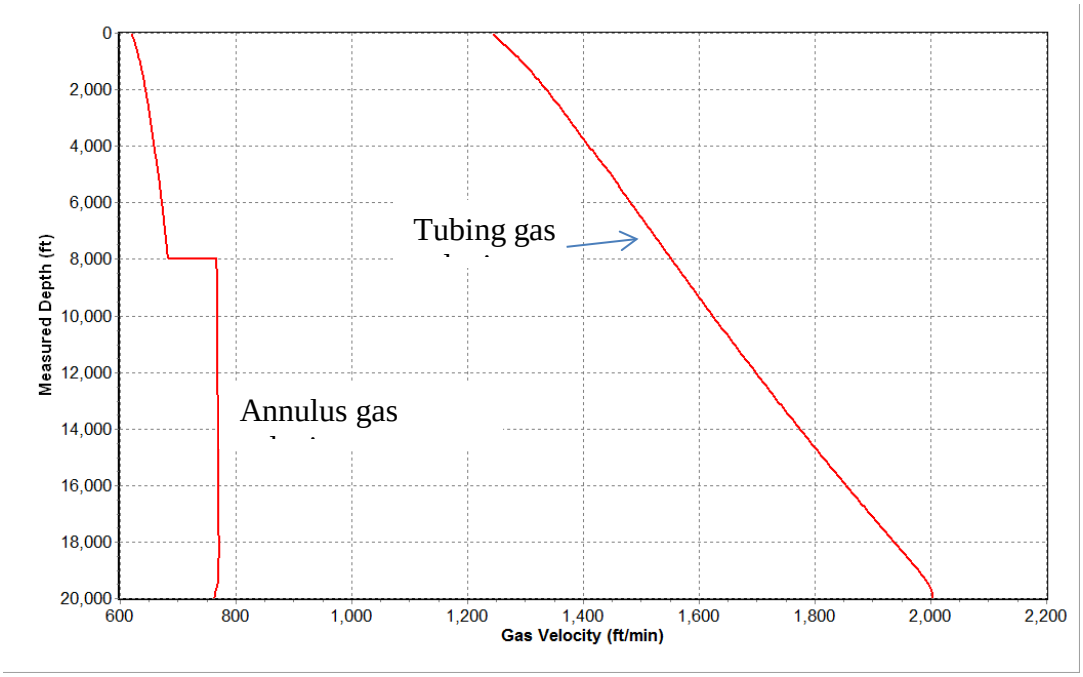


Figure 6-4 Gas velocity profile (185.3 psig surface return pressure, 3.5 MMscf/d injection rate, 20,000 MD ft well depth, 0 bpm brine influx, 600°F formation temperature at depth)

## Chapter 7 Results for the well with 20000 MD ft, 400 °F formation temperature at depth, 1 bpm brine influx, 50 psig surface return pressure, 10 MMscf/D injection rate

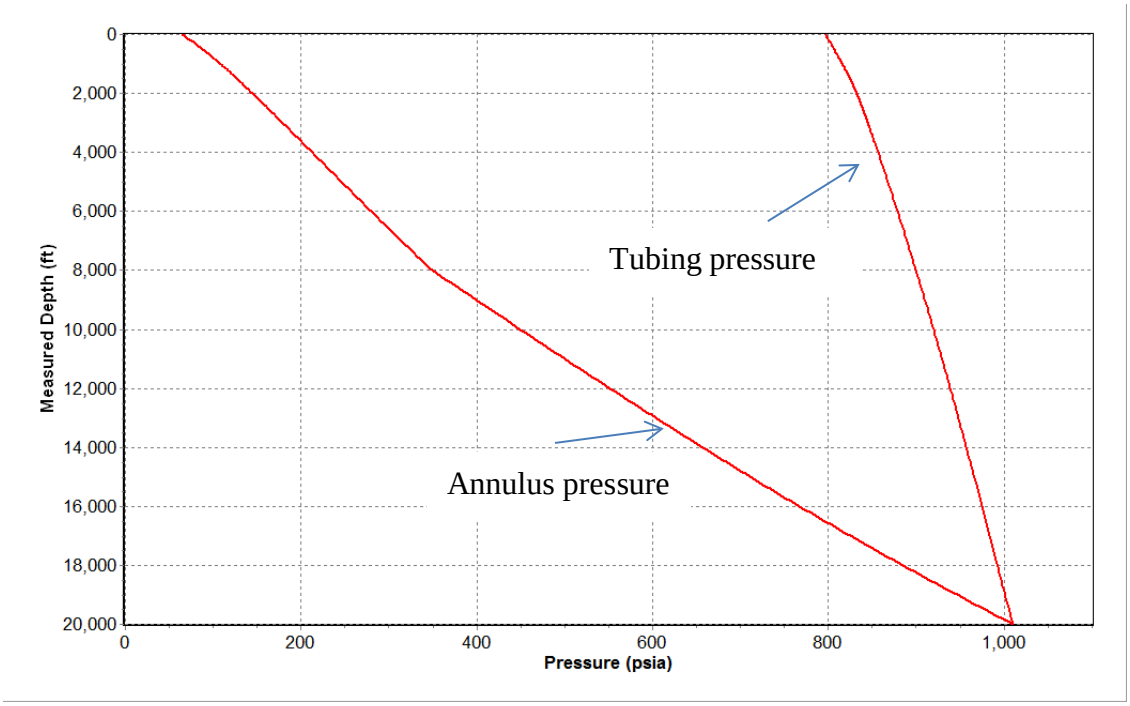


Figure 7-1 Pressure profile (50 psig surface return pressure, 10 MMscf/d injection rate, 20,000 MD ft well depth, 1 bpm brine influx, 400°F formation temperature at depth)

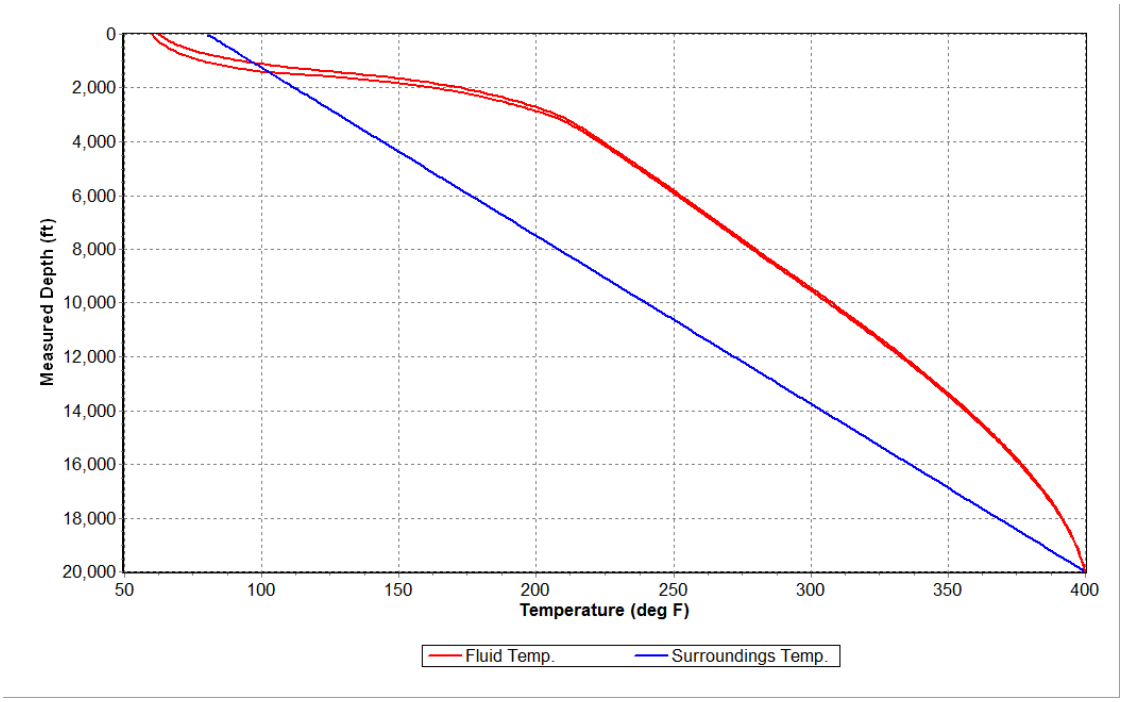


Figure 7-2 Temperature profile (50 psig surface return pressure, 10 MMscf/d injection rate, 20,000 MD ft well depth, 1 bpm brine influx, 400°F formation temperature at depth)

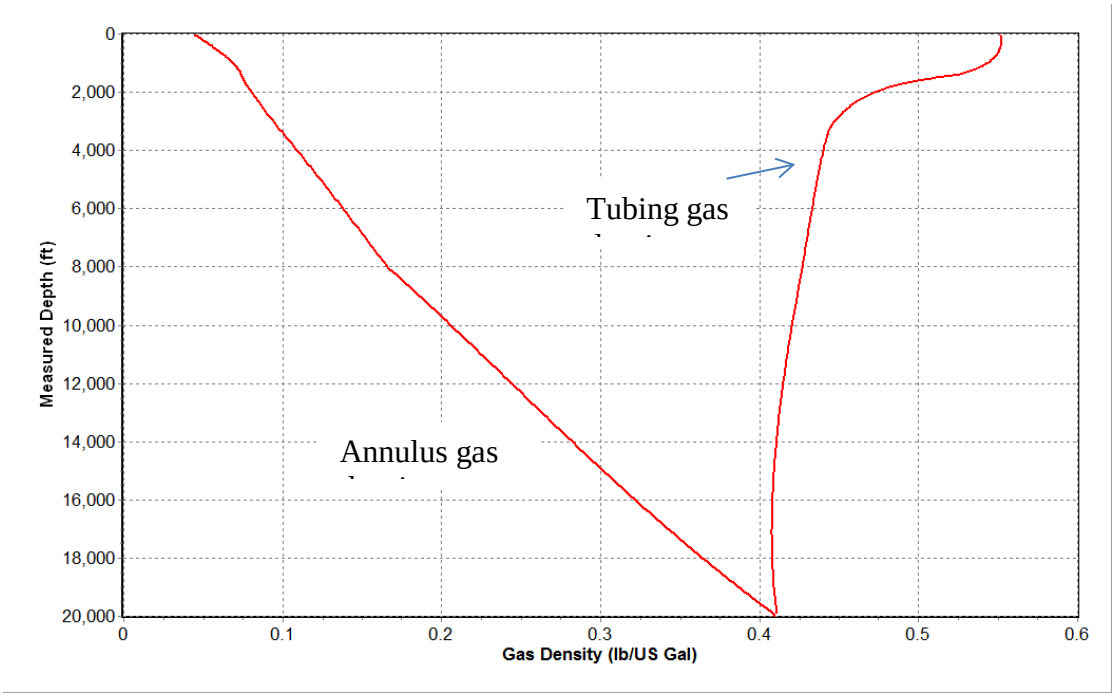


Figure 7-3 Gas density profile (50 psig surface return pressure, 10 MMscf/d injection rate, 20,000 MD ft well depth, 1 bpm brine influx, 400°F formation temperature at depth)

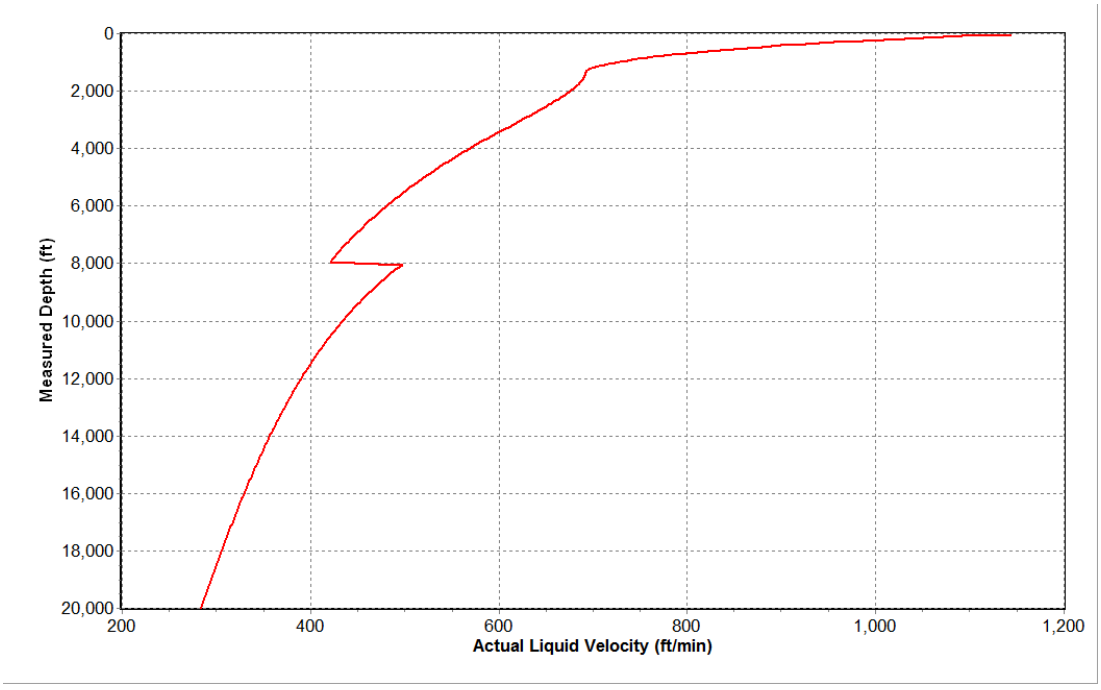


Figure 7-4 Liquid velocity profile (50 psig surface return pressure, 10 MMscf/d injection rate, 20,000 MD ft well depth, 1 bpm brine influx, 400°F formation temperature at depth)

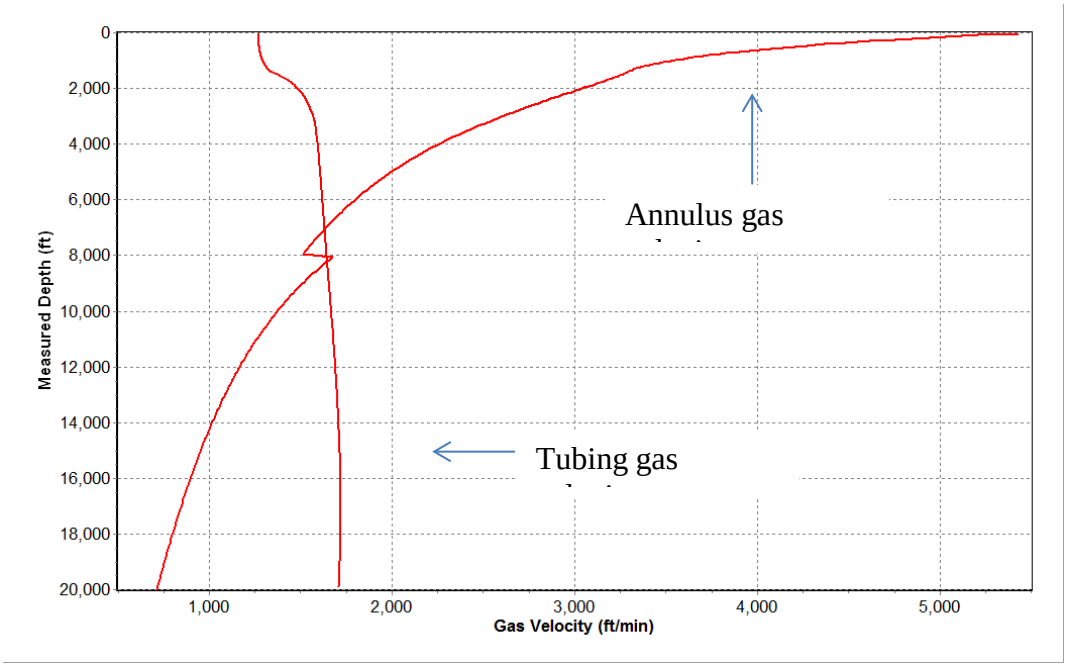


Figure 7-5 Gas velocity profile (50 psig surface return pressure, 10 MMscf/d injection rate, 20,000 MD ft well depth, 1 bpm brine influx, 400°F formation temperature at depth)

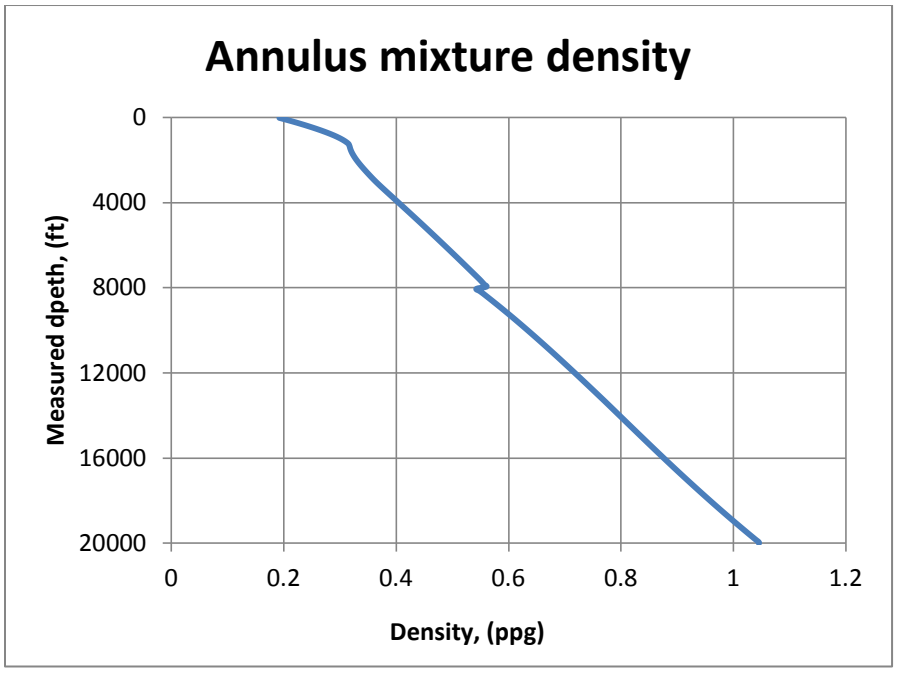


Figure 7-6 Annulus mixture density profile (50 psig surface return pressure, 10 MMscf/d injection rate, 20,000 MD ft well depth, 1 bpm brine influx, 400°F formation temperature at depth)

## Chapter 8 Results for the well with 20000 MD ft, 400 °F formation temperature at depth, 1 bpm brine influx, 50 psig surface return pressure, 3.5 MMscf/D injection rate

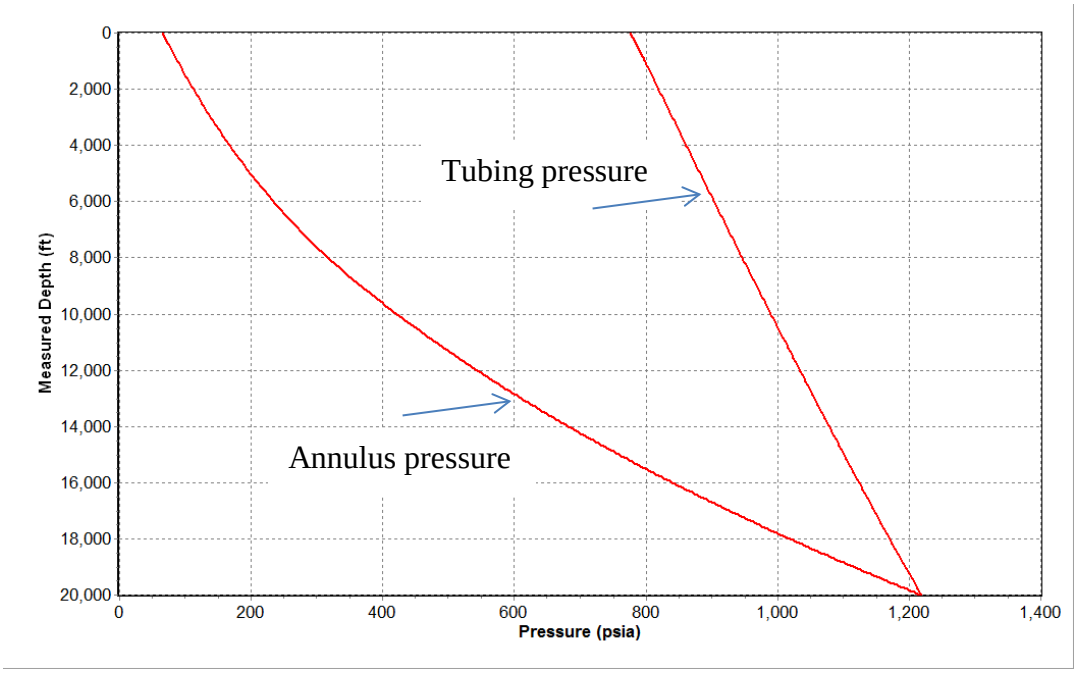


Figure 8-1 Pressure profile (50 psig surface return pressure, 3.5 MMscf/d injection rate, 20,000 MD ft well depth, 1 bpm brine influx, 400°F formation temperature at depth)

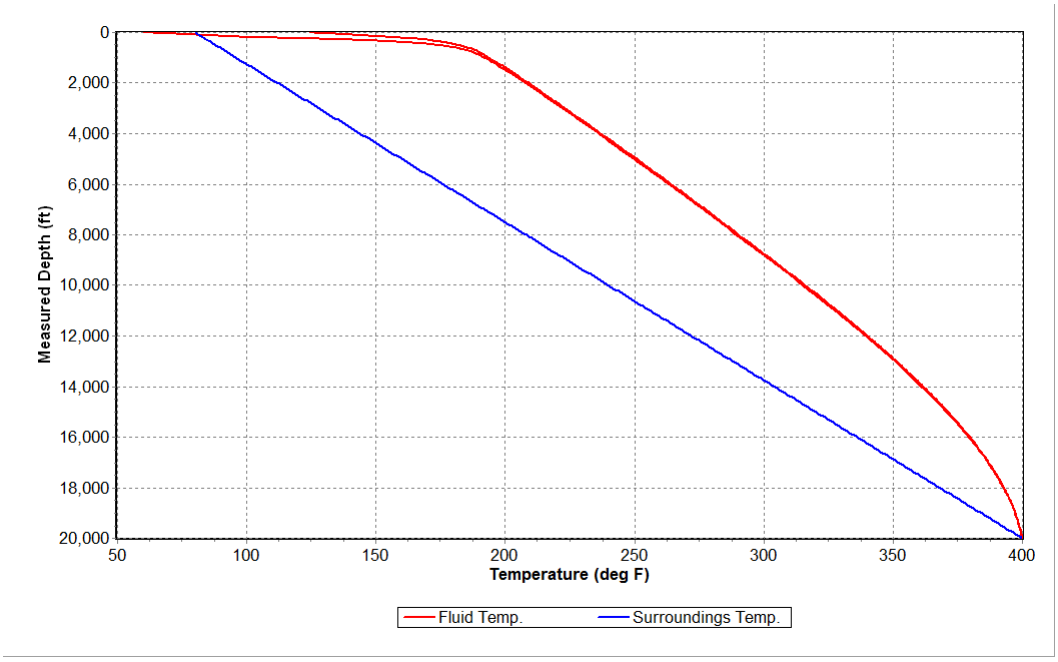


Figure 8-2 Temperature profile (50 psig surface return pressure, 3.5 MMscf/d injection rate, 20,000 MD ft well depth, 1 bpm brine influx, 400°F formation temperature at depth)

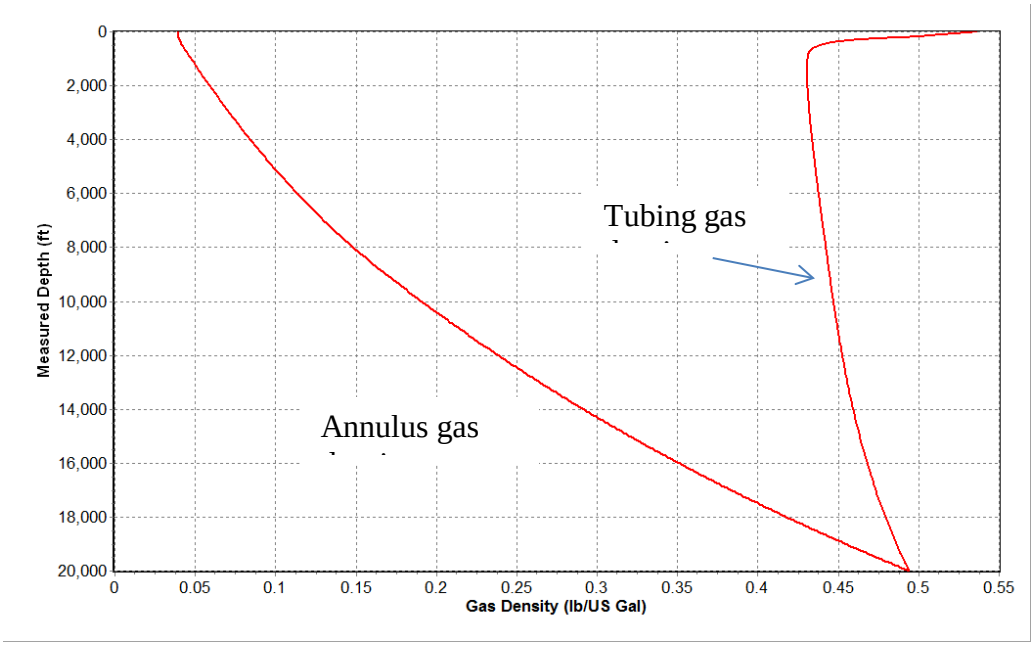


Figure 8-3 Gas density profile (50 psig surface return pressure, 3.5 MMscf/d injection rate, 20,000 MD ft well depth, 1 bpm brine influx, 400°F formation temperature at depth)

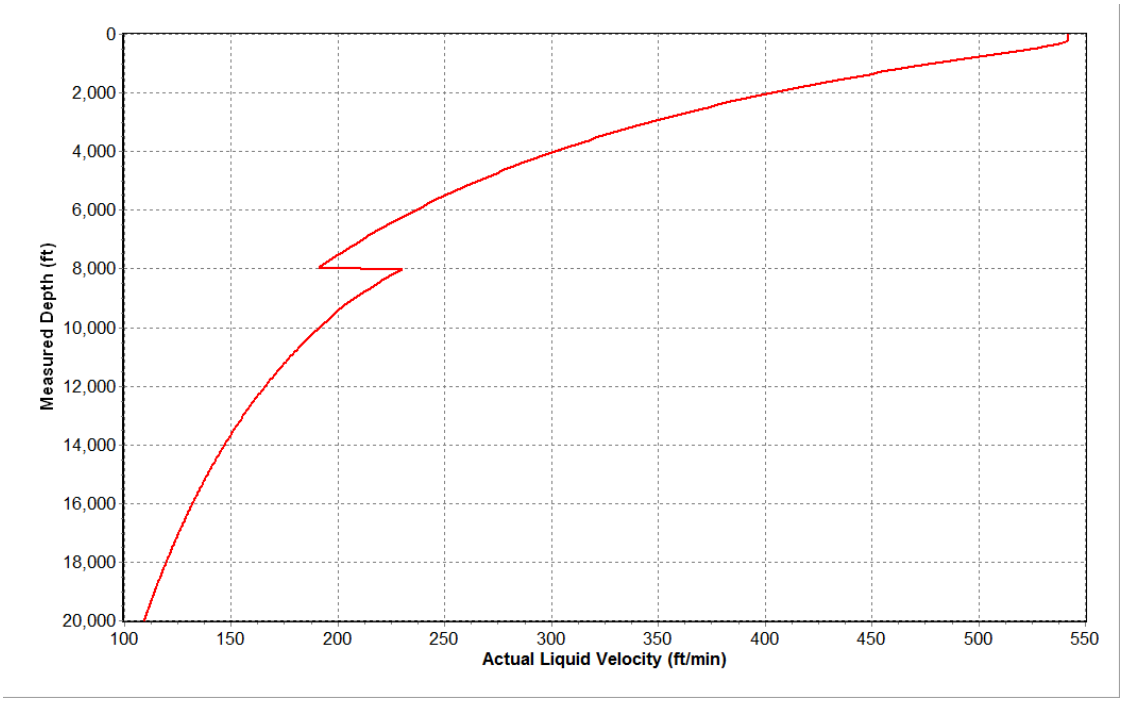


Figure 8-4 Liquid velocity profile (50 psig surface return pressure, 3.5 MMscf/d injection rate, 20,000 MD ft well depth, 1 bpm brine influx, 400°F formation temperature at depth)

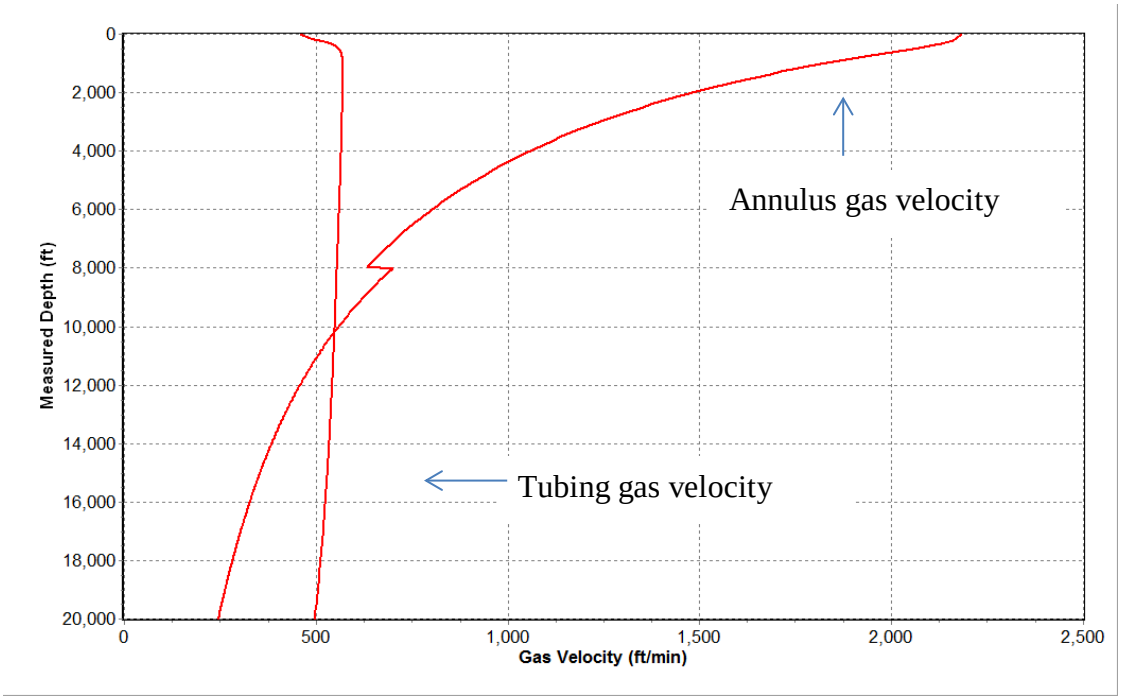


Figure 8-5 Gas velocity profile (50 psig surface return pressure, 3.5 MMscf/d injection rate, 20,000 MD ft well depth, 1 bpm brine influx, 400°F formation temperature at depth)

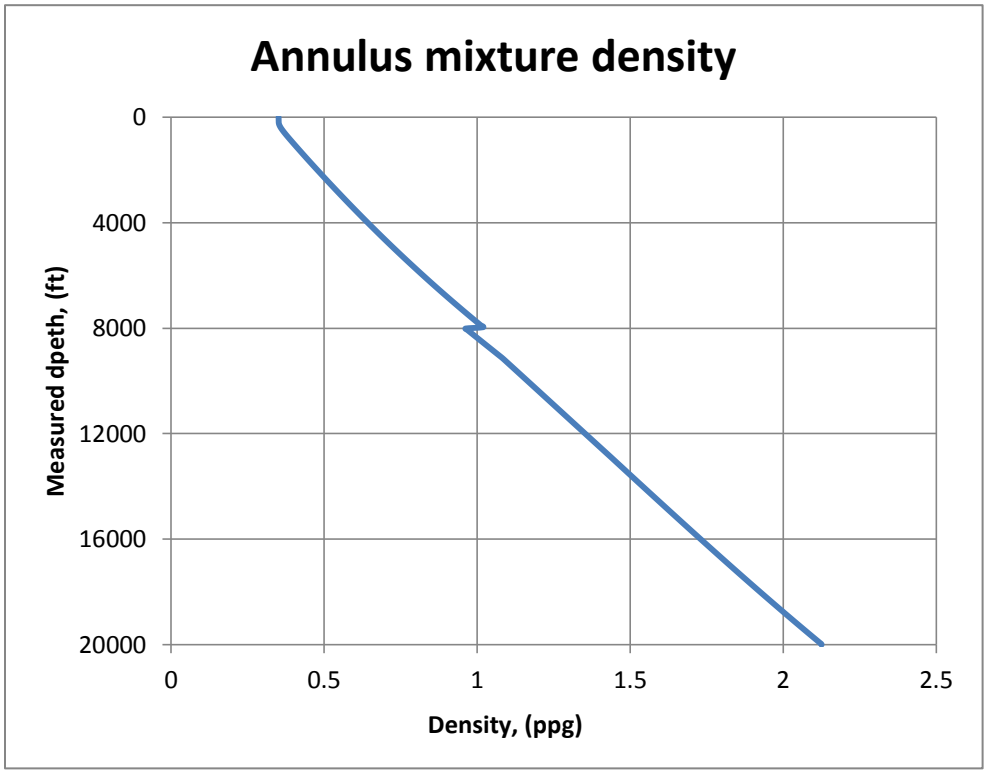


Figure 8-6 Annulus mixture density profile (50 psig surface return pressure, 3.5 MMscf/d injection rate, 20,000 MD ft well depth, 1 bpm brine influx, 400°F formation temperature at depth)

## Chapter 9 Results for the well with 20000 MD ft, 300 °F formation temperature at depth, 1 bpm brine influx, 50 psig surface return pressure, 10 MMscf/D injection rate

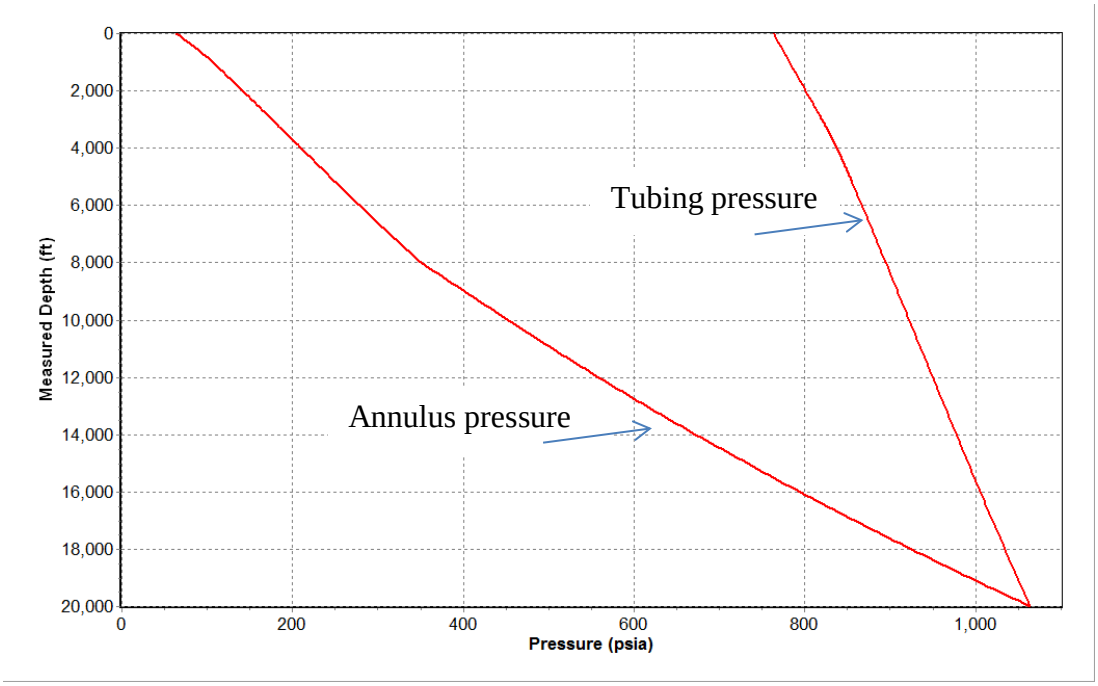


Figure 9-1 Pressure profile (50 psig surface return pressure, 10 MMscf/d injection rate, 20,000 MD ft well depth, 1 bpm brine influx, 300°F formation temperature at depth)

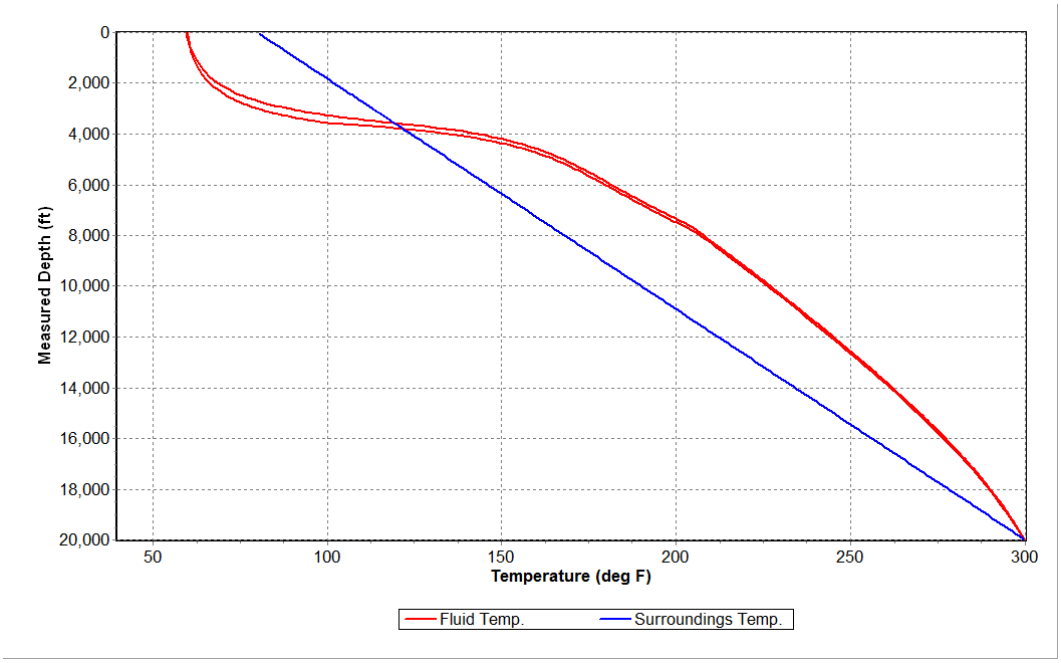


Figure 9-2 Temperature profile (50 psig surface return pressure, 10 MMscf/d injection rate, 20,000 MD ft well depth, 1 bpm brine influx, 300°F formation temperature at depth)

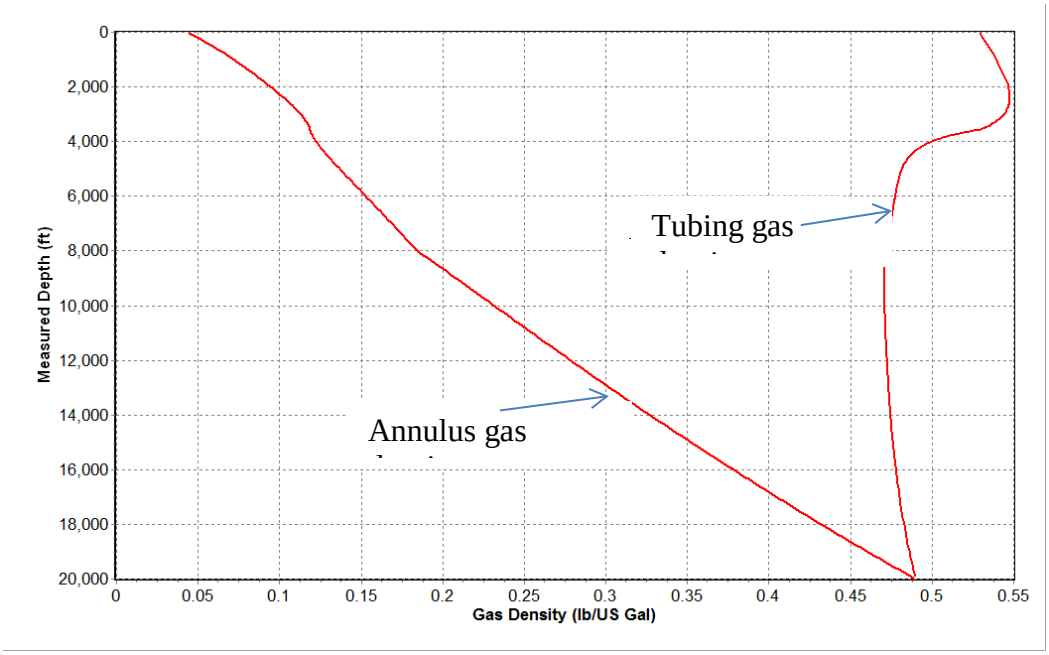


Figure 9-3 Gas density profile
(50 psig surface return pressure, 10 MMscf/d injection rate, 20,000 MD ft well depth, 1 bpm brine influx, 300°F formation temperature at depth)

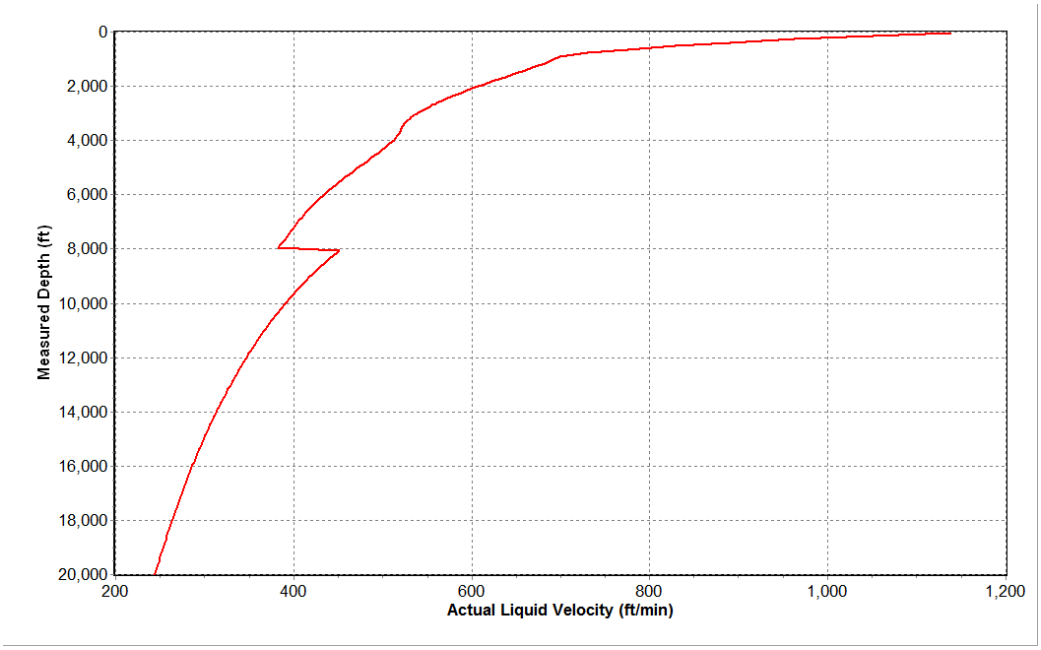


Figure 9-4 Liquid velocity profile (50 psig surface return pressure, 10 MMscf/d injection rate, 20,000 MD ft well depth, 1 bpm brine influx, 300°F formation temperature at depth)

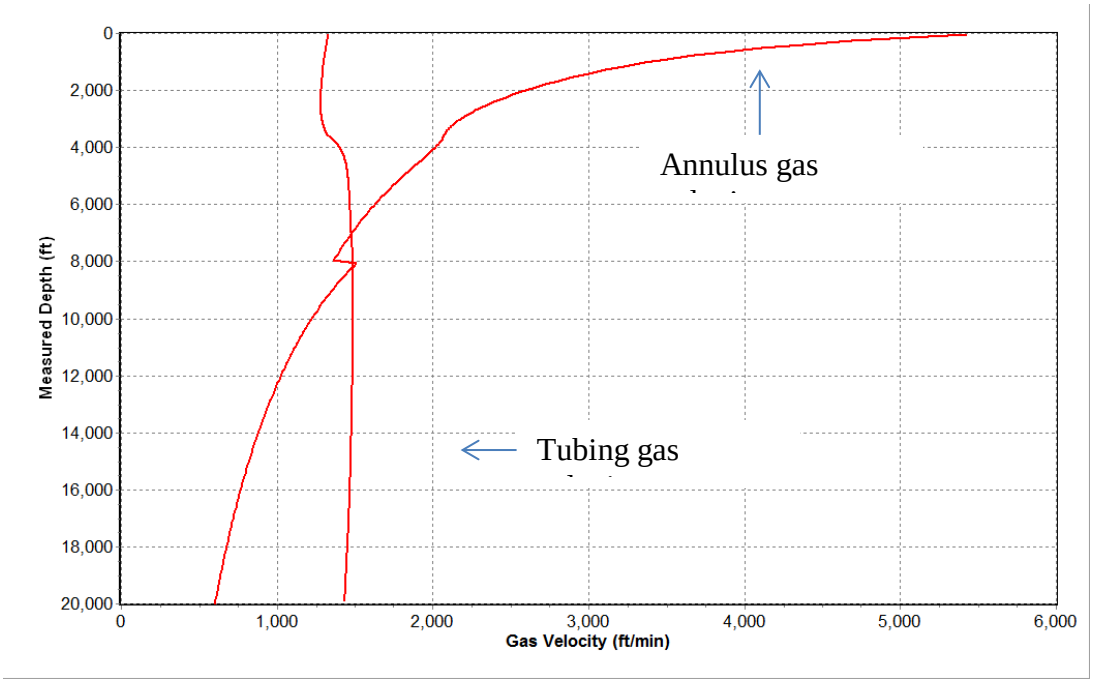


Figure 9-5 Gas velocity profile (50 psig surface return pressure, 10 MMscf/d injection rate, 20,000 MD ft well depth, 1 bpm brine influx, 300°F formation temperature at depth)

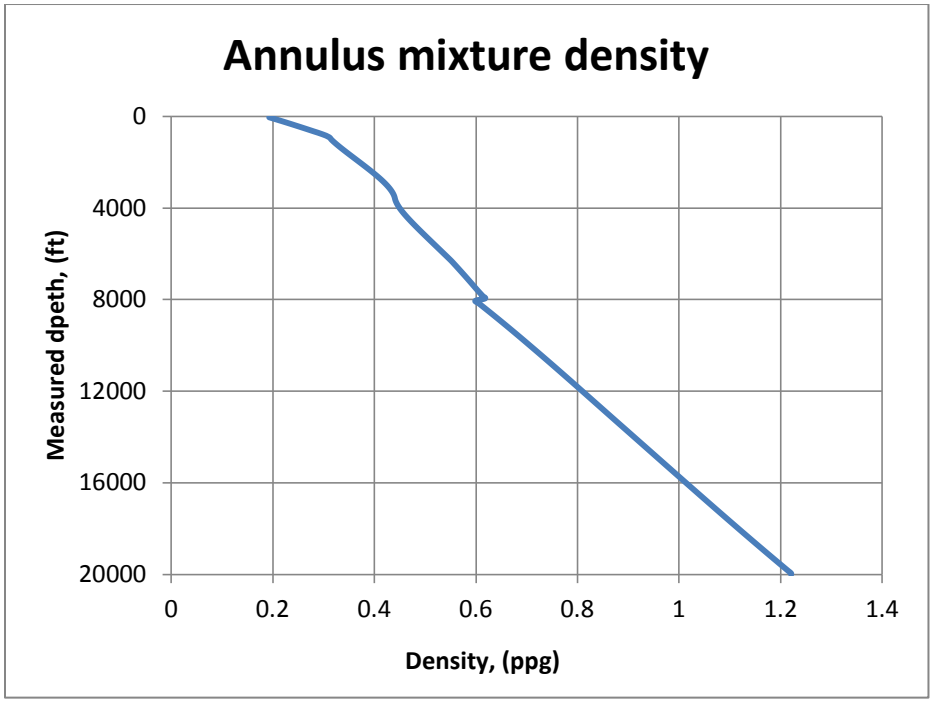


Figure 9-6 Annulus mixture density profile (50 psig surface return pressure, 10 MMscf/d injection rate, 20,000 MD ft well depth, 1 bpm brine influx, 300°F formation temperature at depth)

## Chapter 10 Results for the well with 20000 MD ft, 300 °F formation temperature at depth, 1 bpm brine influx, 50 psig surface return pressure, 3.5 MMscf/D injection rate

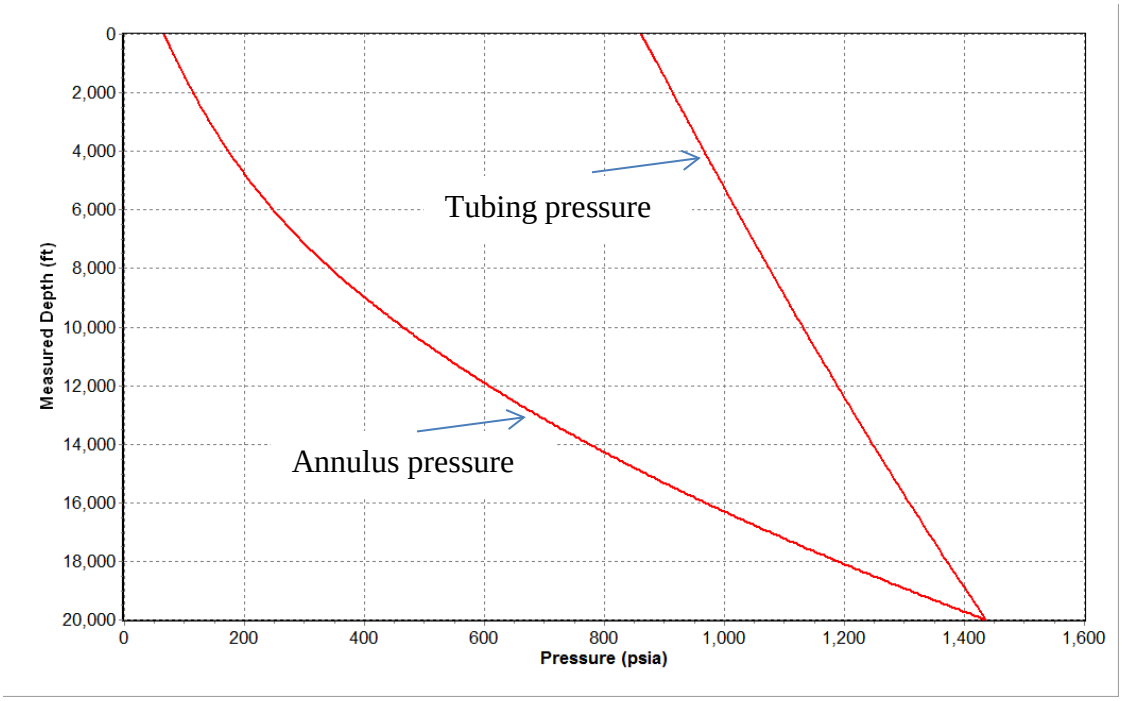


Figure 10-1 Pressure profile (50 psig surface return pressure, 3.5 MMscf/d injection rate, 20,000 MD ft well depth, 1 bpm brine influx, 300°F formation temperature at depth)

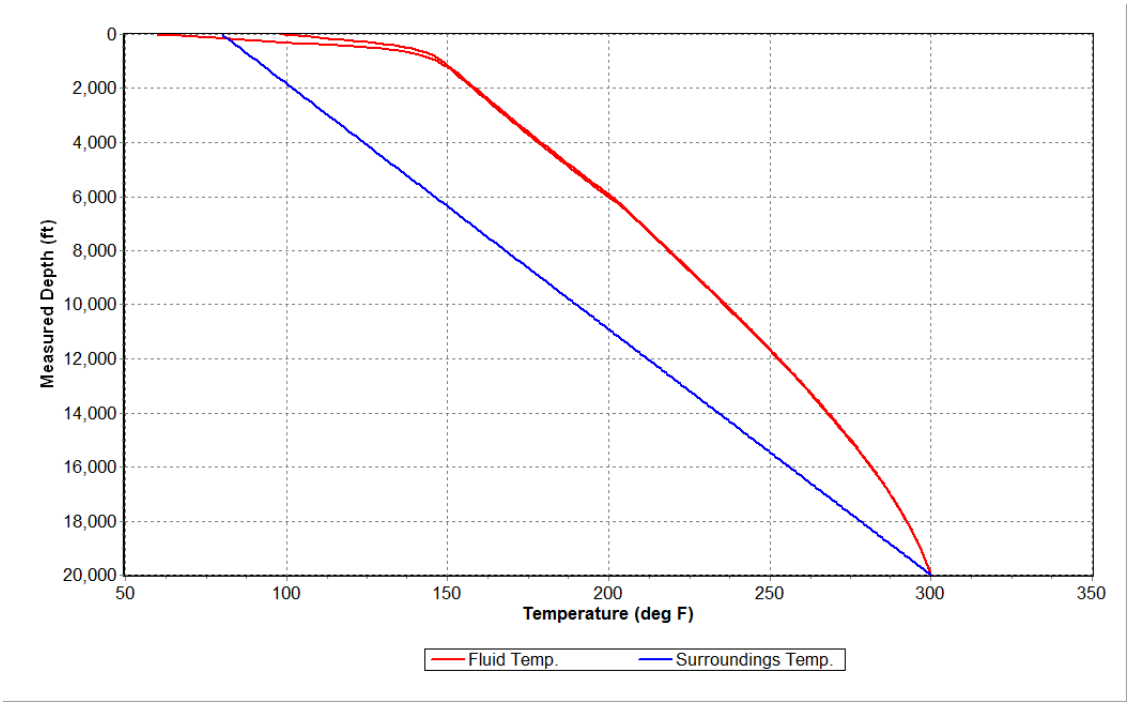


Figure 10-2 Temperature profile (50 psig surface return pressure, 3.5 MMscf/d injection rate, 20,000 MD ft well depth, 1 bpm brine influx, 300°F formation temperature at depth)

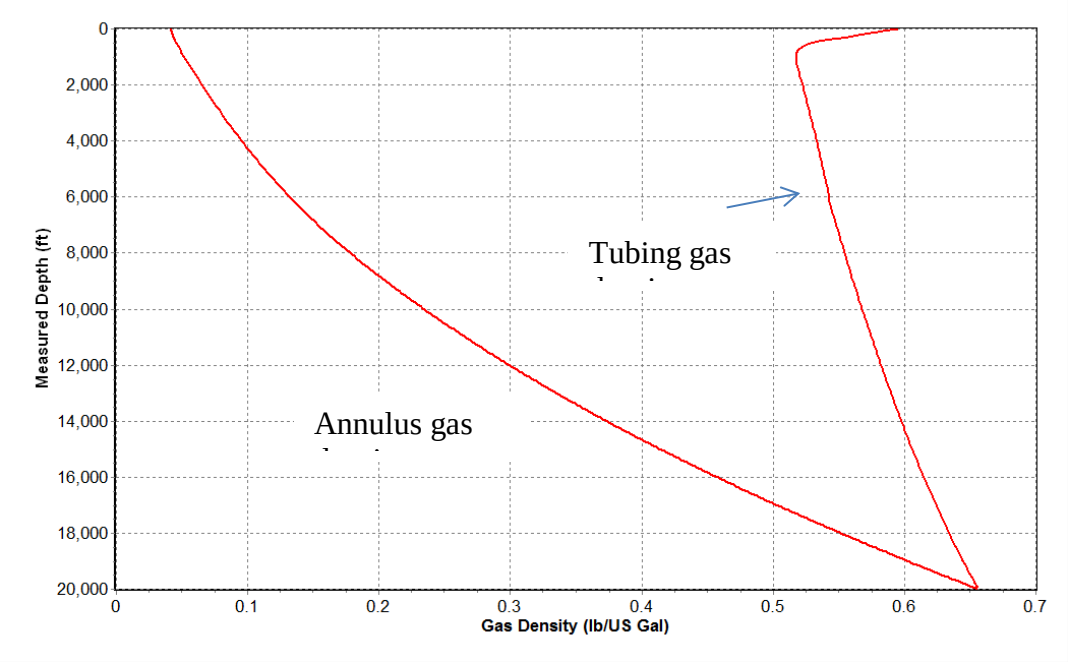


Figure 10-3 Gas density profile (50 psig surface return pressure, 3.5 MMscf/d injection rate, 20,000 MD ft well depth, 1 bpm brine influx, 300°F formation temperature at depth)

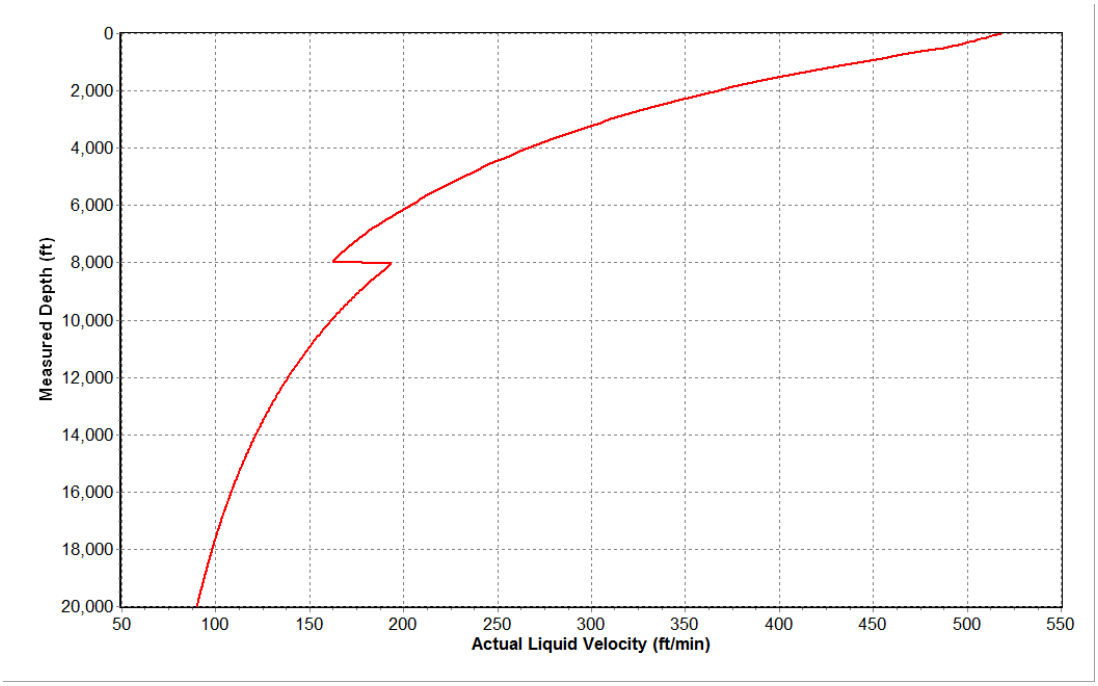


Figure 10-4 Liquid velocity profile (50 psig surface return pressure, 3.5 MMscf/d injection rate, 20,000 MD ft well depth, 1 bpm brine influx, 300°F formation temperature at depth)

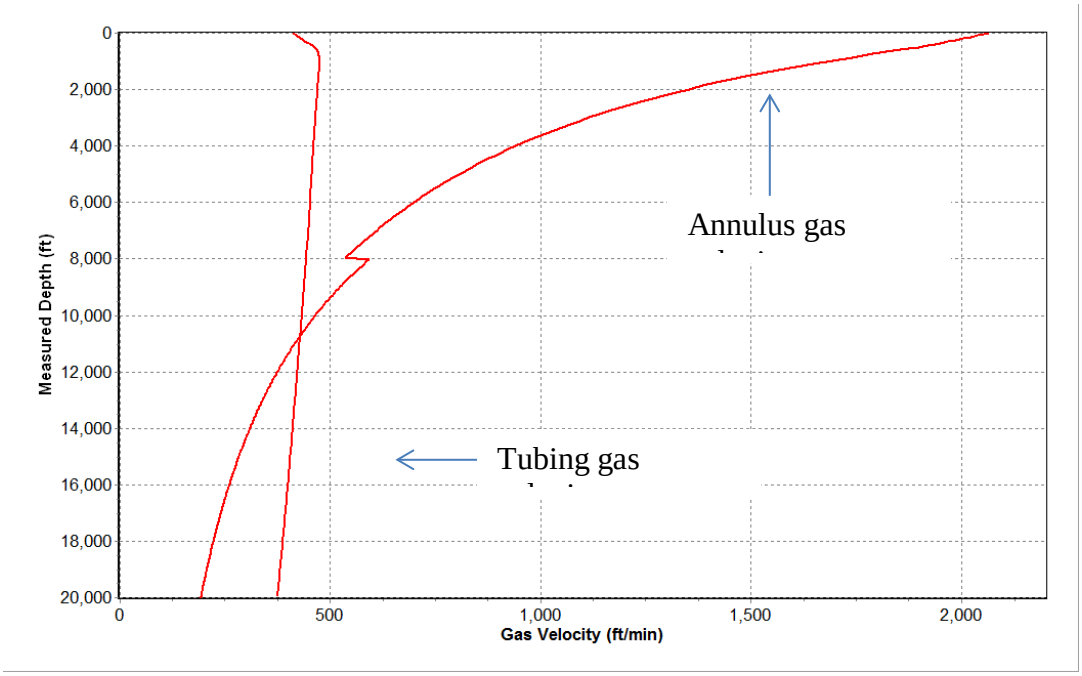


Figure 10-5 Gas velocity profile (50 psig surface return pressure, 3.5 MMscf/d injection rate, 20,000 MD ft well depth, 1 bpm brine influx, 300°F formation temperature at depth)

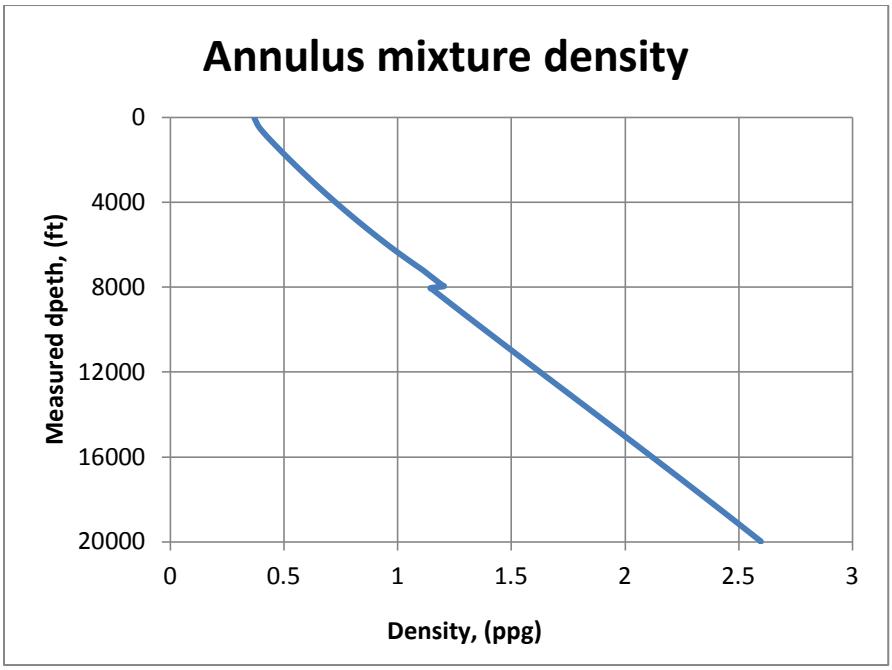


Figure 10-6 Annulus mixture density profile (50 psig surface return pressure, 3.5 MMscf/d injection rate, 20,000 MD ft well depth, 1 bpm brine influx, 300°F formation temperature at depth)

## Chapter 11 Results for the well with 30000 MD ft, 600 °F formation temperature at depth, 0 bpm brine influx, 185.3 psig surface return pressure, 10 MMscf/D injection rate

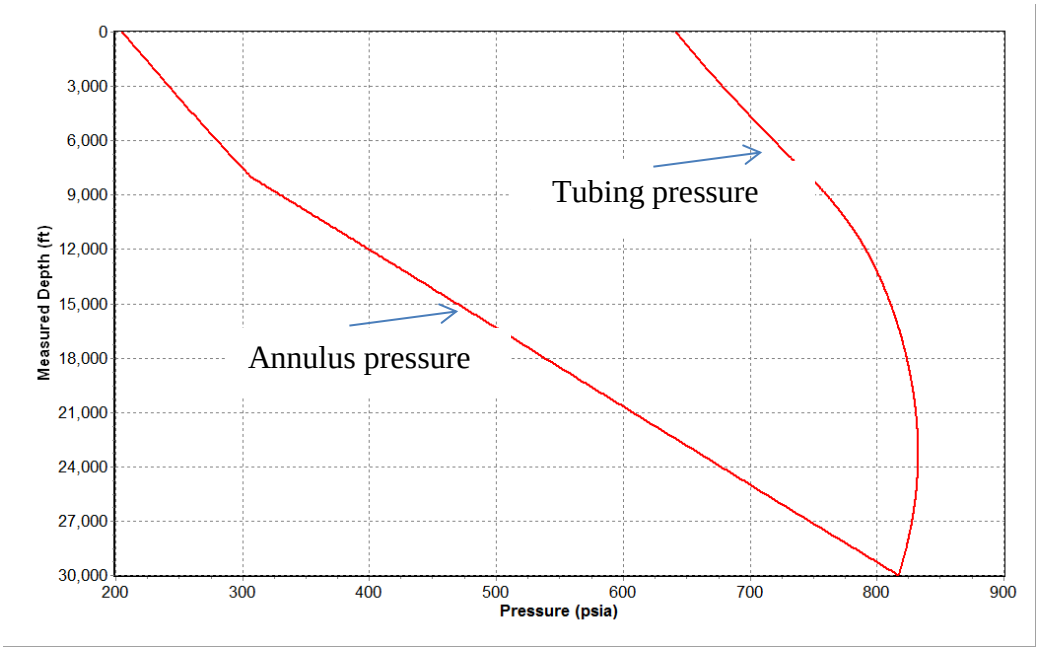


Figure 11-1 Pressure profile (185.3 psig surface return pressure, 10 MMscf/d injection rate, 30,000 MD ft well depth, 0 bpm brine influx, 600°F formation temperature at depth)

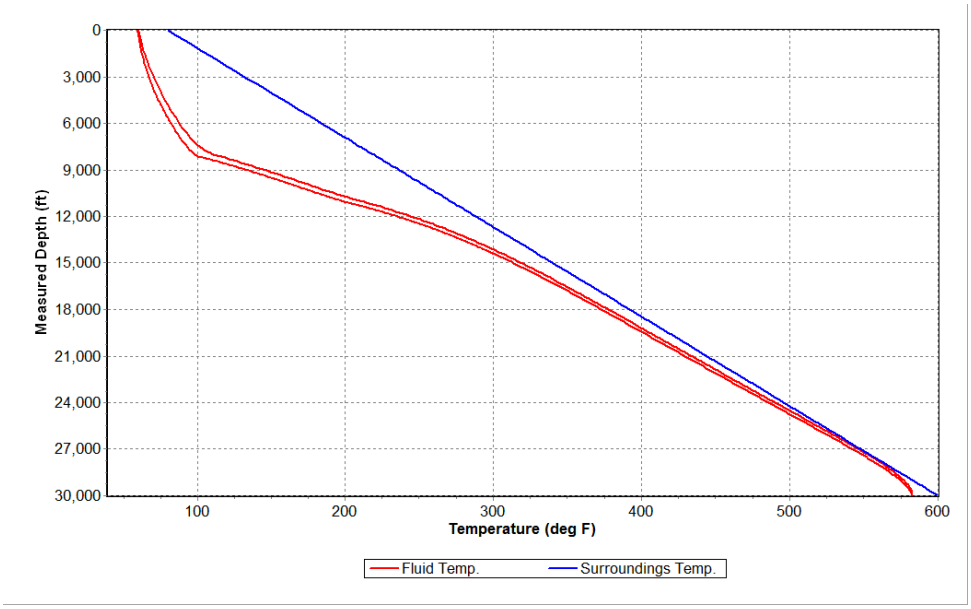


Figure 11-2 Temperature profile (185.3 psig surface return pressure, 10 MMscf/d injection rate, 30,000 MD ft well depth, 0 bpm brine influx, 600°F formation temperature at depth)

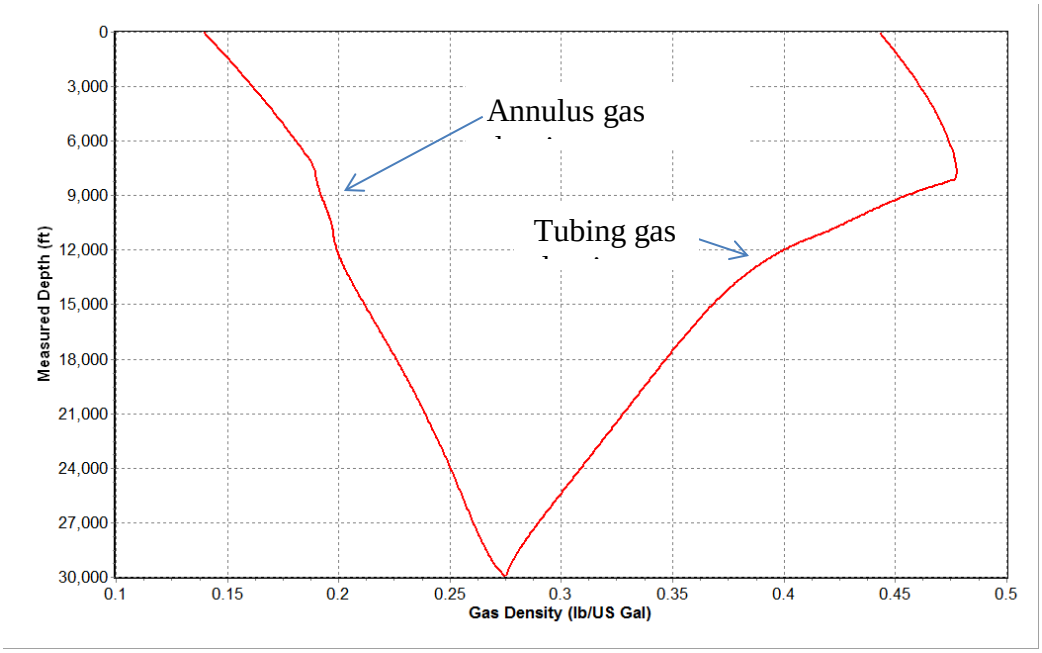


Figure 11-3 Gas density profile (185.3 psig surface return pressure, 10 MMscf/d injection rate, 30,000 MD ft well depth, 0 bpm brine influx, 600°F formation temperature at depth)

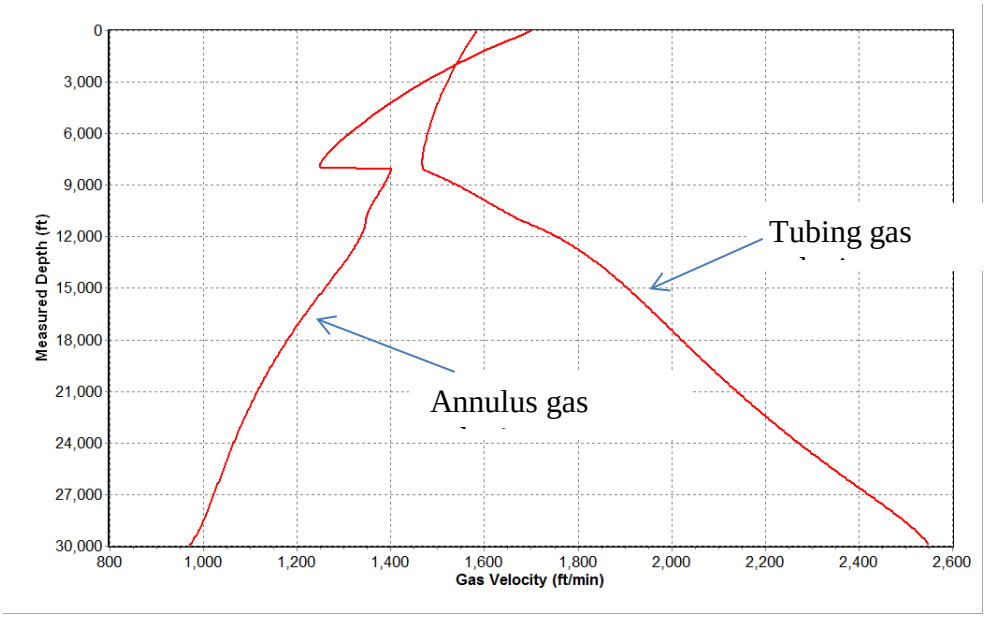


Figure 11-4 Gas velocity profile (185.3 psig surface return pressure, 10 MMscf/d injection rate, 30,000 MD ft well depth, 0 bpm brine influx, 600°F formation temperature at depth)

## Chapter 12 Results for the well with 30000 MD ft, 600 °F formation temperature at depth, 0 bpm brine influx, 185.3 psig surface return pressure, 3.5 MMscf/D injection rate

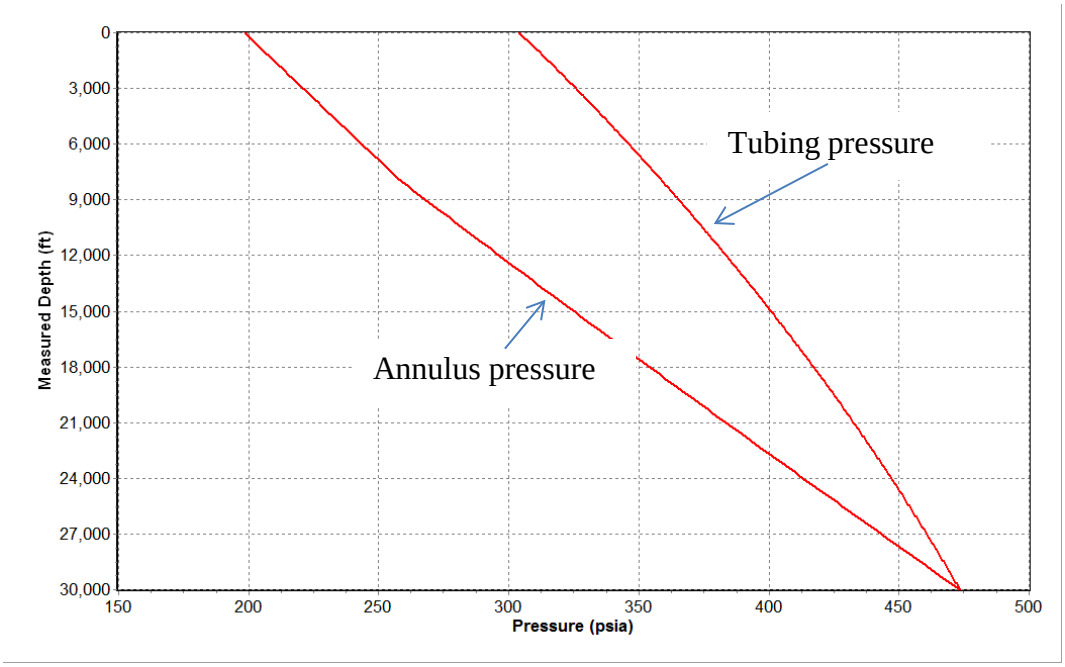


Figure 12-1 Pressure profile (185.3 psig surface return pressure, 3.5 MMscf/d injection rate, 30,000 MD ft well depth, 0 bpm brine influx, 600°F formation temperature at depth)

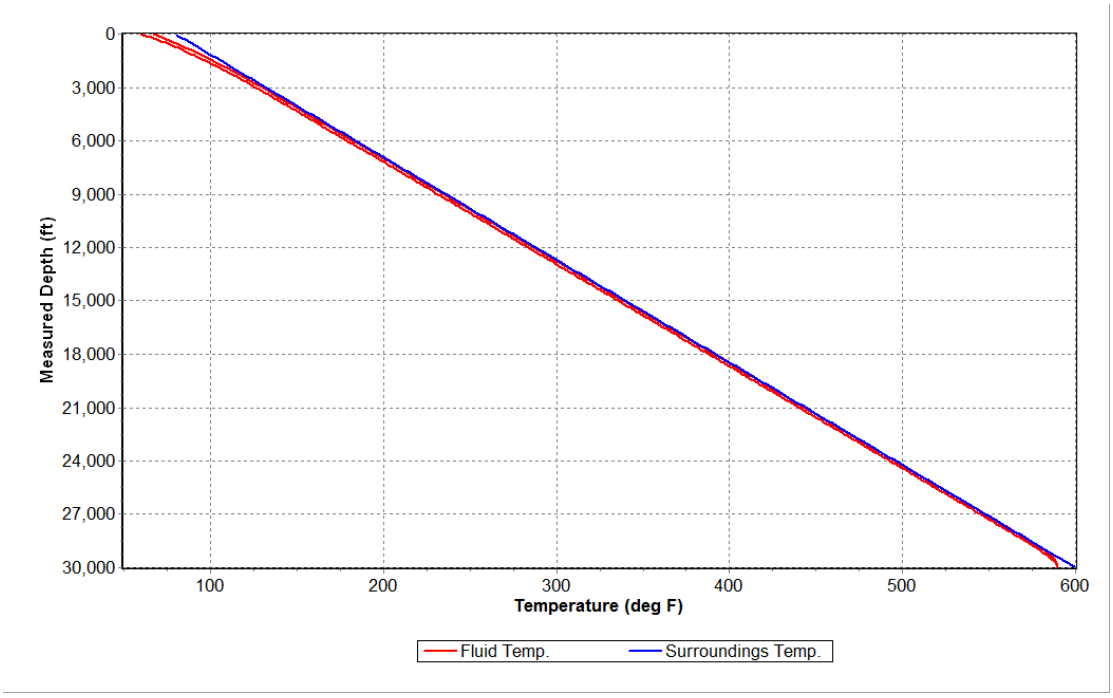


Figure 12-2 Temperature profile (185.3 psig surface return pressure, 3.5 MMscf/d injection rate, 30,000 MD ft well depth, 0 bpm brine influx, 600°F formation temperature at depth)

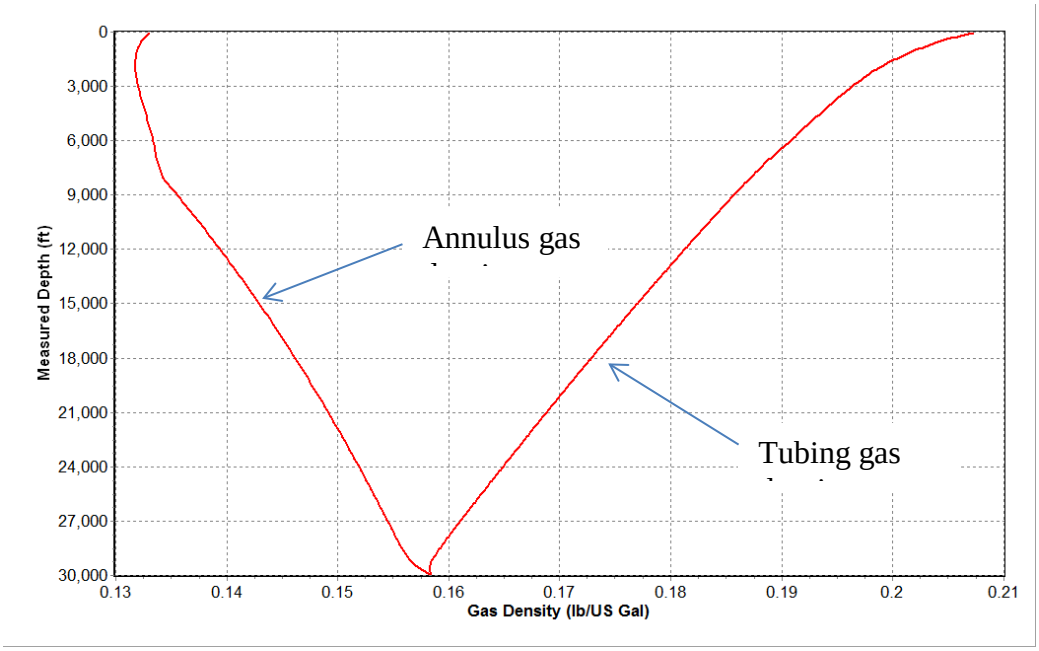


Figure 12-3 Gas density profile (185.3 psig surface return pressure, 3.5 MMscf/d injection rate, 30,000 MD ft well depth, 0 bpm brine influx, 600°F formation temperature at depth)

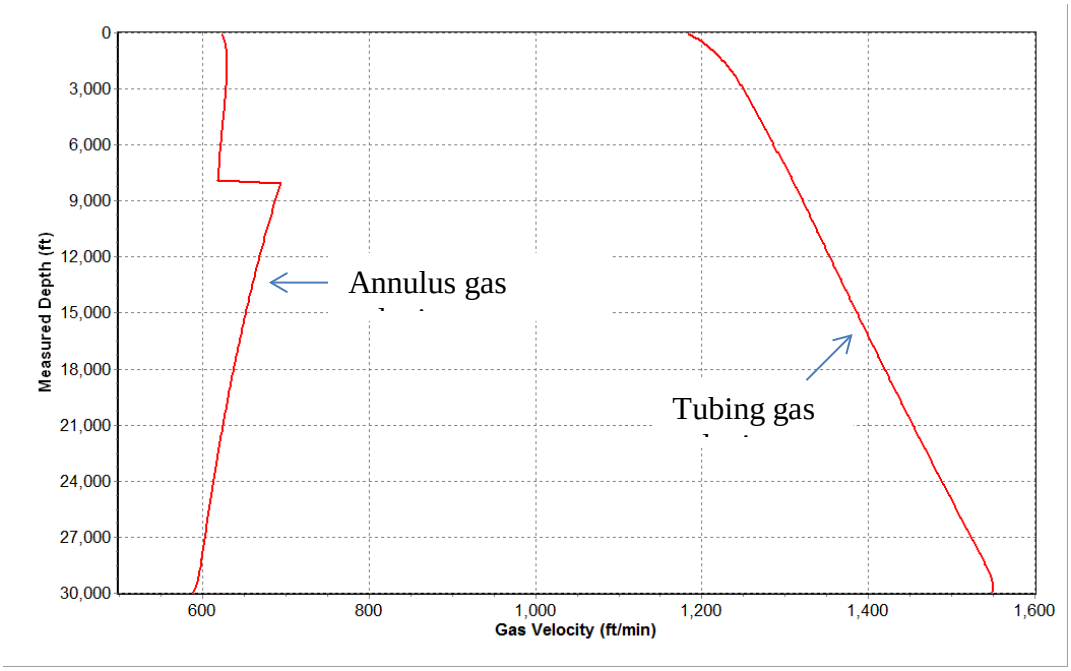


Figure 12-4 Gas velocity profile (185.3 psig surface return pressure, 3.5 MMscf/d injection rate, 30,000 MD ft well depth, 0 bpm brine influx, 600°F formation temperature at depth)

# Appendix C

# Petrographic Report #5EU

# Rock Melt Thin Sections, Photographs and X-Rays Spectrum

# Petrographic Report #5EU

November 12, 2013

for

Paul Woskov
Plasma Fusion Center, NW 16-110
Massachusetts Institute of Technology
190 Albany Street
Cambridge, MA 02139

by

Michael DePangher, Ph.D.
Spectrum Petrographics, Inc.

## Key to Petrographic and Photomicrographic Descriptions

Clay minerals common in altered rocks must often be identified by X-ray diffraction either because their optic properties are not diagnostic or because they are too fine grained to be reliably identified by optical methods. The term "clay" is used herein to denote fine grained phyllosilicates in general. Under ideal conditions, it is often possible to optically discriminate between 4 major groups: kaolinite, smectite, mica (including illite), and chlorite. This is done whenever conditions permit.

The term "sericite" is applied to fine grained colorless phyllosilicates that show upper 2nd order maximum interference colors. These could include muscovite, illite, paragonite, lepidolite, margarite, clintonite, pyrophyllite, and talc. The term "intermediate clay" is applied to fine grained very pale or colorless phyllosilicates that show upper 1st order maximum interference colors. These are probably dominated by chlorite, smectite, and mixed-layer illite/smectite.

The term "opaques" is used to refer to all materials opaque (and sometimes semi-opaque) to transmitted light. The term "FEOH" is herein used to indicate fine grained, yellowish to reddish brown, earthy materials of varying opacity in transmitted light. FEOH is probably mostly Fe oxy-hydroxides but may sometimes include sphalerite, realgar, orpiment, jarosite, a number of Mn oxy-hydroxides, and organic matter.

A question mark after a rock or mineral name in a petrographic description means that there is uncertainty about the identification of that rock or mineral.

Particle size distributions are given as (A-B μm), where A and B are the median and largest particle sizes, respectively, in microns. A question mark (?) in the position of A or B indicates that the value of A or B was indeterminate, probably because of excessively large or small particle size or statistically insignificant numbers of particles.

Mineral abundances are visual estimates for an entire slide. For multi-lithologic materials (cuttings, etc...), mineralogy, textures, and alteration are described only for the dominant lithology.

Section preparation codes are as follows: (1) Format: 27 x 46 mm, 51 x 76 mm, or 1" round; (2) Finish: standard lapping (STD) or polished (POL); (3) Stains: sodium cobaltinitrite (SCN), alizarin red S (ARS), potassium ferricyanide (PF), and barium chloride + potassium rhodizonate (BCPR); and (4) Cover: none, permanent Loctite acrylic (PLA), or removable Canada Balsam (RCB).

Photomicrograph captions/labels contain the following items of information in consecutive order separated by forward slashes: (1) sample identification; (2) JPG image file name composed of concatenated job identification code + sequence number; (3) illumination type; and (5) field of view (FOV). For illumination types, "PPL" indicates plane-polarized light; "XPL indicates cross-polarized light; "R" indicates reflected light. "550" means that a 550 nanometer wavelength plate was inserted in the light path. "C" indicates that the substage condenser was in (sometimes used for Fe-oxides). "O" indicates substage condenser in an oblique position. These various illuminations can be combined. "CON" indicates conoscopic illumination. POL means that a polarizing filter was used with the lens, and DAY means the sample was photographed in diffused daylight.

Features on photomicrographs are indicated by the number of the feature in the ALTERATION section of the text or by a mineral name abbreviation: **Q**uartz, **P**lagioclase, **K**-feldspar, **ser**icite, **b**io**t**ite, **fe**rroan **c**al**c**ite, **act**inolite.

Igneous rock classifications are according to IUGS (1973; 1979); sandstones are classified according to McBride (1963); mudrocks are classified according to Picard (1971); and carbonates are classified according to Folk (1959).

## Hand Specimens

Bedford Granite

1500 C melt

1620 C melt

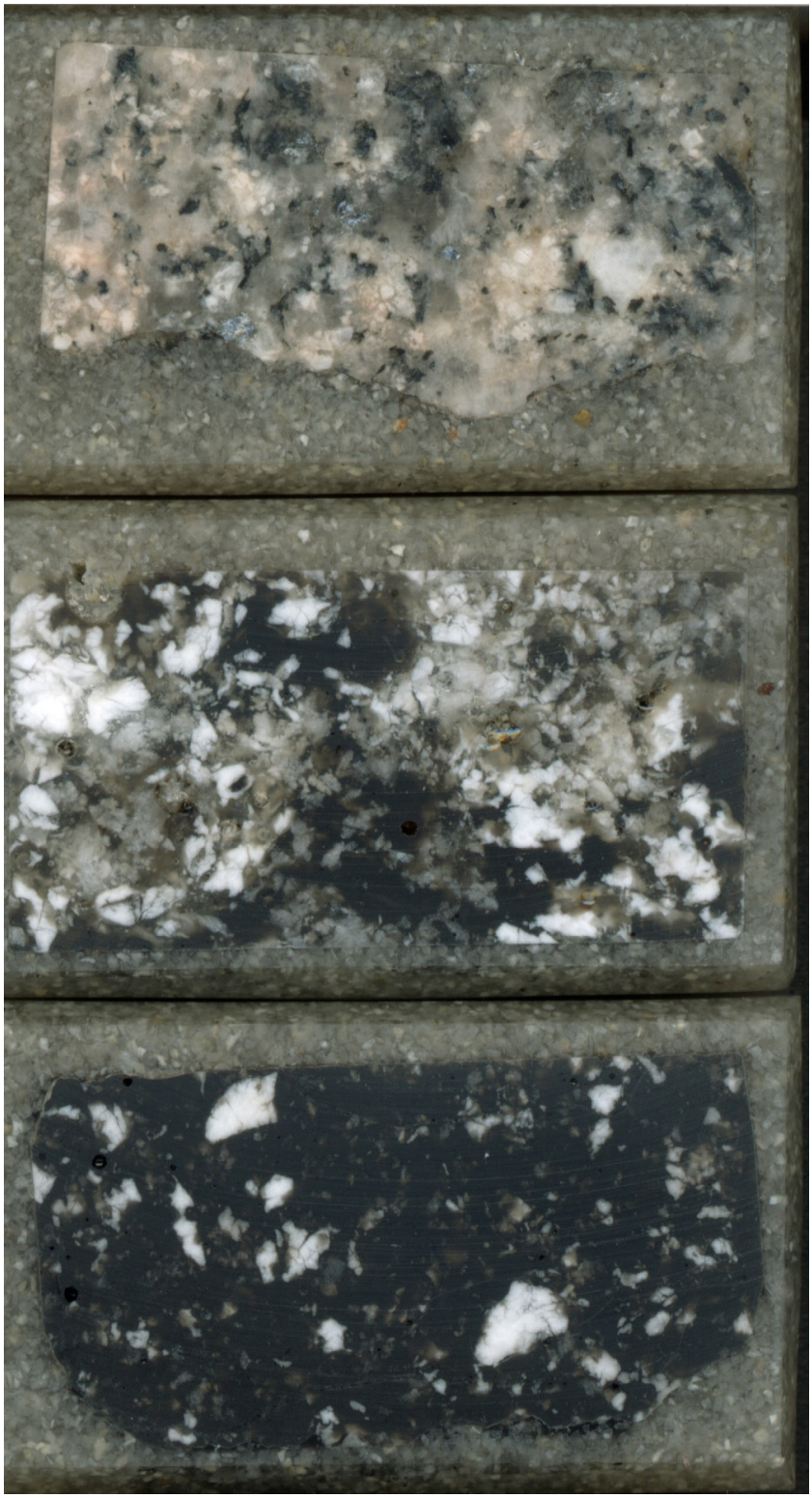

**SAMPLE #** **Bedford Granite** November 12, 2013

**ROCK NAME** ALTERED GRANITE -- probably formed by deformation and alteration (secondary clay + muscovite + chlorite + clinozoisite) of a medium granite protolith.

**MINERALS** Plagioclase (30%) + quartz (30%) + K-feldspar (30%) + biotite (4%) + clay (4%) + muscovite (2%) + chlorite (<1%) + clinozoisite (<1%) + apatite (<1%).

**TEXTURES** Ductile deformation of an intrusive igneous protolith; non-directed fabric.

Phenocrysts (0%) were not observed.

Groundmass (100%) is composed of 800-5600 µm, seriate, [plagioclase weakly altered to clay] + quartz + K-feldspar (mostly microcline) + [biotite weakly altered to muscovite + chlorite + clinozoisite] + apatite.

**ALTERATION** Alteration features of indeterminate relative ages: (1) ductile deformation, possibly metamorphism; (2) local myrmekite.

**SECTIONING** Format: 27 x 46 mm Finish: STD Stains: SCN (top 2/3) + [ARS + PF] (none) Cover: PLA

**IMAGES** Bedford Granite 5EU_001.jpg/XPL/FOV = 4.00 x 5.83 mm ALTERED GRANITE showing typical appearance (same view as 5EU_002.jpg).

Bedford Granite 5EU_002.jpg/PPL/FOV = 4.00 x 5.83 mm ALTERED GRANITE showing typical appearance (same view as 5EU_001.jpg).

**SAMPLE #** **1500 C melt** November 12, 2013

**ROCK NAME** "GRANITE" GLASS -- probably formed by melting of a medium granite protolith.

**MINERALS** Isotropic material (100%).

**TEXTURES** See images; non-directed fabric. No primary textures have survived melting. There are three textural domains: (1) high relief "fragments"; (2) low relief "microspherulitic" "fragments"; and (3) low relief featureless "matrix".

**ALTERATION** Alteration features: (1) granite melting to glass.

**SECTIONING** Format: 27 x 46 mm Finish: STD Stains: SCN (top 2/3) + [ARS + PF] (none) Cover: PLA

**IMAGES** 1500 C melt 5EU_003.jpg/PPL/FOV = 1.85 x 2.69 mm "GRANITE" GLASS showing typical appearance of high relief "fragment".

1500 C melt 5EU_004.jpg/PPL/FOV = 1.85 x 2.69 mm "GRANITE" GLASS showing typical appearance of low relief "microspherulitic" "fragment".

1500 C melt 5EU_005.jpg/PPL/FOV = 0.96 x 1.40 mm "GRANITE" GLASS showing typical appearance of a transitional "fragment" that shows textures of both high and low relief types.

**SAMPLE #** **1620 C melt** November 12, 2013

**ROCK NAME** “GRANITE” GLASS -- probably formed by melting of a medium granite protolith.

**MINERALS** Isotropic material (100%).

**TEXTURES** See images; non-directed fabric. No primary textures have survived melting. There are three textural domains: (1) high relief “fragments”; (2) low relief “fragments”; and (3) low relief featureless “matrix”.

**ALTERATION** Alteration features: (1) granite melting to glass.

**SECTIONING** Format: 27 x 46 mm Finish: STD Stains: SCN (top 2/3) + [ARS + PF] (none) Cover: PLA

**IMAGES** 1620 C melt 5EU_006.jpg/PPL/FOV = 4.00 x 5.83 mm “GRANITE” GLASS showing typical appearance of high relief “fragment”.

1620 C melt 5EU_007.jpg/PPL/FOV = 1.85 x 2.69 mm “GRANITE” GLASS showing typical appearance of low relief “fragment”.

1620 C melt 5EU_008.jpg/PPL/FOV = 0.96 x 1.40 mm “GRANITE” GLASS showing typical closeup appearance of adjacent high and low relief “fragments”.

# Appendix D

# MIT MMW Bench Test Data and Results

## Table 1. Rock Samples Tested and MMW Exposure

| Test Date Duration | Rock Number | Rock Type* | Sample Size | Power [kW] | Guide Mode | Aperture [mm] | |
|---|---|---|---|---|---|---|---|
| 4/3/2013 | 1a | Barre Granite | 3 x 4 x 1" | 1.7 - 4.3 | HE11 | 32.5 | 4 m 20 s |
| 4/4/2013 | 1b | Barre Granite | 4 x 4 x 1" | 1.7 - 4.3 | TE11 | 32.5 | 4 m 39 s |
| 4/5/2013 | 2 | Barre Granite | 2.5 x 3 x 1" | 2.2 - 3.9 | TE11 | 32.5 | 8 m 8 s |
| 4/12/2013 | 3 | Barre Granite | 2 x 3 x 1" | 0.5 - 3.6 | TE11 | 32.5 | 16 m 26 s |
| 4/22/2013 | 4a | Barre Granite | 2 x 6 x 1" | 0.8 - 1.1 | HE11 | 32.5 | 20 m 50 s |
| 4/23/2013 | 4b | Barre Granite | 2 x 6 x 1" | 1.5 - 3.8 | HE11 | 32.5 | 38 m |
| 4/24/2013 | 5a | Barre Granite | 2 x 7 x 1" | 1.5 - 3.9 | HE11 | 32.5 | 25 m 35 s |
| 4/24/2013 | 6 | Granite , MA | irregular ~4" 3D | 0.5 - 3.9 | HE11 | 32.5 | 20 m 30 s |
| 5/24/2013 | 5b | Barre Granite | 2 x 7 x 1" | 1.6 - 2.5 | HE11 | 32.5 | 9 m 20 s |
| 5/31/2013 | 5c | Barre Granite | 2 x 7 x 1" | 1.8 - 4.1 | HE11 | 32.5 | 16 m 21 s |
| 6/14/2013 | 7a | Granite, MA | irregular ~4x3" | 1.3 - 4.0 | HE11 | 32.5 | 4 m 9 s |
| 6/14/2013 | 7b | Granite, MA | irregular ~4x3" | 2.2 - 4.5 | HE11 | 32.5 | 19 m 12 s |
| 6/21/2013 | 8a | Barre Granite | 2 x 3 x 1" | 1.7 - 5.4 | HE11 | 32.5 | 23 m 22 s |
| 6/21/2013 | 8b | Barre Granite | 2 x 3 x 1" | 1.5 - 5.4 | HE11 | 32.5 | 23 m 30 s |
| 7/2/2014 | 8c | Barre Granite | 2 x 3 x 1" | 2.2 - 4.8 | HE11 | 32.5 | 37 m 5 s |
| 7/31/2013 | 9a | Barre Granite | crushed rock | 0.9 - 3.5 | HE11 | 32.5 | 37 m 26 s |
| 8/1/2013 | 9b | Barre Granite | crushed rock | 1.7 - 3.8 | HE11 | 32.5 | 31 m 13 s |
| 8/1/2013 | 9c | Barre Granite | crushed rock | 2.2 - 3.3 | HE11 | 32.5 | 56 m |
| 8/6/2013 | 10 | Granite, MA | irregular, thin | 1.4 - 3.2 | HE11 | 32.5 | 35 m |
| 8/27/2013 | 11a | Granite, Brazil | 4 x 4 x 1 3/16" | 0.8 -2.5 | HE11 | 32.5 | 19 m 34 s |

| | | | | | | | |
|---|---|---|---|---|---|---|---|
| 8/29/2013 | 11b | Granite, Brazil | 5 x 4 x 1 3/16" | 0.8 - 3.5 | HE11 | 32.5 | 19 m 32 s |
| 8/29/2013 | 11c | Granite, Brazil | 6 x 4 x 1 3/16" | 1.1 - 3.9 | HE11 | 32.5 | 37 m 24 s |
| 8/30/2013 | 11d | Granite, Brazil | 7 x 4 x 1 3/16" | 1.6 - 2.8 | HE11 | 32.5 | 24 m 50 s |
| 9/11/2013 | 12a | Granite, MA | irregular~3 x 3" | 1.3 - 2.3 | HE11 | 32.5 | 35 m 31 s |
| 9/11/2013 | 12b | Granite, MA | irregular~3 x 3" | 0.8 - 2.0 | HE11 | 32.5 | 31 m 39 s |
| 9/17/2013 | 13 | Granite, MA | irregular~3.2 x 5" | 1.2 - 3.9 | HE11 | 32.5 | 56 m 49 s |
| 10/18/2013 | 14 | Barre Granite | irregular chip | 2.2 - 3.2 | HE11 | 32.5 | 3 m |
| 10/22/2013 | 15a | Barre Granite | 4" dia. X 1" | 1.6 | HE11 | 32.5 | 2 m 26 s |
| 10/22/2013 | 15b | Barre Granite | 4" dia. X 1" | 1.6 - 2.4 | HE11 | 32.5 | ~40 m |
| 11/8/2013 | 16 | Barre Granite | 4" dia. X 1" | 2.1 - 3.1 | HE11 | 32.5 | 17 m 30 s |
| 12/10/2013 | 17 | Barre Granite | 4 x 4 X 1" | 1.8 - 2.3 | HE11 | 32.5 | 10 m 32 s |
| 12/13/2013 | 18 | Barre Granite | 4 x 4 x 1" | 1.6 - 2.0 | HE11 | 32.5 | 15 m |
| 1/8/2014 | 19 | Barre Granite | 4" dia. X 1" | 1.5 - 3.4 | HE11 | 32.5 | 26 m 20s |
| 1/17/2014 | 20a | Barre Granite | 4" dia. X 1" | 1.8 - 3.5 | TE11, dt** | 20 | 26 m 1 s |
| 3/14/2014 | 21 | Granite, Brazil | 4 x 4 x 1 3/16" | 1.7 - 4.1 | TE11, dt | 20 | 21 m 53 s |
| 3/17/2014 | 20b | Barre Granite | 4" dia. X 1" | 1.8 - 3.7 | TE11, dt | 20 | 13 m 38 s |
| 3/18/2014 | 22 | Basalt | 4 x 4 x 1 1/4" | 2.0 - 3.3 | TE11, dt | 20 | 16 m 51 s |
| 3/19/2014 | 23 | Basalt | 4 x 4 x 1 1/4" | 1.5 - 4.5 | TE11, dt | 20 | 12 m 21s |
| 4/4/2014 | 24 | Basalt | 4 x 4 x 1 1/4" | 1.3 - 4.1 | TE11, dt | 20 | 35 m |

| | | | | | | | |
|---|---|---|---|---|---|---|---|
| 4/23/2014 | 25 | Limestone | 4 x 4 x 2" | 1.6 - 4.2 | TE11, dt | 20 | 31 m 28 s |
| 4/29/2014 | 26 | Basalt | 4 x 4 x 1 1/4" | 1.2 - 3.6 | TE11, dt | 20 | 35 m 8 s |
| | | | | | | | |
| 6/11/2014 | 27a | Basalt | 4 x 4 x 1 1/4" | 0.3 - 3.2 | TE11, dt | 20 | 22 m 15 s |
| 6/18/2014 | 28a | Barre Granite | 4" dia. X 1" | 0.7 - 1.3 | TE11, dt | 20 | 14 m 33 s |
| 6/18/2014 | 28b | Barre Granite | 4" dia. X 1" | 0.7 - 3.4 | TE11, dt | 20 | 33 m 55 s |
| 6/18/2014 | 28c | Barre Granite | 4" dia. X 1" | 0.7 - 3.0 | TE11, dt | 20 | 20 m 54 s |
| 6/20/2014 | 28d | Barre Granite | 4" dia. X 1" | 0.8 - 2.7 | TE11, dt | 20 | 40 m 22 s |
| 6/20/2014 | 27b | Basalt | 4 x 4 x 1 1/4" | 0.7 - 3.1 | TE11, dt | 20 | 30 m 32 s |
| 6/24/2014 | 27c | Basalt | 4 x 4 x 1 1/4" | 0.7 - 4.5 | TE11, dt | 20 | 37 m 58 s |
| 6/27/2014 | 27d | Basalt | 4 x 4 x 1 1/4" | 1.0 - 3.1 | HE11 | 32.5 | 47 m 45 s |
| | | | | | | | |
| 7/2/2014 | 27e | Basalt | 4 x 4 x 1 1/4" | < 2.0 | TE11, dt | 20 | 41 m |
| 7/2/2014 | 27f | Basalt | 4 x 4 x 1 1/4" | < 2.0 | TE11, dt | 20 | 26 m 9 s |
| 7/3/2014 | 27g | Basalt | 4 x 4 x 1 1/4" | < 2.0 | TE11, dt | 20 | 30 m 21 s |
| 7/15/2014 | 27h | Basalt | 4 x 4 x 1 1/4" | 1.6 - 4.4 | TE11, dt | 20 | 39 m 22 s |
| 7/16/2014 | 27i | Basalt | 4 x 4 x 1 1/4" | 1.7 - 4.6 | TE11, dt | 20 | 35 m 46 s |
| 7/17/2014 | 29 | Berea Sandstone | 4" dia. x 1 1/16-1/2" | 1.7 - 4.2 | TE11, dt | 20 | 44 m 13 s |
| 7/23/2014 | 30 | Basalt | 4 x 4 x 1 1/4" | 1.5 - 4.5 | TE11, dt | 20 | 29 m 20 s |
| 7/24/2014 | 31 | Barre Granite | 4 x 4 X 1" | 1.3 - 4.5 | TE11, dt | 20 | 60 m 50 s |
| 7/30/2014 | 32 | Basalt | 4 x 4 x 1 1/4" | 1.7 - 3.3 | HE11 | 32.5 | 37 m 3 s |
| 7/31/2014 | 33 | Basalt | 4 x 4 x 1 1/4" | 1.6 - 4.5 | TE11, dt | 20 | 41 m 1 s |
| | | | | | | | |
| 8/1/2014 | 34a | Barre Granite | 4" dia. X 1" | 1.5 - 4.3 | TE11, dt | 20 | 39 m 2 s |
| 8/6/2014 | 34b | Barre Granite | 4" dia. X 1" | 1.5 - 3.6 | TE11, dt | 20 | 54 m 44 s |
| 8/6/2014 | 34c | Barre Granite | 4" dia. X 1" | 1.8 - 4.0 | HE11 | 32.5 | 36 m 17 s |
| 8/8/2014 | 34d | Barre Granite | 4" dia. X 1" | 1.6 - 4.0 | HE11 | 32.5 | 29 m 2 s |
| 8/13/2014 | 35 | Barre Granite | 4 x 4 X 1" | 1.4 - 4.4 | TE11, dt | 20 | 106 m 24 s |
| 8/19/2014 | 36 | Berea Sandstone | 4" dia. X 0.75 -1 1/16"" | 1.6 - 4.4 | TE11, dt | 20 | 45 m 33 s |

***Rock Types and Sources**

Barre Granite: from Barre, VT quarry

Granite, Brazil: Empire Marble & Granite Sommerville, MA, from quarry in Brazil
Granite, MA: from Bedford, MA
Basalt: Coverall Stone, LLC, SeaTec, WA, from quarry in Mongolia
Berea Sandstone: Cleveland Quarries, Vermilion, OH
Limestone: P & M Brick and Block, Watertown, MA

** waveguide down taper (dt) from 32.5 to 20 mm diameter used in the specified test

## Table 2. Additional MMW Exposure Parameters and Results

| Rock Number | Weight[a] [grams] | Standoff Distance | Purge Gas | Flow[b] [scfh] | Maximum Temp.[c] [°C] |
|---|---|---|---|---|---|
| 1a | | 0.5" | nitrogen | | |
| 1b | | 0.5" | nitrogen | | |
| 2 | | 1.5" | nitrogen | | |
| 3 | | 1.5" | nitrogen | 200/100 | 1,502 |
| 4a | 412.7/412.3 | 1.0" | nitrogen | 200/100 | 1,506 |
| 4b | 412.3/411.4 | 1.0" | nitrogen | 200/100 | 4,000 |
| 5a | 516 | 0.5" | nitrogen | 300/100 | 2,958 |
| 6 | 677.3/675.1 | ~0.5" | nitrogen | 300/100 | 5,916 |
| 5b | /514.6 | 1.0" | nitrogen | 200-320/100 | 20,200 |
| 5c | 514.6/513.7 | 1.0" | nitrogen | 300/100 | 17,880 |
| 7a | 545.9/544.9 | ~1.0" | air | 220/100 | |
| 7b | 544.9/543.3 | ~1.0" | air | 220/100 | |
| 8a | 826.9/826.2 | 1.0" | air | 250/100 | 1,797 |
| 8b | 826.2 | 1.0" | air | 250/100 | 3,547 |
| 8c | /825.9 | 1.0" | air | 300 | 1,867 |
| 9a | 280.5/278.6 | 0.5" | air | 380/100 | 1,912 |
| 9b | 278.0/278.1 | 1.18" | air | 400-490 | 1,307 |
| 9c | | 1.18" | air | 400 | 2,930 |
| 10 | | ~0.55" | air | 450/100 | 3,012 |
| 11a | | 0.5" | air | 450 | 2,400 |
| 11b | | 1.0" | air | 450 | 2,431 |
| 11c | | 0.75" | air | 350-450 | 2,856 |
| 11d | | 0.75" | air | 35-450 | 3,403 |
| 12a | 569.3 | 0" | air | 350/100 | 2,392-5,110 |
| 12b | | 0" | air | 400-450/100 | 2,245-5,065 |
| 13 | | 0" | air | 500/100 | 3,287 |
| 14 | 162.4 | ~0.5" | air | 500/50 | 1,945 |
| 15a | 552.9 | 0.75" | air | 0 | |
| 15b | /551.8 | 0.75" | air | 500/50 | 1,914 |
| 16 | 553.1 | 1.0" | air | 500 | 1,468 |

| | | | | | |
|---|---|---|---|---|---|
| 17 | 664.5/663.8 | 0.31" | air | 460/40 | 2,230 |
| 18 | | 0.62" | air | 460/40 | 1,458 |
| | | | | | |
| 19 | 570.8 | 0.31" | air | 460 | 2,422 |
| 20a | 577.8 | 0.5 - 1.38" | air | 450 | 1,878 |
| | | | | | |
| 21 | 860.8/859.5 | 0.75" | air | 460 | 2,538 |
| 20b | 572.8/572.7 | 0.75" | air | 350 | 3,006 |
| 22 | 891.5 | 0.75" | air | 350 | 2,003 |
| 23 | | 0.75" | air | 350 | 548 |
| | | | | | |
| 24 | 889.2/877.9 | 0.75" | air | 350 | 2,983 |
| 25 | 1260.4/1208.0 | 0.75" | air | 360 | 3,350 |
| 26 | 912.8/909.9 | 0.75" | air | 380 | 3,523 |
| | | | | | |
| 27a | 906.6/895.4 | 0.75" | air | 450 | 2,455 |
| 28a | 578.0/577.4 | 0.75" | air | 450 | 1,075 |
| 28b | 577.4/576.9 | 0.75 | air | 450 | 2,503 |
| 28c | 576.9/576.7 | 1.0" | air | 450 | 1,790 |
| 28d | 576.7/576.4 | 1.18" | air | 450 | 2,005 |
| 27b | 895.4/894.0 | 1.18" | air | 450-420 | 1,180 |
| 27c | 890.7/888.9 | 1.57" | air | 450 | 1,730 |
| 27d | 888.9/888.4 | 1.71" | air | 450 | 1,140 |
| | | | | | |
| 27e | | 1.57" | air | 450 | |
| 27f | | 1.57" | air | 450 | |
| 27g | | 1.57" | air | 460 | |
| 27h | /884.6 | 1.57" | air | 460 | 2,697 |
| 27i | 884.6/884.3 | 1.57" | air | 460 | 1,993 |
| 29 | 560.1/555.0 | 1.42" | air | 460 | 3,150 |
| 30 | 891.0/715.1 | 1.38" | air | 460 | 1,490 |
| 31 | 686.9 | 1.46" | air | 460 | 1,996 |
| 32 | 892.9/865.4 | 1.50" | air | 460 | 1,880 |
| 33 | 895.5/686.7 | 1.38" | air | 460 | 1,050 |
| | | | | | |
| 34a | 597.5/592.0 | 1.46" | air | 460 | 2,100 |
| 34b | 585.7/584.2 | 1.46" | air | 460 | 2,130 |
| 34c | 580.1/577.7 | 1.57" | air | 460 | 1,830 |
| 34d | 573/572.7 | 1.85" | air | 460 | 2,260 |
| 35 | 694.0/679.7 | 1.46" | air | 480 | 2,240 |
| 36 | 383.9/377.9 | 1.38" | air | 470 | 2,180 |

[a]Second number after slash is weigth after MMW exposure
[b]Flow after slash is from side pipe blowing across
launch aperture
[c]Average temperature over radiometer view uncorrected for emissivity or background
heating temperatures above 3,000 °C suggest presences of plasma breakdown

## Table 3. MMW Expossure Observations

| Rock Number | Comments/ Results |
|---|---|
| 1a | 1 3/8" dia. borehole, no melting |
| 1b | 1 3/8" dia. borehole, no melting |
| 2 | Rock #1 borehole on top, ~1/4" melt spot |
| 3 | Rock #1 borehole on top, ~1 1/4" melt spot and stalactite |
| 4a | direct surface exposure, ~ 1" dia. melt spot |
| 4b | Rock 4a translated ~1 1/4" melt spot |
| 5a | 1 3/8" dia. 1" long mullite tube on top, ~1 3/8" melt spot |
| 6 | direct surface exposure, backyard rock ~1" dia. melt spot |
| 5b | TV camera used, plasma breakdown seen after surface temperature > 1000 °C |
| 5c | TV camera used, airflow can suppress plasma |
| 7a | backyard rock, ~1 3/8" dia. melt spot |
| 7b | repeat same rock, ~ 1 3/8" dia. melt spot with large bubble void |
| 8a | Rock #1 borehole on top, borehole circum. melted, < 1" dia. melt on bottom rock |
| 8b | Rock #8 again through hole, borehole wall melting increased (off center) |
| 8c | Rock #8 again, 1 3/8" dia. 1" long mullite tube on top , enlarged melt spot slightly |
| 9a | 3" dia. crucible with 1 3/8" dia. borehole through 4" diameter by 1 1/4" thick granite on top |
| 9b | without granite borehole top |
| 9c | without granite borehole top, surface melt dia. ~1 3/4" and 1" peak depth |
| 10 | backyard rock about 1/2" to 1" thick, melt crater about 1 5/8" dia. and 5/8" deep at center |
| 11a | melt spot dia. ~ 1 3/8", fracture from melt to edge |
| 11b | repeat Rock #11 |
| 11c | repeat Rock #11 |

| | |
|---|---|
| 11d | repeat Rock #11, melt spot reaches about 1 3/4" diameter, peak depth ~ 5/8" |
| 12a | backyard rock through 1.3" dia. 1 1/4" deep granite borehole on top, parial me lting of borehole |
| 12b | repeat Rock #12 with granite borehole on top, melt area about 1 3/4" in size wi th 1" flow to one side |
| 13 1/4" long | rock with sloping ridged surfaces and propagation through 1 3/8" dia., 1 granite bore on top, 3" melt flow down side of rock, borehole vitrification observed |
| 14 | max. thick 0.59", 4 x 4.0 - 2.5", melt and shattered |
| 15a | breakdown in waveguide, airflow not on |
| 15b | multiple gyrotron trips, ~1 1/2" dia. melt spot |
| 16 | direct surface exposure, one gyrotron trip ~ 1 1/2" melt diameter |
| 17 | waveguide gap installed, ~1 3/8" melt spot on top and ~1/2" melt spot on bottom 18 multiple gyrotron trips |
| 19 | direct surface exposure, two samples stacked, ~ 1 1/2" dia. melt spot |
| 20a | 2 cm dia. down taper (dt), rock slipped down, ~2" dia. melt spot with 3/8" raised edge |
| 21 | direct surface exposure, ~1 3/4" dia. melt crater ~ 3/8" deep |
| 20b | re-exposed Rock #20 Jan17th sample, crater slightly larger, large bubble in center |
| 22 | complete breakup and scatter throughout test chamber without outer clamp |
| 23 | beam off center partially missing rock clamped around side, breakup from upper surface |
| 24 | Gap water cooling added, ~ 1 7/8" diameter shallow melt crater, post weight may miss fracture fragments |
| 25 | vaporized black carbon like coating on surfaces inside test chamber, small translucent glassy melt spot |
| 26 | direct surface exposure, ~ 1 1/2" dia. shallow melt crater thoroughly fractured |
| 27a | significant chipping, fragment missing from top, ~7/8" melt spot inner dia. with some flow to side |
| 28a | ~ 1" dia. melt spot, 3/4" long stalactite formed on bottom |
| 28b | Rock #28, 1 3/4" by 1 7/8" melt crater, ~ 0.40" deep with raised rim |

| | |
|---|---|
| 28c | Rock #28, 1 11/16" by 1 7/8" melt crater, ~ 0.45" deep with raised rim |
| 28d | Rock #28 melt crater 1 7/8" by 2.0 ", depth about the same |
| 27b | Rock #27 melt crater dia. ~ 1.18" inside raised ridge, off center flow |
| 27c | Rock #27 melt crater size ~ 1.50" to 1.65" inside raised ridge, ~0.5 deep below raised ridge |
| 27d | Rock #27 off center melting non-symmetrical crater about same size as before |
| 27e | Rock #27 down taper installed backwards inefficient heating |
| 27f | Rock #27 down taper installed backwards inefficient heating |
| 27g | Rock #27 down taper installed backwards inefficient heating |
| 27h | Rock #27, down taper corrected, melt crater about 1.5" by 1.65" |
| 27i | Rock #27 no significant increase in crater size, but more flow outside ridge |
| 29 | diameter to crater ridge peak 1.50", penciled depth to 0.83" at center |
| 30 | 1/2" leak hole, complete melt through ~2" dia., 165.4 g melt collected |
| 31 | 1/2" leak hole, complete melt through 1.54"/1.0" dia. at top/bottom, 2" long melt tube below, 25 g melt collected |
| 32 | 1/2" leak hole, crater 1.46" by 1.69" , 0.39" deep, 0.35" long stalactite below, breakdown limit in crater |
| 33 | 1/2" leak hole, complete melt through 2.05 X 1.93" top to 1.77" x1.69" bottom larger diameter inside, 198.6 g melt collected |
| 34a | 1/2" leak hole, no melt through large 2.20" dia. melt crater 1/2" leak hole plugged up |
| 34b | Rock #34 1/2" leak hole redrilled, crater diameter about the same, depth ~0.61" leak hole plugged |
| 34c | Rock #34 1/2" leak hole redrilled, crater diameter about same, depth ~0.71" leak hole plugged |
| 34d | Rock #34 1/2" leak hole redrilled, 1/2 tea spoon sodium carbonate, no melt through but can see light through plugged leak hole |
| 35 | 1/2" leak hole, almost melt through, 1.5" inner dia. 2.25" outer, ~1" deep from 0.5" high ridge, 1.5" long stalactite from bottom leak hole |
| 36 | 1/2" leak hole, no melt through, 3.0" inner dia. 1.65 outer, ~1" deep in center from 0.375" high surface ridge |

# Appendix E

# Publications

IMPACT Technologies LLC

U. S. DEPARTMENT OF ENERGY | Energy Efficiency & Renewable Energy

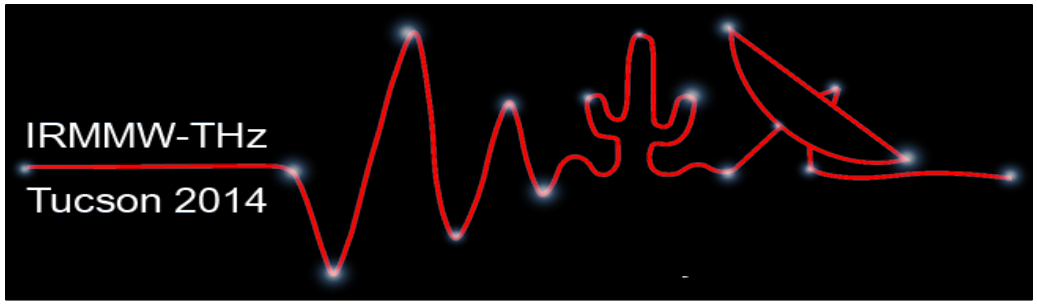


# Penetrating Rock with Intense Millimeter-Waves

Paul P. Woskov[1], Herbert H. Einstein[2] and Kenneth D. Oglesby[3]

[1]*Plasma Science and Fusion Center, MIT*
[2]*Civil and Environmental Engineering, MIT*
[3]*Impact Technologies LLC*

# Motivation

- **Current mechanical drilling technologies are fully mature**
  - Drill rate decreases, and cost increases, exponentially with depth
  - Penetrating hard crystalline rock formations particularly challenging
  - A new approach is needed to make a breakthrough

- **Important applications in need of advance in drilling**
  - Enhanced Geothermal Systems (EGS)* in hot crystal rock formations
    - A large potential energy resource second only to fusion**
  - Nuclear waste storage in deep boreholes***
    - Better biosphere isolation than near surface mined repositories

* J.W. Tester et al, The Future of Geothermal Energy, MIT, 2006

** H.C.H. Armstead and J.W. Tester, Heat Mining, Chapman & Hall, 1987

*** P.V. Brady *et al*, Deep Borehole Disposal of High-Level Radioactive Waste, Sandia Report, 2009

# Directed Energy Drilling

- **Advantages of <u>full bore</u> directed energy drilling**
  - Drill rate expected to be constant, and cost increase linear, with depth
  - Rock hardness and temperature not limiting parameters
  - No mechanical systems to wear out
    - *Opening wellbores in rock could be reduced into a fundamental interaction between energy and matter*
  - Potential for vitrified casing with drilling in one process, but need to deal with initial heat weakening
- **Pursued since the invention of the laser in 1960**
  - Military laser experiments (MIRCAL & COIL) in 1997-1999 showed potential for 10-100 times faster drilling*
  - No practical implementation to date
    - Infrared physics and laser technology limitations

* R. M. Graves & D. G. O'Brien, "StarWars laser technology applied to drilling and completing gas wells", *Proc.- SPE Annual Technical Conference,* pp. 761-770, 1998

# Millimeter-Waves

## Can make full bore directed energy drilling practical

- **Physics Reasons**
  - Compatible with dirty environment and small particle plumes
    - Rayleigh scattering scales as $1/\lambda^4$
      *(1 mm versus 1 $\mu$m $\lambda$, $10^{12}$ less scattering loss than IR)*
  - Absorption in hot rock melt more efficient than in IR *($\mathcal{E}_{MMW} > \mathcal{E}_{IR}$)*
  - Wavelengths and typical borehole sizes are ideally suited for efficient beam guiding and wellbore diameter control

- **Technology Reasons**
  - Commercially available efficient, megawatt gyrotron sources*
  - Efficient long distance, megawatt transmission technology
  - Remote real-time diagnostic monitoring technology available
    - Radiometry, radar, spectroscopy

* G.S. Nusinovich, M.K.A. Thumm, M.I. Petelin, "The Gyrotorn at 50: Historical Overview", J Infrared Milli Terahz Waves, 2014

# Analytic Basis - MMW Rock Melting/Vaporization

**Total energy, *H [kJ/cm³]*, needed vaporize rock:***

$$H = c_s\left(T_m - T_i\right) + H_f + c_m\left(T_v - T_m\right) + H_v$$

$c_s$ = mean heat capacity of solid rock, J/g/°C
$c_m$ = mean heat capacity of molten rock, J/g/°C
$H_v$ = latent heat of vaporization, J/g
$H_f$ = latent heat of fusion, J/g

$T_i$ = initial temperature of rock, °C
$T_m$ = melting temperature of rock, °C
$T_v$ = vaporization temperature of rock, °C
*(at 1 – 3 atmospheres in calculations here)*

| Rock | $c_s$ [J/g/°C] | $T_m$ [°C] | $H_f$ [J/g] | $c_m$ [J/g/°C] | $T_v$** [°C] | $H_v$** [kJ/g] | H** [kJ/cm³] |
|---|---|---|---|---|---|---|---|
| Granite | 1.05 | 1215-1260 | 335 | 1.57 | 2960-3230 | 4.8 - 5.3 | 25 - 28 |
| Basalt | 1.05 | 984-1260 | 419 | 1.65 | 2960-3230 | 3.9 - 4.2 | 25 - 28 |
| Sandstone | 1.04 | 1650 | 335 | 1.51 | 2800-3010 | 4.3 – 4.5 | 19 - 20 |
| Limestone | 1.04 | 2600 | 498 | 1.61 | 3360-3620 | 6.0 – 6.5 | 31 - 33 |

* W. C. Maurer, Novel Drilling Techniques, Pergamon Press, London, pp. 87-91, 1968

** P. Woskov and D. Cohn, MIT Report #PSFC/RR-09-11, 2009

# Drill Rate/ Energy Cost Estimates

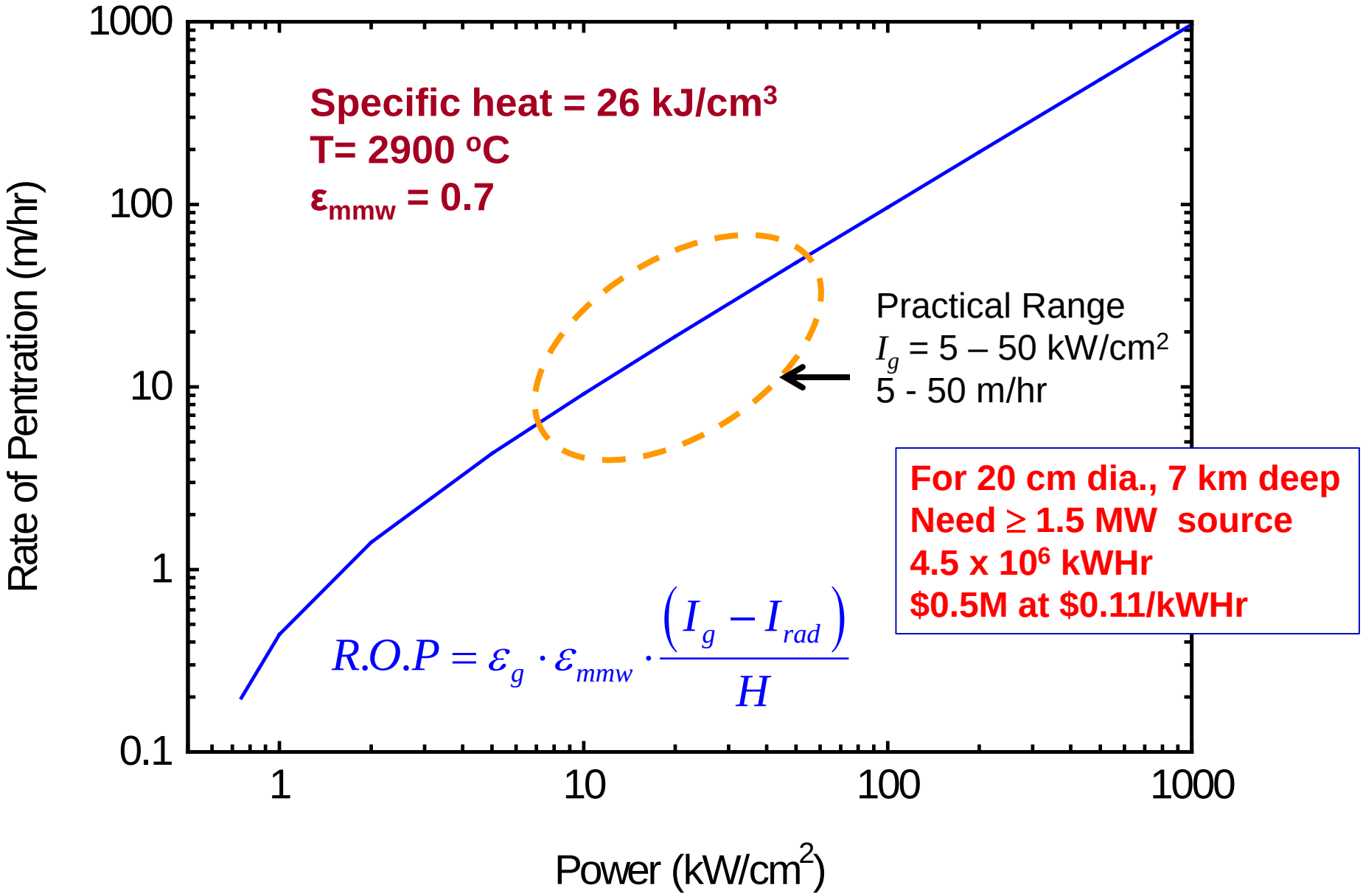

# Experiments - MMW Rock Melting/Vaporization

## Main Features

- **10 kW, 28 GHz HeatWave CPI gyrotron**
- **Transmission line/ reflected power isolation**
  - with forward gas purge, water cooling
- **Collinear 137 GHz radiometer diagnostic**
- **Calorimeter rock ablation test chamber**
- **Granite, basalt, sandstone, and limestone test samples**




**Size - 10 cm (4”) square or diameter, thickness 2.5 – 5 cm (1” – 2”)**

# Experimental Layout

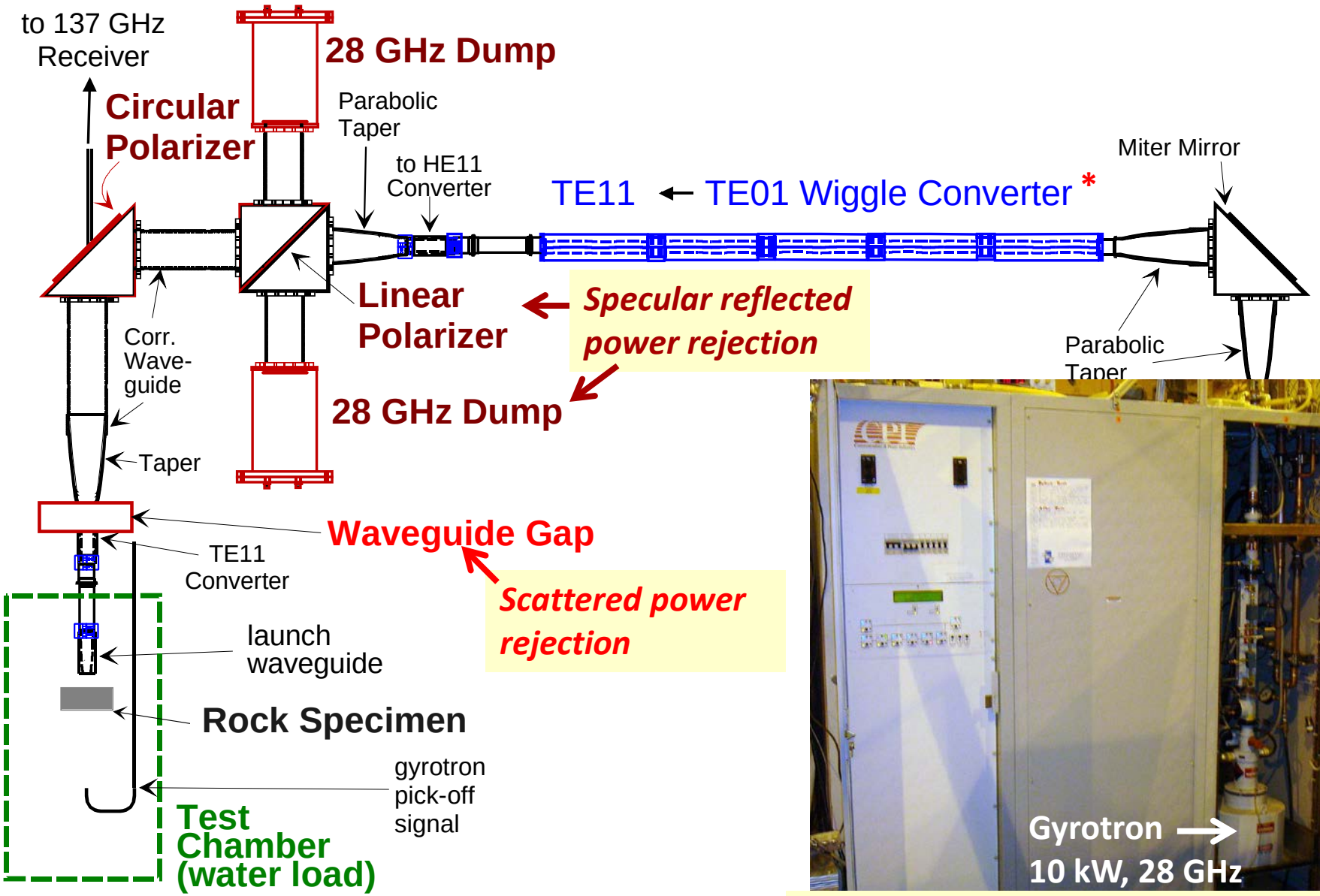





CPI HeatWave Model VIA-301

* M. Thumm, Int. J. Electronics, vol. 57, p. 1225, 1984

# 28 GHz Transmission Line

- Four up and down tapers between 32.5 and 76 mm
- Up to three conversions between TE11 and HE11
- Two miter bends, two polarizers, and one gap
- Forward gas purge
- Collinear 137 GHz radiometer view

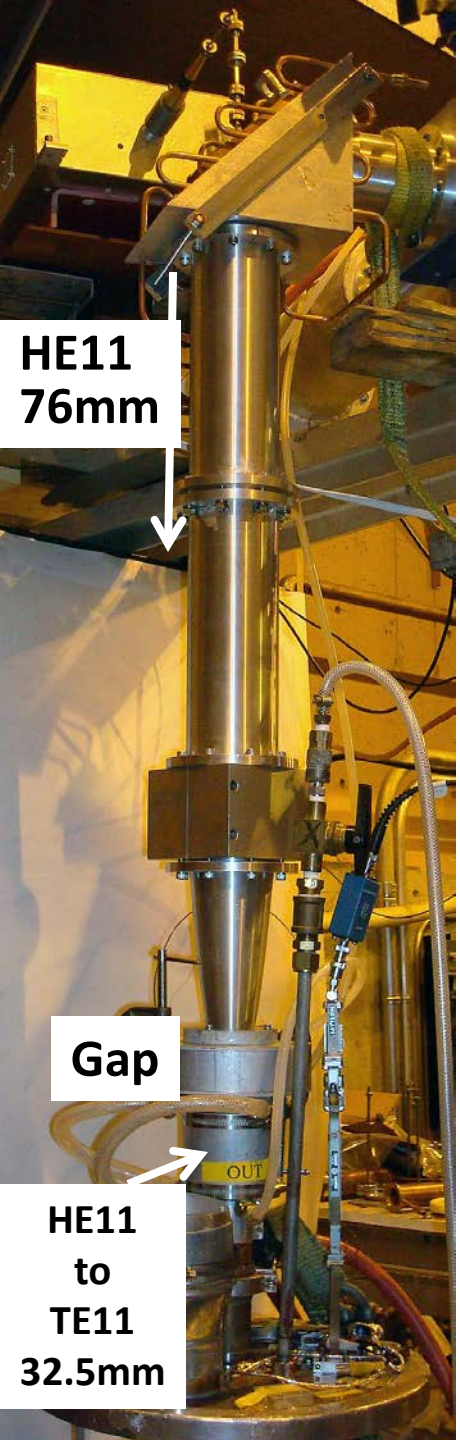


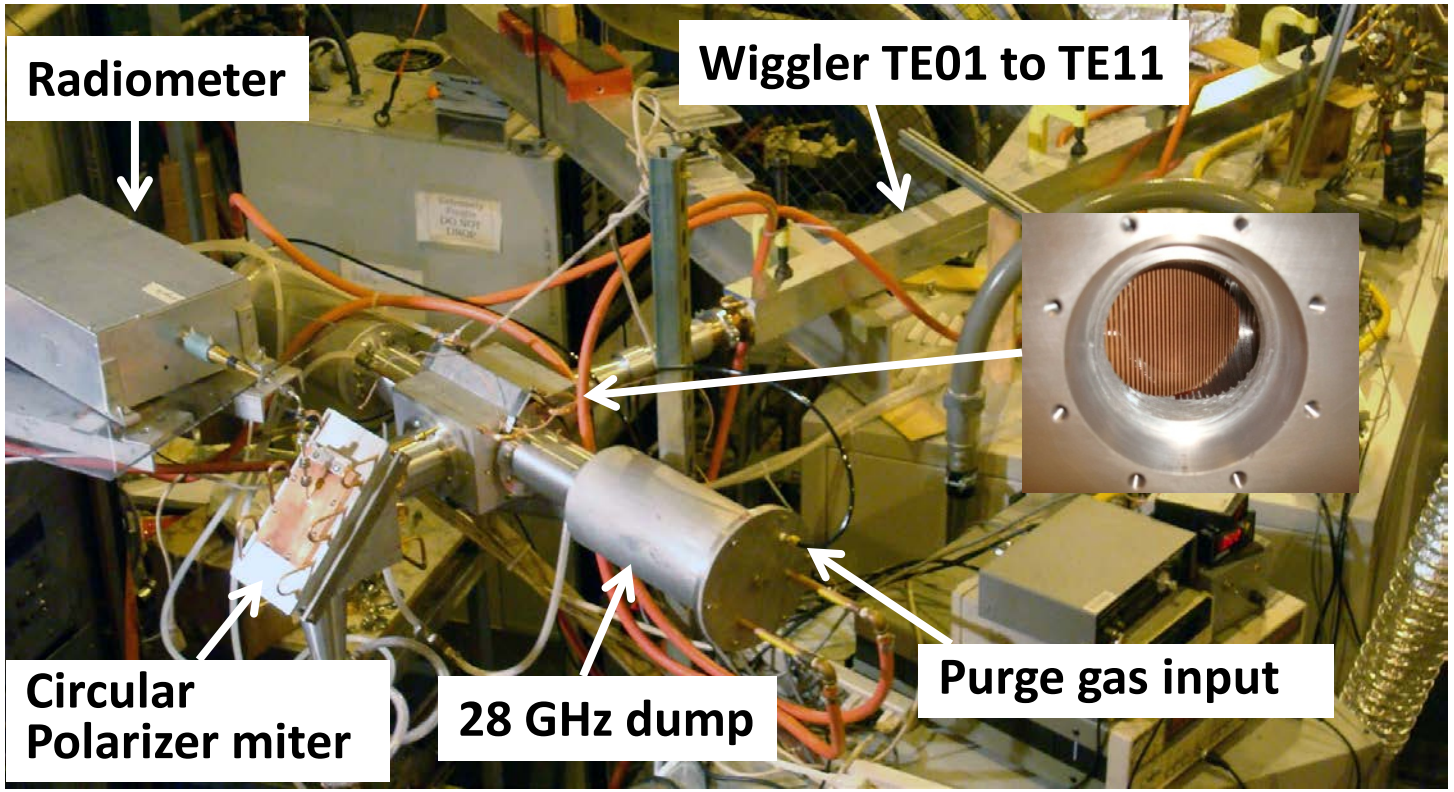

# Rock Test Chamber (& water load)

## Outside View


## Inside View

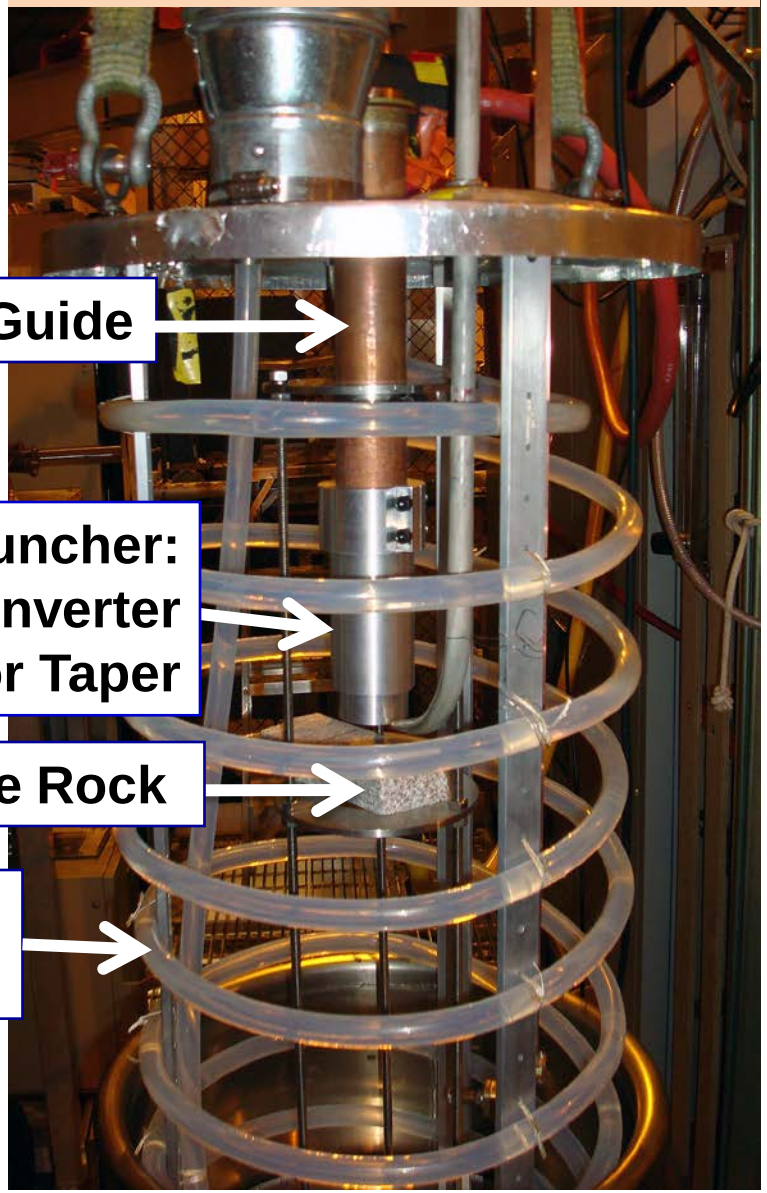

# Transmission Line Calibration

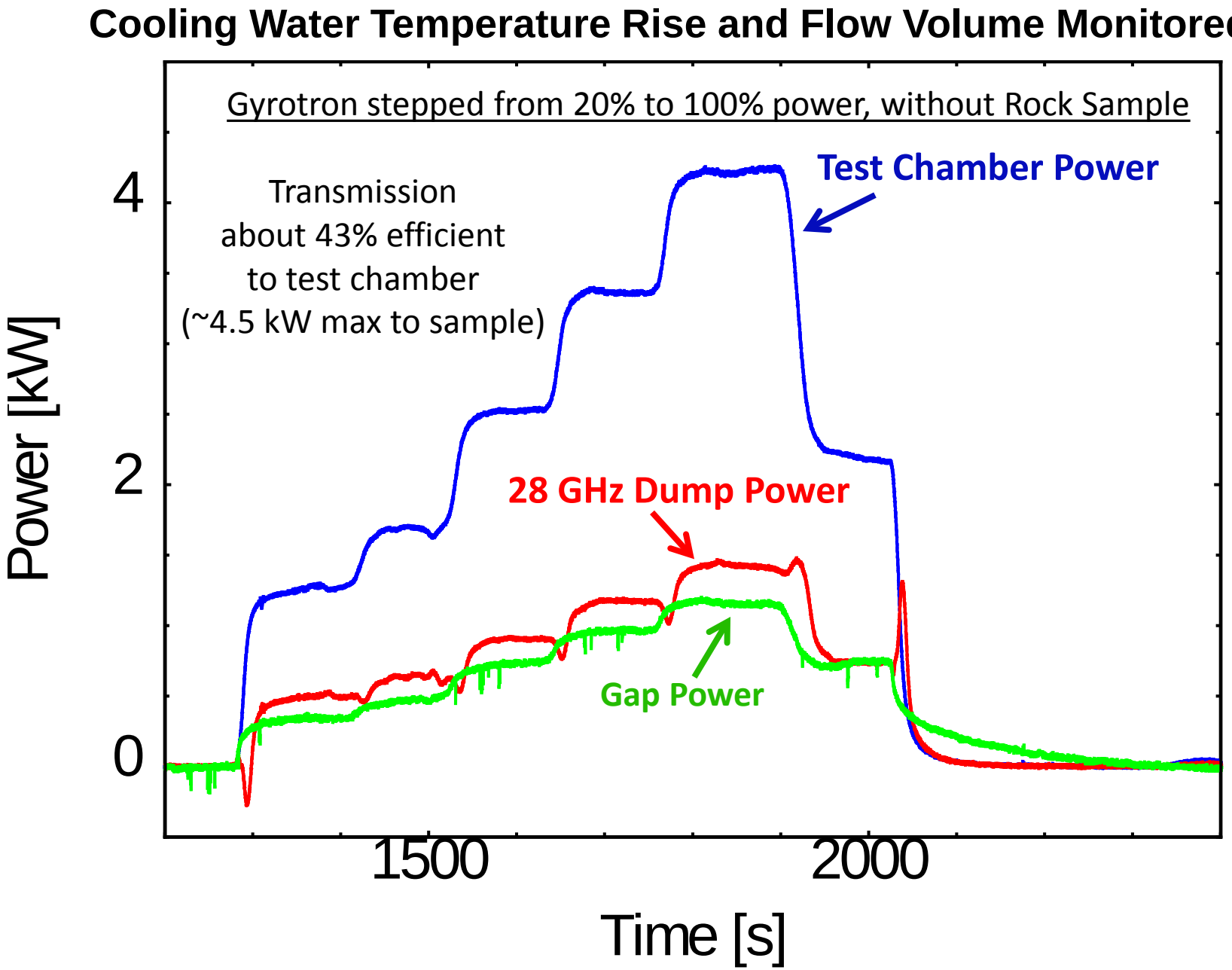

# Initial Granite Exposures

## Plasma breakdown observed with low purge gas flow

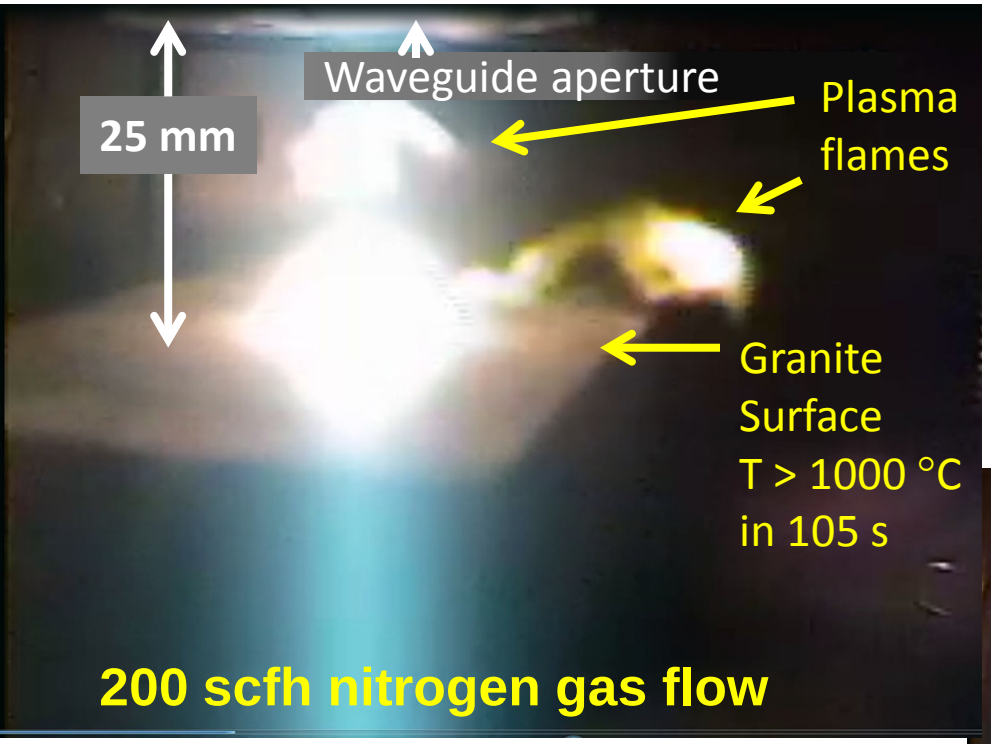


**Incident Power ~ 2.2 kW**
**Peak Intensity ~ 1.3 kW/cm²**

HE11 launched from 32.5 mm dia. waveguide about 25 mm from sample

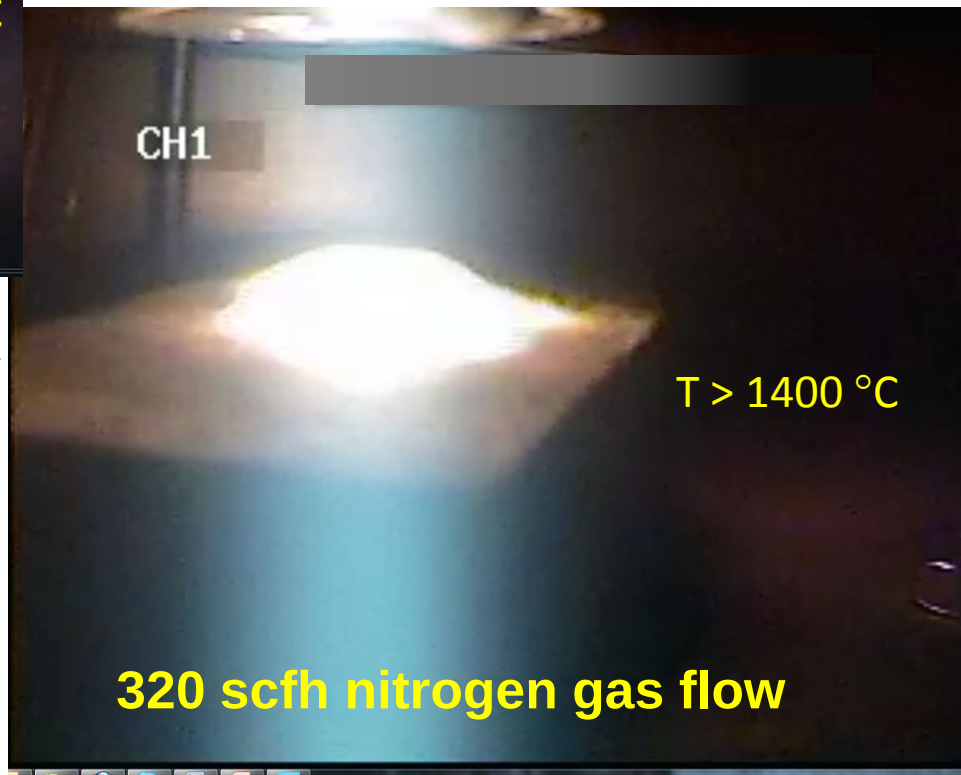


**Higher gas flow suppresses plasma flames**

**Real deep drilling applications would occur at pressures over 100 Atmospheres where breakdown is less likely**

# Directed Energy vs. Plasma

## Plasma Heating is Omni Directional and Inefficient

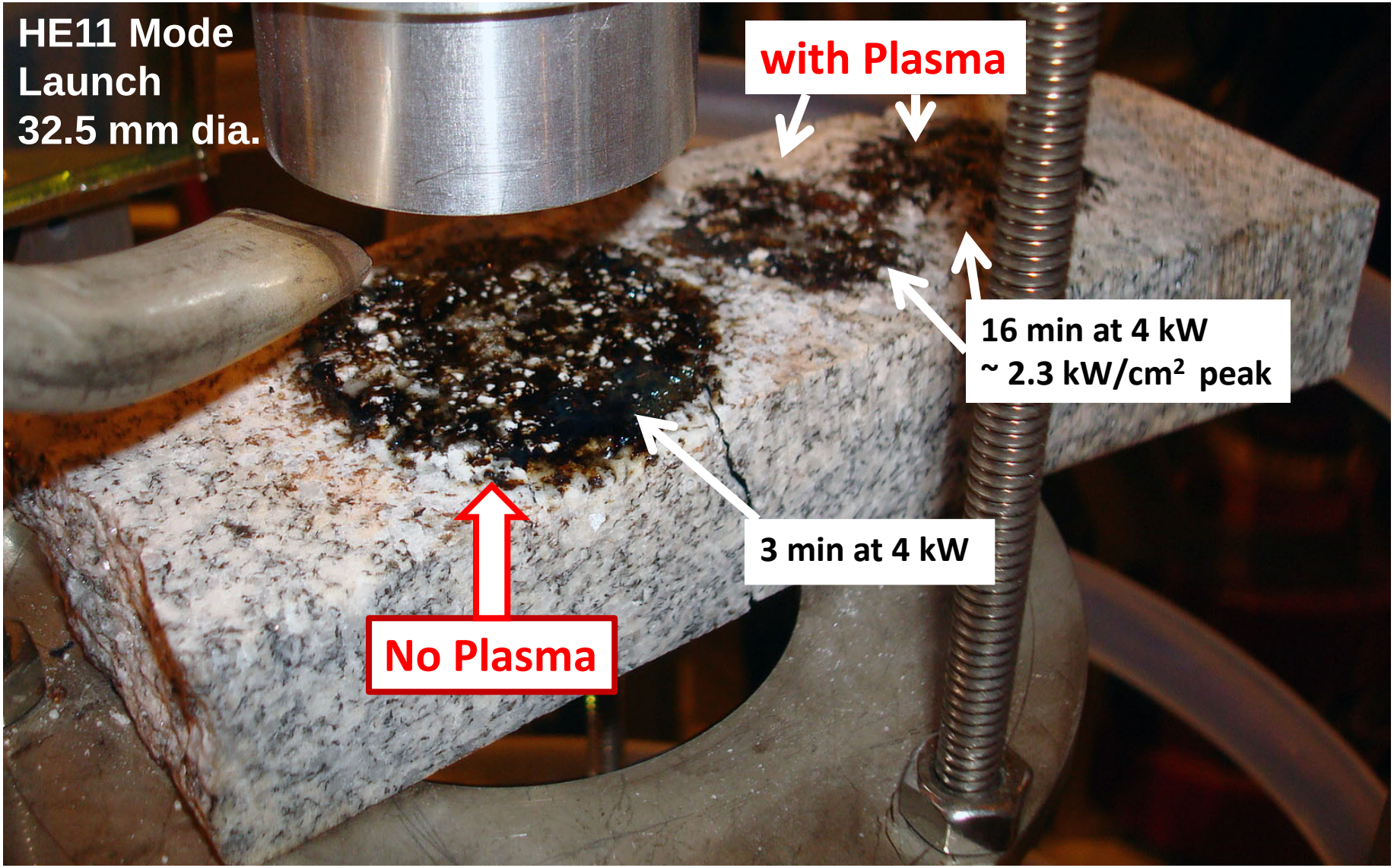

# Results on Flat Surface Samples

## With Circular TE11 Down Taper to 20 mm Dia. Launch Aperture

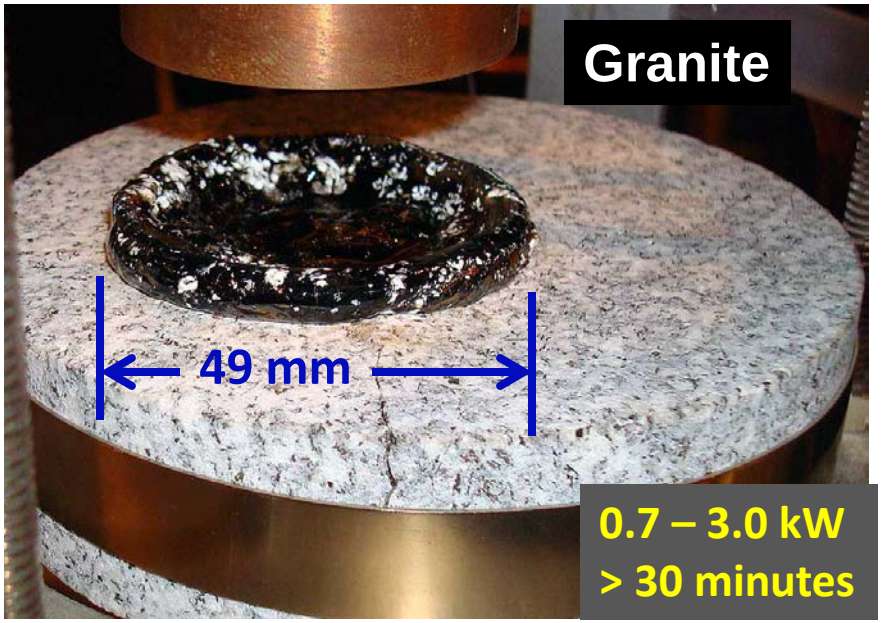


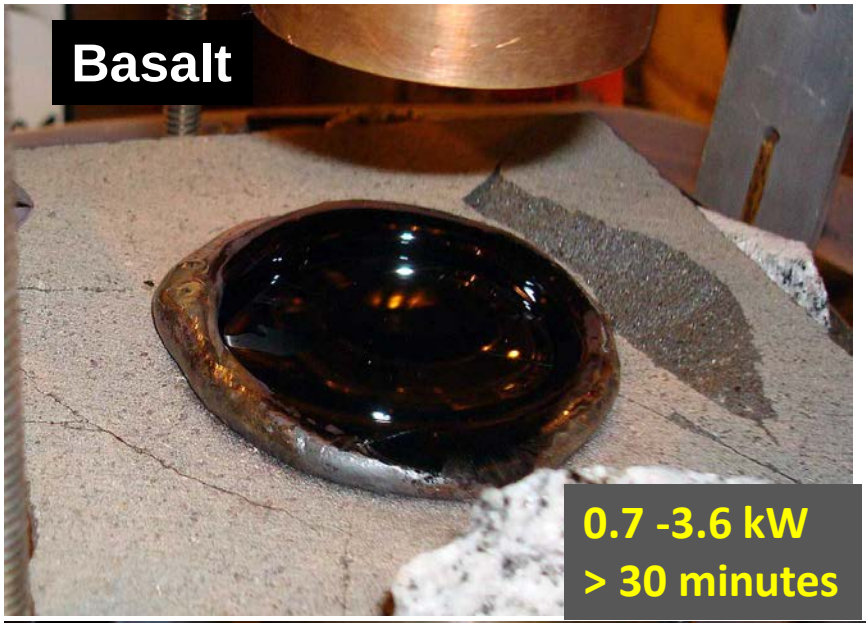


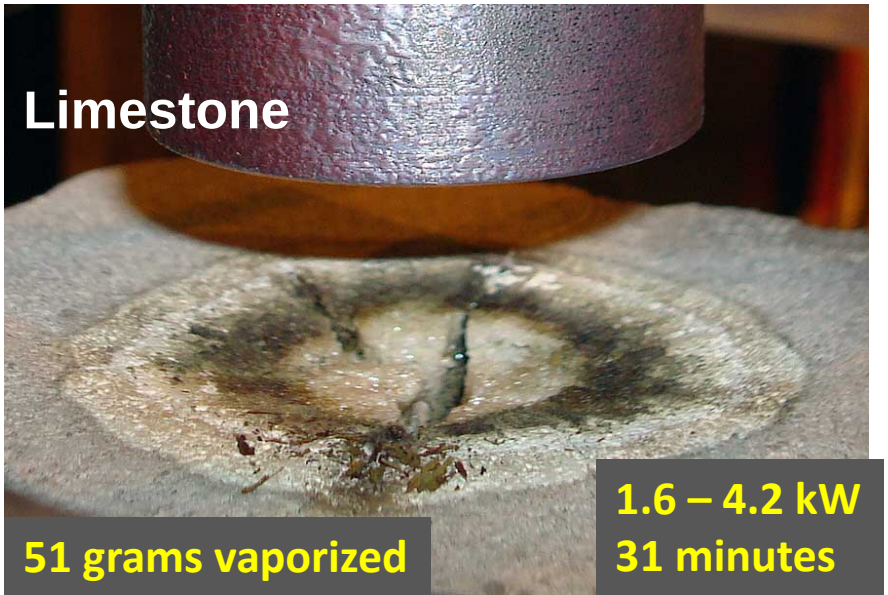


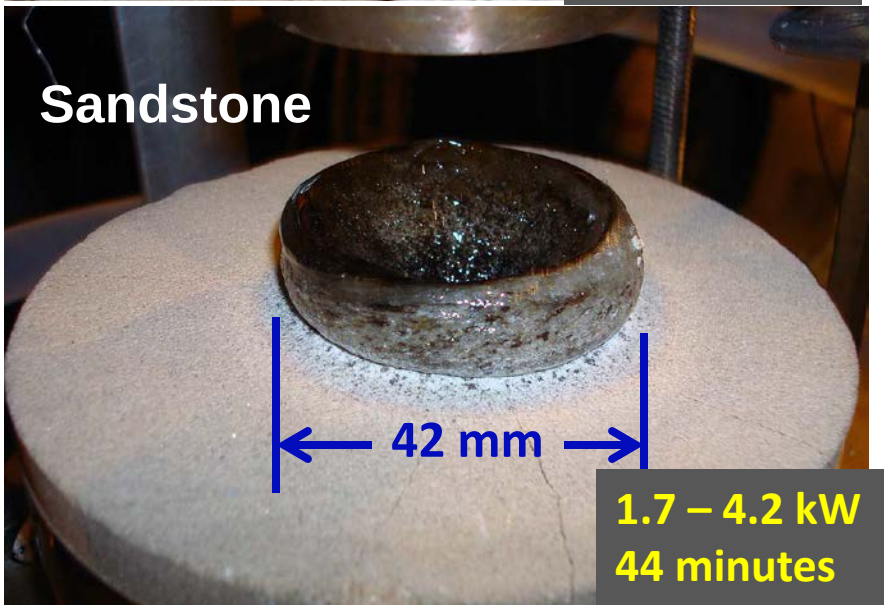

# Power and Temperature Measurements

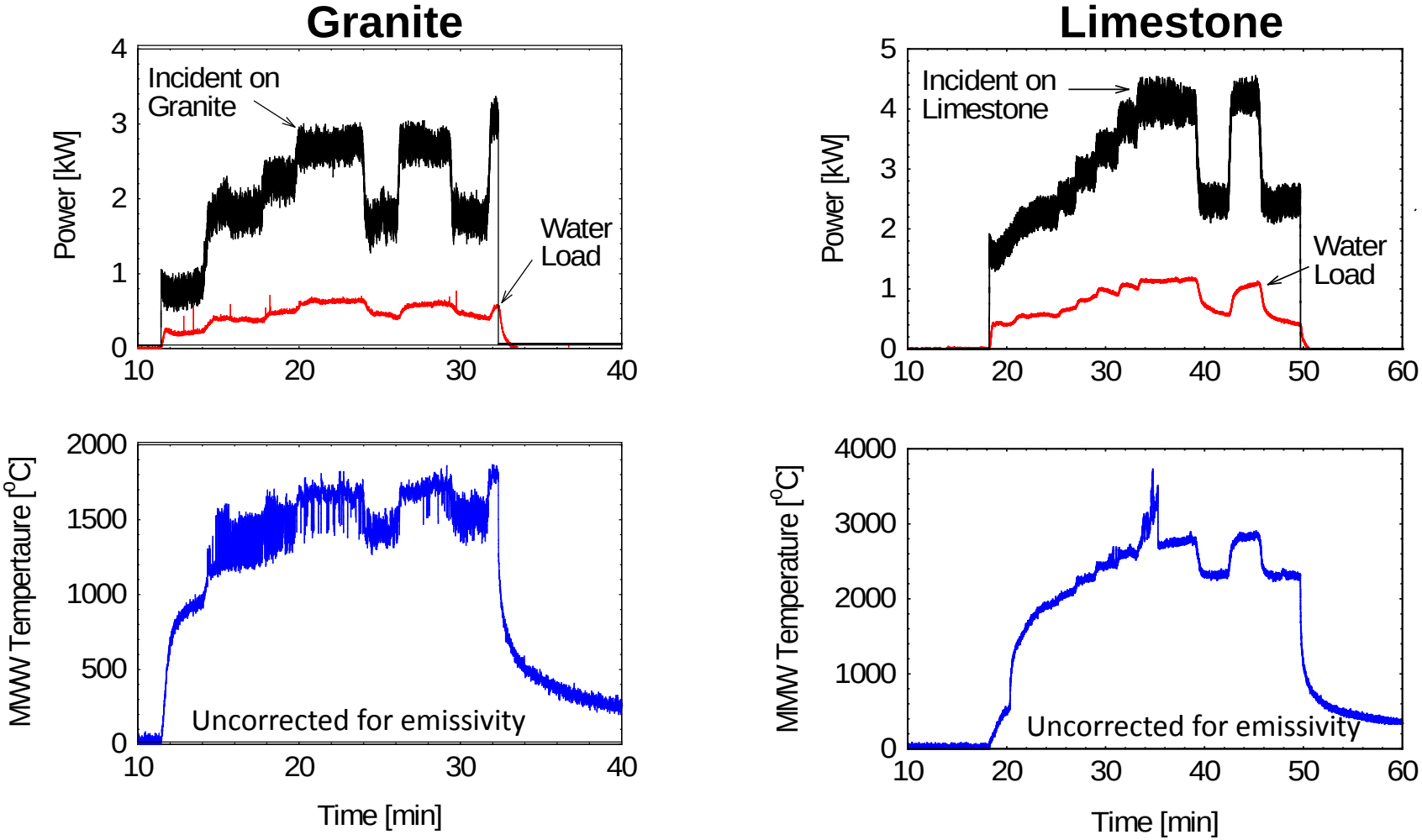


- **Measurements of water load power (along with reflected power) relative to incident power indicates efficiency of 28 GHz absorption by rock melt**
  - *Granite ~ 70%, basalt ~ 50%, sandstone ~ 65%, limestone ~ 75%*
- **Note that surface temperature change is not linear with power change**

# Heat Transfer Modeling

Granite Sample
10 cm (4”) square, 2.5 cm (1”) thick

Gaussian beam incident
10.4 mm waist

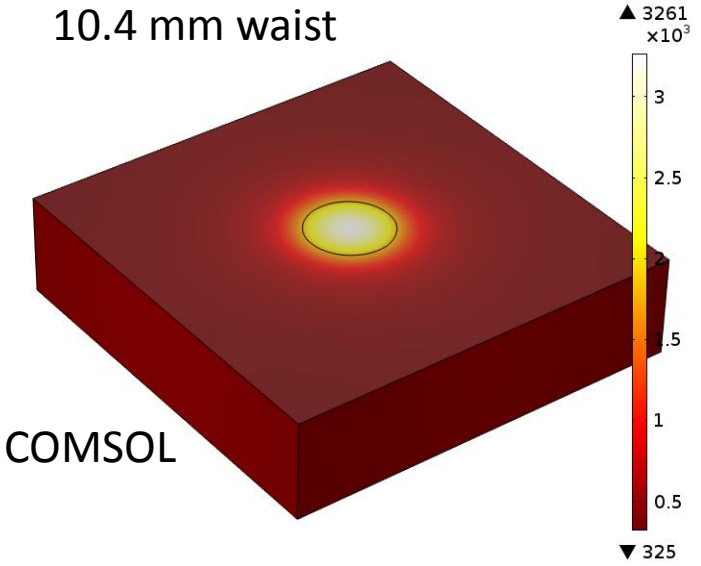


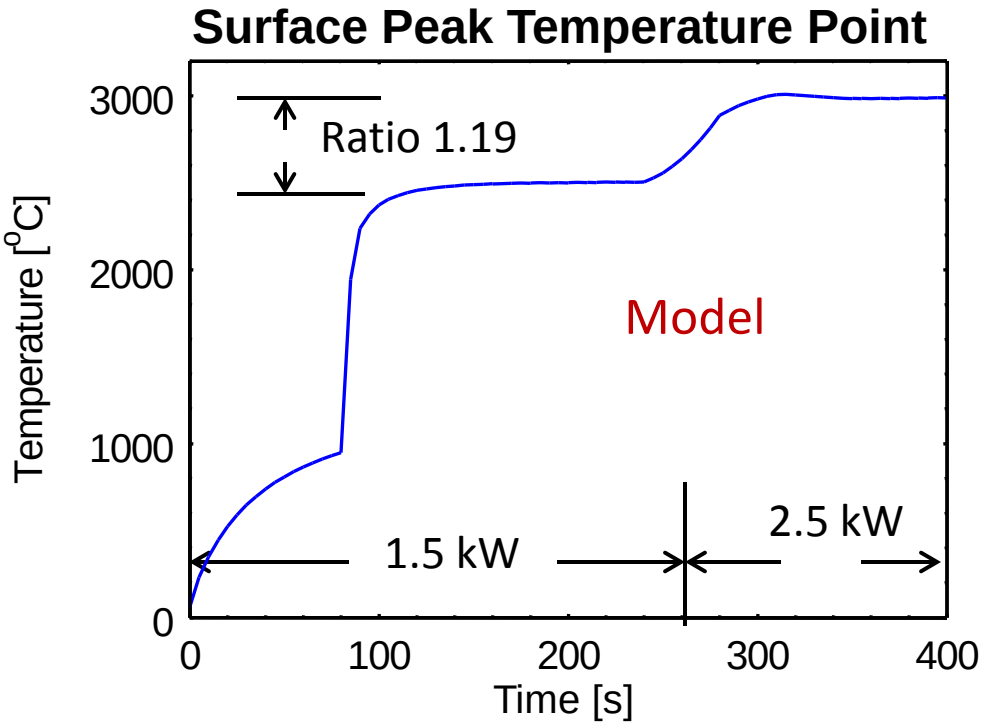


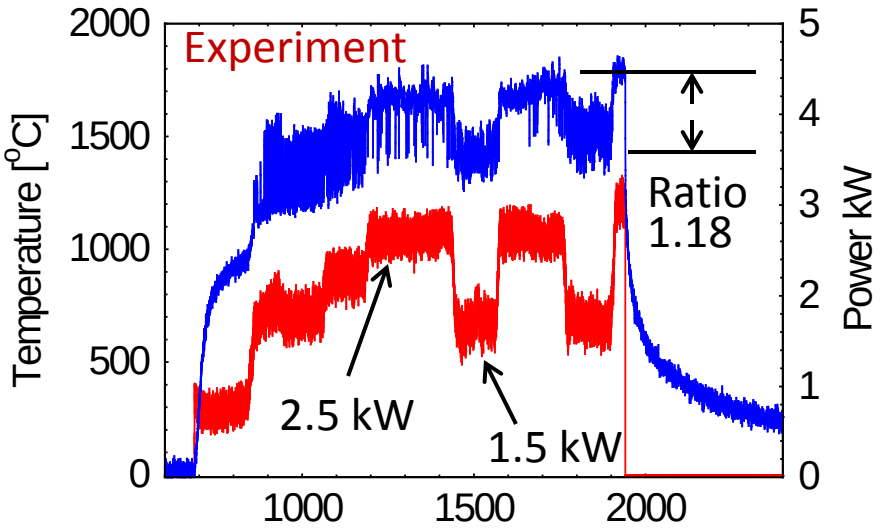


- **Computer modeling qualitatively shows the observed temperature behavior**
- **Radiated heat loss is dominate**

# Power Balance

## For Granite Measurements on Previous Slides

| | |
|---|---|
| Observed peak 137 GHz thermal emission: | 1700 °C |
| Corrected for emissivity (1700/0.7 ): | 2430 °C |
| Measured peak incident power: | 2.2 kW |
| Corrected for emissivity (2.2 x 0.7): | 1.54 kW Absorbed |

## Stefan-Boltzmann Law (radiative heat transfer)

$$q = \varepsilon_{IR}\sigma(T_{hot}^4 - T_{cold}^4)A$$

| | |
|---|---|
| Observed melt spot diameter: | 30 mm |
| Area (A): | 7.1E-4 m^2 |
| Stefan-Boltzmann constant: | 5.67e-8 W/m^2/K^4 |

If $\varepsilon_{IR} = 1.0$ 3.1 kW Radiated

$\varepsilon_{IR}$ = 0.7, 2.1 kW

**Infrared emissivity needs to be less than 0.5 to balance power***

***($\varepsilon_{MMW} > \varepsilon_{IR}$)***

*A.A. Abtahi *et al*, American Geophysical Meeting, Fall 2002

# Experiments with Melt Flow

## and Radiative Heat Loss Trapping

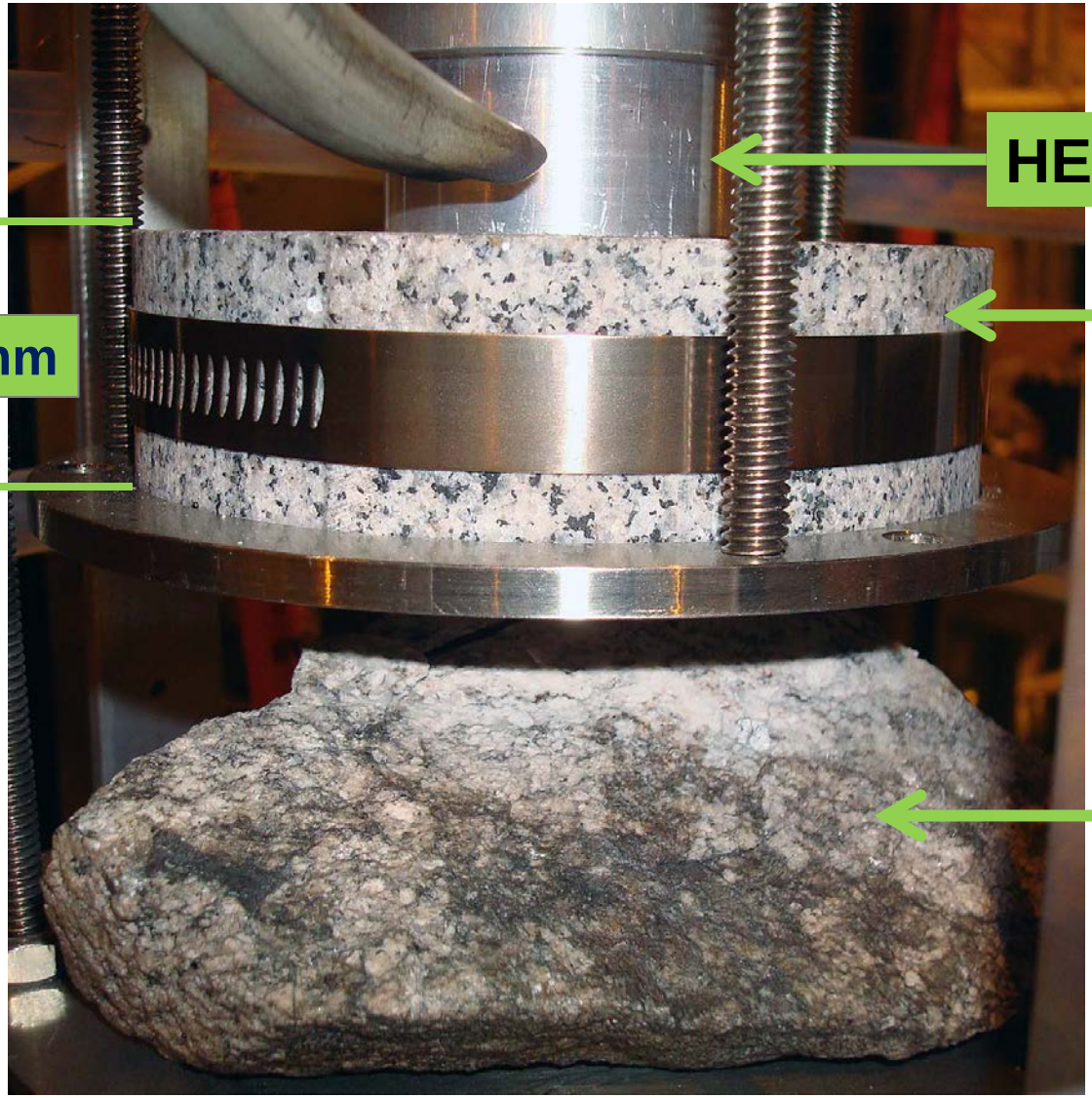


**HE11 launch waveguide**

**Granite borehole waveguide**

(33 mm diameter)

17% dielectric waveguide transmission loss at 28 GHz

**Massachusetts granite**

Sloping rock in beam path allows melt to flow down

# Full Bore Melt Flow

## Before Gyrotron Turned On

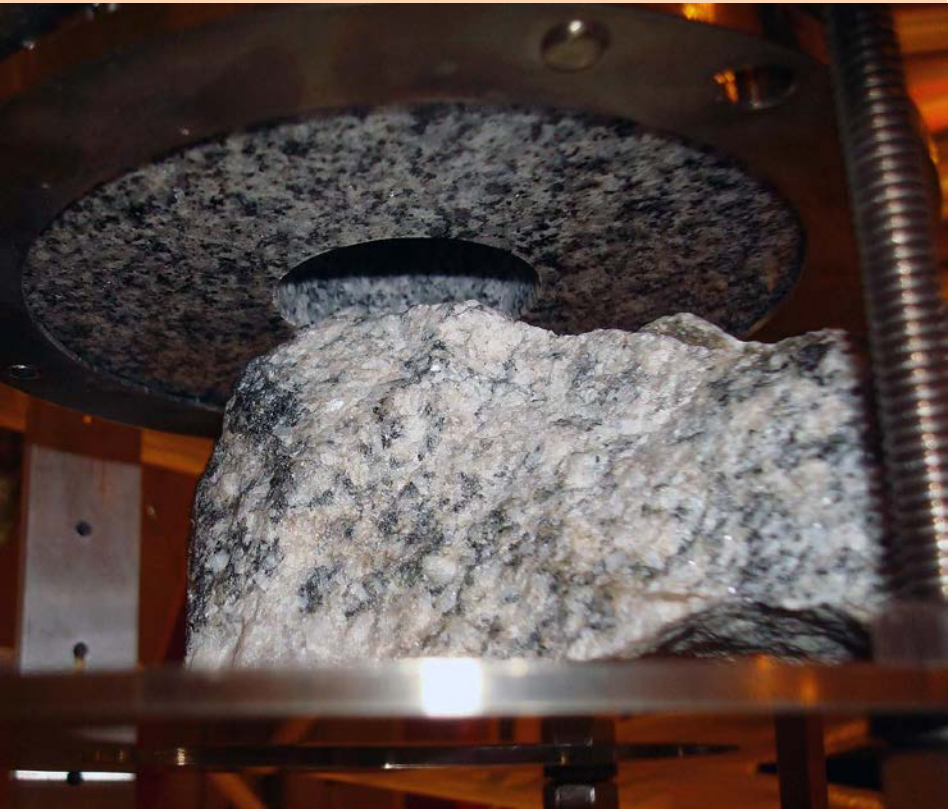

## After

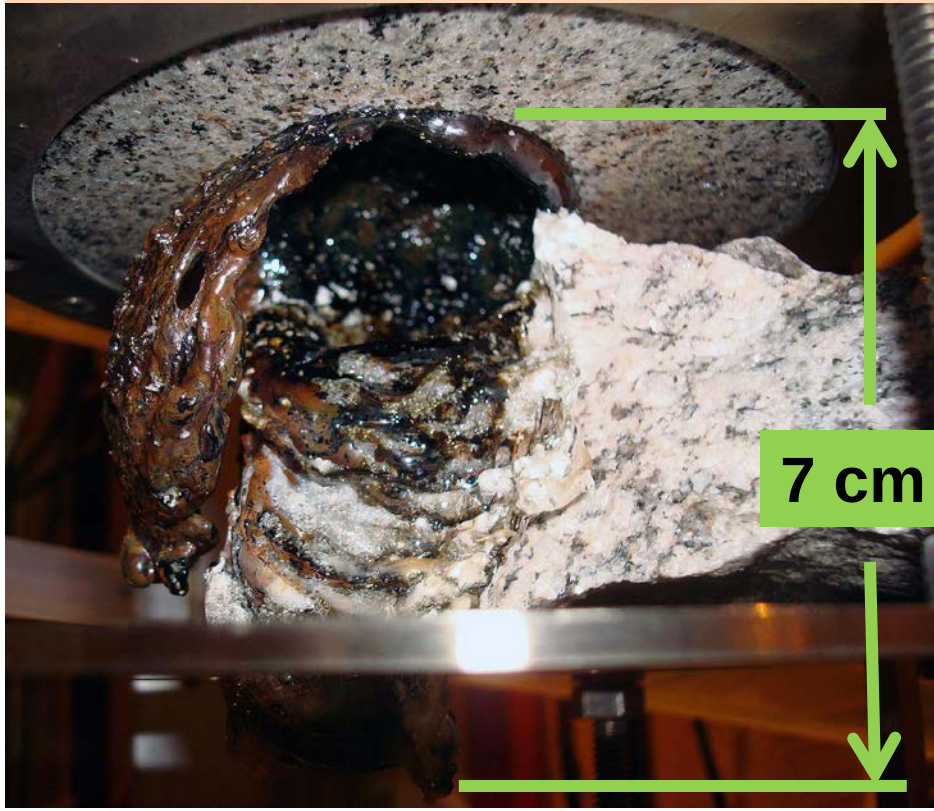


**57 min exposure 1.1 - 3.9 kW, 500 scfh air flow**

- **Radiative heat loss trapping and beam wall losses partially vitrify borehole wall**

# Experiments with a Leak Hole


**Providing a path for melt flow allows large holes**

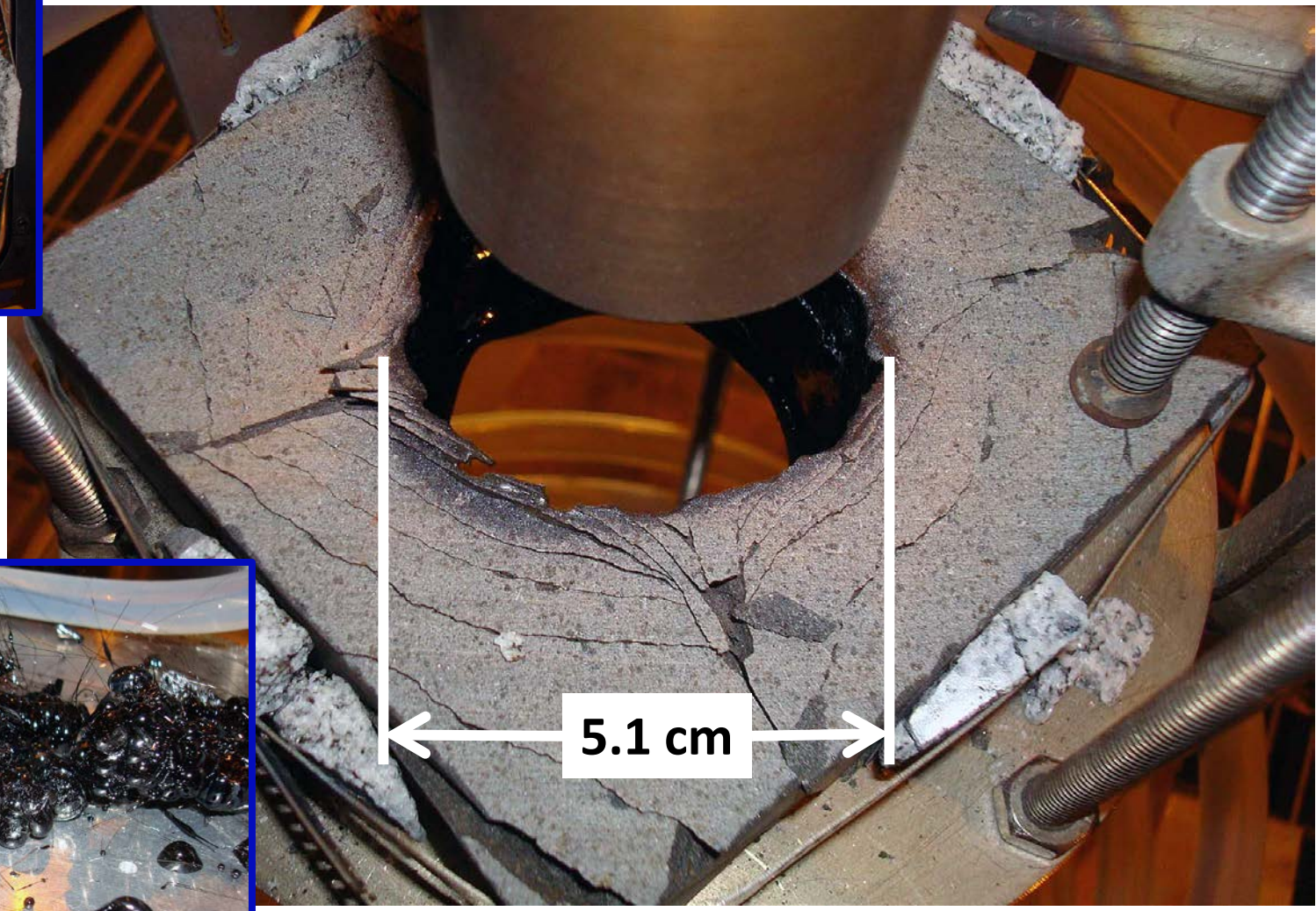


**Rock melt collected on bottom of test chamber**

**Basalt exposed to 28 GHz, 1.6 to 4.5 kW beam for 29 minutes, TE11, 20 mm dia., 35 mm distant**

# Analytic basis- Hole Size/ Wall Melt

- Hole wall will heat up from beam losses and radiated heat from the bottom
- Diameter will increase until too large to sustain wall melt *($H_{wall} < H_f$)*

$$P_{wall} = (1 - Pe^{-\alpha L})$$

$$P_{rad} = \varepsilon_{IR}\sigma[(T_h)^4 - (T_c)^4]\pi a^2$$

$$\alpha = \left(\frac{X_{nm}}{2\pi}\right)^2 \frac{\lambda^2}{a^3} \frac{\frac{1}{2}(n^2+1)}{\sqrt{n^2-1}} \quad *$$

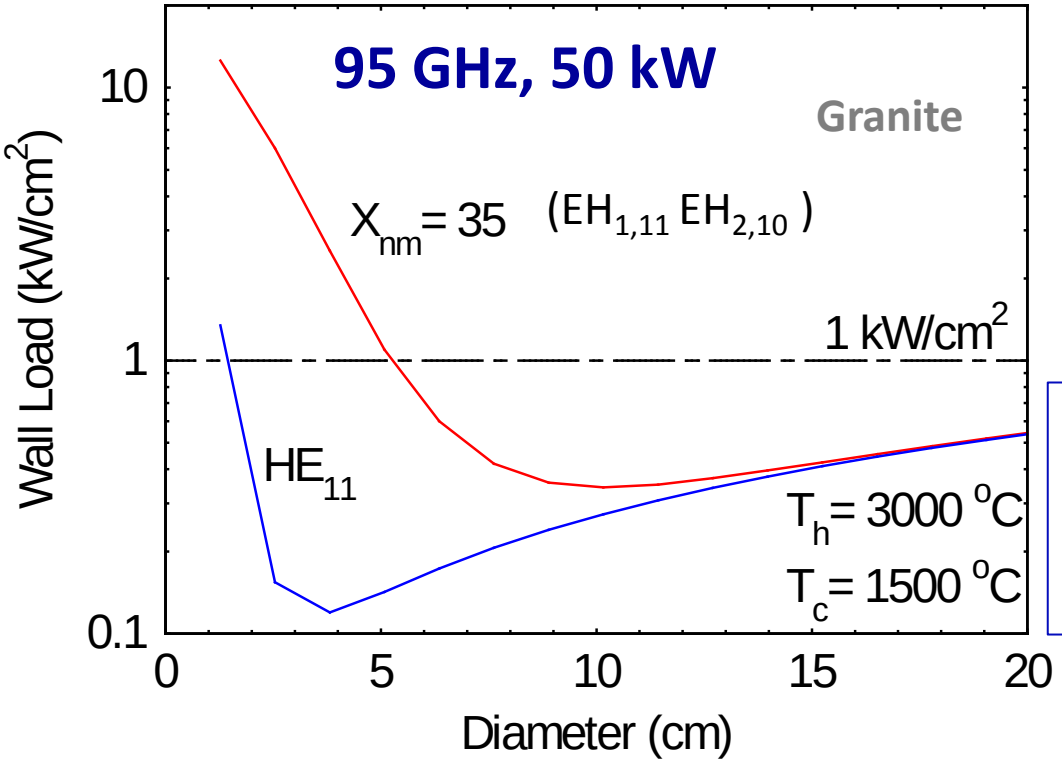


Diameter will depend on frequency, mode, material, rate of penetration

***Opening a borehole could be reduced to a fundamental interaction between energy and matter no mechanics required***

* Marcatili and Schmeltzer, The Bell System Tech. J., v43, 1763, 1964

# Future Plans

**Current experiments are limited by too low a frequency and too low power**

- **Need to get above vaporization point to limit radiative losses**
- **The current gyrotron is limited to 10 kW**
- **At 28 GHz the 20 mm aperture beam can not be focused anymore**

**Plans are in the works to use an Air Force active denial 95 GHz, 100 kW gyrotron to advance rock melting/ vaporization studies next year**

**Fixed system will be used (not shown here)**

# Challenges

- Vitrification for casing will need to develop strategies to deal with heat weakened rock.

- MMW transmission in super critical fluids must be understood
  - Initial tests of $N_2$ to 330 Atmospheres and 1 meter path do not show significant losses
  - More tests needed to study kilometer transmission

- High pressure windows needed 100s' of atmospheres

# Conclusions

## MMWs can make full bore directed energy drilling practical

- **Physics is Favorable**
  - Compatible with dirty environment and small particle plumes
  - Absorption in hot rock melt more efficient than in IR ($\mathcal{E}_{MMW} > \mathcal{E}_{IR}$)
  - Wavelengths and typical borehole sizes are ideally suited for efficient beam guiding and wellbore diameter control
- **Technology is Available**
  - Commercially available efficient, megawatt gyrotron sources
  - Efficient long distance, megawatt transmission technology
  - Remote real-time diagnostic monitoring technology available
    - Radiometry, radar, spectroscopy
- **We have shown necessary features on small scale**
  - Reflected power isolation, forward gas purge, collinear diagnostics, borehole propagation/ vitrification